BioMed Research International

Molecular Mechanism of Muscle Contraction: New Perspectives and Ideas

Guest Editors: Oleg S. Matusovsky, Olga Mayans, and Danuta Szczesna-Cordary

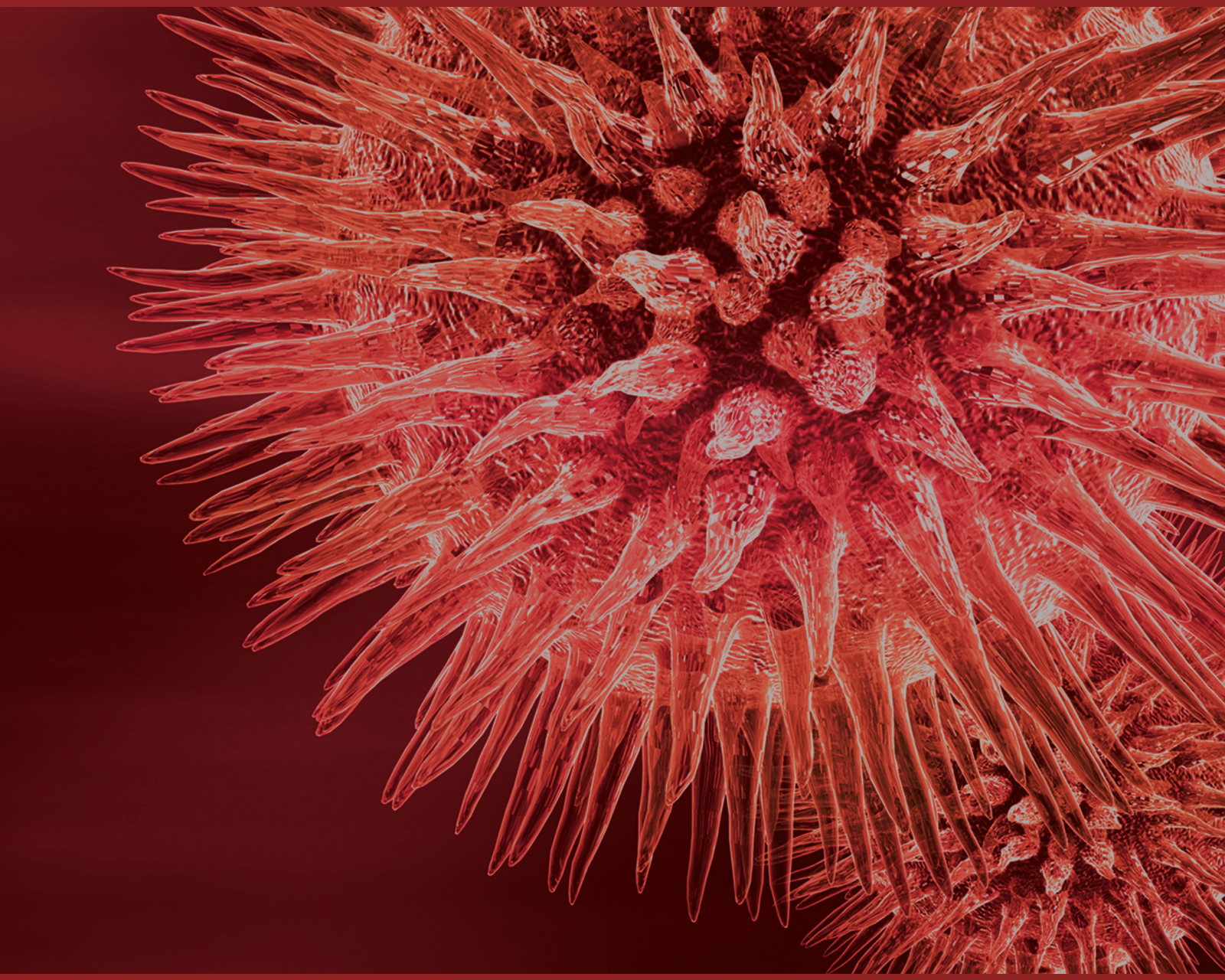

Molecular Mechanism of Muscle Contraction: New Perspectives and Ideas

BioMed Research International

Molecular Mechanism of Muscle Contraction: New Perspectives and Ideas

Guest Editors: Oleg S. Matusovsky, Olga Mayans, and Danuta Szczesna-Cordary

Contents

Hindawi Publishing Corporation
BioMed Research International
Volume 2015, Article ID 694345, 2 pages
http://dx.doi.org/10.1155/2015/694345

Editorial

Molecular Mechanism of Muscle Contraction: New Perspectives and Ideas

Oleg S. Matusovsky,[1,2] Olga Mayans,[3] and Danuta Szczesna-Cordary[4]

[1] *Meakins-Christie Laboratories, McGill University, Research Institute of the MUHC, Centre for Translational Biology, Montreal, QC, Canada H4A 3J1*
[2] *A.V. Zhirmunsky Institute of Marine Biology, FEB RAS, Vladivostok 690041, Russia*
[3] *Institute of Integrative Biology, University of Liverpool, Liverpool L69 7ZB, UK*
[4] *Department of Molecular & Cellular Pharmacology, University of Miami Miller School of Medicine, Miami, FL 33136, USA*

Correspondence should be addressed to Oleg S. Matusovsky; oleg.matusovskiy@mcgill.ca

Received 22 March 2015; Accepted 22 March 2015

Movement, motility, and conformational dynamics of proteins are the basic phenomena of life underlying various physiological and pathological processes of the cell. Muscle cells use an extensively organized but still poorly understood actin-myosin contractile apparatus to generate force and movement and respond to various physiological stimuli. In this special issue we present several invited original and review articles from researchers who study muscle structure and function from different perspectives and emphases.

During the last decades we have seen a major revision of the immutable postulates underlying the molecular mechanisms of muscle contraction. One of the best examples is the discovery of giant proteins widely distributed in nature from nematodes to humans. It was shown that giant proteins are involved in some *fascinating phenomena*; molluscan twitchin regulates the so-called catch state, which permits generation of force with little expenditure of energy. The twitchin-like protein in insects called projectin is implicated in stretch activation of flight muscle, which allows insects to beat their wings at frequencies higher than possible by neural stimulation. The function of titin, the biggest protein involved in various processes in vertebrate skeletal muscle including sarcomere assembly, passive elasticity, myofibrillogenesis, gene regulation, and signaling in health and disease, is still not fully understood.

J. Bogomolovas et al. evaluated the clinical potential of titin ligands in the progression of cardiac remodeling associated with the end-stage idiopathic dilated cardiomyopathy (IDCM). The authors showed that one of the tested ligands, ANKRD1, is a potential marker for cardiac remodeling and disease progression in IDCM and that its greater expression correlated with reduced cardiac contractility.

In skeletal muscle, titin spans each half-sarcomere from the Z-band to M-line. The review of L. Y. Hu et al. is an elegant summary of the recent vast volume of data concerning the M-band region of striated muscle. While the role of the M-region in supporting myofibrillar structure and contractility is well established, its role in mediating additional cellular processes has only recently started to emerge. As such, the M-region is a hub of key protein players contributing to cytoskeletal remodeling, signal transduction, mechanosensing, metabolism, and proteasomal degradation.

Another comprehensive review by A. Månsson et al. pointed out the poorly understood aspects of striated muscle contraction and, in particular, the relationship between the force generation process and the phosphate-release step in the ATP-turnover cycle. The authors discuss in-depth the role of the two heads of myosin II and whether they are independent or cooperative in their interaction with actin. The structure and function of actin filaments in muscle contraction are also discussed.

Four original research articles in the issue were devoted to heart muscle and cardiac disease. J. Liang et al. tested the effect of the hypertrophic cardiomyopathy-linked mutation in human cardiac troponin I (cTnI) on the contractile properties and myofilament protein phosphorylation in papillary

muscle preparations from the left (LV) and right (RV) ventricles of R21C+/+-knock-in mice. The authors showed a significant functional difference in contractile force generation between the LV and RV in the disease model which is not present in wild-type mice. They concluded that the presence of the effect of the mutation only in the LV is a testimony to the power of the mutation exerting its detrimental effects on the function of the LV.

H. B. Lin et al., in their original study, showed that inhibition of MMP-2, the matrix metalloproteinase, is instrumental in enhancing cardiomyocyte contractility and protecting the heart against simulated ischemia-reperfusion (I/R) injury. In another paper by D. Bialy et al., the authors tested the effects of low frequency electromagnetic field conditioning in a model of ex vivo cardiac I/R and demonstrated that when applied prior to, during, and after the ischemic insult, it protects the heart against I/R-induced cardiac contractile dysfunction.

In a well-executed work, K. M. Haizlip et al. showed that during muscle contraction force and calcium transients are not changing in parallel and that a change in steady-state conditions occurs in multiple phases. A rapid phase, characterized by a fast change in force production, is mirrored by a change in calcium transient amplitude. But during a slow phase that occurs as the muscle proceeds to stabilize at the new frequency, dissociation between the calcium transient amplitude and developed force occurs. This dynamic relationship between force and calcium upon a switch in stimulation frequency unveils the dynamic involvement of a myofilament-based regulation during a change in the cardiac contractile steady-state.

The paper of J. Karolczak et al. addressed a unique actin-based motor protein, myosin VI, and performed a search for its binding partners in mouse myoblasts and myotubes. A kinase anchoring protein 9 (AKAP9), a regulator of the protein kinase A (PKA) activity, was identified as a binding partner for myosin VI. The authors concluded that this novel interaction between myosin VI and AKAP9 links myosin VI with the PKA pathway, which could be important for the regulatory activity of myosin VI in the cell.

The present issue constitutes an important update in a constantly developing field. The efforts to carry on these studies may generate new opportunities in the near future.

Acknowledgment

The editors of this special issue are indebted to all the authors who provided either original data or contributed a comprehensive review of the previous and current literature, making this volume appealing to a diverse audience of muscle researchers.

Oleg S. Matusovsky
Olga Mayans
Danuta Szczesna-Cordary

Hindawi Publishing Corporation
BioMed Research International
Volume 2015, Article ID 742536, 9 pages
http://dx.doi.org/10.1155/2015/742536

Research Article

The R21C Mutation in Cardiac Troponin I Imposes Differences in Contractile Force Generation between the Left and Right Ventricles of Knock-In Mice

Jingsheng Liang, Katarzyna Kazmierczak, Ana I. Rojas, Yingcai Wang, and Danuta Szczesna-Cordary

Department of Molecular & Cellular Pharmacology, University of Miami Miller School of Medicine, Miami, FL 33136, USA

Correspondence should be addressed to Danuta Szczesna-Cordary; dszczesna@med.miami.edu

Received 16 September 2014; Revised 16 December 2014; Accepted 19 December 2014

Academic Editor: Luis Loura

We investigated the effect of the hypertrophic cardiomyopathy-linked R21C (arginine to cysteine) mutation in human cardiac troponin I (cTnI) on the contractile properties and myofilament protein phosphorylation in papillary muscle preparations from left (LV) and right (RV) ventricles of homozygous R21C$^{+/+}$ knock-in mice. The maximal steady-state force was significantly reduced in skinned papillary muscle strips from the LV compared to RV, with the latter displaying the level of force observed in LV or RV from wild-type (WT) mice. There were no differences in the Ca^{2+} sensitivity between the RV and LV of R21C$^{+/+}$ mice; however, the Ca^{2+} sensitivity of force was higher in RV-R21C$^{+/+}$ compared with RV-WT and lower in LV- R21C$^{+/+}$ compared with LV-WT. We also observed partial loss of Ca^{2+} regulation at low [Ca^{2+}]. In addition, R21C$^{+/+}$-KI hearts showed no Ser23/24-cTnI phosphorylation compared to LV or RV of WT mice. However, phosphorylation of the myosin regulatory light chain (RLC) was significantly higher in the RV versus LV of R21C$^{+/+}$ mice and versus LV and RV of WT mice. The difference in RLC phosphorylation between the ventricles of R21C$^{+/+}$ mice likely contributes to observed differences in contractile force and the lower tension monitored in the LV of HCM mice.

1. Introduction

The pump function of the heart is achieved by a sequence of alternating contraction and relaxation of the heart muscle. Although both the left (LV) and right (RV) ventricles contract simultaneously, there are functional and structural differences between them. Since the LV is responsible for pumping blood throughout most vessels in the body, it generates more pressure and therefore it is thicker than the RV. A normal LV has a near conical geometry with its long-axis directed from apex to base and irregular endocardial surface due to the presence of papillary muscles and trabeculae [1]. Several studies using experimental mechanics and computational modeling have proved that the helical geometry of the muscle fibers of the LV changes gradually from right-handed in the subendocardium to left-handed in the subepicardium, which produces a distinctive counter directional movement of the fiber layers in a beating heart [2–5]. The RV is less muscular because it operates at a lower pressure compared to the LV and pumps blood through the shorter distance to the lungs. In addition, the RV does very little work against gravity. The stroke work for RV is approximately 25% of that for LV because of low resistance of the pulmonary vasculature. Morphologically, the RV is distinguished from the LV by having coarser trabeculae and a lack of fibrous continuity between its inflow and outflow valves [6, 7].

Despite efforts by many, the contractile differences between the RV and LV in the healthy and/or diseased heart are poorly understood. For example, no differences were observed in the stress development, twitch duration, work performance, or shortening power between the RV and LV in dogs [8, 9]. On the other hand, small differences were observed in the contractile performance and growth of the LV and RV myocytes in dilated cardiomyopathy [10] and in

myofilament function in congestive heart failure [11]. Likewise, molecular analysis of the myocardial tissue of the explanted heart of familial hypertrophic cardiomyopathy (HCM) patients showed similar mRNA and β-MHC protein expression levels in both ventricles but the hypertrophic phenotype was only observed in the LV [12].

This report aimed to examine the functional differences between the LV and RV at the level of papillary muscle fibers from the knock-in (KI) mice expressing the HCM-linked R21C (arginine to cysteine) mutation in cardiac troponin I (cTnI) shown to cause a malignant HCM phenotype [13]. The animal model of R21C-HCM was produced and characterized previously [14, 15]. Here we show a significant functional difference in contractile force generation between the LV and RV in the disease model expressing the R21C cTnI mutation which is not present in wild-type (WT) control mice. The presence of the effect of the mutation only in the LV is the testimony to the power of the mutation exerting detrimental effects on the function of the LV.

2. Materials and Methods

All animal studies were conducted in accordance with institutional guidelines. The University of Miami has an Animal Welfare Assurance (A-3224-01, effective November 23, 2011) on file with the Office of Laboratory Animal Welfare (OLAW), National Institutes of Health. The mouse model of R21C-HCM was generated and characterized earlier [14]. Seven nine-month-old homozygote R21C$^{+/+}$ KI mice were used in the experiments and the results were compared to those of age and gender matched WT controls.

2.1. Histopathological Characterization. After euthanasia, the hearts from ~7-month-old WT and R21C$^{+/+}$ KI mice were excised and immersed in 10% buffered formalin. Slides of whole mouse hearts were prepared at the Histology Laboratory (University of Miami Miller School of Medicine, Miami, FL). Paraffin-embedded longitudinal sections of whole mouse hearts stained with hematoxylin and eosin (H&E) and Masson's trichrome were examined for overall morphology and fibrosis using a Dialux 20 microscope, 40/0.65 NA (numerical aperture) Leitz Wetzlar objective, and an AxioCam HRc (Zeiss) as described previously [16, 17].

2.2. Preparation of Glycerinated Left and Right Ventricular Muscle Strips. The papillary muscles of the left and right ventricles from flash frozen hearts of R21C$^{+/+}$ KI mice were isolated, dissected into muscle bundles in the buffer containing pCa 8 solution (10^{-8} M [Ca^{2+}], 1 mM free [Mg^{2+}] (total MgPr (propionate) = 3.88 mM), 7 mM EGTA, 2.5 mM [Mg-ATP^{2-}], 20 mM MOPS, pH 7.0, 15 mM creatine phosphate, and 15 units/mL of phosphocreatine kinase, ionic strength = 150 mM adjusted with KPr), 15% glycerol, and 30 mM BDM. Solutions of increasing Ca^{2+} concentrations from pCa 8 ([Ca^{2+}] = 10^{-8} M) to pCa 4 ([Ca^{2+}] = 10^{-4} M) were prepared based on the "pCa-Calculator" program developed by Dweck et al. [18]. Muscle bundles were skinned in 50% pCa 8 solution and 50% glycerol containing 1% Triton X-100 for 24 hr at 4°C. Muscle bundles were then transferred to the same solution without Triton X-100 and stored at −20°C for experiments within ~5 days [19].

2.3. Steady-State Force Development. Small muscle strips of approximately 1.4 mm in length and 100 μm in diameter were isolated from a batch of glycerinated skinned mouse papillary muscle bundles and attached by tweezer clips to a force transducer. The strips were placed in a 1 mL cuvette and freshly skinned in 1% Triton X-100 dissolved in pCa 8 buffer for 30 min. The sarcomere length was adjusted to ~2.1 μm and the maximal steady-state force was measured in pCa 4 solution (composition is the same as pCa 8 buffer except the [Ca^{2+}] = 10^{-4} M). Maximal tension readings (in pCa 4) were taken before and after the force-pCa curve, averaged, and expressed in kN/m^2. The cross-sectional area of the muscle strip was assumed to be circular [16].

2.4. The Ca^{2+} Dependence of Force Development. After determination of initial steady-state force, muscle strips were relaxed in pCa 8 buffer and exposed to solutions of increasing Ca^{2+} concentrations from pCa 8 to pCa 4 [18]. The level of force was measured in each "pCa" solution. Data were analyzed using the Hill equation [20], where "$[Ca^{2+}]_{50}$ or pCa_{50}" is the free Ca^{2+} concentration which produces 50% of the maximal force and n_H is the Hill coefficient. The pCa_{50} represents the measure of Ca^{2+} sensitivity of force and the n_H is the measure of myofilament cooperativity.

2.5. Passive Force Measurements. The measurement of passive force (in pCa 8 solution) in response to muscle stretch was performed as described in [16]. Briefly, after skinning the strips were washed in the relaxing solution and their length was adjusted to remove the slack. This procedure resulted in sarcomere length (SL) of ~2.1 μm as judged by the first order optical diffraction using a He–Ne laser [21, 22]. This point was set as zero for both the passive force and starting length of the muscle strip. Then, the strips were stretched by 10% of its length ×4 consecutive times, and the passive force per cross-section of muscle (in kN/m^2) was determined.

2.6. Analysis of Protein Phosphorylation. Flash frozen LV and RV from all groups were homogenized in CMF buffer consisting of 5 mM NaH_2PO_4, 5 mM Na_2HPO_4 (pH 7.0), 0.1 mM NaCl, 5 mM $MgCl_2$, 0.5 mM EGTA, 5 mM ATP, 5 nM microcystin, 0.1% Triton X-100, 20 mM NaF (phosphatase inhibitor), 5 mM DTT, and 1 μL/mL protease inhibitor cocktail. The samples were homogenized for 2 min in a Mixer-Mill MM301 at 30 Hz, chilled on ice, and homogenized again for 2 min. Homogenates were then centrifuged for 4 min at 1800 g and the supernatants were discarded. The pellets were resuspended in the CMF buffer and the myofibrils were subsequently dissolved in SDS-PAGE sample buffer and loaded on 15% SDS-PAGE. The phosphorylated form of myosin regulatory light chain (RLC) was detected with phosphospecific RLC antibodies (produced earlier [23]), which recognize the phosphorylated form of the RLC followed by a secondary goat anti-rabbit antibody conjugated with the fluorescent

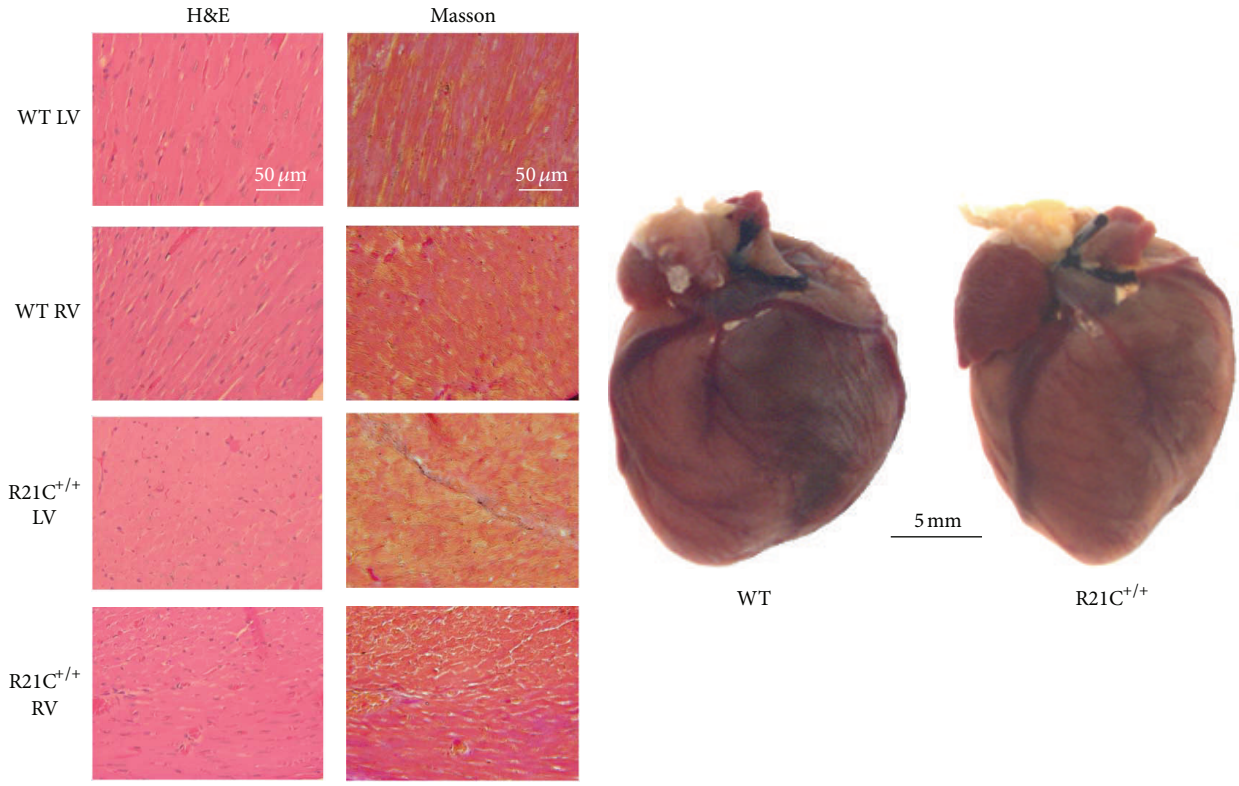

FIGURE 1: Representative hearts and H&E and Masson's trichrome-stained LV and RV sections from R21C$^{+/+}$ and WT mice. LV and RV sections from the hearts of ~7-month-old male R21C$^{+/+}$ and WT mice were imaged. Note: no mutation-induced abnormalities in H&E stained sections from the hearts of R21C$^{+/+}$ compared with WT mice. Very mild histopathological changes could infrequently be observed in Masson's trichrome-stained LV sections from R21C$^{+/+}$ mice.

dye, IR red 800. The total RLC protein was detected with polyclonal RLC CT-1 antibodies produced in this laboratory [19] (raised against 15 residues from the C-terminus of human cardiac RLC) and served as a loading control. Mouse cardiac myofibrils from LV and RV were also used to determine sarcomeric protein phosphorylation by ProQ/Coomassie [17]. After separation of the samples on 15% SDS-PAGE ProQ Diamond phosphoprotein gel stain reagent (Invitrogen) was used (as described in the manufacturer's manual) to assess phosphorylation of troponin (TnT, TnI) and myosin RLC. The total protein was further detected in the same gel using the Coomassie brilliant blue staining. Myofilament protein phosphorylation ratio (ProQ) was calculated relative to the corresponding Coomassie brilliant blue staining (ProQ/Coomassie) using Image J software.

2.7. Statistical Analysis. All values are shown as means ± SEM (standard error of the mean). Statistically significant differences between two groups were determined using an unpaired Student's t-test, with significance defined as $P < 0.05$. Comparisons between multiple groups were performed using one-way ANOVA (Sigma Plot 11; Systat Software, San Jose, CA). Passive tension measurements were analyzed using one-way repeated measures ANOVA (IBM SPSS statistics version 21).

3. Results

3.1. Histology. Representative H&E and Masson's trichrome-stained LV and RV sections from the hearts of ~7-month-old male R21C$^{+/+}$ and WT mice and images of the whole hearts are presented in Figure 1. The heart tissue morphology pictured in H&E stained slides showed no mutation-induced abnormalities in LV or RV of R21C$^{+/+}$ mice. Very mild histopathological changes could occasionally be seen in Masson's trichrome-stained LV sections from R21C$^{+/+}$ mice compared to WT controls, but no obvious signs of fibrosis or myofilament disarray were observed. These results are in accord with previous findings on R21C$^{+/+}$ mice showing no abnormalities in the hearts of 3–6-month-old mutant versus WT mice [14]. Substantial morphological changes with severe fibrotic lesions were observed in animals as old as 18 months [14].

3.2. The R21C Mutation in cTnI Imposes Differences in Maximal Steady-State Force in the LV but Not in RV. Measurements of steady-state force were performed in skinned papillary muscle strips from the LV and RV of R21C$^{+/+}$ KI homozygous mice and the results were compared to WT mice (Figures 2(a) and 2(b)). Three to four hearts per group were used with each heart yielding 5–8 muscle strips from LV

Table 1: The effect of R21C mutation in TnI on steady-state force measurements in KI R21C$^{+/+}$ mice.

Parameter	LV-WT mice Three mice; 22 fibers	RV-WT mice Three mice; 16 fibers	LV-R21C$^{+/+}$ mice Four mice; 30 fibers	RV-R21C$^{+/+}$ mice Four mice; 30 fibers
Maximal tension/cross-section (kN/m^2)	41.8 ± 0.8	41.7 ± 0.6	36.9 ± 1.2	43.5 ± 1.0
pCa_{50} (calcium sensitivity)	5.76 ± 0.02	5.67 ± 0.03	5.71 ± 0.01	5.73 ± 0.01
n_H (Hill coefficient)	2.16 ± 0.14	1.90 ± 0.10	2.19 ± 0.10	2.20 ± 0.09

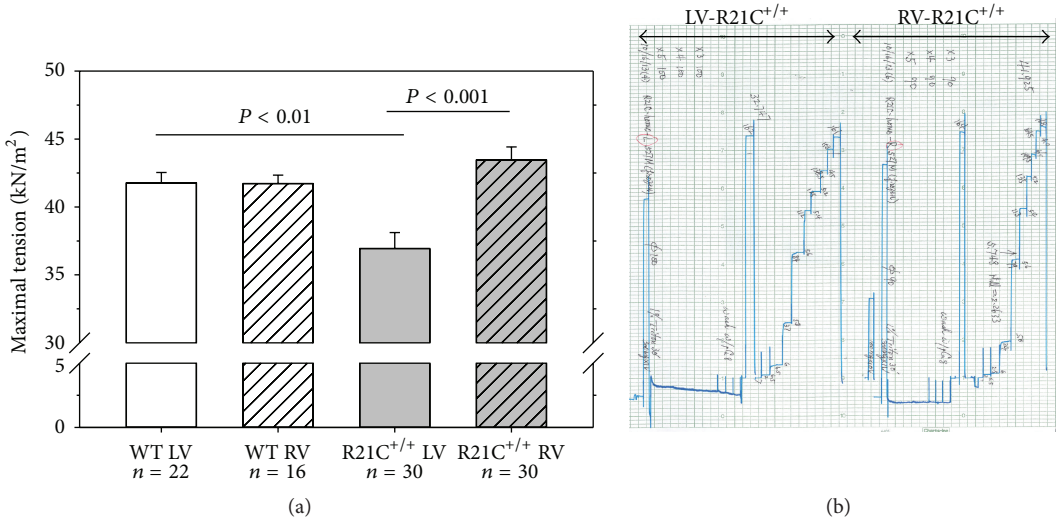

Figure 2: The effect of the HCM-R21C mutation in cTnI on steady-state force development in LV versus RV papillary muscle strips in genetically altered mice. (a) Maximal tension per cross-section of muscle strip. Note that the R21C mutation in cTnI imposes differences in maximal steady-state force in the LV but not in RV. Sixteen to thirty independent measurements on skinned cardiac muscle strips from the left and right ventricles of three WT hearts and four homozygous R21C$^{+/+}$ knock-in hearts have been performed. ~8-month-old mice were used yielding, respectively, $n = 22$ and $n = 16$ muscle strips from the LV and RV of WT mice and $n = 30$ muscle strips from LV and RV of R21C$^{+/+}$ mice. Error bars are SEM. (b) Representative force traces in the LV and RV papillary muscle fibers of R21C$^{+/+}$ mice.

and RV that were used in mechanical experiments (Table 1). A significantly lower maximal isometric force was observed in LV of R21C$^{+/+}$ mice (36.9 ± 1.2 kN/m^2, $n = 30$ strips) compared to LV-WT (41.8 ± 0.8 kN/m^2, $n = 22$) strips (Figure 2 and Table 1). The differences in the level of force in LV- R21C$^{+/+}$ versus all other muscles including RV- R21C$^{+/+}$ (43.5 ± 1.0 kN/m^2, $n = 30$) were also statistically significant (Figure 2, $P < 0.001$). There were no differences between WT-LV and WT-RV (41.7 ± 0.6 kN/m^2, $n = 16$) or RV-R21C$^{+/+}$ (Figure 2(a) and Table 1). Therefore, the mutation exerted its effect only on the LV and not RV while there were no differences between ventricles of WT mice.

3.3. Force-pCa Relationship Is Rightward Shifted in the LV but Leftward Shifted in RV in R21C$^{+/+}$ Compared to WT Mice. As shown in Figures 3(a) and 3(b), there was a significant difference in the Ca^{2+} sensitivity of force between LV-WT ($pCa_{50} = 5.76 \pm 0.02$, $n = 22$) and RV-WT (5.67 ± 0.03, $n = 16$) muscles and the Ca^{2+} sensitivity of force was rightward shifted in the RV of WT mice compared to LV-WT (Figure 3(b), Table 1). The Hill coefficient (parameter of cooperativity) was also slightly lower in RV-WT ($n_H = 1.90 \pm 0.10$) compared to LV-WT ($n_H = 2.16 \pm 0.14$), but the difference was not statistically significant (Table 1). Considering the HCM R21C$^{+/+}$ heart, the mutation exerted no statistically significant changes in the Ca^{2+}-sensitivity of contraction between the LV and RV (Figure 3). The HCM phenotype of the R21C mutation was manifested by a small but significant change in the Ca^{2+} sensitivity in the LV-R21C$^{+/+}$ (5.71 ± 0.01, $n_H = 2.19 \pm 0.10$, $n = 30$) compared to the LV-WT. However, as observed for other HCM mutations, the force-pCa relation was leftward shifted in the RV of R21C$^{+/+}$ mice (5.73±0.01, $n_H = 2.20 \pm 0.09$, $n = 30$) compared to RV-WT (Figure 3, $P < 0.05$).

3.4. The R21C Mutation in cTnI Imposes Differences in Passive Force in the LV but Not in RV. The measurement of passive tension in response to muscle stretch was performed in pCa 8 relaxing solution as described in [16]. The data are expressed as fold change over the active force measured in kN/m^2 in pCa 4 solution before the first 10% stretch of the fiber length (Figure 4). Data are average of 9-10 experiments performed on skinned papillary muscle strips from flash frozen hearts of 9-month-old male mice. The effect of mutation on passive tension followed the trend observed in active tension development presented in Figure 2. Passive

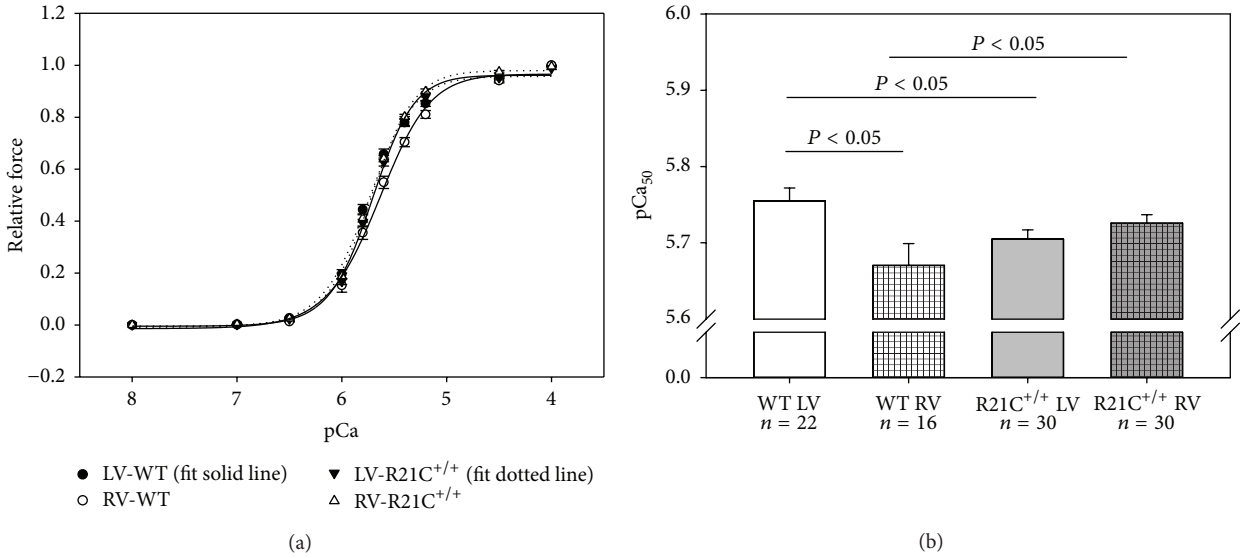

Figure 3: Force-pCa dependence (a) and Ca^{2+}-sensitivity (b) in LV and RV of R21C$^{+/+}$ mice compared with LV and RV of WT mice. Note that the Ca^{2+} sensitivity of force was lower in RV-WT compared to LV-WT ($P < 0.05$). The Ca^{2+} sensitivity of force was also lower in the LV of R21C$^{+/+}$ mice versus LV-WT. The pCa_{50} was larger in the RV-R21C$^{+/+}$ compared to RV of WT mice ($P < 0.05$). No differences in the force-pCa dependence were observed between the LV versus RV of R21C$^{+/+}$ mice. Number of mice and muscle strips are as in Figure 2. Error bars are SEM.

tension was significantly higher in LV-R21C$^{+/+}$ compared to LV-WT for all points of stretch (Figure 4, $P = 0.015$). No significant changes in the resistance to stretch were noted for other groups of strips. The level of passive tension for 10% stretch (in kN/m^2) was 2.2 ± 0.4 (LV-WT); 2.9 ± 0.5 (RV-WT); 7.1 ± 2.2 (LV-R21C$^{+/+}$); and 4.4 ± 1.0 (RV-R21C$^{+/+}$). Interestingly, the difference between LV-R21C$^{+/+}$and LV-WT was statistically significant ($P = 0.027$) indicating partial loss of Ca^{2+} regulation at low [Ca^{2+}] in the mutant LV. Therefore, once again, it is important to note that the effect of a disease causing mutation was manifested in the papillary muscle strips from the LV (and not RV), the ventricle which is predominantly affected by HCM disease.

3.5. The R21C Mutation Prevents cTnI Phosphorylation in Both Ventricles but Imposes Differences in RLC Phosphorylation between the LV and RV. As shown in Figures 5(a) and 5(c), there were no differences in cTnI phosphorylation between the LV and RV of WT mice. Consistent to what was observed earlier in this R21C$^{+/+}$-KI mouse model of HCM [14, 15], the mutation prevented β-adrenergic-activated protein kinase A- (PKA-) mediated phosphorylation of cTnI at Ser 23 and 24. Data were derived from four independent ProQ/Coomassie gels assessed in 2-3 preparations from LV and RV of R21C$^{+/+}$ and WT mice. No changes in phosphorylation of troponin T (TnT) or myosin binding protein C (MyBP-C) were observed between the groups of fibers (Figure 5(a)). However, the mutation imposed a significant alteration in the myosin RLC phosphorylation between the LV and RV of R21C$^{+/+}$ mice (Figures 5(b) and 5(d)). Data for RLC phosphorylation were derived from six independent SDS-PAGE (Western blots and ProQ/Coomassie gels) analyses of two to three LV and RV preparations per group. Interestingly, phosphorylation of myosin RLC was significantly higher in the RV versus LV of R21C$^{+/+}$ mice (Figures 5(b) and 5(d), $P = 0.007$) and also significantly higher than in LV-WT (Figures 5(b) and 5(d), $P = 0.027$). Elevated RLC phosphorylation in the RV of R21C$^{+/+}$ mice may play rescuing role in preventing the right ventricle from abnormalities in force development that are observed in the LV of R21C$^{+/+}$ mice. No statistically significant differences in myosin RLC phosphorylation were observed between the LV and RV of WT mice (Figure 5(d), $P > 0.05$).

4. Discussion

In this study, we aimed to examine the effect of the HCM-linked R21C in cTnI on the function and protein phosphorylation and pinpoint potential differences between the LV and RV using papillary muscle fibers from the KI homozygous mice compared to WT. The R21C mutation was identified in a cardiomyopathy patient, who presented with atrial fibrillation shortly after the sudden death of her child at the age of 18 years [13]. Three surviving mutation carriers from the family had asymmetrical septal hypertrophy, left atrial enlargement, and normal cardiac dimensions. The mutation was also identified in another HCM family with 4 mutation carriers having subaortic asymmetrical hypertrophy and one mutation carrier with normal cardiac dimensions, who was resuscitated from sudden death [13]. The animal model of R21C-HCM used in this study was produced and characterized previously [14, 15]. In agreement with those reports, we show that the mutation renders no obvious histopathological changes in ~7-month-old mice compared to age and gender matched

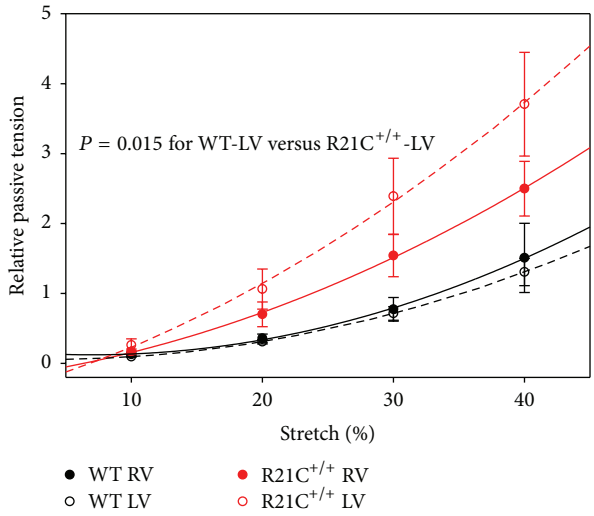

FIGURE 4: Passive tension per cross-section of muscle strip in LV and RV of R21C$^{+/+}$ mice compared with LV and RV of WT mice. After skinning the strips were washed in the relaxing solution and their length was adjusted to remove the slack to sarcomere length (SL) = ~2.1 μm. This point was set as zero for both the passive force and starting length of the muscle strip. Then, the strips were stretched by 10% of its length ×4 consecutive times, and the passive force per cross-section of muscle (in kN/m^2) was determined. Note that the R21C mutation exerted its effect on passive tension in the LV compared to LV-WT ($P = 0.015$ as established by repeated measures ANOVA). The values of passive tension (in kN/m^2) for 10%, 20%, 30%, and 40% stretch were 2.2 ± 0.4; 7.9 ± 0.7; 19.6 ± 1.8; and 38.7 ± 3.5 for LV-WT and 6.4 ± 2.1; 26.6 ± 7.5; 59.7 ± 15.5; and 92.1±21.7 for LV-R21C$^{+/+}$. No statistical differences in the resistance to stretch were observed between the LV versus RV of WT mice. Interestingly, the passive tension for 10% stretch (in kN/m^2) was 2.2 ± 0.4 (LV-WT); 2.9 ± 0.5 (RV-WT); 7.1 ± 2.2 (LV-R21C$^{+/+}$); and 4.4 ± 1.0 (RV-R21C$^{+/+}$). The difference between LV-mutant and LV-WT was statistically significant ($P = 0.027$) indicating mutation-induced partial loss of Ca^{2+} regulation at low Ca^{2+}. Data are average of n = 9-10 experiments performed on skinned muscle strips from 9-month-old male mice. Error bars are SEM.

WT (Figure 1). Likewise, as shown earlier, we observed no cTnI phosphorylation in R21C$^{+/+}$ mice (Figure 5). However, we show here that the R21C mutation in cTnI imposes significant functional differences in contractile force generation in genetically altered KI-R21C$^{+/+}$ compared to WT mice. In contrast to Wang et al., 2012 [14], a significantly lower maximal pCa 4 force was observed in R21C$^{+/+}$ compared with WT mice (Figure 2). Importantly, this difference in maximal tension per cross-section of muscle occurred only in the LV and not in the RV of R21C$^{+/+}$ mice (Figure 2). This result highlights the importance of testing cardiac muscle preparations from both ventricles when studying the effect of HCM causing mutations in mice. Interestingly, passive tension in R21C$^{+/+}$ mice followed the active force measurements and the only difference between R21C$^{+/+}$ and WT fibers was observed in the LV. A significantly larger value for passive tension was observed in LV-R21C$^{+/+}$ compared to LV-WT (Figure 4, $P = 0.015$). No statistically significant changes in the resistance to stretch were noted for other groups of muscle strips. In addition, the value of passive tension for 10% stretch was 3.2-fold larger in LV-R21C$^{+/+}$ than in LV-WT ($P = 0.027$). Elevated passive tension measured in the LV of R21C$^{+/+}$ versus WT mice indicated partial loss of Ca^{2+} regulation at low [Ca^{2+}]. Therefore, once again, it is important to note that the effect of a disease causing mutation was manifested in the papillary muscle strips from the LV (and not RV), the ventricle which is predominantly affected due to HCM disease.

There are various functional differences between the LV and RV of WT mice that could arise from differences in external loads of both ventricles, differently occurring post-translational modifications, and so forth, and be manifested by changes in the myofilament Ca^{2+} sensitivity between LV and RV. In agreement with the study by Perreault et al. [24] and Belin et al. [11], we observed a rightward shift in the force-pCa curve in the RV versus LV of WT mice (Figure 3). There were no differences in the Ca^{2+} sensitivity between the RV and LV of R21C$^{+/+}$-KI mice. In R21C$^{+/+}$ mice, the R21C mutation disrupts the PKA consensus sequence preventing PKA-dependent phosphorylation of Ser 23/24 of TnI that occurs in response to β-adrenergic stimulation in WT mice resulting in faster relaxation and desensitization of myofilaments to calcium [25–28]. As seen for the majority of HCM causing mutations, especially for the regulatory troponin proteins [29, 30], the R21C mutation left shifted the Ca^{2+} sensitivity of force but only in the RV compared to RV-WT. The HCM phenotype in the LV of R21C$^{+/+}$-KI mice was manifested by a rightward shift in the Ca^{2+} sensitivity of force compared to LV of WT mice. A mutation-elicited response in the LV of R21C$^{+/+}$ mice was similar to that observed on β-adrenergic stimulation causing desensitization of myofilaments to calcium. However, the latter did not occur due to the PKA-dependent phosphorylation of TnI, which was absent in R21C$^{+/+}$ mice. Regarding the phenotypes between the LV and RV, the mutant showed a significantly lower Ca^{2+} sensitivity (pCa_{50}) than WT in the LV, while it resulted in larger pCa_{50} than WT in the RV (Figure 3(b)). In conclusion, the HCM phenotype in R21C$^{+/+}$ mice was manifested by the lack of differences in the Ca^{2+} sensitivity of force between the LV and RV that were clearly observed in the ventricles of WT mice.

To elucidate the reason for contractile differences (in force and calcium sensitivity) observed in R21C$^{+/+}$ versus WT mice, we have examined sarcomeric protein phosphorylation in the LV and RV of mice (Figure 5). The phosphorylation level of cTnI was not different between the LV and RV of WT mice, while no phosphorylation of cTnI was seen in LV-R21C$^{+/+}$ and RV-R21C$^{+/+}$ (Figures 5(a) and 5(c)). As observed in this study, the R21C mutation was shown before to prevent the PKA-dependent phosphorylation of Ser 23 and Ser 24 of cTnI [14, 29]. In addition, no mutation exerted changes were observed in phosphorylation of TnT or MyBP-C (Figure 5(a)). However, a significant R21C-mediated enhancement of myosin RLC phosphorylation was observed in the RV compared with LV of R21C$^{+/+}$-KI mice

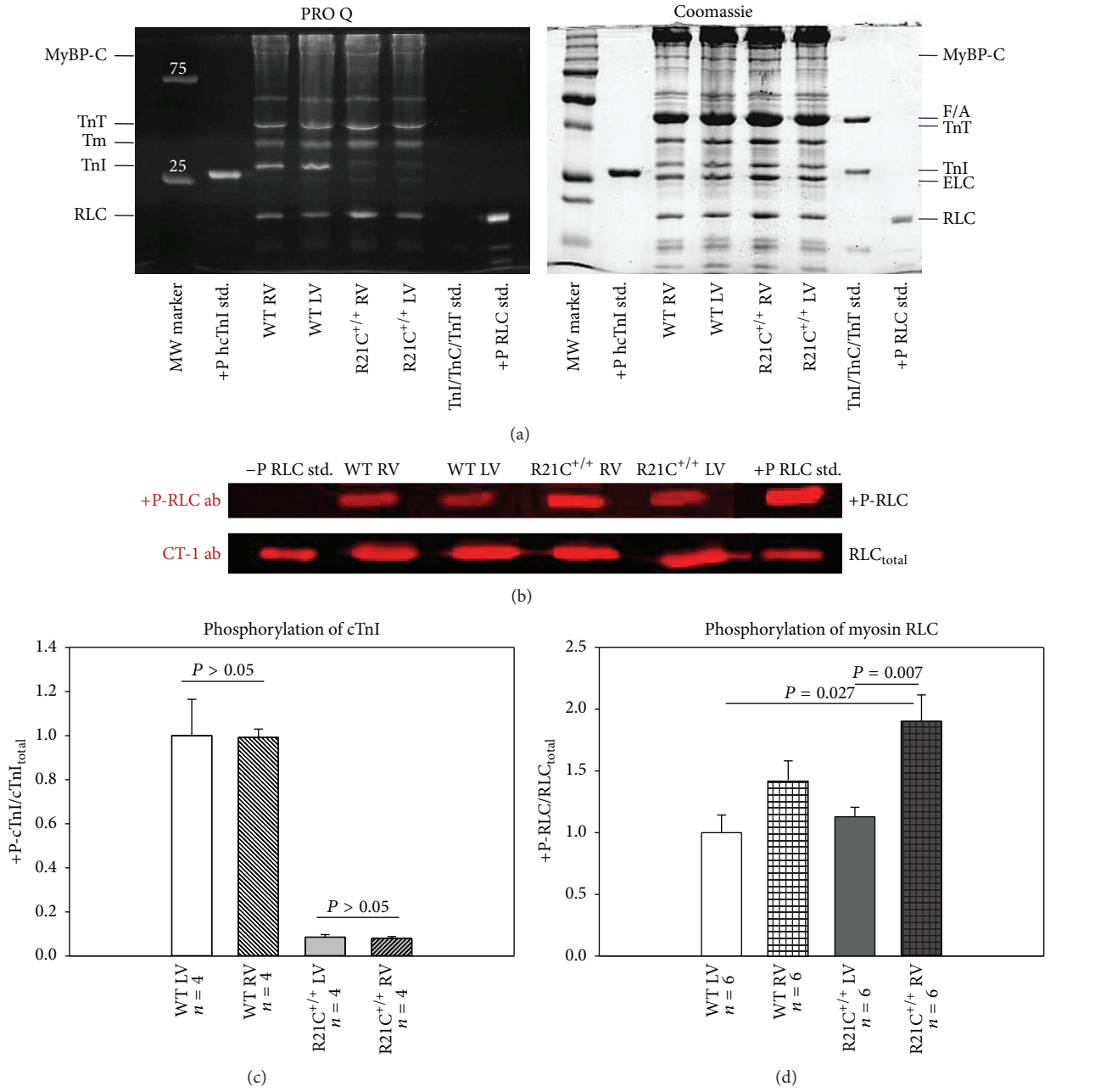

Figure 5: Assessment of protein phosphorylation in LV and RV of R21C$^{+/+}$ mice compared with LV and RV of WT mice. (a) Representative ProQ/Coomassie gels of myofibrillar preparations from LV and RV of R21C$^{+/+}$ mice compared with LV and RV of WT mice. MyBP-C, myosin binding protein C; F/A, F-actin; TnT, troponin T; Tm, tropomyosin; TnI, troponin I, ELC, myosin essential light chain; RLC, myosin regulatory light chain; +P hcTnI std., phosphorylated human cardiac TnI standard; and +P RLC std., phosphorylated human cardiac RLC standard. (b) Representative Western blot of myofibrillar preparations from LV and RV of R21C$^{+/+}$ mice compared with LV and RV of WT mice. The level of RLC phosphorylation was determined with phosphospecific RLC antibodies (+P-RLC ab) and compared to the total RLC content assessed with a rabbit polyclonal RLC antibody (CT-1 ab) recognizing total RLC protein. −P RLC std., nonphosphorylated RLC and +P RLC std., phosphorylated RLC standard proteins. (c) Quantification of phosphorylated cTnI was assessed by $n = 4$ independent SDS-PAGE (ProQ/Coomassie gels) analyses of two to three preparations from LV and RV ventricles per group. (d) Quantification of RLC phosphorylation was assessed by $n = 6$ SDS-PAGE analyses (Western blots and ProQ/Coomassie gels) of two to three LV and RV preparations from WT and R21C$^{+/+}$ mice. Note no cTnI phosphorylation in R21C$^{+/+}$-KI mouse model. There were no differences in cTnI phosphorylation between the LV and RV of WT mice. Note significantly enhanced phosphorylation in the RV-R21C$^{+/+}$ compared to LV-R21C$^{+/+}$ ($P = 0.007$) and to LV-WT ($P = 0.027$). No statistically significant differences in myosin RLC phosphorylation were observed between the LV and RV of WT mice. Errors bars are SEM.

(Figures 5(a), 5(b), and 5(d)). Cardiac myosin RLC is a major regulatory subunit of muscle myosin and a modulator of the Ca^{2+}-controlled regulation of muscle contraction [31]. It is localized at the head-rod junction of the myosin heavy chain and it contains the myosin light chain kinase- (MLCK-) specific phosphorylatable Ser15. The level of RLC phosphorylation has been shown by us and others to play a critical role in cardiac muscle contraction and in the Ca^{2+}-sensitive interaction of myosin cross-bridges with the actin-containing thin filaments [32–35]. Largely reduced RLC phosphorylation was reported in patients with heart failure [36, 37] and observed in animal models of cardiac disease [38–41]. Increased myosin RLC phosphorylation was also observed as a preventive measure of cardiac hypertrophy in mice [42]. Since no significant differences in RLC phosphorylation were noted between the LV and RV of WT mice and LV of $R21C^{+/+}$ mice (Figure 5(d)), one can speculate that elevated RLC phosphorylation in the RV of $R21C^{+/+}$ mice may play a rescue role alleviating or preventing mutation-induced contractile abnormalities and maintaining the RV tension at the level of WT. Our results indicate that the lower level of RLC phosphorylation in the LV versus RV of $R21C^{+/+}$-KI mice may contribute to the HCM phenotype that can be clearly observed in the LV and not in the RV of $R21C^{+/+}$ mice.

Conflict of Interests

The authors declare that there is no conflict of interests regarding the publication of this paper.

Acknowledgments

The authors thank Ms. Michelle Jones for help in editing the paper. This work was supported, in whole or in part, by National Institutes of Health Grants R01 HL042325 and HL108343 (to Danuta Szczesna-Cordary).

References

[1] J. S. Rankin, P. A. McHale, C. E. Arentzen, D. Ling, J. C. Greenfield Jr., and R. W. Anderson, "The three dimensional dynamic geometry of the left ventricle in the conscious dog," *Circulation Research*, vol. 39, no. 3, pp. 304–313, 1976.

[2] J. Chen, W. Liu, H. Zhang et al., "Regional ventricular wall thickening reflects changes in cardiac fiber and sheet structure during contraction: quantification with diffusion tensor MRI," *The American Journal of Physiology—Heart and Circulatory Physiology*, vol. 289, no. 5, pp. H1898–H1907, 2005.

[3] P. M. F. Nielsen, I. J. Le Grice, B. H. Smaill, and P. J. Hunter, "Mathematical model of geometry and fibrous structure of the heart," *The American Journal of Physiology—Heart and Circulatory Physiology*, vol. 260, part 2, no. 4, pp. H1365–H1378, 1991.

[4] P. P. Sengupta, B. K. Khandheria, J. Korinek, J. Wang, and M. Belohlavek, "Biphasic tissue Doppler waveforms during isovolumic phases are associated with asynchronous deformation of subendocardial and subepicardial layers," *Journal of Applied Physiology*, vol. 99, no. 3, pp. 1104–1111, 2005.

[5] M. Vendelin, P. H. M. Bovendeerd, J. Engelbrecht, and T. Arts, "Optimizing ventricular fibers: uniform strain or stress, but not ATP consumption, leads to high efficiency," *American Journal of Physiology—Heart and Circulatory Physiology*, vol. 283, no. 3, pp. H1072–H1081, 2002.

[6] R. Foale, P. Nihoyannopoulos, W. McKenna et al., "Echocardiographic measurement of the normal adult right ventricle," *British Heart Journal*, vol. 56, no. 1, pp. 33–44, 1986.

[7] A. M. Gerdes, J. A. Moore, J. M. Hines, P. A. Kirkland, and S. P. Bishop, "Regional differences in myocyte size in normal rat heart," *Anatomical Record*, vol. 215, no. 4, pp. 420–426, 1986.

[8] J. Wikman-Coffelt, C. Fenner, R. Walsh, A. Salel, T. Kamiyama, and D. T. Mason, "Comparison of mild vs severe pressure overload on the enzymatic activity of myosin in the canine ventricles," *Biochemical Medicine*, vol. 14, no. 2, pp. 139–146, 1975.

[9] J. Wikman-Coffelt, R. Walsh, C. Fenner, T. Kamiyama, A. Salel, and D. T. Mason, "Activity and molecular changes in right and left ventricular myosins during right ventricular volume overload," *Biochemical Medicine*, vol. 14, no. 1, pp. 33–41, 1975.

[10] W. S. McMahon, R. Mukherjee, P. C. Gillette, F. A. Crawford, and F. G. Spinale, "Right and left ventricular geometry and myocyte contractile processes with dilated cardiomyopathy: myocyte growth and β-adrenergic responsiveness," *Cardiovascular Research*, vol. 31, no. 2, pp. 314–323, 1996.

[11] R. J. Belin, M. P. Sumandea, G. A. Sievert et al., "Interventricular differences in myofilament function in experimental congestive heart failure," *Pflügers Archiv European Journal of Physiology*, vol. 462, no. 6, pp. 795–809, 2011.

[12] B. Borchert, S. Tripathi, A. Francino, F. Navarro-Lopez, and T. Kraft, "The left and right ventricle of a patient with a R723G mutation of the beta-myosin heavy chain and severe hypertrophic cardiomyopathy show no differences in the expression of myosin mRNA," *Cardiology Journal*, vol. 17, no. 5, pp. 518–522, 2010.

[13] M. Arad, M. Penas-Lado, L. Monserrat et al., "Gene mutations in apical hypertrophic cardiomyopathy," *Circulation*, vol. 112, no. 18, pp. 2805–2811, 2005.

[14] Y. Wang, J. R. Pinto, R. S. Solis et al., "Generation and functional characterization of knock-in mice harboring the cardiac troponin I-R21C mutation associated with hypertrophic cardiomyopathy," *Journal of Biological Chemistry*, vol. 287, no. 3, pp. 2156–2167, 2012.

[15] D. Dweck, M. A. Sanchez-Gonzalez, A. N. Chang et al., "Long term ablation of protein kinase A (PKA)-mediated cardiac troponin I phosphorylation leads to excitation-contraction uncoupling and diastolic dysfunction in a knock-in mouse model of hypertrophic cardiomyopathy," *The Journal of Biological Chemistry*, vol. 289, no. 33, pp. 23097–23111, 2014.

[16] W. Huang, J. Liang, K. Kazmierczak et al., "Hypertrophic cardiomyopathy associated Lys104Glu mutation in the myosin regulatory light chain causes diastolic disturbance in mice," *Journal of Molecular and Cellular Cardiology*, vol. 74, pp. 318–329, 2014.

[17] K. Kazmierczak, E. C. Paulino, W. Huang et al., "Discrete effects of A57G-myosin essential light chain mutation associated with familial hypertrophic cardiomyopathy," *The American Journal of Physiology—Heart and Circulatory Physiology*, vol. 305, no. 4, pp. H575–H589, 2013.

[18] D. Dweck, A. Reyes-Alfonso Jr., and J. D. Potter, "Expanding the range of free calcium regulation in biological solutions," *Analytical Biochemistry*, vol. 347, no. 2, pp. 303–315, 2005.

[19] D. Szczesna-Cordary, G. Guzman, J. Zhao, O. Hernandez, J. Wei, and Z. Diaz-Perez, "The E22K mutation of myosin RLC that

causes familial hypertrophic cardiomyopathy increases calcium sensitivity of force and ATPase in transgenic mice," *Journal of Cell Science*, vol. 118, no. 16, pp. 3675–3683, 2005.

[20] T. L. Hill, E. Eisenberg, and L. Greene, "Theoretical model for the cooperative equilibrium binding of myosin subfragment 1 to the actin-troponin-tropomyosin complex.," *Proceedings of the National Academy of Sciences of the United States of America*, vol. 77, no. 6, pp. 3186–3190, 1980.

[21] P. Muthu, L. Wang, C.-C. Yuan et al., "Structural and functional aspects of the myosin essential light chain in cardiac muscle contraction," *The FASEB Journal*, vol. 25, no. 12, pp. 4394–4405, 2011.

[22] L. Wang, P. Muthu, D. Szczesna-Cordary, and M. Kawai, "Characterizations of myosin essential light chain's N-terminal truncation mutant Δ43 in transgenic mouse papillary muscles by using tension transients in response to sinusoidal length alterations," *Journal of Muscle Research and Cell Motility*, vol. 34, no. 2, pp. 93–105, 2013.

[23] K. Kazmierczak, P. Muthu, W. Huang, M. Jones, Y. Wang, and D. Szczesna-Cordary, "Myosin regulatory light chain mutation found in hypertrophic cardiomyopathy patients increases isometric force production in transgenic mice," *Biochemical Journal*, vol. 442, no. 1, pp. 95–103, 2012.

[24] C. L. Perreault, O. H. L. Bing, W. W. Brooks, B. J. Ransil, and J. P. Morgan, "Differential effects of cardiac hypertrophy and failure on right versus left ventricular calcium activation," *Circulation Research*, vol. 67, no. 3, pp. 707–712, 1990.

[25] R. J. Solaro, A. J. G. Moir, and S. V. Perry, "Phosphorylation of troponin I and the inotropic effect of adrenaline in the perfused rabbit heart," *Nature*, vol. 262, no. 5569, pp. 615–617, 1976.

[26] P. J. M. Wijnker, A. M. Murphy, G. J. M. Stienen, and J. van der Velden, "Troponin I phosphorylation in human myocardium in health and disease," *Netherlands Heart Journal*, vol. 22, no. 10, pp. 463–469, 2014.

[27] R. Zhang, J. Zhao, A. Mandveno, and J. D. Potter, "Cardiac troponin I phosphorylation increases the rate of cardiac muscle relaxation," *Circulation Research*, vol. 76, no. 6, pp. 1028–1035, 1995.

[28] J. C. Kentish, D. T. McCloskey, J. Layland et al., "Phosphorylation of troponin I by protein kinase A accelerates relaxation and crossbridge cycle kinetics in mouse ventricular muscle," *Circulation Research*, vol. 88, no. 10, pp. 1059–1065, 2001.

[29] A. V. Gomes, K. Harada, and J. D. Potter, "A mutation in the N-terminus of Troponin I that is associated with hypertrophic cardiomyopathy affects the Ca^{2+}-sensitivity, phosphorylation kinetics and proteolytic susceptibility of troponin," *Journal of Molecular and Cellular Cardiology*, vol. 39, no. 5, pp. 754–765, 2005.

[30] S. B. Marston and P. P. de Tombe, "Troponin phosphorylation and myofilament Ca^{2+}-sensitivity in heart failure: Increased or decreased?" *Journal of Molecular and Cellular Cardiology*, vol. 45, no. 5, pp. 603–607, 2008.

[31] D. Szczesna, "Regulatory light chains of striated muscle myosin. Structure, function and malfunction," *Current Drug Targets—Cardiovascular and Haematological Disorders*, vol. 3, no. 2, pp. 187–197, 2003.

[32] P. Muthu, K. Kazmierczak, M. Jones, and D. Szczesna-Cordary, "The effect of myosin RLC phosphorylation in normal and cardiomyopathic mouse hearts," *Journal of Cellular and Molecular Medicine*, vol. 16, no. 4, pp. 911–919, 2012.

[33] P. Muthu, J. Liang, W. Schmidt, J. R. Moore, and D. Szczesna-Cordary, "In vitro rescue study of a malignant familial hypertrophic cardiomyopathy phenotype by pseudo-phosphorylation of myosin regulatory light chain," *Archives of Biochemistry and Biophysics*, vol. 552-553, pp. 29–39, 2014.

[34] S. B. Scruggs and R. J. Solaro, "The significance of regulatory light chain phosphorylation in cardiac physiology," *Archives of Biochemistry and Biophysics*, vol. 510, no. 2, pp. 129–134, 2011.

[35] C. Toepfer, V. Caorsi, T. Kampourakis et al., "Myosin regulatory light chain (RLC) phosphorylation change as a modulator of cardiac muscle contraction in disease," *The Journal of Biological Chemistry*, vol. 288, no. 19, pp. 13446–13454, 2013.

[36] J. van der Velden, Z. Papp, N. M. Boontje et al., "The effect of myosin light chain 2 dephosphorylation on Ca^{2+}-sensitivity of force is enhanced in failing human hearts," *Cardiovascular Research*, vol. 57, no. 2, pp. 505–514, 2003.

[37] J. van der Velden, Z. Papp, R. Zaremba et al., "Increased Ca^{2+}-sensitivity of the contractile apparatus in end-stage human heart failure results from altered phosphorylation of contractile proteins," *Cardiovascular Research*, vol. 57, no. 1, pp. 37–47, 2003.

[38] T. P. Abraham, M. Jones, K. Kazmierczak et al., "Diastolic dysfunction in familial hypertrophic cardiomyopathy transgenic model mice," *Cardiovascular Research*, vol. 82, no. 1, pp. 84–92, 2009.

[39] W. Glenn L Kerrick, K. Kazmierczak, Y. Xu, Y. Wang, and D. Szczesna-Cordary, "Malignant familial hypertrophic cardiomyopathy D166V mutation in the ventricular myosin regulatory light chain causes profound effects in skinned and intact papillary muscle fibers from transgenic mice," *The FASEB Journal*, vol. 23, no. 3, pp. 855–865, 2009.

[40] S. B. Scruggs, A. C. Hinken, A. Thawornkaiwong et al., "Ablation of ventricular myosin regulatory light chain phosphorylation in mice causes cardiac dysfunction in situ and affects neighboring myofilament protein phosphorylation," *Journal of Biological Chemistry*, vol. 284, no. 8, pp. 5097–5106, 2009.

[41] F. Sheikh, K. Ouyang, S. G. Campbell et al., "Mouse and computational models link Mlc2v dephosphorylation to altered myosin kinetics in early cardiac disease," *The Journal of Clinical Investigation*, vol. 122, no. 4, pp. 1209–1221, 2012.

[42] J. Huang, J. M. Shelton, J. A. Richardson, K. E. Kamm, and J. T. Stull, "Myosin regulatory light chain phosphorylation attenuates cardiac hypertrophy," *Journal of Biological Chemistry*, vol. 283, no. 28, pp. 19748–19756, 2008.

Hindawi Publishing Corporation
BioMed Research International
Volume 2015, Article ID 245154, 28 pages
http://dx.doi.org/10.1155/2015/245154

Review Article

Poorly Understood Aspects of Striated Muscle Contraction

Alf Månsson,[1] Dilson Rassier,[2] and Georgios Tsiavaliaris[3]

[1]*Department of Chemistry Biomedical Sciences, Linnaeus University, 39182 Kalmar, Sweden*
[2]*Department of Kinesiology and Physical Education, McGill University, Montreal, QC, Canada H3A 2T5*
[3]*Institute for Biophysical Chemistry, Medizinische Hochschule Hannover, 30625 Hannover, Germany*

Correspondence should be addressed to Alf Månsson; alf.mansson@lnu.se

Received 22 August 2014; Accepted 28 October 2014

Academic Editor: Oleg S. Matusovsky

Muscle contraction results from cyclic interactions between the contractile proteins myosin and actin, driven by the turnover of adenosine triphosphate (ATP). Despite intense studies, several molecular events in the contraction process are poorly understood, including the relationship between force-generation and phosphate-release in the ATP-turnover. Different aspects of the force-generating transition are reflected in the changes in tension development by muscle cells, myofibrils and single molecules upon changes in temperature, altered phosphate concentration, or length perturbations. It has been notoriously difficult to explain all these events within a given theoretical framework and to unequivocally correlate observed events with the atomic structures of the myosin motor. Other incompletely understood issues include the role of the two heads of myosin II and structural changes in the actin filaments as well as the importance of the three-dimensional order. We here review these issues in relation to controversies regarding basic physiological properties of striated muscle. We also briefly consider actomyosin mutation effects in cardiac and skeletal muscle function and the possibility to treat these defects by drugs.

1. Introduction

Muscle contraction is the result of cyclic interactions between the contractile proteins myosin and actin, driven by the turnover of adenosine triphosphate (ATP) [1–8]. In vertebrate striated muscle (heart and skeletal muscle), actin and myosin are organized with several accessory proteins in highly ordered sets of interdigitating thin and thick filaments, respectively, forming repetitive 2.0–2.5 μm long sarcomeres [2]. The functional units of muscle are the half-sarcomeres. These are connected in series to each other forming ~1 μm wide myofibrils (Figures 1(a) and 1(b)) that run the entire length of the muscle cell (muscle fiber) and in parallel over the muscle fiber cross-section. During muscle contraction, globular myosin motor domains (heads) extend from the thick filaments to interact cyclically with actin binding sites on the thin filaments forming so-called cross-bridges (Figure 1(b)). The ordered arrangement on different hierarchical levels in muscles is highly beneficial to the effectiveness of the contractile process which is reflected in the independent evolution [9] of similar sarcomere organizations in phylogenetically distant organisms such as mammalians and Cnidaria (e.g., jellyfish). Some of the advantages of this arrangement are obvious, such as effective summation of length changes produced by sarcomeres arranged in series and forces over the muscle cross-section. However, there are likely additional, subtle benefits and even inbuilt imperfections of the ordered arrangement have been found to be of physiological importance [10–12].

Generally, there has been formidable progress [6, 13–16] in the understanding of striated muscle function since the elucidation of its basic principles [2, 17–19]. Initially, this progress relied mainly on mechanical and ultrastructural studies of muscle cells and biochemical studies of isolated actin and soluble myosin motor fragments. Key developments in the late eighties and early nineties transformed the field substantially with a shift of focus to a more reductionist approach (reviewed in [13]) and with complementary insights gained from studies of a range of newly discovered nonmuscle myosins. One of the major technical developments in this period was the in vitro motility assay [7, 20] where fluorescent actin filaments are observed [21] while being propelled by

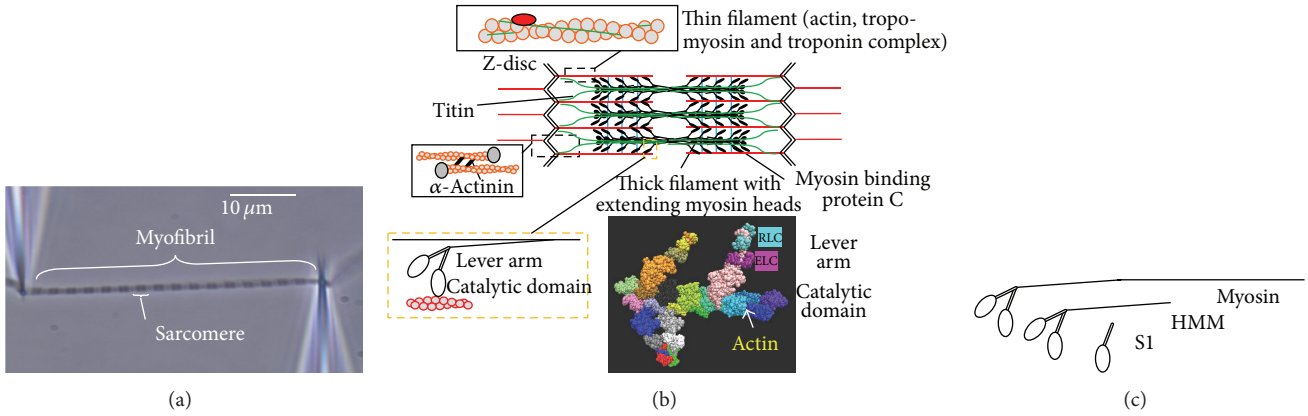

Figure 1: Hierarchical organization of myofibril. (a) Segment of myofibril captured between two microneedles for force measurements or application of length changes. (b) The sarcomere (structure between two Z-discs), with key protein components schematically illustrated. The resting length of the sarcomere is approximately 2.0 μm in the human heart and 2.5 μm in human skeletal muscle. Insets: the thin filament (top); critical molecular arrangement of the Z-disc (middle); extending myosin catalytic domain and lever arm interacting with actin filament (bottom; left) and 4 molecules of myosin subfragment 1 interacting with actin filament in the absence of ATP (PDB 1MQ8; bottom right). Regulatory light chain (RLC) and essential light chain (ELC) stabilize the lever arm. (c) Schematic illustration of myosin molecule (approximately to scale; see also (b)) and soluble motor fragments, heavy meromyosin (HMM) and subfragment 1 (S1) obtained by proteolytic cleavage under different conditions [356, 357].

myosin or more often proteolytic myosin motor fragments (Figure 1(c)) such as subfragment 1 (S1) or heavy meromyosin (HMM). The latter contains two myosin heads, that is, two complete catalytic domains each with lever arm and two light chains, connected to a coiled-coil tail domain. Other key developments include (i) single molecule mechanics (optical tweezers based [22–24]) and single molecule fluorescence microscopy techniques [25] related to the in vitro motility assays, (ii) crystallization of actin [26] and the myosin motor domain (S1) [5, 27] allowing determination of their molecular structure with atomic resolution, and, finally, (iii) development of techniques for genetic engineering of myosin [28, 29]. While recent technical progress allowed a number of long-standing issues to be settled (cf. [30]), several important features of muscle contraction remain incompletely understood. This includes central issues such as (1) the molecular basis for the high maximum power-output [31, 32], (2) the mechanism of effective resistance to stretch of active muscle [33–35], and (3) the mechanisms by which myopathy mutations [36–43] and certain drugs affect muscle function.

The difficulties in addressing the problems (1)–(3) are due to limited understanding of important molecular mechanisms of the actomyosin interaction. This limitation is, in turn, attributed to challenges when integrating information derived from studies on different levels of hierarchical order (e.g., muscle cell versus single molecules) or using different techniques (e.g., biochemical solution studies versus muscle cell mechanics or single molecule mechanics). In this paper, we will review incompletely understood aspects of the actomyosin interaction. Other general aspects of muscle physiology and regulation are not included—the reader is instead referred to previous comprehensive reviews [15, 44, 45] and references therein.

2. The Molecular Basis of Muscle Contraction: Current View

Molecular motors may be classified as processive or nonprocessive depending on whether they take several steps or only one step along their track before detaching. A typical example of a processive motor is the nonmuscular myosin V with roles in certain forms of intracellular transport, for example, in the nervous system [46]. This motor is characterized by a slow and strongly strain-dependent detachment from the actin filament and appropriate coordination of its two motor domains (heads). Such characteristics allow the motor to move processively several steps along an actin filament.

The myosin II motor of muscle, generally denoted by "myosin" below, is, on the other hand, classified as nonprocessive. Thus, each myosin II motor domain spends most of its ATPase cycle time detached from actin and a single myosin motor is believed to take only one single step along an actin filament before detaching. Efficient operation of muscle therefore relies on a large assembly of myosin II motors working together. Consequently, the production of force and displacement by actomyosin in striated muscle is the result of cyclic interactions of billions of myosin motor domains with actin filaments. The efficiency and control of this process are optimized by the assembly of actin, myosin, and accessory (e.g., regulatory) proteins into highly ordered structures on different levels of hierarchical organization (Figure 1). The force-generating interaction cycles between actin and myosin are powered by the turnover of MgATP (denoted by ATP below) and are, except in response to rapid perturbations of length or tension [47–49], asynchronous between different motors as a basis for smooth shortening and force-development.

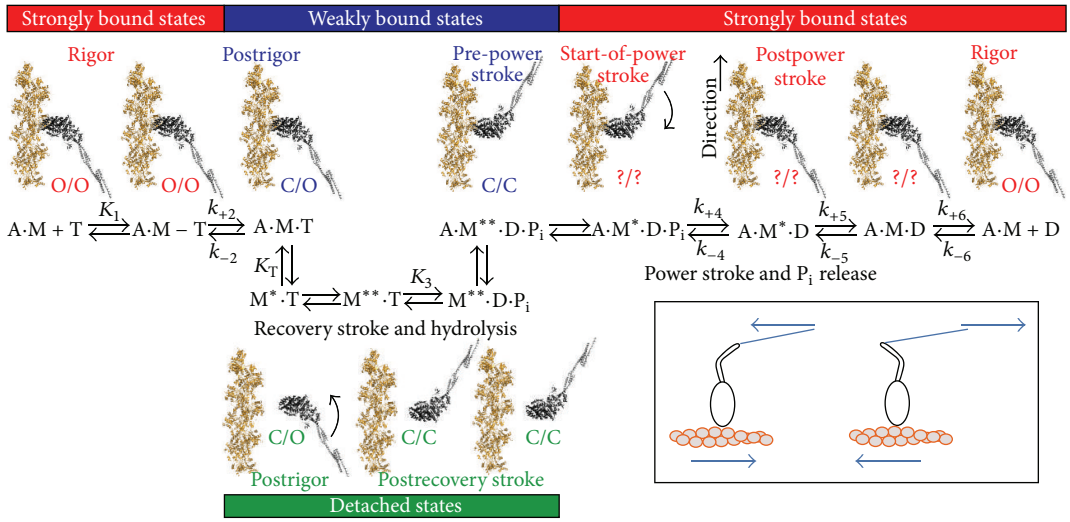

FIGURE 2: Simplified schematic representation of the predominant biochemical and structural states of the actomyosin ATPase cycle. Actin is depicted in orange; the myosin motor domain with artificial lever arm (X-ray structure PDB:1G8X [358]) is shown in grey colors (A = actin, M = myosin motor domain, T = ATP, D = ADP, and P = P_i). The open (O) or closed (C) conformation of the active site elements switch 1 and switch 2 is indicated with switch 1 designated as the first. The power stroke corresponds to the switch 2 closed-to-open transition while the motor domain is bound to actin. The recovery stroke occurs in the detached state. It is assumed that the two heads of myosin act independently from each other and only one head is shown. Equilibrium constants and rate constants are denoted by upper case and lower case letters, respectively. Inset: Schematic illustration of tension in lever arm that causes muscle shortening (left) and that resists shortening (right).

The basic principles of the force-generating cross-bridge cycle in striated muscle have been elucidated on basis of biochemical, mechanical, and structural data [1, 2, 4–6, 23, 27, 47, 50–68]. Binding of ATP to the myosin motor domain first causes a structural change with a swing of the myosin lever arm (a "recovery stroke," bottom Figure 2) that prepares the myosin head for executing a force-generating power stroke upon the next binding to actin. This event is also associated with altered disposition of loops (switch 1, switch 2, and P-loop) at the catalytic site (see further below). Subsequently, ATP is hydrolyzed to ADP and inorganic phosphate (P_i) but the hydrolysis products remain bound to the active site of myosin. The subsequent, critical step in the force-generating cycle is the binding of the myosin head to the actin filament, forming a so-called cross-bridge. The initial binding is nonspecific [69, 70] and dynamically disordered with a range of azimuthal and axial angles of both motor domain and the light chain binding lever arm [71–73] relative to the actin filament. Furthermore, this initial weak binding is mainly electrostatic in nature [69, 70] with attached and detached states in rapid equilibrium. The transition from the initial weakly and non-stereo-specifically bound state of the myosin head to a stereospecifically bound state has been suggested to involve an average rolling transition of the myosin head on the actin filament [72–74] followed by locking in the stereospecifically attached state. This "roll and lock" transition may both increase the effective attachment rate [75] and contribute to the translation of the thin filaments [71] as well as the tension recovery following rapid length steps [72, 74].

Binding of the myosin head to an actin filament causes ~100-fold activation of the rate of P_i release. In the absence of actin, the P_i release, or rather a preceding conformational transition related to the reversal of the recovery stroke, is rate limiting for ATP turnover by myosin. The release of P_i from actin-bound myosin is associated with a strongly increased actomyosin affinity and a large drop in free energy. Further, there is an appreciable structural change that, in the absence or presence of a counteracting load, causes a swing of the light chain binding myosin lever arm or a tendency for such a swing, respectively. This swing of the lever arm, often termed the power stroke (Figure 2, step 4), is the basis for force-generation of muscle and the myosin induced sliding motion between the thin and thick filaments in the sarcomere. The type of structural change that actually occurs in this process depends on stretching elastic elements in the myosin head and elsewhere and, as just mentioned, the magnitude of the structural change varies depending on the external load on the cross-bridge (see further below).

Under certain physiological conditions, the muscle does not produce any mechanical power in spite of active cross-bridge cycles, such as during isometric contractions (without length changes), equivalent to isovolumetric contraction in a cardiac muscle contracting against closed valves. Further, eccentric contraction, when the muscle is stretched during activity, is associated with work done on the muscle rather than by the muscle [76]. Such eccentric contractions occur physiologically in skeletal and cardiac muscle [77]. During eccentric contractions, there is formation of actomyosin cross-bridges but the biochemical cycle in Figure 2 is not

completed, as evident from the very low ATP turnover under these conditions [78]. Instead, the myosin cross-bridges are forcibly broken [34, 79–82] after pulling their elastic element backwards (corresponding to counterclockwise turning of lever arm in Figure 2). Thus, eventually, the backward pull leads to higher tension in the cross-bridge than sustainable by the actomyosin bond [81, 83–87]. The myosin head then detaches from actin, without release of ADP and subsequent rebinding of ATP, in contrast to the situation during shortening and isometric contraction. Indeed, cross-bridge detachment is also quite slow during isometric contraction, associated with key properties of the AM*ADP state in Figure 2. This state has long been inferred in skeletal muscle [88–91] but its detailed properties were first studied more directly using different slow, nonstriated muscle myosins [92–99]. However, more recently a state with similar properties was found in skeletal muscle [61, 100]. It has also been essential to include in models of striated muscle contraction to accommodate findings that the ADP release occurs in two steps where the first step is an isomerization reaction that is accelerated by negative strain in the myosin lever arm (corresponding to clockwise turning in Figure 2). This results in opening of the nucleotide binding pocket (with a strain (x)-dependent rate constant $k_{+5}(x)$; cf. Figure 2) before ADP leaves rapidly with rate constant k_{+6}.

The numerical value of $k_{+5}(x)$ is believed to be high for low x-values (dominating during rapid shortening), intermediate at intermediate x-values (dominating in isometric contraction), and very low for large x-values (dominating during forcible lengthening). Clearly, the AM*ADP state and the strain-dependent transition $k_{+5}(x)$ are responsible for differences in cross-bridge kinetics between different conditions. For instance, at high physiological ATP concentration, if $k_{+6} \gg k_{+2}$ [101] and if $k_{+5}(x)$ is large ($k_{+5}(x) \gg k_{+2}$), the overall dissociation constant $k_{\text{off}}(x, [\text{ATP}])$ is given by

$$k_{\text{off}}(x, [\text{ATP}]) \approx \frac{k_{+2}[\text{ATP}]}{1/K_1 + (k_{+2}/k_{+6} + 1)[\text{ATP}]}. \quad (1)$$

This applies for myosin heads that are brought into the drag-stroke region ($x < 0$ nm) during shortening where they resist sliding. In contrast, during isometric and eccentric contraction, when $k_{+5}(x)$ is small, then

$$\begin{aligned} k_{\text{off}}(x, [\text{ATP}]) &= \frac{k_{+2}[\text{ATP}]}{1/K_1 + (k_{+2}/k_{+5}(x))[\text{ATP}]} \\ &= \frac{k_{+5(x)}[\text{ATP}]}{k_{+5}(x)/k_{+2}K_1 + [\text{ATP}]}. \end{aligned} \quad (2)$$

In this connection it is of interest to consider the concept of duty ratio [102], f, that is, the fraction of the ATP turnover time that myosin molecules spend attached to actin. This ratio (see further [103, 104]) that is close to 1 for processive motors and <0.5 for nonprocessive motors is approximated by the following expression:

$$f = \frac{k_{\text{on}}}{k_{\text{on}} + k_{\text{off}}}, \quad (3)$$

where k_{on} and k_{off} are the cross-bridge attachment and detachment rate constant, respectively. Together with (1)-(2), this suggests that the duty ratio for myosin II while low during rapid shortening (e.g., ~0.05 in unloaded shortening) may be quite high in isometric and eccentric contraction as well as very slow shortening (with low k_{off}).

3. Poorly Understood Phenomena in Muscle Contraction

Because muscle contraction is due to the action of a very large ensemble of actomyosin motors it is necessary to use statistical models to relate contractile properties, such as force-velocity relationships, to actomyosin interaction kinetics and mechanics [1, 105–108]. Several models of this type have been developed, often incorporating the above-mentioned principles [31, 49, 109–111] and the additional assumption that all myosin heads act independently. The latter assumption deserves clarification. In most current cross-bridge models, it is assumed that (i) the myosin heads (even the two heads of one myosin molecule) do not compete for the same site on actin and (ii) the binding of one head does not affect the kinetics (nor its strain-dependence) for any transition involving another head (whether belonging to the same myosin molecule or not). This view is similar to the definition outlined in detail by Hill [105, 106]. It means that observable properties of muscle fibers can be readily obtained from mean values calculated from a given number of state probabilities without changing the model parameters between different conditions. For instance, if the myosin heads are assumed to act independently, it means that neither propagating structural changes in the thin filaments nor sequential actions of the two partner head are assumed to alter any parameter value such as attachment rate. Importantly, however, this independence does not prevent myosin heads from interacting (cooperating) by collectively altering the strain of other heads that are attached to a given surface or thick filament past which actin filaments move [1, 49, 112–114].

Statistical cross-bridge models with independent force-generators based on a kinetic scheme similar to Figure 2, but where each biochemical state exists for a range of elastic strains, account well for several contractile phenomena. This includes the information-rich relationship between velocity and load on a muscle (the load-velocity or force-velocity relationship; Figure 3; [115]). However, some key aspects of muscle function cannot be explained in a straightforward way by the most recent cross-bridge models. For instance, if the low myosin attachment rate to actin, suggested by the rate of rise of isometric force, is plugged into a statistical model (e.g., [1] or [31]), a velocity lower than that observed experimentally is predicted for shortening against intermediate loads. Thus, the high maximal power-output during muscle shortening [116] is not accounted for ([31, 32] and references therein; see also Figure 3). Neither is a low attachment rate consistent with the high steady-state resistance to forcible lengthening in eccentric contractions [79, 80, 110, 117]. Related to the difficulty in accounting for the high power-output during shortening, it is also difficult to account for the rapid repriming of the working stroke after

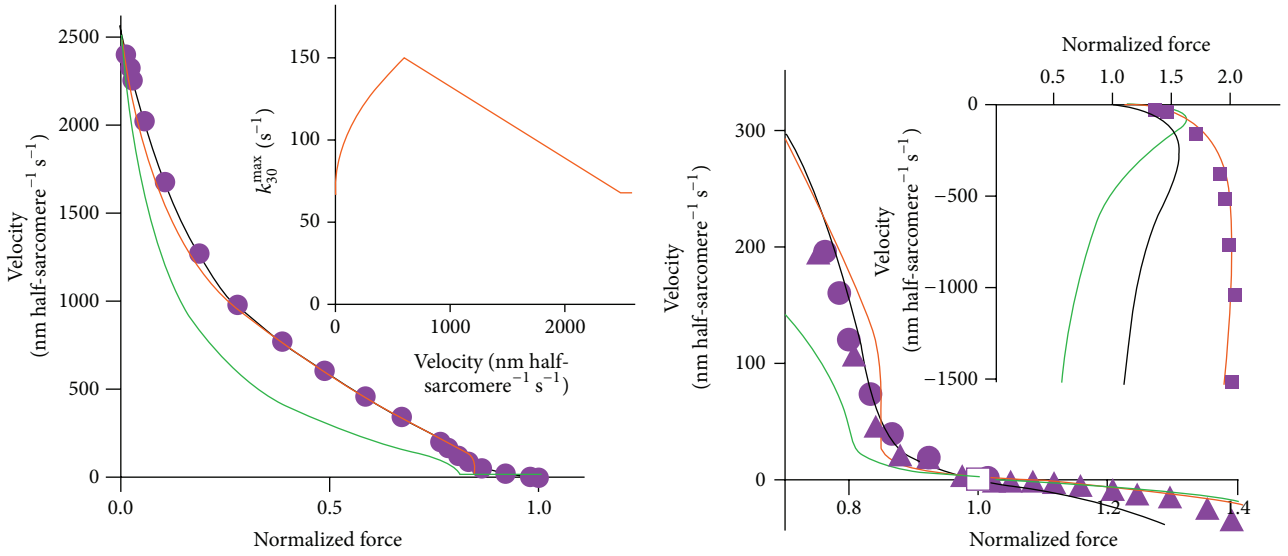

Figure 3: Force-velocity (load-velocity) relationship of frog muscle fiber. (a) Force-velocity relationship for shortening (positive velocity). Inset: assumed velocity dependence of attachment rate (k_{30}^{max}) for certain model predictions in (a) and (b). (b) Force-velocity relationship for loads (forces) close to isometric (normalized force: 1.0) and for eccentric contractions (negative velocities). Inset: extended region for eccentric contraction. Purple symbols in (a) and (b): experimental data from [31] (circles), [191] (triangles), and [79] (squares). Green lines: model [110] with same attachment rate that would fit rise of tension in isometric contraction. Black lines: model [110] with attachment rate accounting well for the maximum power-output during shortening. Orange lines: model [110] with velocity dependent attachment rate for shortening (inset in (a)) and lengthening. In the latter case, the attachment rate constant increased from a maximum value of 67 s^{-1} in isometric contraction (inset (a)) to 335 s^{-1} at lengthening velocities ≥ 600 nm hs^{-1} s^{-1}. Figures from Biophysical Journal [110] reprinted with permission from Elsevier/The Biophysical Society.

a rapid length step, that is, the fact that the amplitude of the tension relaxation upon a rapid release recovers appreciably faster than tension after a priming release step. These phenomena may be reproduced by modifying existing models (e.g., [110]) to make the attachment rate velocity dependent so that it is low during isometric contraction, intermediate during shortening, and fast during lengthening [33–35, 79, 80, 110]. However, a velocity dependent attachment rate is not physically reasonable. Therefore, several alternative mechanisms have been proposed to account for the apparent velocity dependence of this rate [31, 35, 75, 110, 118–124]. Some of the alternative suggestions have kept the idea of independent myosin heads but appreciably increased the number of states and/or included the possibility for myosin heads to rapidly "jump" between neighboring sites on the actin filaments. Others have instead assumed important roles of cooperativity between the two heads of a given myosin molecule. However, there is still no consensus about these models. A third possibility is that the apparent velocity dependence of the attachment rate is related to myosin- or tension-induced structural changes along the actin filament [21, 125–133]. These could cooperatively alter the myosin binding properties of neighboring or even distant actin sites. The above considered alternative explanations are addressed in further detail below.

Another poorly understood issue is the pathogenesis of hereditary sarcomere myopathies which generally are due to single point mutations in myosin or regulatory proteins. The development of protein expression techniques for striated muscle myosin II [134–137] has enabled studies of the underlying functional deficit on the molecular level. However, the complex and multidimensional pathogenesis of the diseases [36–43] is the result of disturbed function on the whole muscle/heart level. This calls for new experimental approaches for studies of ensemble function on sarcomere or even super-sarcomere levels [43]. Whereas a reductionist approach will give important clues into the mechanisms of disease, a full understanding is likely to require studies on different levels of organization.

The challenges in understanding myopathies are very similar to those in understanding drug effects. Drugs with effects on muscle contraction are of interest for several reasons. For instance, there are compounds with activating potential [138, 139] that stimulate the actomyosin ATPase activity and enhance the contractility or even act as a kind of chemical chaperon that reactivates misfolded myosin molecules [140]. These substances represent a new generation of drugs, and improvements in their efficacy could provide new disease treatment strategies targeted against various hereditary myopathies, acute or chronical heart failure, and other forms of cardiovascular disease. Myosin inhibitors, on the other hand, could be useful for the treatment of myopathies caused by mutations in myosin that increase the active force while reducing the efficiency of muscle contractility [37, 141, 142].

More generally, any small chemical compound that effectively binds to the myosin motor domain and allosterically modulates the functional performance is of great interest in research on myosin and muscle [87, 100, 111, 143–157]. In contrast to point mutations, specific drug effects can be studied not only using expressed single molecules or disordered ensembles but also using muscle fiber preparations with maintained order of the myofilament lattice.

4. Different Experimental Systems

Below we consider why studies using different techniques and on different levels of hierarchical organization give results that are sometimes challenging to reconcile with each other (see also [158]). We also further consider model studies [1, 47, 52, 105, 107, 108, 112] because these have contributed to bridging the gap between different levels of hierarchical organization and integrated information from different experimental systems and from different scientific disciplines. Developments along these lines include studies [109, 117] attempting to integrate molecular structural models, biochemical schemes, and results from muscle mechanics. Furthermore, more recently, efforts have been made to achieve detailed fits of model predictions to a range of experimental data [31, 75, 103, 110, 111, 121, 122, 159].

Problems in integrating results of different types of studies are related to specific features and limitations that distinguish different experimental systems and approaches as outlined below.

4.1. Biochemical Solution Studies. Biochemical solution studies [4, 6, 50–54, 56–58, 63–65] have deciphered dominant parts of the kinetic scheme for the turnover of ATP by myosin and actin (Figure 2; reviewed in [16, 55, 57, 104]). Most of these studies have employed myosin subfragment 1 (S1) that contains the catalytic and actin binding sites of myosin and part of the lever arm (Figure 1(c)). Using this preparation, actomyosin states are generally probed under low ionic strength and unstrained conditions, corresponding to an elastic equilibrium position in muscle [107]. The lack of elastic strain is in contrast to the situation in muscle contraction where elastic strain is the basis for force-development and effects of force on actomyosin transition rate constants.

Whereas strain-dependent transitions cannot be probed in solution studies using S1, they can be studied in single molecule mechanics and in vitro motility assays where the myosin motor fragments are immobilized to surface substrates (Figure 4). Some aspects of strain-dependent transitions can also be investigated in solution using heavy meromyosin (HMM) motor fragments [99, 100, 160] because both of its motor domains can bind to actin filaments. This leads to strain between the heads although most likely different than that present in the ordered sarcomere lattice.

An interesting model, the so-called 3G model, was proposed in two influential papers [57, 58] based on evidence that myosin head binding to actin occurs in two steps. This led to the idea that each biochemical state (Figure 2) exists in three different structural states, with high, low, and very low affinity for actin. The 3G model furthermore assumes that the equilibrium between these states depends on the nucleotide occupancy of the active site. These ideas are relevant for the understanding of force-generation in muscle and have been incorporated into several more advanced statistical cross-bridge models (see below).

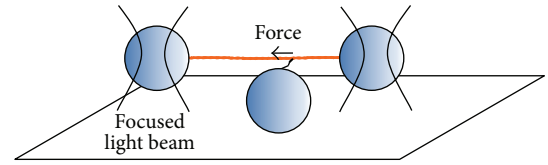

Figure 4: Optical trap system with actin filaments captured on two dielectric beads (optical traps) to which forces may be applied by a focused beam of near-infrared light. The actin filament held in the traps will interact with a single myosin motor on a third bead.

4.2. In Vitro Motility Assays and Mechanical Measurements from Small Ensembles and Single Molecules. In vitro motility assays may be viewed as extensions of biochemical solution studies with the key difference that the myosin motor fragments are immobilized to surfaces. Whereas the surface immobilization may affect protein function and complicate some aspects of data interpretation ([161, 162]) it ensures that strain-dependence of the actomyosin interaction is maintained. Therefore it also allows development of motion and forces. In vitro motility assay techniques [7] allow the observation of single actin filaments [21] when interacting with different numbers of myosin motor fragments and under different experimental conditions, for example, ATP concentration and ionic strength [163, 164]. This assay was later supplemented with a "laser trap" ("optical tweezers" technique [22–24, 68, 165, 166]). In this system, assumedly one myosin molecule attaches to an actin filament that is captured at the ends by beads "trapped" between two focused laser beams (Figure 4). Upon myosin-actin interactions, the displacement of actin filaments can be measured by tracking the position of the beads, showing that myosin II produces forces of 1–10 pN and maximum displacements of ~10 nm per interaction with actin [23, 94, 167–171]. In physiological conditions, however, the force and displacements produced by myosin and any other molecular motor are heavily influenced by the external load which dictates their functioning and mechanics.

The load dependence of the power stroke in single molecule studies has been investigated mostly in processive motors (e.g., myosin V) due to slow detachment kinetics and processivity, putting reduced demands on time resolution. The mechanics of myosin V has been studied when the motor was subjected to "pushing" and "pulling" forces, which corresponds to reduced and increased external load, respectively. The duration of attachments between the motor and actin filaments was decreased when the motors were pushed and increased when the motors were pulled [168, 172–174]. Furthermore, the attachment times were shortened with increasing ATP concentrations, suggesting that attachment was terminated when ATP binds to myosin following ADP release [168, 172–175]. Subsequent studies with myosins I and

V and smooth muscle myosin II [94, 97, 98, 175, 176] suggest that increasing loads delay ADP release, resulting in a longer attachment time.

Single molecule mechanics studies using skeletal muscle myosin II [23, 169–171, 177, 178] are challenging due to high detachment rate and associated low *duty ratio*. Therefore, studying the effects of load of myosin II must occur during actomyosin attachments that are extremely short. A study performed with smooth muscle myosin, which has a longer average attachment time than striated muscle myosin, suggested that increasing loads increases this time [98]. Assuming that the total attachment/detachment cycle does not change during the actomyosin cycle, an increase in attachment time results in an increased duty ratio. The authors [98] also investigated the kinetics of the load dependence of attachment times and distinguished between two phases of attachment of myosin, consistent with structural studies showing two distinct myosin bond conformations: one conformation in the presence (phase 1) and the other in the absence (phase 2) of bound ADP. Increasing loads prolonged the duration of phase 1 but did not affect phase 2, suggesting that load dependence may be attributed to a transition between an actomyosin state with and without bound ADP (cf. k_{+5} in Figure 2). Later, using a laser trap system with improved time resolution [61], similar results were obtained using fast and slow myosin II from skeletal muscle.

The in vitro motility assays and related force-measuring techniques have answered a number of central questions with regard to striated muscle contraction suggesting that (i) only one myosin II head is necessary for production of motion and force [8, 179, 180], (ii) an unloaded displacement of 5–10 nm is produced by a myosin motor domain upon binding to an actin filament [23, 61, 67, 168, 171, 177] with the highest values in this range for two-headed myosin preparations and optimized orientations, (iii) a maximum force of about 10 pN is actively developed by a myosin motor domain [23, 170], (iv) there are target zones with sites, ~36 nm apart, along the actin filament to which an immobilized myosin II motor binds more readily [177, 181] than to other sites (see also [71, 74]), and (v) the displacement induced by a given strongly actin-attached motor domain occurs in two steps [61] where the second step is believed to be associated with the strain-dependent transition from the AM*ADP to the AMADP state. Finally, recent developments [182] have allowed quite detailed probing of the force-dependence of several kinetic steps in the actomyosin turnover of ATP.

The importance of the surface-based assays is hard to overestimate. However, it is challenging to relate single molecule mechanics data to mechanics of muscle cells or myofibrils where very large ensembles of myosin motors interact simultaneously with the actin filaments (see below). Moreover, key aspects of muscle function such as the detailed shape of the force-velocity relationship and the apparent velocity dependence of the attachment rate constant have not been addressed because they result from interactions of a large ensemble of myosin motor domains with actin filaments in an ordered arrangement. In only few cases have the interaction between several (but not a large number of) motors and an actin filament been investigated using optical tweezers [183]. Furthermore, even if the interaction of a large number of myosin motors with actin filaments could be studied, it is difficult to assess cooperative phenomena properly. Such phenomena include that related to the role of the two myosin heads and their possible interaction with two actin filaments [160] or that due to an ordered arrangement of myosin motors in three dimensions around each actin filament.

Statistical and kinetic models of the type mentioned above (e.g., [1, 103, 108]) form an excellent basis for explaining results both from muscle cells, conventional in vitro motility assays and single molecule mechanical studies. However, there is risk of confusion when results from these different experimental systems are compared. This is exemplified by the myosin working stroke (power stroke) distance, as follows. First, we define this distance, h, as the average displacement of the actin filament actively produced when one myosin head binds to actin and completes its ATP turnover in the absence of counteracting load. The distance would be that measured in single molecule optical tweezers studies with low trap stiffness. It does not involve excursion of the myosin head elasticity into strains with negative forces (that resist sliding), that is, into the drag-stroke region [184]. This value for the working stroke would be identical to that: $h = v_f \tau_{on}(0)$ obtained from the in vitro sliding velocity (v_f) and the myosin on time ($\tau_{on}(0)$) at zero strain (e.g., measured in solution) if it is assumed that precisely one myosin head at a time propels an actin filament. These conditions imply immediate execution of a power stroke (to reach its zero-strain elastic equilibrium) upon myosin head attachment to actin and subsequent detachment with time constant $\tau_{on}(0)$ immediately followed, but not preceded, by attachment of a new myosin head and repetition of the cycle. Such ideal conditions are not fulfilled in reality. Therefore, the magnitude of the step length obtained from velocities measured in the vitro motility assay and optical tweezers studies differs by a factor up to ~2. This is clear by examining the condition with a very large ensemble of myosin heads that work together to propel the actin filament. This condition is fulfilled in muscle cells and approximately fulfilled in the in vitro motility assay if an actin filament is propelled over a surface with saturating density of myosin motor fragments. Under these conditions the elastic element of a large fraction of the myosin heads will be shortened to the extent that these cross-bridges resist sliding in the shortening direction (execute a drag-stroke). During steady-state unloaded shortening, the negative cross-bridge forces that counteract sliding are exactly balanced by the positive forces due to cross-bridges that undergo their power stroke. These force-levels are determined by the average strain of negatively ($v_f \tau_{on^-}$) and positively ($\langle h \rangle$) strained cross-bridges, respectively, each factor multiplied by the cross-bridge stiffness. If the stiffness is Hookean the stiffness-values on the left and right sides of the equation cancel out and $\langle h \rangle = v_f \tau_{on^-}$. This expression is deceivingly similar to that for h, given above. However, $\langle h \rangle$ is always smaller than h [103, 111, 184], generally $0.5h < \langle h \rangle < h$, consistent with $\tau_{on^-} < \tau_{on}(0)$ which, in turn, is consistent with $\tau_{on}(x) = 1/k_{off}(x)$ (see (1)-(2)).

These relationships can be further expanded by considering also h_{∞} and $\tau_{on}\infty$, defined as the average sliding distance and time, respectively, over which a given myosin head stays attached to the actin filament while executing first positive and then negative force (executing working-stroke followed by drag-stroke) in a large ensemble. Naturally, it also applies that $h_{\infty} = v_f \tau_{on}\infty$. Finally, it is readily shown (cf. [103]) that $\tau_{on}(0) > \tau_{on}\infty > \tau_{on}-$ and $2h > h_{\infty} > h > \langle h \rangle > 0.5h$, where the last inequality is approximate.

4.3. Muscle Fiber Mechanics and Statistical Models. In the field of muscle mechanics, mechanical and optical sensor systems are used to relate length changes of muscle sarcomeres to the stiffness and forces developed by muscle cells (muscle fibers). The experiments can be performed either on intact [19, 185, 186] or on skinned [187–189] muscle fibers. The intact muscle cells are dissected from a living muscle using micromechanical tools (scissors, forceps, needles, etc.) leaving the cell membrane intact. In contrast, the membrane of skinned muscle cell segments is removed, chemically or mechanically, allowing the myofilament environment to be controlled from the bath fluid.

Of central importance in muscle mechanics are studies relating the imposed steady load on a muscle cell to the resulting steady velocity of the length change or equivalently the force developed upon imposition of a ramp shaped length change of a given velocity [1, 32, 115, 187, 190–195]. Force-velocity relationships obtained in either of these ways have demonstrated, although indirectly, that increased load increases the duration of the myosin power stroke [1, 196–198]. The velocity in response to increasing loads is continuously reduced, approximately according to a rectangular hyperbola [190] (however see [191]) from its maximum value in unloaded shortening to zero during isometric contraction (without length change). At this point the derivative of steady velocity versus steady load is continuous [191] when load increases above isometric force to cause lengthening with constant velocity (negative shortening velocity; Figure 3(b)). When a stretch is performed at low speeds (less than 2 muscle lengths s^{-1}; L_0 s^{-1}), the increase in force during a length ramp has two components: (i) a fast phase, in which force increases substantially over a few nanometers per half-sarcomere and (ii) a slow phase, in which force increases a small amount or remains unchanged [79, 80, 86, 199–204]. The latter phase approximates the steady force during lengthening. The transition between these two phases occurs at a critical stretch amplitude of ~10 nm half-sarcomere, commonly associated with a critical strain of attached cross-bridges beyond which they are forcibly detached from actin [33, 34, 79, 80, 85, 86, 199–202, 204–206].

The mechanism behind the increase in force during stretch is still controversial. Several investigators have suggested that it is primarily due to an increased force per cross-bridge (increased strain) during stretch [33, 34, 80, 86, 207]. It has been made likely that this effect is caused by prepower stroke cross-bridges, in a state that precedes phosphate release [86, 201, 202, 208, 209]. Interestingly, in this connection, recent X-ray diffraction studies [124] suggested an increased fraction of non-stereo-specifically bound myosin heads during stretch, properties usually attributed to weakly bound prepower stroke cross-bridges. However, the idea of increased force-resistance being attributed to weakly bound myosin heads is not easy to reconcile with the above-mentioned critical strain of ~10 nm. Nevertheless, any model must account for the findings that the phosphate analogues vanadate and aluminium fluoride (AlF_4), which are known to bias cross-bridges into a prepower stroke position, reduce isometric force of fibers treated with polyethylene glycol (which promotes myosin-actin interactions) considerably more than stretch forces [86, 208]. Similarly, the drugs butanedione monoxime (BDM) [207, 210] benzyl-toluene sulfonamide (BTS) [202] and blebbistatin [197], that are believed to inhibit main force-generating transitions, have similar effects. In this connection it is also of interest to mention that increased tonicity of the extracellular solution that causes volume shrinkage of intact muscle cells appreciably reduces the maximum isometric tension without affecting the maximum force during stretch [80, 204]. A similar result is seen at reduced temperature [211].

Many aspects of muscle mechanics have been strongly influenced by the pioneering work of AF Huxley from both a theoretical [1, 47] and experimental [19, 47, 212–215] perspective. Accordingly, muscle mechanical studies are often interpreted in terms of cross-bridge models that incorporate features of the Huxley and Simmons (1971; [47]) and the Huxley (1957; [1]) models. The latter model explains the basic steady-state properties of muscle (such as the force-velocity relationship) whereas the Huxley and Simmons (1971) model (Figure 5) accounts for the tension responses to rapid length changes imposed on a muscle cell. The combination of these two models accounts well for several aspects of muscle function [216].

The Huxley and Simmons model was inspired by the swinging cross-bridge model proposed by H. E. Huxley [2] on basis of ultrastructural evidence. Interestingly, in similarity to later results based on the atomic structure of myosin [5] the model incorporates ideas with an increasing number of attachment points between actin and myosin that stabilize high-force states. However, the model also raises critical questions. First, an independent elastic structure has not been unequivocally identified in the actomyosin cycle. Bending of the entire light chain stabilized alpha helical lever arm [217] or structural changes in the neighboring regions in the converter domain [141, 218] have been implicated to represent the elastic element (see also [219]). However, this region has also been implicated as the main component that swings during the force-recovery after a length step [66, 220].

This so-called swinging lever arm model followed the swinging cross-bridge model upon accumulating evidence against large-scale orientation changes of the entire myosin motor domain during force-generation [30] (however, see [71]). A second problem with the Huxley and Simmons [47] model is related to the number of states and force-generating structural transitions required. In their original paper, two stable attached states were assumed where transition from the low-force to the high-force state was accompanied by ~10 nm extension of the elastic element. As already was pointed out by the authors, two states are insufficient to account for the

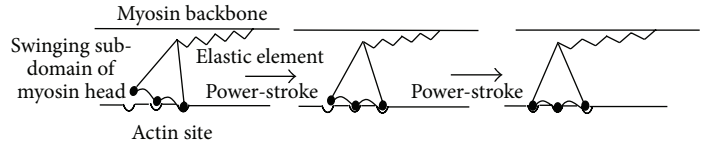

Figure 5: Model of the Huxley and Simmons type [47]. Force development is assumed to occur by thermally excited swing of a myosin head subdomain that stretches an independent elastic element. The swing is forward-biased (producing a power stroke) by progressively increased binding affinity between the myosin head and actin for each transition (to the right) that stretches the elastic element.

high power-output of muscle as well as for the rate of the tension transients using a model with an independent elastic element. This issue has become increasingly challenging after emerging evidence that the stiffness of the elastic element is somewhere in the range 1.7–3.3 pN/nm [32, 67, 221], considerably higher than previously believed.

Whereas a cross-bridge stiffness of ~1.7 pN/nm seems to be consistent with two tension generating steps [114, 222], a larger number of structurally and mechanically distinct states are required for a cross-bridge stiffness of ~3 pN/nm [75, 121, 122, 222, 223]. There is limited evidence for such a large number of states with different stable positions of the lever arm. Possibly, the issue would be resolved if the lever arm swing is preceded by a "roll and lock" transition of the entire myosin head that also contributes to force-recovery after a length step ([72]; see above). However, for any model with a large number of states, validation is difficult because a wide range of experimental findings can be reproduced with several free parameters whether the model is correct or not. A final complication related to the Huxley and Simmons [47] model is that the rates of relevant biochemical transitions observed in solution studies are considerably lower than the rates required to account for the rapid tension transients. This complication is related to the incompletely understood relationship between the rapid tension transients in response to length steps and the P_i release step in the ATP turnover by actomyosin, that is, the biochemical transition being most closely associated with the force-generating structural change in the actomyosin cross-bridge (see below). This is suggested by comparison of solution studies and rapid perturbations of contraction in intact and skinned muscle cells including rapid length steps (see above) and sinusoidal oscillations [89, 224, 225], rapid changes in load [48, 122], temperature (temperature jumps; [209, 225–231]), hydrostatic pressure (pressure jump; [232]), and phosphate concentration (phosphate jump; [151, 233–235]). Moreover, in skinned fibers, insight into the force-generating step and its relationship to, for example, P_i release (see below), has been obtained by investigating the $[P_i]$-dependence of steady-state isometric tension and force-velocity data ([122, 192, 209, 236]).

An issue that has severely complicated the interpretation of a large number of muscle mechanical studies is the possibility of a nonlinear (non-Hookean) elasticity of the cross-bridges [67, 111, 237] and/or myofilaments [33, 238–242] or the presence of a time-invariant parallel-elastic element, possibly attributed to a fixed number of cross-bridges [243]. These issues (reviewed in [222]) have been considered further recently [244] but are not yet resolved making it challenging to interpret stiffness data in terms of the number of attached cross-bridges. This uncertainty is highlighted by experiments investigating the number of attached cross-bridges during shortening at different velocities [32, 85] and during slow stretch [33, 35, 120]. During shortening, stiffness measurements (after correction for presumed linear series elasticity) suggest that force and the number of attached cross-bridges are approximately proportional (at least at loads close to the isometric one) [32]. In contrast, an alternative approach for obtaining the number of attached cross-bridges based on the maximum tension response to very rapid stretches [206] suggests lack of such proportionality [85]. Furthermore, the assumption of linear filament elasticity suggests ([35] and later [120]) that the resistance to slow stretch of active muscle is mainly attributed to increased recruitment of cross-bridges. In contrast, Nocella et al. [33] found evidence for a nonlinear filament compliance suggesting the force-enhancement during stretch is mainly attributed to increased average cross-bridge strain (see also [34, 80]). Another type of studies that is not always easy to interpret is those based on time resolved low-angle X-ray scattering from contracting muscle cells. Whereas these studies have led to new important insights [217, 220, 238, 239, 245] there are conflicting views about the interpretation in some cases [246]. The interested reader is referred to other review-articles [247–249] for details.

Muscle fiber experiments have the advantage of maintained three-dimensional arrangement between the myofilaments in half-sarcomeres and preservation of accessory proteins that may affect contraction. On the other hand, the large number of protein components makes it necessary to use statistical models [1, 105] for interpretation of the experimental results and several different models are likely to account for a given data set. Furthermore, the interpretations of muscle mechanical and structural data (e.g., from low-angle X-ray diffraction) in terms of cross-bridge properties often rely on high degree of uniformity between half-sarcomeres along the length of a studied muscle fiber and over the muscle cross-section. In the absence of such order and uniformity, unpredictable emergent properties are possible. Model studies have suggested that the nonuniformities may cause residual force enhancement after stretch [250] and the suppression of oscillatory motion under certain conditions [43, 49]. Different types of nonuniformities between segments along muscle cells have also been observed experimentally [11, 19, 251–254] and found to play important physiological roles, for example, in speeding up relaxation after an isometric contraction [10] (see also [255, 256]) and

contributing to aspects of the tension response to stretch [11, 12, 257].

The results of muscle fiber experiments may be affected, in unpredictable ways, by muscle fiber type, that is, by using fast or slow muscle (e.g., [61, 101, 258–260]) or due to mixtures of myosin isoforms in a given cell [251, 254] (see also [261, 262]). Furthermore, the level of activation and the presence of regulatory proteins ([151, 187, 263]) may affect the kinetics of the actomyosin interaction in different ways. Finally, a range of posttranslational modifications may affect function. This expanding field is not considered further here but it may be worth mentioning that the drug blebbistatin affected unloaded shortening velocity in skinned fibers differently in the presence and absence of phosphorylation of the regulatory myosin light chains [264].

4.4. Myofibril Mechanics. Myofibrils can be isolated both from skeletal and cardiac muscles and mounted for force-measurements and imposition of length perturbations (e.g., [207, 256, 265, 266]). Myofibrils are of particular interest to study because they are the smallest experimental units that maintain the three-dimensionally ordered myofilament lattice of striated muscle. The myofibrils are formed basically by sarcomeres arranged in series and with all major proteins intact (i.e., myosin, actin, troponin, tropomyosin, titin, and myosin binding protein C). Results from studies with myofibrils have been used to link studies on single molecules or proteins in solution with studies performed using muscle fibers. The length of myofibril segments to be studied can be virtually chosen by the investigators, and their diameter is substantially smaller (~1.0–1.5 μm) than that of muscle fibers (~10 μm). This is important, because it makes the diffusion time during activation of myofibrils very short, eliminating gradients of activation from the periphery to the core of the preparation. In contrast, the longer diffusion distances in muscle fibers can cause substantial gradients, not only in the activation level but also of ATP, ADP, and P_i concentrations, making interpretations at the actomyosin level complex.

The development of techniques for rapid solution exchanges during experiments with myofibrils enables exact determination of the rates of force development and relaxation during contraction, important indicators of the acto-myosin interactions. Furthermore, the use of myofibril activation, in association with fast length changes imposed to the preparation, allows precise evaluation of the rate of force redevelopment (Ktr) following a shortening-stretching protocol [265] that was originally developed for application to muscle fibers [267]. The Ktr has been used effectively to define the kinetics of cross-bridges transiting between weakly bound and strongly bound states. The Ktr determined with high time resolution has been used not only for probing the steps of the actomyosin cycle, but also for comparison of myosin kinetics in muscles of different conditions, health, and disease (e.g., [268–270]). Finally, myofibril studies allow investigators to elucidate the detailed relation between force development, relaxation, and sarcomeres dynamics. Since myofibrils are formed by a single chain of sarcomeres, the force produced by the myofibril at both ends can only be produced and shared by these interconnected structures. Such structural geometry has been explored to infer the mechanical behavior of myofibrils upon activation and during/after loads that are imposed to the preparation [257, 266].

Recently, there have been studies using single sarcomeres [271] and isolated half-sarcomeres [272], preparations that by nature avoid sarcomere length nonuniformities, and thus open possibilities for investigations of contractile performance without confounding effects. The limitation of these preparations is their fragility—it is virtually impossible to activate single sarcomeres for more than 5-6 activation cycles.

4.5. Molecular Structure: X-Ray Crystallography and Cryo-Electron Microscopy. Structural insights (Figure 6(a)) into the acto-myosin interaction have been obtained by combining crystallographic data for the myosin motor domain with information derived by electron microscopy and small angle X-ray scattering studies from myosin-decorated actin filaments [27, 59, 273–275]. The X-ray structures of the myosin motor domains crystallized so far fall into three categories dependent on the structural state they represent in the ATPase cycle (Figure 2). The distinctions are made on basis of the relative position of the active site elements (switch 1 and switch 2 closed or open; Figure 6(b)), the lever arm orientation (up or down), and the conformation of the actin-binding cleft (open, closed, or partially closed). The switch elements act as nucleotide sensors responsible for communication between the nucleotide biding pocket and the actin binding sites. Their reversible switching between two conformations opens and closes the active site around the γ-phosphate enabling hydrolysis and the coupling of internal conformational changes to larger rearrangements and rigid body movements of subdomains in the myosin motor that eventually lead to force generation. When considering states based on X-ray scattering and cryo-electron microscopy it is important to emphasize that they only capture metastable structural states.

The majority of the myosin structures crystallized with ADP.P_i analogs represent the prepower stroke state after ATP hydrolysis with weak affinity of the myosin cross-bridge for actin [157, 274, 276–279]. The cleft in most of these structures is partially closed. Further, switch 1 and switch 2 adopt closed conformations and the lever arm is in the up position. The second group of structures comprises states of the myosin motor domain assigned as postrigor [280–283]. These are thought to represent the prehydrolysis state (cf. Figure 2) of the myosin from which the recovery stroke takes place, transferring the motor to a catalytically competent prepower stroke state. In the postrigor states, the cleft is open, switch1 is closed, switch 2 is open, and the lever arm is down. A third group of structures, defined as rigor-like, have been obtained for myosin V and myosin VI [284–286]. According to the functional properties of these high duty ratio myosins, the crystallized states are thought to represent high actin affinity binding at a time after the power stroke has occurred. Characteristic for the majority of these nucleotide-free structures is a closed-cleft conformation and the lever arm down. Of relevance here, the rigor-like structure has also been obtained for muscle and nonmuscle myosin II

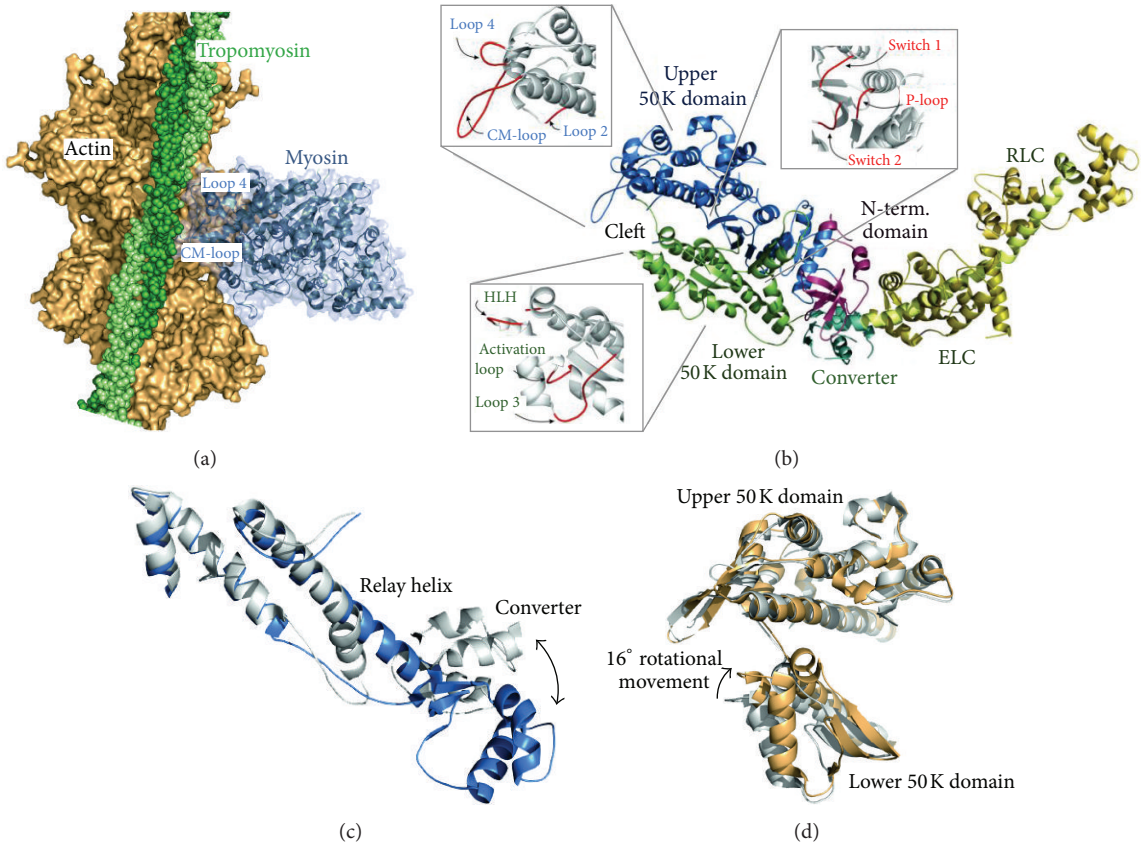

Figure 6: Structures of the rigor actomyosin complex and the myosin motor domain (S1) at different nucleotide states. (a) High resolution structure of the nucleotide-free actin-myosin- tropomyosin complex as obtained by cryo-electron microscopy (ref. [291], PDB IDs 4a7n, 4a7l, 4a7h, and 4a7f). (b) Ribbon representation of the atomic structure of chicken skeletal muscle myosin S1 fragment (PDB: 2MYS). S1 comprises 843 amino acid residues of the myosin heavy chain and two light chains (RLC and ELC) bound to the C-terminal neck region of the molecule. The central core comprises a seven-stranded β-sheet surrounded by several α helices. Characteristic is the deep cleft in the molecule. The cleft extends from the active site (P-loop, switch 1, and switch 2) to the actin binding elements, which are located in the upper (blue) and lower 50 K (green) domains. The N-terminus is adjacent to the C-terminus forming a protruding SH3-like β-barrel structure (red). The long C-terminal helix (light green) contains two IQ motifs that bind the light chains (ELC and RLC) and acts as a lever arm and conveys together with the converter domain local conformational changes to large movements. Highlighted in red in the insets are the actin binding and nucleotide coordinating loop and switch elements. (c) Conformational rearrangements of the relay helix (unwinding and kinking) and the converter (rotational movement) during the recovery stroke. The recovery stroke drives the detached myosin from the postrigor state to the prepower stroke state. The structures depicted are PDB ID: 2JHR and PDB ID: 1G8X. (d) Structural model for the strong binding start-of-power stroke (ref. [145]). The myosin power stroke is initiated by a transition from a weak-to-strong actin binding state. A rotational movement of the lower 50 K domain from the prepower stroke state (light grey, PDB ID: 2JJ9) enables a rigor-like strong binding geometry of the myosin at the actin interface (shown in brown ribbon representation) without changing the position of the converter domain. The structures were prepared with the PyMOL Molecular Graphics System, Version 1.7.2, Schrödinger, LCC.

[287, 288]. Despite the small differences seen in the extent and location of the cleft closure between the different rigor-like structures, it becomes apparent that cleft closure, although enthalpically unfavorable [289], is essential for facilitating the release of the hydrolysis products.

There is no crystal structure of the myosin motor domain bound to actin, but the rigor-like structures all exhibit features of an actin-bound state and high resolution cryo-electron microscopy support this view [290, 291]. Other limitations of available structural data are the lack of crystal structures showing states between the prepower stroke states and the rigor-like state.

In view of the limited availability of structural data, determining the sequence of events by which the myosin cross-bridge generates force has been made possible only by the combined analysis of structural information and biochemical data from solution kinetics together with model building including molecular dynamic simulations. In the absence of ATP, myosin forms a high affinity complex with actin (Figure 6(a)). In this strongly bound rigor state, the active site elements, switch 1 and switch 2, are thought to adopt an open conformation with the lever arm in a down position (Figure 2) [59]. The state subsequently turns into a low affinity state as Mg^{2+}-ATP irreversibly binds to the myosin active site [292].

The Mg^{2+}-ATP binding induces a closing of switch 1, which drives the formation of several new interactions such

as a salt-bridge between switch 1 and switch 2 that assists in stabilizing the β-phosphate and enables the coordination of the Mg^{2+}-ion and proper positioning of the surrounding water molecules for ATP hydrolysis. Kinetic studies with myosin mutants in which the formation of the salt bridge is disrupted are not capable of hydrolysis, emphasizing the critical role of the switch 1/switch 2 interaction [293–296]. At the same time, the active site rearrangements induced by Mg^{2+}-ATP binding are coupled to the distortion of the seven-stranded β-sheet forcing the upper 50 kDa subdomain to undergo a large movement, which reduces the contact area and weakens the affinity to actin. This enables cleft opening and the full dissociation of the actomyosin complex [297]. The dissociated state is the hydrolysis competent state of myosin. According to current data, the hydrolysis reaction requires the closing of switch 2 [298, 299], which is coupled to larger rearrangements of the relay helix and the converter [300–302]. The 6 Å shift of switch 2—as seen between the postrigor and prepower stroke state structures (Figure 6(c))—causes a partial unwinding of the relay helix and a kink. Since the tip of the relay-helix is connected via hydrogen bonds and hydrophobic interactions with the converter, the relatively small switch 2 movement is amplified via the relay helix to a 65° rotation of the converter and a swinging of the lever arm from the initial down to the up position. This structural transition is known as the recovery-stroke [275, 282, 303–309].

The up position of the lever arm is the starting point of the force producing working stroke or power stroke, which requires rebinding of myosin to actin (Figure 2). Otherwise P_i is released from myosin without actin-binding, following a lever arm swing that represents the reversal of the power stroke and that is futile with regard to force-production [62].

Characterization of the actin binding elements by mutational analysis assumes that actin binding occurs sequentially through the contribution of at least six flexible myosin loops (Figure 6(b), close-up views) that modulate, in a nucleotide-dependent manner, the interaction strength and coupling to actin [296, 310–315] (see also [316]). According to solution kinetics, binding of myosin heads to the actin filament occurs in two distinct ways, weak and strong [57, 58, 317], that cannot entirely be explained by the current set of structures. The rigor-like structures allow predictions of how cleft closure induced by actin binding accelerates product release [284, 287]. However, what cannot be deduced from the rigor-like structural state are details of the conformational changes that initiate the power stroke and that accompany the transition from an initial weakly bound acto-myosin-ADP.P_i state to the actin-myosin rigor complex (Figure 2). A priori, there are several possibilities [62], including the presence of a start-of-power stroke state in which the myosin motor domain is strongly bound to actin and the lever arm is in an up position. Structure-based modeling of this putative state [318] suggests that the power stroke is not a reversal of the recovery-stroke, because the tight actin-binding constrains the relative motion of the upper and lower 50 K domain [59]. Rather, the power stroke is thought to be realized in at least two steps, involving a transition from the prepower stroke state to the proposed start-of-power stroke state. This could be accomplished by a rotational movement of the lower 50 K domain (Figure 6(d)), which subsequently closes the cleft thereby putting a torsional strain on the β4-strand of the central β-sheet via the W-helix forcing the molecule to subsequently straighten the relay helix, which in turn drives power stroke. The exact position of the active site switch elements in this transition state and their mutual interplay in the following states with respect to additional coupled rearrangements of the relay-helix and core β-strand cannot be accurately predicted from the current structures and models. With the help of kinetic studies, some speculations about the series of switch movements coupled to the power stroke can be made [319, 320]. However, additional structural and biochemical work is necessary to resolve the exact communication pathway that links actin binding to force production.

5. Poorly Understood Molecular Mechanisms in relation to Contractile Properties

An explanation for poorly understood phenomena in muscle contraction (Section 3) requires better understanding of the incompletely understood molecular mechanisms considered below.

5.1. Attachment of Myosin Head to Actin, Phosphate Release, and the Main Force-Generating Transition. There is currently rather incomplete understanding of the biochemical, mechanical, and structural events associated with myosin head attachment to actin and subsequent force-production.

Whereas we here focus on the force-generating transition it is of relevance to describe some uncertainties about the rate-limiting step for the ATP turnover cycle that has been placed somewhere between the ATP-hydrolysis and P_i release step (Figure 2) [16, 55, 65, 108, 321, 322]. The issue is important for explaining the increased apparent attachment rate during shortening against intermediate loads compared to isometric contraction (see above). For instance, if the attachment rate is limited by the rate of the hydrolysis process rather than by the attachment step or P_i release one may foresee higher apparent attachment rate during shortening. This is due to completion of the hydrolysis step during the time that actin target sites (with 36 nm separation) move past myosin heads that are incorrectly oriented for binding. This means that any sterically feasible cross-bridge attachment is faster under these conditions than during isometric contraction. The situation is similar if the rate-limiting step is between a so-called refractory and nonrefractory M.ADP.P_i state. This was the case in the model of Eisenberg et al. [108] and it is the basis for the capability of this model to account for the fast repriming of the power stroke by rapid reattachment of cross-bridges from a nonrefractory M.ADP.P_i state into a low-force state that is competent to undergo a force-generating transition upon a length step [118].

With regard to the relationship between the force-generating transition and P_i release, several issues are controversial. First, the major component of the fast tension recovery in response to length steps [47, 212, 225] is an order of magnitude faster than the tension responses to sudden

Table 1: Conflicting evidence from experimental studies and theoretical considerations related to temporal relationship between P_i release and force-generating step in actomyosin cross-bridge cycle in muscle.

Force-gen. before P_i release	P_i release before force-gen.	Loose coupling
Kawai and Halvorson [89] P_i release fast	Davis and Epstein [230]. L-jumps and T-jumps in skinned muscle fibers	Caremani et al. [122]. Load-clamp expts. in skinned muscle fibers at varied $[P_i]$
Dantzig et al. [233] based on P_i jump experiments in skinned muscle fibers P_i release fast	Davis and Rodgers [229]	
Tesi et al. [235] P_i-jumps and tension versus $[P_i]$ in myofibrils P_i release fast	Spudich [16]	
Smith and Sleep [324] based on comparison of kinetic models P_i release slow	Sweeney and Houdusse [60] from reviewing structural data from several studies	
Ranatunga [209] from reviewing own work and work by others P_i release fast	Conibear et al. [359]	
Caremani et al. [236]. Contraction of skinned fibres at different $[P_i]$ P_i release fast		
Muretta et al. [323]. Spectroscopy applied to Dictyostelium myosin II P_i release slow		

changes in P_i concentration [233] hydrostatic pressure [232], temperature ([228–230] reviewed in [209]), and the force-generating process detected in spectroscopic studies [323]. Furthermore, the rate of tension recovery after length steps depended on the phosphate concentration after stretches but not after rapid releases. Thus, clearly the physical basis of the tension response to length steps and the other perturbations is not identical and the relationship between the length perturbation responses and phosphate release is complex. The idea of different molecular basis for the tension response to length jumps and temperature jumps is consistent with different structural changes according to X-ray diffraction patterns of skinned muscle fibers [217] but the relationship is complex. Thus, the tension response to temperature jumps seems to correspond to a slow phase of the tension relaxation in response to rapid length steps [225, 229, 230] and the overall rate of the tension response to length steps increases with temperature. The observed complexities (see also [230]) add to concerns [114, 158] that rather large number of states found necessary to account for the length-step response [122, 152] are not readily associated with states observed in biochemical and structural studies.

In order to elucidate the apparent incommensurability between results from different perturbation studies one may consider the characteristics of the observed tension responses in some detail. First, the dominant rate observed in the tension response to steps in pressure and temperature is rather similar [209] and the response to jumps in P_i concentration has a similar rate. Accordingly, temperature jumps have been claimed to affect an endothermic force-generating transition [209] in series with a rapid P_i-binding equilibrium. Whereas most available data suggest that the force-generating transition occurs prior to the P_i release (see Table 1) there has been appreciable controversy about the exact temporal relationship (Table 1) and the possibility has also been considered that the P_i release is more or less loosely coupled to the force-generating transition [75, 121, 122]. Furthermore, whether force-generation occurs before or after phosphate release, there is controversy about the exact number of substeps and their rates [122, 151, 209, 229, 230, 236, 321, 323, 324]. If P_i release occurs before the force-generating transition (Table 1), then it seems that P_i release must be rate-limiting for force-generation because direct measurements of P_i release in solution [65] yield a similar rate as that attributed to tension generation following temperature jumps, phosphate jumps, and so forth. A slow P_i release has also been favored on basis of kinetic modeling [324], but in this case, the P_i release was believed to occur after the force-generating transition. Under such conditions, an AM.ADP.P_i state would be the main force-generating state and phosphate release would be rate-limiting for cross-bridge detachment. This is consistent with findings that an AM.ADP.P_i state is the dominant biochemical species in contracting myofibrils [325] and with spectroscopic studies of relay-helix motion in Dictyostelium myosin II catalytic domain [323]. The latter motion precedes a slower P_i release. However, numerous other findings suggest that P_i release is fast [122, 209, 236] and that an AM.ADP state (AM^*ADP in Figure 2) rather than and AM.ADP.P_i state dominates during steady-state contraction [89, 100, 326, 327].

Difficulties to reconcile results from experimental systems with different ionic strength, strain dependence, and so forth may contribute to the different views about the temporal relationship between P_i release and force-generation. The importance of strain, for instance, is reflected in 500-fold faster ^{18}O exchange (reflecting P_i-exchange) in isometric

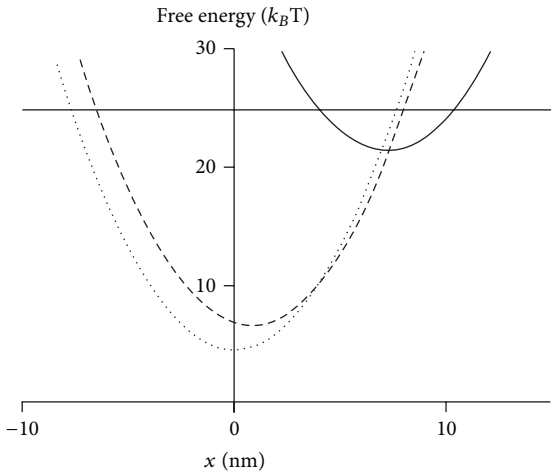

FIGURE 7: Free energy of main cross-bridge states in Figure 2 as function of the strain parameter x. Straight full line: detached states M.ATP and M.ADP.P_i lumped together into one state. Curved full line: AM.ADP.P_i. Dashed line: AM*ADP. Dotted line: AM, AM.ADP, and AM.ATP states lumped together. The parameter $x = 0$ when force is zero in the AM, AM.ADP, and AM.ATP states.

contraction of skinned fibers than in acto-S1 in solution [328]. Moreover, P_i release was inhibited during ramp stretches in cardiac muscle [329] and, finally, the P_i-concentration affected the tension recovery after rapid stretches but not after rapid releases ([225]; see also [330]).

Another possibility is that the conflicting interpretations are due to models that do not capture certain critical features of cross-bridge operation. Furthermore, the lack of generality and stringency in definition of terms such as "main force-generating step" and "power stroke" contribute to the problems. These terms are used differently between researchers and between subfields such as muscle mechanics, single molecule mechanics, and actomyosin structural biology and biochemistry. The ambiguity is reflected in the discussion of the power stroke distance in Section 4.2 (see also [67, 114, 184, 222]).

A direct identity of the force-generating transition associated with P_i release and length jumps was assumed in some early model studies [52, 107, 331] before the broad availability of data from perturbation studies other than length steps. The simplification was also used in recent models [111, 114] where the relationship between P_i release and force-generation was not in focus. In these cases, with key model states and their free energies illustrated in Figure 7, it is of interest to note that the model had high explanatory power accounting for both length-jump responses and a range of steady-state properties, for example, the force-velocity relationship, both in the presence and in absence of a drug affecting the strain-dependent transition from the AM*ADP to the AM.ADP state [100, 110]. Later developments of the same model [111] also accounted for the effects of varying concentrations of ATP and ADP. Whereas temperature jump and P_i-effects were not considered it was found that some temperature effects could be accounted for by increasing the free energy between the AM.ADP.P_i and AM*ADP states [111]. These models could, however, not account for the high power-output of muscle during steady-state shortening or the high steady-state resistance to lengthening without assuming velocity dependent attachment rates (Section 3). Furthermore, due to the very fast detachment from pretension AM.ADP.P_i states, suggested by single molecule studies [182] and the associated weak actin affinity of these states, it seems unlikely that prepower stroke AM.ADP.P_i states can account for the high resistance to slow stretch. Thus, under slow stretches, the rupture force of a majority of the force-resistant cross-bridges seems to be high and with appreciable elastic strain [33, 81], seemingly incompatible with properties of AM.ADP.P_i states. However, future models must reconcile this finding with results (see above), based on effects of nucleotide analogs and drugs [197, 202, 208, 210], varied temperature, and altered P_i-concentration [209], suggesting that prepower stroke cross-bridges in the AM.ADP.P_i state contribute appreciably to the stretch response.

A further problem of current models for force-generation is, as pointed out above, that they assume an independent elastic element and require that the force-generating transition occurs in a large number of steps. An interesting alternative possibility, similar to that originally proposed in [107] is to assume an elastic element that is not independent from the swinging component and that is strained by a subnanometer structural change (in contrast to ~10 nm in the Huxley and Simmons model). This may be termed an Eyring like model [104, 110] where a local chemical change causes a transition into the new state, followed by ~10 nm relaxation of the elastic element into the minimum free energy of the new state. One model for how this could occur is schematically illustrated in Figure 8. Here, the localized structural changes strain the elastic element. The latter is here attributed to bending of the lever arm but the bending could also occur in the converter domain [141, 218]. The localized structural changes, on the other hand, involve thermal fluctuations of structural domains (e.g., related to relay helix, converter domain, central beta-sheet, and the loops around the nucleotide binding site), fluctuations that may precede P_i release [323]. A difference from the original Huxley and Simmons model [47] is the very small amplitude of the structural changes that lead to the high force-state in Figure 8, a fact that substantially reduces the energy barrier to be overcome. This Eyring mechanism [104] is in contrast to a more Kramers-like process, that is where a large scale diffusional straining of an elastic element against a load (as in the Huxley and Simmons [47] model) precedes the chemical change.

Something that further hampers our understanding of the force-generating transition is the fact that the atomic structural correlates of P_i release and force-generation in response to different perturbations are not well-defined. First, a question about the P_i release mechanism, including the exact time point in the ATPase cycle (does P_i release precede the power stroke or does the power stroke precede P_i release?), cannot be readily answered with the present structural models (see Section 4.5). On the other hand, structural information and computational analysis of the hydrolysis reaction postulate different equally feasible escape

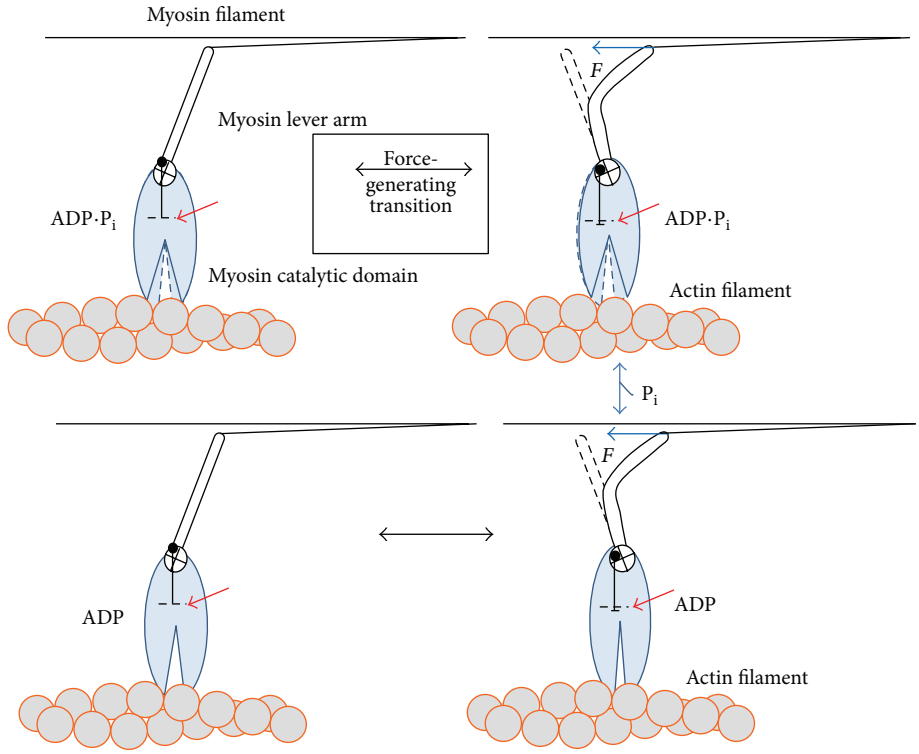

Figure 8: Tentative model. The elastic element is represented by bending of the lever arm being an integral part of the myosin head. This elastic element is stretched by a small amplitude structural change in the catalytic domain (from left to right). The schematic illustration is for isometric contraction. The position of the lever arm at elastic equilibrium of the main force-generating state (right) is illustrated by the lever arm drawn in dashed lines. The force-generating transition from left to right is orthogonal to the phosphate release step (vertical).

routes [62]. However, as touched upon above, a recent study based on solution kinetics and time-resolved fluorescence resonance energy transfer (FRET) experiments revealed that actin binding straightens the relay helix before phosphate dissociation assuming that the power stroke occurs before P_i-release [323]. Structural details of the P_i release state of myosin are needed to understand how actin triggers product release and how active site switch elements rearrange to facilitate the P_i release.

The difficulty of crystallizing the actin-bound state of myosin has hampered detailed insights into the mechanism of force production. One possible way to overcome this problem would be the production of stable dimeric or trimeric actin oligomers. This minimal number of actin subunits could form a functional and crystallizable rigor complex for detailed analysis. In this way it would be possible to resolve, both the exact actin-myosin binding interface, the structural state and interactions between actin and the second myosin head [332], resolving the functional role of the latter. Optical trap experiments with native myosin II have shown that the degree of flexibility of the heads is sufficient to allow attachment to at least three subsequent binding sites on one actin filament [181].

In order to account for some of the apparently conflicting evidence it is interesting to consider ideas that each biochemical state exists in different mechanical/structural states in rapid equilibrium with each other [57, 58, 215, 333] (cf. Figures 5 and 8). More recently, these ideas have gained additional support [334] and been incorporated into rather complete cross-bridge models [75, 109, 117, 121, 122]. In the latter types of model each biochemical state in Figure 2 would be composed of several substates that differ mechanically and structurally by different extension of their elastic element, different degree of completion of the lever-arm swing and different affinity between actin and myosin (cf. Figures 5 and 8).

In terms of such a model, the tension response to length steps is due to very rapid transitions between mechanical/structural states (similar to those in Figure 5) without transitions between biochemical states (horizontal transitions in Figure 8).

The tension response to other perturbations, for example, temperature and phosphate jumps, is due to slower chemical reactions, for example, an isomerization prior to phosphate release that may or may not be strain-dependent.

Whereas models of this type account well for several experimental phenomena it will be important to limit the number of states to an absolute minimum and firmly define the properties of these states, including strain-dependence of interstate transitions, on basis of a range of different experiments. A further challenge will be to relate the structural course of events as defined by X-ray crystallography to the events seen in response to rapid perturbation experiments such as length-jumps, P_i jumps, and temperature jumps in

muscle fibers. Possibly, mechanical experiments on different levels of hierarchical organization from single molecules over small ordered ensembles and myofibrils to muscle cells can help to bridge the gap if they are combined with spectroscopic techniques, for example, single-molecule FRET.

5.2. Number of Actin Sites within Reach for a Given Myosin Head. Several models of muscle contraction assume that only one binding site on the actin filament is within reach for binding of a given myosin head. This approximation allows simulation of most aspects of muscle contraction without severe limitations [110]. However, some additional phenomena may be accounted for if more binding sites are available. For steric reasons, such as the helical arrangement of the actin binding sites on the actin filament, it is likely that only groups of few (3–5) neighboring sites at 5.5 nm intersite distance are reached by myosin heads belonging to a given crown on the thick filament. This idea was supported by laser trap studies showing target zones for myosin binding corresponding to the helical repeat of 36–38 nm of the actin filament. The presence of neighboring sites on the same filament allows extension of the above models such as rapid reattachment to the neighboring actin binding site of a myosin head forcibly detached into an M^*ADP or $MADPP_i$ state during shortening or stretch [75, 121, 122]. Such behavior may form the basis for an apparent velocity dependence of the cross-bridge attachment rate.

5.3. Role of Two Myosin Heads. The role of the second head in the dimeric myosin II molecule remains enigmatic, for example, whether the two heads are independent or cooperative in their interaction with actin and whether there is an alternating stepping behavior, where the heads subsequently bind to actin in a processive manner, thus enhancing force-output [160, 335–339].

Some studies have indicated that interhead cooperativity between the two heads of each myosin II molecule may not be important and the two heads are often viewed as independent force generators ([68, 171, 179]; see further above). However, there are a range of experimental results suggesting different forms of cooperativity of the two heads [74, 100, 124, 160, 168, 338, 340, 341]. One possibility is negative cooperativity between the two heads, that is, binding of one head to actin inhibits binding of the other [342] or one head prevents dissociation of the other head. Negative cooperativity of the latter type would enable maintenance of tension without energy consumption.

On the other hand, positive cooperativity has also been proposed [110, 160, 168, 341]. This may take different forms but one possibility is that binding of one head promotes binding of the other in a way that sequential actions of the two heads are promoted [110, 160]. Such effects may play a role in explaining the apparently faster attachment rate of cross-bridges during shortening and during lengthening. For instance, a mechanism with attachment of the second head was suggested [35], based on muscle X-ray diffraction data (see also [120]), to account for the effective resistance to lengthening. A similar model was proposed more recently [124], but with additional details, suggesting that a large fraction of the actomyosin cross-bridges during stretch are non-stereo-specifically bound (see also above). On the other hand, the idea that the appreciable resistance to stretch of active muscle is attributed mainly to increased number of attached myosin heads could not be corroborated in another recent study [33].

Modeling based on data showing two-headed attachment of fast myosin II [100] hinted [110] that sequential actions of the two heads of myosin II may become important in shortening against intermediate loads [60, 110] (intermediate velocities) when power-output is maximal. The rapid repriming of the working stroke [203] mentioned above has also been explained on this basis. Whereas recent in vitro motility assay tests [111] failed to corroborate the idea of sequential head actions they could neither falsify the hypothesis with certainty. Thus the predicted changes that were looked for were small and it is possible that the loss of cellular order in the in vitro motility assay was the reason for the failure to detect cooperativity [160]. Furthermore, effective interhead cooperativity may also require binding of the two myosin heads to neighboring actin filaments at interfilament distances similar to that in muscle [160] or there may be other forms of interhead cooperativity where the presence of two heads facilitates attachment of one of them but where sequential force-producing actions are not occurring [168, 340, 341].

5.4. Role of Structural Changes in Actin Filaments. The active role of myosin in force-production by actomyosin is universally accepted, but the actin filaments are generally [6], except for their allosteric activation of phosphate release from myosin, viewed as rope-like passive interaction partners. However, the actin filament structure is highly dynamic and altered during the force-generating process [21, 129, 132, 343, 344]. It is therefore reasonable to assume that structural changes in the actin filament are important for effective generation of force and power. Some authors have even proposed a dominant role of the actin filaments, for example, in providing gross structural changes that cause translation of actin over myosin or an asymmetric potential for biased diffusion of the myosin head. However, there is firm evidence for more facilitating and modulatory roles of the actin filaments. Thus, several studies [21, 127–133, 345, 346] suggest that myosin binding to actin or tension on the actin filament causes structural changes that propagate along the actin filament.

6. Understanding of Muscle Function Requires the Combination of Top-Down Disassembly and Bottom-Up Assembly of the Contractile Machinery

In addressing incompletely understood molecular mechanisms of muscle contraction, it will be critical to integrate results from experimental systems on different levels of hierarchical organization. It will also be essential to use a stringent joint terminology so that key concepts, such as "power stroke" have a similar meaning among muscle

physiologists, biochemists, single molecule biophysicists, and structural biologists. Such an integrated approach should lead to models with a minimal number of states that integrate structural, biochemical, and mechanical information from fibers and single molecules, thereby laying a solid foundation for insight into poorly understood phenomena in normal muscle contraction as well as into effects of drugs and myopathy mutations.

Naturally, any cooperative interactions between myosin motors are lost in single molecule studies but detailed nonambiguous information about the strain-dependence of transition rates [61, 98, 182] is more readily derived using single molecules than ensembles. Such studies are now also possible using expressed myosin II from human striated muscle, both normal and with myopathy mutations [135]. On the other hand, the force-velocity relationship of striated muscle is a property of an ordered ensemble that cannot be fully characterized using single myosin motors. However, other challenges plague studies on muscle cells and myofibrils. Thus, there may be uncertainties about interpretation of mechanical and structural data from muscle fiber and myofibril mechanics due to incompletely characterized elastic components, emerging properties in the large ensemble of motors [347] that are not readily extrapolated back to actomyosin interactions or related effects of sarcomere nonuniformities. Clearly, it would be of great interest with new types of experiments to bridge the gap between the ordered system and single molecule studies. One may consider two complementary approaches. First, top-down disassembly, or rather a combined top-down disassembly and bottom-up assembly, of the contractile systems may be achieved by starting with skinned fibers or myofibrils [66, 348, 349] and removing more and more components, possibly followed by reconstitution. The other approach is pure bottom-up assembly of ordered contractile systems from single molecules. Simple versions of such experimental systems, for example, using different number of myosin motors randomly adsorbed to surfaces [183, 350] or incorporated into synthetic myosin filaments on a pedestal [67, 171], would allow studies of force-velocity relationships of ordered and disordered ensembles of myosin motors with one or two heads [179] interacting with actin filaments. Next, it may be of relevance to add other protein components one molecule after the other such as troponin and tropomyosin and protein C.

On more advanced level one may consider the use of DNA-origami scaffolds (cf. [351]) and engineered attachment points of the motors [135] to produce well-defined ordered arrays. Furthermore, if the scaffold could be produced inside a hollow nanowire [352] it may even be possible to build up in vitro assay systems with maintained 3D order similar to that in the myofilament lattice. Finally, it is of interest to use extensively engineered myosins [353–355] to investigate specific properties.

Interesting questions that may be possible to answer by combining single molecule studies and modelling with new experimental systems featuring few to many protein components in different ordered arrangements would be the following.

(i) Overall, are there emerging properties when going from single molecules to ordered ensembles or are the ensemble properties fully characterized on basis of single molecule components?

(ii) What is the role of the two heads in single molecules and in ordered ensembles of different size?

(iii) What is the role of 3D order, for example, the possibility of a given two-headed myosin motor to interact with two or more actin filaments at similar inter-filament distances as in a muscle cell?

(iv) What are the roles of different accessory proteins?

(v) What is the importance of variations between half-sarcomeres in overlap between the thick and thin filaments and other variability in contractile properties over the fiber cross-section and along the length of a myofibril?

(vi) What are the mechanisms determining the force-velocity relationship, for example, the role of two-myosin heads, structural changes in actin filaments, 3D order, and single myosin heads rapidly "jumping" from one actin site to the next when they are part of an ensemble. These issues may be accessible by studying force-velocity relationships of ordered ensembles of different sizes, using one-headed and two-headed myosin fragments and myosin motors with critical mutations, for example, affecting attachment properties or P_i release.

(vii) Can ensemble effects of myopathy mutations and drugs be predicted from single molecule studies and solution biochemistry?

Conflict of Interests

The authors declare that there is no conflict of interests regarding the publication of this paper.

Acknowledgments

Alf Månsson is grateful to the Faculty of Health and Life Sciences of the Linnaeus University for funding and to the Wenner-Green Foundation for funding a sabbatical in the lab of Dilson Rassier at McGill University during which period the present study was initiated. Dilson Rassier acknowledges support from NSERC of Canada and Georgios Tsiavaliaris is grateful to the German Research Foundation and the State of Lower Saxony for funding.

References

[1] A. F. Huxley, "Muscle structure and theories of contraction," *Progress in biophysics and biophysical chemistry*, vol. 7, pp. 255–318, 1957.

[2] H. E. Huxley, "The mechanism of muscular contraction," *Science*, vol. 164, no. 3886, pp. 1356–1366, 1969.

[3] A. F. Huxley, "Muscular contraction," *The Journal of Physiology*, vol. 243, no. 1, pp. 1–43, 1974.

[4] R. W. Lymn and E. W. Taylor, "Mechanism of adenosine triphosphate hydrolysis by actomyosin," *Biochemistry*, vol. 10, no. 25, pp. 4617–4624, 1971.

[5] I. Rayment, H. M. Holden, M. Whittaker et al., "Structure of the actin-myosin complex and its implications for muscle contraction," *Science*, vol. 261, no. 5117, pp. 58–65, 1993.

[6] M. A. Geeves and K. C. Holmes, "The molecular mechanism of muscle contraction," *Advances in Protein Chemistry*, vol. 71, pp. 161–193, 2005.

[7] S. J. Kron and J. A. Spudich, "Fluorescent actin filaments move on myosin fixed to a glass surface," *Proceedings of the National Academy of Sciences of the United States of America*, vol. 83, no. 17, pp. 6272–6276, 1986.

[8] Y. Y. Toyoshima, S. J. Kron, E. M. McNally, K. R. Niebling, and J. A. Spudich, "Myosin subfragment-1 is sufficient to move actin filaments in vitro," *Nature*, vol. 328, no. 6130, pp. 536–539, 1987.

[9] P. R. H. Steinmetz, J. E. M. Kraus, C. Larroux et al., "Independent evolution of striated muscles in cnidarians and bilaterians," *Nature*, vol. 487, no. 7406, pp. 231–234, 2012.

[10] K. A. P. Edman and F. W. Flitney, "Laser diffraction studies of sarcomere dynamics during 'isometric' relaxation in isolated muscle fibres of the frog," *Journal of Physiology*, vol. 329, pp. 1–20, 1982.

[11] K. A. P. Edman, "Residual force enhancement after stretch in striated muscle. A consequence of increased myofilament overlap?" *Journal of Physiology*, vol. 590, no. 6, pp. 1339–1345, 2012.

[12] D. E. Rassier, "Residual force enhancement in skeletal muscles: one sarcomere after the other," *Journal of Muscle Research and Cell Motility*, vol. 33, no. 3-4, pp. 155–165, 2012.

[13] C. Batters, C. Veigel, E. Homsher, and J. R. Sellers, "To understand muscle you must take it apart," *Frontiers in Physiology*, vol. 5, Article ID Article 90, 2014.

[14] H. E. Huxley, "A personal view of muscle and motility mechanisms," *Annual Review of Physiology*, vol. 58, pp. 1–19, 1996.

[15] S. Schiaffino and C. Reggiani, "Fiber types in Mammalian skeletal muscles," *Physiological Reviews*, vol. 91, no. 4, pp. 1447–1531, 2011.

[16] J. A. Spudich, "The myosin swinging cross-bridge model," *Nature Reviews Molecular Cell Biology*, vol. 2, no. 5, pp. 387–392, 2001.

[17] A. F. Huxley and R. Niedergerke, "Structural changes in muscle during contraction: interference microscopy of living muscle fibres," *Nature*, vol. 173, no. 4412, pp. 971–973, 1954.

[18] H. Huxley and J. Hanson, "Changes in the cross-striations of muscle during contraction and stretch and their structural interpretation," *Nature*, vol. 173, no. 4412, pp. 973–976, 1954.

[19] A. M. Gordon, A. F. Huxley, and F. J. Julian, "The variation in isometric tension with sarcomere length in vertebrate muscle fibres.," *Journal of Physiology*, vol. 184, no. 1, pp. 170–192, 1966.

[20] J. A. Spudich, S. J. Kron, and M. P. Sheetz, "Movement of myosin-coated beads on oriented filaments reconstituted from purified actin," *Nature*, vol. 315, no. 6020, pp. 584–586, 1985.

[21] T. Yanagida, M. Nakase, K. Nishiyama, and F. Oosawa, "Direct observation of motion of single F-actin filaments in the presence of myosin," *Nature*, vol. 307, no. 5946, pp. 58–60, 1984.

[22] A. Ashkin and J. M. Dziedzic, "Optical trapping and manipulation of viruses and bacteria," *Science*, vol. 235, no. 4795, pp. 1517–1520, 1987.

[23] J. T. Finer, R. M. Simmons, and J. A. Spudich, "Single myosin molecule mechanics: piconewton forces and nanometre steps," *Nature*, vol. 368, no. 6467, pp. 113–119, 1994.

[24] S. M. Block, L. S. B. Goldsteint, and B. J. Schnapp, "Bead movement by single kinesin molecules studied with optical tweezers," *Nature*, vol. 348, no. 6299, pp. 348–352, 1990.

[25] T. Funatsu, Y. Harada, M. Tokunaga, K. Saito, and T. Yanagida, "Imaging of single fluorescent molecules and individual ATP turnovers by single myosin molecules in aqueous solution," *Nature*, vol. 374, no. 6522, pp. 555–559, 1995.

[26] W. Kabsch, H. G. Mannherz, D. Suck, E. F. Pai, and K. C. Holmes, "Atomic structure of the actin:DNase I complex," *Nature*, vol. 347, no. 6288, pp. 37–44, 1990.

[27] I. Rayment, W. R. Rypniewski, K. Schmidt-Bäse et al., "Three-dimensional structure of myosin subfragment-1: a molecular motor," *Science*, vol. 261, no. 5117, pp. 50–58, 1993.

[28] A. De Lozanne and J. A. Spudich, "Disruption of the Dictyostelium myosin heavy chain gene by homologous recombination," *Science*, vol. 236, no. 4805, pp. 1086–1091, 1987.

[29] E. W. Kubalek, T. Q. P. Uyeda, and J. A. Spudich, "A dictyostelium myosin II lacking a proximal 58-kDa portion of the tail is functional in vitro and in vivo," *Molecular Biology of the Cell*, vol. 3, no. 12, pp. 1455–1462, 1992.

[30] R. Cooke, "The mechanism of muscle contraction," *CRC Critical Reviews in Biochemistry*, vol. 21, no. 1, pp. 53–118, 1986.

[31] K. A. P. Edman, A. Månsson, and C. Caputo, "The biphasic force-velocity relationship in frog muscle fibres and its evaluation in terms of cross-bridge function," *The Journal of Physiology*, vol. 503, part 1, pp. 141–156, 1997.

[32] G. Piazzesi, M. Reconditi, M. Linari et al., "Skeletal muscle performance determined by modulation of number of Myosin motors rather than motor force or stroke size," *Cell*, vol. 131, no. 4, pp. 784–795, 2007.

[33] M. Nocella, M. A. Bagni, G. Cecchi, and B. Colombini, "Mechanism of force enhancement during stretching of skeletal muscle fibres investigated by high time-resolved stiffness measurements," *Journal of Muscle Research and Cell Motility*, vol. 34, no. 1, pp. 71–81, 2013.

[34] G. Piazzesi, F. Francini, M. Linari, and V. Lombardi, "Tension transients during steady lengthening of tetanized muscle fibres of the frog," *The Journal of Physiology*, vol. 445, pp. 659–711, 1992.

[35] E. Brunello, M. Reconditi, R. Elangovan et al., "Skeletal muscle resists stretch by rapid binding of the second motor domain of myosin to actin," *Proceedings of the National Academy of Sciences of the United States of America*, vol. 104, no. 50, pp. 20114–20119, 2007.

[36] P. A. Harvey and L. A. Leinwand, "The cell biology of disease: cellular mechanisms of cardiomyopathy," *The Journal of Cell Biology*, vol. 194, no. 3, pp. 355–365, 2011.

[37] J. A. Spudich, "Hypertrophic and dilated cardiomyopathy: four decades of basic research on muscle lead to potential therapeutic approaches to these devastating genetic diseases," *Biophysical Journal*, vol. 106, no. 6, pp. 1236–1249, 2014.

[38] P. Teekakirikul, R. F. Padera, J. G. Seidman, and C. E. Seidman, "Hypertrophic cardiomyopathy: translating cellular cross talk into therapeutics," *The Journal of Cell Biology*, vol. 199, no. 3, pp. 417–421, 2012.

[39] N. G. Laing, "Congenital myopathies," *Current Opinion in Neurology*, vol. 20, no. 5, pp. 583–589, 2007.

[40] H. Tajsharghi and A. Oldfors, "Myosinopathies: pathology and mechanisms," *Acta Neuropathologica*, vol. 125, no. 1, pp. 3–18, 2013.

[41] M. Memo and S. Marston, "Skeletal muscle myopathy mutations at the actin tropomyosin interface that cause gain-or loss-of-function," *Journal of Muscle Research and Cell Motility*, vol. 34, no. 3-4, pp. 165–169, 2013.

[42] J. Ochala, D. S. Gokhin, I. Pénisson-Besnier et al., "Congenital myopathy-causing tropomyosin mutations induce thin filament dysfunction via distinct physiological mechanisms," *Human Molecular Genetics*, vol. 21, no. 20, Article ID dds289, pp. 4473–4485, 2012.

[43] A. Månsson, "Hypothesis and theory: mechanical instabilities and non-uniformities in hereditary sarcomere myopathies," *Frontiers in Physiology*, vol. 5, article 350, 2014.

[44] A. M. Gordon, E. Homsher, and M. Regnier, "Regulation of contraction in striated muscle," *Physiological Reviews*, vol. 80, no. 2, pp. 853–924, 2000.

[45] S. S. Lehrer, "The 3-state model of muscle regulation revisited: is a fourth state involved?" *Journal of Muscle Research and Cell Motility*, vol. 32, no. 3, pp. 203–208, 2011.

[46] J. R. Sellers, *Myosins*, Oxford University Press, Oxford, UK, 2nd edition, 1999.

[47] A. F. Huxley and R. M. Simmons, "Proposed mechanism of force generation in striated muscle," *Nature*, vol. 233, no. 5321, pp. 533–538, 1971.

[48] K. A. P. Edman and N. A. Curtin, "Synchronous oscillations of length and stiffness during loaded shortening of frog muscle fibres," *Journal of Physiology*, vol. 534, no. 2, pp. 553–563, 2001.

[49] T. A. J. Duke, "Molecular model of muscle contraction," *Proceedings of the National Academy of Sciences of the United States of America*, vol. 96, no. 6, pp. 2770–2775, 1999.

[50] E. Eisenberg and C. Moos, "The adenosine triphosphatase activity of acto-heavy meromyosin. A kinetic analysis of actin activation," *Biochemistry*, vol. 7, no. 4, pp. 1486–1489, 1968.

[51] E. Eisenberg and C. Moos, "Actin activation of heavy meromyosin adenosine triphosphatase. Dependence on adenosine triphosphate and actin concentrations.," *Journal of Biological Chemistry*, vol. 245, no. 9, pp. 2451–2456, 1970.

[52] E. Eisenberg and L. E. Greene, "The relation of muscle biochemistry to muscle physiology.," *Annual Review of Physiology*, vol. 42, pp. 293–309, 1980.

[53] S. P. Chock, P. B. Chock, and E. Eisenberg, "The mechanism of the skeletal muscle myosin ATPase. II. Relationship between the fluorescence enhancement induced by ATP and the initial Pi burst," *The Journal of Biological Chemistry*, vol. 254, no. 9, pp. 3236–3243, 1979.

[54] L. A. Stein, P. B. Chock, and E. Eisenberg, "The rate-limiting step in the actomyosin adenosinetriphosphatase cycle," *Biochemistry*, vol. 23, no. 7, pp. 1555–1563, 1984.

[55] E. W. Taylor, "Mechanism of actomyosin ATPase and the problem of muscle contraction," *CRC Critical Reviews in Biochemistry*, vol. 6, no. 2, pp. 103–164, 1979.

[56] Y.-Z. Ma and E. W. Taylor, "Kinetic mechanism of myofibril ATPase," *Biophysical Journal*, vol. 66, no. 5, pp. 1542–1553, 1994.

[57] M. A. Geeves, R. S. Goody, and H. Gutfreund, "Kinetics of acto-S1 interaction as a guide to a model for the crossbridge cycle," *Journal of Muscle Research and Cell Motility*, vol. 5, no. 4, pp. 351–361, 1984.

[58] M. A. Geeves, "The dynamics of actin and myosin association and the crossbridge model of muscle contraction," *Biochemical Journal*, vol. 274, no. 1, pp. 1–14, 1991.

[59] K. C. Holmes, R. R. Schröder, H. L. Sweeney, and A. Houdusse, "The structure of the rigor complex and its implications for the power stroke," *Philosophical Transactions of the Royal Society B: Biological Sciences*, vol. 359, no. 1452, pp. 1819–1828, 2004.

[60] H. L. Sweeney and A. Houdusse, "Structural and functional insights into the myosin motor mechanism," *Annual Review of Biophysics*, vol. 39, no. 1, pp. 539–557, 2010.

[61] M. Capitanio, M. Canepari, P. Cacciafesta et al., "Two independent mechanical events in the interaction cycle of skeletal muscle myosin with actin," *Proceedings of the National Academy of Sciences of the United States of America*, vol. 103, no. 1, pp. 87–92, 2006.

[62] A. Málnási-Csizmadia and M. Kovács, "Emerging complex pathways of the actomyosin powerstroke," *Trends in Biochemical Sciences*, vol. 35, no. 12, pp. 684–690, 2010.

[63] C. R. Bagshaw and D. R. Trentham, "The characterization of myosin product complexes and of product release steps during the magnesium ion dependent adenosine triphosphatase reaction," *Biochemical Journal*, vol. 141, no. 2, pp. 331–349, 1974.

[64] S. Highsmith, "The effects of temperature and salts on myosin subfragment 1 and F actin association," *Archives of Biochemistry and Biophysics*, vol. 180, no. 2, pp. 404–408, 1977.

[65] H. D. White, B. Belknap, and M. R. Webb, "Kinetics of nucleoside triphosphate cleavage and phosphate release steps by associated rabbit skeletal actomyosin, measured using a novel fluorescent probe for phosphate," *Biochemistry*, vol. 36, no. 39, pp. 11828–11836, 1997.

[66] M. Irving, T. St Clair-Allen, C. Sabido-David et al., "Tilting of the light-chain region of myosin during step length changes and active force generation in skeletal muscle," *Nature*, vol. 375, no. 6533, pp. 688–691, 1995.

[67] M. Kaya and H. Higuchi, "Nonlinear elasticity and an 8-nm working stroke of single myosin molecules in myofilaments," *Science*, vol. 329, no. 5992, pp. 686–689, 2010.

[68] J. E. Molloy, J. E. Burns, J. Kendrick-Jones, R. T. Tregear, and D. C. S. White, "Movement and force produced by a single myosin head," *Nature*, vol. 378, no. 6553, pp. 209–212, 1995.

[69] B. Brenner, M. Schoenberg, J. M. Chalovich, L. E. Greene, and E. Eisenberg, "Evidence for cross-bridge attachment in relaxed muscle at low ionic strength.," *Proceedings of the National Academy of Sciences of the United States of America*, vol. 79, no. 23, pp. 7288–7291, 1982.

[70] M. A. Geeves and K. C. Holmes, "Structural mechanism of muscle contraction," *Annual Review of Biochemistry*, vol. 68, pp. 687–728, 1999.

[71] K. A. Taylor, H. Schmitz, M. C. Reedy et al., "Tomographic 3D reconstruction of quick-frozen, Ca^{2+}-activated contracting insect flight muscle," *Cell*, vol. 99, no. 4, pp. 421–431, 1999.

[72] M. A. Ferenczi, S. Y. Bershitsky, N. Koubassova et al., "The "roll and lock" mechanism of force generation in muscle," *Structure*, vol. 13, no. 1, pp. 131–141, 2005.

[73] B. A. J. Baumann, H. Liang, K. Sale, B. D. Hambly, and P. G. Fajer, "Myosin regulatory domain orientation in skeletal muscle fibers: application of novel electron paramagnetic resonance spectral decomposition and molecular modeling methods," *Biophysical Journal*, vol. 86, no. 5, pp. 3030–3041, 2004.

[74] S. Wu, J. Liu, M. C. Reedy et al., "Electron tomography of cryofixed, isometrically contracting insect flight muscle reveals novel actin-myosin interactions," *PLoS ONE*, vol. 5, no. 9, Article ID e12643, 2010.

[75] D. A. Smith, M. A. Geeves, J. Sleep, and S. M. Mijailovich, "Towards a unified theory of muscle contraction. I: foundations," *Annals of Biomedical Engineering*, vol. 36, no. 10, pp. 1624–1640, 2008.

[76] B. C. Abbott, X. M. Aubert, and A. V. Hill, "The absorption of work when a muscle is stretched," *The Journal of Physiology*, vol. 111, no. 1-2, pp. 41p–42p, 1950.

[77] H. Ashikaga, T. I. G. van der Spoel, B. A. Coppola, and J. H. Omens, "Transmural myocardial mechanics during isovolumic contraction," *JACC: Cardiovascular Imaging*, vol. 2, no. 2, pp. 202–211, 2009.

[78] N. A. Curtin and R. E. Davies, "Very high tension with very little ATP breakdown by active skeletal muscle," *Journal of Mechanochemistry and Cell Motility*, vol. 3, no. 2, pp. 147–154, 1975.

[79] V. Lombardi and G. Piazzesi, "The contractile response during steady lengthening of stimulated frog muscle fibres," *Journal of Physiology*, vol. 431, pp. 141–171, 1990.

[80] A. Mansson, "The tension response to stretch of intact skeletal muscle fibres of the frog at varied tonicity of the extracellular medium," *Journal of Muscle Research and Cell Motility*, vol. 15, no. 2, pp. 145–157, 1994.

[81] B. Colombini, M. Nocella, G. Benelli, G. Cecchi, P. J. Griffiths, and M. A. Bagni, "Reversal of the myosin power stroke induced by fast stretching of intact skeletal muscle fibers," *Biophysical Journal*, vol. 97, no. 11, pp. 2922–2929, 2009.

[82] B. Colombini, M. Nocella, G. Benelli, G. Cecchi, and M. A. Bagni, "Crossbridge properties during force enhancement by slow stretching in single intact frog muscle fibres," *The Journal of Physiology*, vol. 585, no. 2, pp. 607–615, 2007.

[83] T. Nishizaka, H. Miyata, H. Yoshikawa, S. Ishiwata, and K. Kinosita Jr., "Unbinding force of a single motor molecule of muscle measured using optical tweezers," *Nature*, vol. 377, no. 6546, pp. 251–254, 1995.

[84] B. Guo and W. H. Guilford, "Mechanics of actomyosin bonds in different nucleotide states are tuned to muscle contraction," *Proceedings of the National Academy of Sciences of the United States of America*, vol. 103, no. 26, pp. 9844–9849, 2006.

[85] M. A. Bagni, G. Cecchi, and B. Colombini, "Crossbridge properties investigated by fast ramp stretching of activated frog muscle fibres," *Journal of Physiology*, vol. 565, part 1, pp. 261–268, 2005.

[86] E. B. Getz, R. Cooke, and S. L. Lehman, "Phase transition in force during ramp stretches of skeletal muscle," *Biophysical Journal*, vol. 75, no. 6, pp. 2971–2983, 1998.

[87] F. C. Minozzo, L. Hilbert, and D. E. Rassier, "Pre-power-stroke cross-bridges contribute to force transients during imposed shortening in isolated muscle fibers," *PLoS ONE*, vol. 7, no. 1, Article ID e29356, 2012.

[88] J. A. Sleep and R. L. Hutton, "Exchange between inorganic phosphate and adenosine 5′-triphosphate in the medium by actomyosin subfragment," *Biochemistry*, vol. 19, no. 7, pp. 1276–1283, 1980.

[89] M. Kawai and H. R. Halvorson, "Two step mechanism of phosphate release and the mechanism of force generation in chemically skinned fibers of rabbit psoas muscle," *Biophysical Journal*, vol. 59, no. 2, pp. 329–342, 1991.

[90] J. A. Dantzig, M. G. Hibberd, D. R. Trentham, and Y. E. Goldman, "Cross-bridge kinetics in the presence of MgADP investigated by photolysis of caged ATP in rabbit psoas muscle fibres," *The Journal of Physiology*, vol. 432, pp. 639–680, 1991.

[91] M. Nyitrai and M. A. Geeves, "Adenosine diphosphate and strain sensitivity in myosin motors," *Philosophical Transactions of the Royal Society B: Biological Sciences*, vol. 359, no. 1452, pp. 1867–1877, 2004.

[92] J. D. Jontes, E. M. Wilson-Kubalek, and R. A. Milligan, "A 32° tail swing in brush border myosin I on ADP release," *Nature*, vol. 378, no. 6558, pp. 751–753, 1995.

[93] M. Whittaker, E. M. Wilson-Kubalek, J. E. Smith, L. Faust, R. A. Milligant, and H. L. Sweeney, "A 35-A movement of smooth muscle myosin on ADP release," *Nature*, vol. 378, no. 6558, pp. 748–751, 1995.

[94] C. Veigel, L. M. Coluccio, J. D. Jontes, J. C. Sparrow, R. A. Milligan, and J. E. Molloy, "The motor protein myosin-I produces its working stroke in two steps," *Nature*, vol. 398, no. 6727, pp. 530–533, 1999.

[95] J. Gollub, C. R. Cremo, and R. Cooke, "ADP release produces a rotation of the neck region of smooth myosin but not skeletal myosin," *Nature Structural Biology*, vol. 3, no. 9, pp. 796–802, 1996.

[96] S. S. Rosenfeld and H. L. Sweeney, "A model of myosin V processivity," *The Journal of Biological Chemistry*, vol. 279, no. 38, pp. 40100–40111, 2004.

[97] C. Veigel, F. Wang, M. L. Bartoo, J. R. Sellers, and J. E. Molloy, "The gated gait of the processive molecular motor, myosin V," *Nature Cell Biology*, vol. 4, no. 1, pp. 59–65, 2002.

[98] C. Veigel, J. E. Molloy, S. Schmitz, and J. Kendrick-Jones, "Load-dependent kinetics of force production by smooth muscle myosin measured with optical tweezers," *Nature Cell Biology*, vol. 5, no. 11, pp. 980–986, 2003.

[99] M. Kovács, K. Thirumurugan, P. J. Knight, and J. R. Sellers, "Load-dependent mechanism of nonmuscle myosin 2," *Proceedings of the National Academy of Sciences of the United States of America*, vol. 104, no. 24, pp. 9994–9999, 2007.

[100] N. Albet-Torres, M. J. Bloemink, T. Barman et al., "Drug effect unveils inter-head cooperativity and strain-dependent ADP release in fast skeletal actomyosin," *The Journal of Biological Chemistry*, vol. 284, no. 34, pp. 22926–22937, 2009.

[101] M. Nyitrai, R. Rossi, N. Adamek, M. A. Pellegrino, R. Bottinelli, and M. A. Geeves, "What limits the velocity of fast-skeletal muscle contraction in mammals?" *Journal of Molecular Biology*, vol. 355, no. 3, pp. 432–442, 2006.

[102] T. Q. P. Uyeda, S. J. Kron, and J. A. Spudich, "Myosin step size: estimation from slow sliding movement of actin over low densities of heavy meromyosin," *Journal of Molecular Biology*, vol. 214, no. 3, pp. 699–710, 1990.

[103] S. Walcott, D. M. Warshaw, and E. P. Debold, "Mechanical coupling between myosin molecules causes differences between ensemble and single-molecule measurements," *Biophysical Journal*, vol. 103, no. 3, pp. 501–510, 2012.

[104] J. Howard, *Mechanics of Motor Proteins and the Cytoskeleton*, Sinauer Associates, Sunderland, Mass, USA, 2001.

[105] T. L. Hill, "Theoretical formalism for the sliding filament model of contraction of striated muscle .Part I," *Progress in Biophysics and Molecular Biology*, vol. 28, pp. 267–340, 1974.

[106] T. L. Hill, "Theoretical formalism for the sliding filament model of contraction of striated muscle part II," *Progress in Biophysics & Molecular Biology*, vol. 29, pp. 105–159, 1976.

[107] E. Eisenberg and T. L. Hill, "A cross-bridge model of muscle contraction," *Progress in Biophysics and Molecular Biology*, vol. 33, no. 1, pp. 55–82, 1978.

[108] E. Eisenberg, T. L. Hill, and Y. Chen, "Cross-bridge model of muscle contraction. Quantitative analysis," *Biophysical Journal*, vol. 29, no. 2, pp. 195–227, 1980.

[109] D. A. Smith and M. A. Geeves, "Strain-dependent cross-bridge cycle for muscle," *Biophysical Journal*, vol. 69, no. 2, pp. 524–537, 1995.

[110] A. Månsson, "Actomyosin-ADP states, interhead cooperativity, and the force-velocity relation of skeletal muscle," *Biophysical Journal*, vol. 98, no. 7, pp. 1237–1246, 2010.

[111] M. Persson, E. Bengtsson, L. ten Siethoff, and A. Månsson, "Nonlinear cross-bridge elasticity and post-power-stroke events in fast skeletal muscle actomyosin," *Biophysical Journal*, vol. 105, no. 8, pp. 1871–1881, 2013.

[112] F. Jülicher and J. Prost, "Cooperative molecular motors," *Physical Review Letters*, vol. 75, no. 13, pp. 2618–2621, 1995.

[113] A. Vilfan and E. Frey, "Oscillations in molecular motor assemblies," *Journal of Physics Condensed Matter*, vol. 17, no. 47, pp. S3901–S3911, 2005.

[114] G. Offer and K. W. Ranatunga, "A cross-bridge cycle with two tension-generating steps simulates skeletal muscle mechanics," *Biophysical Journal*, vol. 105, no. 4, pp. 928–940, 2013.

[115] C. Y. Seow, "Hill's equation of muscle performance and its hidden insight on molecular mechanisms," *The Journal of General Physiology*, vol. 142, no. 6, pp. 561–573, 2013.

[116] C. J. Barclay, "Estimation of cross-bridge stiffness from maximum thermodynamic efficiency," *Journal of Muscle Research and Cell Motility*, vol. 19, no. 8, pp. 855–864, 1998.

[117] D. A. Smith and M. A. Geeves, "Strain-dependent cross-bridge cycle for muscle II. Steady-state behavior," *Biophysical Journal*, vol. 69, no. 2, pp. 538–552, 1995.

[118] Y.-D. Chen and B. Brenner, "On the regeneration of the actin-myosin power stroke in contracting muscle," *Proceedings of the National Academy of Sciences of the United States of America*, vol. 90, no. 11, pp. 5148–5152, 1993.

[119] A. F. Huxley and S. Tideswell, "Rapid regeneration of power stroke in contracting muscle by attachment of second myosin head," *Journal of Muscle Research and Cell Motility*, vol. 18, no. 1, pp. 111–114, 1997.

[120] L. Fusi, M. Reconditi, M. Linari et al., "The mechanism of the resistance to stretch of isometrically contracting single muscle fibres," *The Journal of Physiology*, vol. 588, no. 3, pp. 495–510, 2010.

[121] D. A. Smith and S. M. Mijailovich, "Toward a unified theory of muscle contraction. II. Predictions with the mean-field approximation," *Annals of Biomedical Engineering*, vol. 36, no. 8, pp. 1353–1371, 2008.

[122] M. Caremani, L. Melli, M. Dolfi, V. Lombardi, and M. Linari, "The working stroke of the myosin II motor in muscle is not tightly coupled to release of orthophosphate from its active site," *The Journal of Physiology*, vol. 591, part 20, pp. 5187–5205, 2013.

[123] G. Piazzesi and V. Lombardi, "A cross-bridge model that is able to explain mechanical and energetic properties of shortening muscle," *Biophysical Journal*, vol. 68, no. 5, pp. 1966–1979, 1995.

[124] M. A. Ferenczi, S. Y. Bershitsky, N. A. Koubassova et al., "Why muscle is an efficient shock absorber," *PLoS ONE*, vol. 9, no. 1, Article ID e85739, 2014.

[125] J. Kozuka, H. Yokota, Y. Arai, Y. Ishii, and T. Yanagida, "Dynamic polymorphism of single actin molecules in the actin filament," *Nature Chemical Biology*, vol. 2, no. 2, pp. 83–86, 2006.

[126] E. Prochniewicz, E. Katayama, T. Yanagida, and D. D. Thomas, "Cooperativity in F-actin: chemical modifications of actin monomers affect the functional interactions of myosin with unmodified monomers in the same actin filament," *Biophysical Journal*, vol. 65, no. 1, pp. 113–123, 1993.

[127] V. E. Galkin, A. Orlova, and E. H. Egelman, "Actin filaments as tension sensors," *Current Biology*, vol. 22, no. 3, pp. R96–R101, 2012.

[128] V. E. Galkin, A. Orlova, G. F. Schröder, and E. H. Egelman, "Structural polymorphism in F-actin," *Nature Structural and Molecular Biology*, vol. 17, no. 11, pp. 1318–1323, 2010.

[129] A. Orlova and E. H. Egelman, "A conformational change in the actin subunit can change the flexibility of the actin filament," *Journal of Molecular Biology*, vol. 232, no. 2, pp. 334–341, 1993.

[130] T. Q. P. Uyeda, Y. Iwadate, N. Umeki, A. Nagasaki, and S. Yumura, "Stretching actin filaments within cells enhances their affinity for the myosin ii motor domain," *PLoS ONE*, vol. 6, no. 10, Article ID e26200, 2011.

[131] K. Tokuraku, R. Kurogi, R. Toya, and T. Q. P. Uyeda, "Novel mode of cooperative binding between myosin and Mg^{2+} -actin filaments in the presence of low concentrations of ATP," *Journal of Molecular Biology*, vol. 386, no. 1, pp. 149–162, 2009.

[132] P. G. Vikhorev, N. N. Vikhoreva, and A. Månsson, "Bending flexibility of actin filaments during motor-induced sliding," *Biophysical Journal*, vol. 95, no. 12, pp. 5809–5819, 2008.

[133] E. Prochniewicz, T. F. Walseth, and D. D. Thomas, "Structural dynamics of actin during active interaction with myosin: different effects of weakly and strongly bound myosin heads," *Biochemistry*, vol. 43, no. 33, pp. 10642–10652, 2004.

[134] G. Miller, J. Maycock, E. White, M. Peckham, and S. Calaghan, "Heterologous expression of wild-type and mutant β-cardiac myosin changes the contractile kinetics of cultured mouse myotubes," *Journal of Physiology*, vol. 548, no. 1, pp. 167–174, 2003.

[135] R. F. Sommese, J. Sung, S. Nag et al., "Molecular consequences of the R453C hypertrophic cardiomyopathy mutation on human β-cardiac myosin motor function," *Proceedings of the National Academy of Sciences of the United States of America*, vol. 110, no. 31, pp. 12607–12612, 2013.

[136] M. Bloemink, J. Deacon, S. Langer et al., "The hypertrophic cardiomyopathy myosin mutation R453C alters ATP binding and hydrolysis of human cardiac β-myosin," *Journal of Biological Chemistry*, vol. 289, no. 8, pp. 5158–5167, 2014.

[137] D. I. Resnicow, J. C. Deacon, H. M. Warrick, J. A. Spudich, and L. A. Leinwand, "Functional diversity among a family of human skeletal muscle myosin motors," *Proceedings of the National Academy of Sciences of the United States of America*, vol. 107, no. 3, pp. 1053–1058, 2010.

[138] F. I. Malik, J. J. Hartman, K. A. Elias et al., "Cardiac myosin activation: a potential therapeutic approach for systolic heart failure," *Science*, vol. 331, no. 6023, pp. 1439–1443, 2011.

[139] B. P. Morgan, A. Muci, P.-P. Lu et al., "Discovery of omecamtiv mecarbil the first, selective, small molecule activator of cardiac myosin," *ACS Medicinal Chemistry Letters*, vol. 1, no. 9, pp. 472–477, 2010.

[140] M. B. Radke, M. H. Taft, B. Stapel, D. Hilfiker-Kleiner, M. Preller, and D. J. Manstein, "Small molecule-mediated refolding and activation of myosin motor function," *eLife*, vol. 2014, no. 3, Article ID e01603, 2014.

[141] J. Kohler, G. Winkler, I. Schulte et al., "Mutation of the myosin converter domain alters cross-bridge elasticity," *Proceedings of the National Academy of Sciences of the United States of America*, vol. 99, no. 6, pp. 3557–3562, 2002.

[142] C. Ferrantini, A. Belus, N. Piroddi, B. Scellini, C. Tesi, and C. Poggesi, "Mechanical and energetic consequences of HCM-causing mutations," *Journal of Cardiovascular Translational Research*, vol. 2, no. 4, pp. 441–451, 2009.

[143] L. M. Bond, D. A. Tumbarello, J. Kendrick-Jones, and F. Buss, "Small-molecule inhibitors of myosin proteins," *Future Medicinal Chemistry*, vol. 5, no. 1, pp. 41–52, 2013.

[144] S. M. Heissler, J. Selvadurai, L. M. Bond et al., "Kinetic properties and small-molecule inhibition of human myosin-6," *FEBS Letters*, vol. 586, no. 19, pp. 3208–3214, 2012.

[145] M. Preller, K. Chinthalapudi, R. Martin, H.-J. Knölker, and D. J. Manstein, "Inhibition of myosin ATPase activity by halogenated pseudilins: a structure-activity study," *Journal of Medicinal Chemistry*, vol. 54, no. 11, pp. 3675–3685, 2011.

[146] R. Fedorov, M. Böhl, G. Tsiavaliaris et al., "The mechanism of pentabromopseudilin inhibition of myosin motor activity," *Nature Structural & Molecular Biology*, vol. 16, no. 1, pp. 80–88, 2009.

[147] K. Chinthalapudi, M. H. Taft, R. Martin et al., "Mechanism and specificity of pentachloropseudilin-mediated inhibition of myosin motor activity," *The Journal of Biological Chemistry*, vol. 286, no. 34, pp. 29700–29708, 2011.

[148] I. Ramachandran, M. Terry, and M. B. Ferrari, "Skeletal muscle myosin cross-bridge cycling is necessary for myofibrillogenesis," *Cell Motility and the Cytoskeleton*, vol. 55, no. 1, pp. 61–72, 2003.

[149] M. Kovács, J. Tóth, C. Hetényi, A. Málnási-Csizmadia, and J. R. Seller, "Mechanism of blebbistatin inhibition of myosin II," *The Journal of Biological Chemistry*, vol. 279, no. 34, pp. 35557–35563, 2004.

[150] A. F. Straight, A. Cheung, J. Limouze et al., "Dissecting temporal and spatial control of cytokinesis with a myosin II inhibitor," *Science*, vol. 299, no. 5613, pp. 1743–1747, 2003.

[151] M. Regnier, C. Morris, and E. Homsher, "Regulation of the cross-bridge transition from a weakly to strongly bound state in skinned rabbit muscle fibers," *American Journal of Physiology*, vol. 269, no. 6, part 1, pp. C1532–C1539, 1995.

[152] M. Linari, G. Piazzesi, and V. Lombardi, "The effect of myofilament compliance on kinetics of force generation by myosin motors in muscle," *Biophysical Journal*, vol. 96, no. 2, pp. 583–592, 2009.

[153] D. F. A. McKillop, N. S. Fortune, K. W. Ranatunga, and M. A. Geeves, "The influence of 2,3-butanedione 2-monoxime (BDM) on the interaction between actin and myosin in solution and in skinned muscle fibres," *Journal of Muscle Research and Cell Motility*, vol. 15, no. 3, pp. 309–318, 1994.

[154] M. A. Bagni, G. Cecchi, F. Colomo, and P. Garzella, "Effects of 2,3-butanedione monoxime on the crossbridge kinetics in frog single muscle fibres," *Journal of Muscle Research and Cell Motility*, vol. 13, no. 5, pp. 516–522, 1992.

[155] Y.-B. Sun, F. Lou, and K. A. P. Edman, "The effects of 2,3-butanedione monoxime (BDM) on the force-velocity relation in single muscle fibres of the frog," *Acta Physiologica Scandinavica*, vol. 153, no. 4, pp. 325–334, 1995.

[156] M. Webb, D. R. Jackson, T. J. Stewart et al., "The myosin duty ratio tunes the calcium sensitivity and cooperative activation of the thin filament," *Biochemistry*, vol. 52, no. 37, pp. 6437–6444, 2013.

[157] J. S. Allingham, R. Smith, and I. Rayment, "The structural basis of blebbistatin inhibition and specificity for myosin II," *Nature Structural & Molecular Biology*, vol. 12, no. 4, pp. 378–379, 2005.

[158] A. Månsson, "ATP-driven mechanical work performed by molecular motors," in *Encyclopedia of Biophysics*, pp. 135–141, 2013.

[159] L. Chin, P. Yue, J. J. Feng, and C. Y. Seow, "Mathematical simulation of muscle cross-bridge cycle and force-velocity relationship," *Biophysical Journal*, vol. 91, no. 10, pp. 3653–3663, 2006.

[160] P. B. Conibear and M. A. Geeves, "Cooperativity between the two heads of rabbit skeletal muscle heavy meromyosin in binding to actin," *Biophysical Journal*, vol. 75, no. 2, pp. 926–937, 1998.

[161] A. Månsson, "Translational actomyosin research: fundamental insights and applications hand in hand," *Journal of Muscle Research and Cell Motility*, vol. 33, no. 3-4, pp. 219–233, 2012.

[162] A. Mansson, M. Balaz, N. Albet-Torres, and K. J. Rosengren, "In vitro assays of molecular motors—impact of motor-surface interactions," *Frontiers in Bioscience*, vol. 13, no. 15, pp. 5732–5754, 2008.

[163] E. Homsher, F. Wang, and J. R. Sellers, "Factors affecting movement of F-actin filaments propelled by skeletal muscle heavy meromyosin," *American Journal of Physiology: Cell Physiology*, vol. 262, no. 3, part 1, pp. C714–C723, 1992.

[164] I. Chizhov, F. K. Hartmann, N. Hundt, and G. Tsiavaliaris, "Global fit analysis of myosin-5b motility reveals thermodynamics of Mg^{2+}-sensitive acto-myosin-ADP states," *PLoS ONE*, vol. 8, no. 5, Article ID e64797, 2013.

[165] A. Ashkin, "Forces of a single-beam gradient laser trap on a dielectric sphere in the ray optics regime," *Methods in Cell Biology*, vol. 55, pp. 1–27, 1998.

[166] A. Ashkin, "Applications of laser radiation pressure," *Science*, vol. 210, no. 4474, pp. 1081–1088, 1980.

[167] R. M. Simmons, J. T. Finer, S. Chu, and J. A. Spudich, "Quantitative measurements of force and displacement using an optical trap," *Biophysical Journal*, vol. 70, no. 4, pp. 1813–1822, 1996.

[168] M. J. Tyska, D. E. Dupuis, W. H. Guilford et al., "Two heads of myosin are better than one for generating force and motion," *Proceedings of the National Academy of Sciences of the United States of America*, vol. 96, no. 8, pp. 4402–4407, 1999.

[169] C. Veigel, M. L. Bartoo, D. C. S. White, J. C. Sparrow, and J. E. Molloy, "The stiffness of rabbit skeletal actomyosin cross-bridges determined with an optical tweezers transducer," *Biophysical Journal*, vol. 75, no. 3, pp. 1424–1438, 1998.

[170] Y. Takagi, E. E. Homsher, Y. E. Goldman, and H. Shuman, "Force generation in single conventional actomyosin complexes under high dynamic load," *Biophysical Journal*, vol. 90, no. 4, pp. 1295–1307, 2006.

[171] H. Tanaka, A. Ishijima, M. Honda, K. Saito, and T. Yanagida, "Orientation dependence of displacements by a single one-headed myosin relative to the actin filament," *Biophysical Journal*, vol. 75, no. 4, pp. 1886–1894, 1998.

[172] W. H. Guilford, D. E. Dupuis, G. Kennedy, J. Wu, J. B. Patlak, and D. M. Warshaw, "Smooth muscle and skeletal muscle myosins produce similar unitary forces and displacements in the laser trap," *Biophysical Journal*, vol. 72, no. 3, pp. 1006–1021, 1997.

[173] M. Rief, R. S. Rock, A. D. Mehta, M. S. Mooseker, R. E. Cheney, and J. A. Spudich, "Myosin-V stepping kinetics: a molecular model for processivity," *Proceedings of the National Academy of Sciences of the United States of America*, vol. 97, no. 17, pp. 9482–9486, 2000.

[174] K. Visscher, M. J. Schnltzer, and S. M. Block, "Single kinesin molecules studied with a molecular force clamp," *Nature*, vol. 400, no. 6740, pp. 184–189, 1999.

[175] C. Veigel, S. Schmitz, F. Wang, and J. R. Sellers, "Load-dependent kinetics of myosin-V can explain its high processivity," *Nature Cell Biology*, vol. 7, no. 9, pp. 861–869, 2005.

[176] E. M. de la Cruz, A. L. Wells, S. S. Rosenfeld, E. M. Ostap, and H. L. Sweeney, "The kinetic mechanism of myosin V," *Proceedings of the National Academy of Sciences of the United States of America*, vol. 96, no. 24, pp. 13726–13731, 1999.

[177] J. E. Molloy, J. E. Burns, J. C. Sparrow et al., "Single-molecule mechanics of heavy meromyosin and S1 interacting with rabbit or *Drosophila* actins using optical tweezers," *Biophysical Journal*, vol. 68, no. 4, pp. 298S–305S, 1995.

[178] J. E. Molloy, J. Kendrick-Jones, C. Veigel, and R. T. Tregear, "An unexpectedly large working stroke from chymotryptic fragments of myosin II," *FEBS Letters*, vol. 480, no. 2-3, pp. 293–297, 2000.

[179] Y. Harada, A. Noguchi, A. Kishino, and T. Yanagida, "Sliding movement of single actin filaments on one-headed myosin filaments," *Nature*, vol. 326, no. 6115, pp. 805–808, 1987.

[180] A. Kishino and T. Yanagida, "Force measurements by micromanipulation of a single actin filament by glass needles," *Nature*, vol. 334, no. 6177, pp. 74–76, 1988.

[181] W. Steffen, D. Smith, R. Simmons, and J. Sleep, "Mapping the actin filament with myosin," *Proceedings of the National Academy of Sciences of the United States of America*, vol. 98, no. 26, pp. 14949–14954, 2001.

[182] M. Capitanio, M. Canepari, M. Maffei et al., "Ultrafast force-clamp spectroscopy of single molecules reveals load dependence of myosin working stroke," *Nature Methods*, vol. 9, no. 10, pp. 1013–1019, 2012.

[183] E. P. Debold, J. B. Patlak, and D. M. Warshaw, "Slip sliding away: load-dependence of velocity generated by skeletal muscle myosin molecules in the laser trap," *Biophysical Journal*, vol. 89, no. 5, pp. L34–L36, 2005.

[184] E. Pate, H. White, and R. Cooke, "Determination of the myosin step size from mechanical and kinetic data," *Proceedings of the National Academy of Sciences of the United States of America*, vol. 90, no. 6, pp. 2451–2455, 1993.

[185] R. W. Ramsey and S. F. Street, "The isometric length-tension diagram of isolated skeletal muscle fibers of the frog," *Journal of Cellular and Comparative Physiology*, vol. 15, no. 1, pp. 11–34, 1940.

[186] J. Lannergren and H. Westerblad, "The temperature dependence of isometric contractions of single, intact fibres dissected from a mouse foot muscle," *Journal of Physiology*, vol. 390, pp. 285–293, 1987.

[187] F. J. Julian, "The effect of calcium on the force-velocity relation of briefly glycerinated frog muscle fibres," *The Journal of Physiology*, vol. 218, no. 1, pp. 117–145, 1971.

[188] R. Natori, "The role of myofibrils, sarcoplasm and sarcolemma," *Jikeikai Medical Journal*, vol. 1, pp. 177–192, 1954.

[189] A. Szent-Gyorgyi, "Free-energy relations and contraction of actomyosin," *The Biological Bulletin*, vol. 96, no. 2, pp. 140–161, 1949.

[190] A. V. Hill, "The heat of shortening and the dynamic constants of muscle," *Proceedings of the Royal Society B*, vol. 126, pp. 136–195, 1938.

[191] K. A. P. Edman, "Double-hyperbolic force-velocity relation in frog muscle fibres," *Journal of Physiology*, vol. 404, pp. 301–321, 1988.

[192] R. Cooke and E. Pate, "The effects of ADP and phosphate on the contraction of muscle fibers," *Biophysical Journal*, vol. 48, no. 5, pp. 789–798, 1985.

[193] R. Cooke and W. Bialek, "Contraction of glycerinated muscle fibers as a function of the ATP concentration," *Biophysical Journal*, vol. 28, no. 2, pp. 241–258, 1979.

[194] M. A. Ferenczi, Y. E. Goldman, and R. M. Simmons, "The dependence of force and shortening velocity on substrate concentration in skinned muscle fibres from Rana temporara," *The Journal of Physiology*, vol. 350, pp. 519–543, 1984.

[195] G. Cecchi, F. Colomo, and V. Lombardi, "Force-velocity relation in normal and nitrate-treated frog single muscle fibres during rise of tension in an isometric tetanus," *Journal of Physiology*, vol. 285, pp. 257–273, 1978.

[196] M. Reconditi, M. Linari, L. Lucii et al., "The myosin motor in muscle generates a smaller and slower working stroke at higher load," *Nature*, vol. 428, no. 6982, pp. 578–581, 2004.

[197] F. C. Minozzo and D. E. Rassier, "Effects of blebbistatin and Ca^{2+} concentration on force produced during stretch of skeletal muscle fibers," *American Journal of Physiology: Cell Physiology*, vol. 299, no. 5, pp. C1127–C1135, 2010.

[198] F. C. Minozzo and D. E. Rassier, "The effects of Ca2+ and MgADP on force development during and after muscle length changes," *PLoS ONE*, vol. 8, no. 7, Article ID e68866, 2013.

[199] K. A. P. Edman, G. Elzinga, and M. I. M. Noble, "Critical sarcomere extension required to recruit a decaying component of extra force during stretch in tetanic contractions of frog skeletal muscle fibers," *The Journal of General Physiology*, vol. 78, no. 4, pp. 365–382, 1981.

[200] F. W. Flitney and D. G. Hirst, "Cross-bridge detachment and sarcomere "give" during stretch of active frog's muscle," *The Journal of Physiology*, vol. 276, pp. 449–465, 1978.

[201] G. J. Pinniger, K. W. Ranatunga, and G. W. Offer, "Crossbridge and non-crossbridge contributions to tension in lengthening rat muscle: Force-induced reversal of the power stroke," *Journal of Physiology*, vol. 573, part 3, pp. 627–643, 2006.

[202] H. Roots, G. W. Offer, and K. W. Ranatunga, "Comparison of the tension responses to ramp shortening and lengthening in intact mammalian muscle fibres: crossbridge and non-crossbridge contributions," *Journal of Muscle Research and Cell Motility*, vol. 28, no. 2-3, pp. 123–139, 2007.

[203] V. Lombardi, G. Piazzesi, and M. Linari, "Rapid regeneration of the actin-myosin power stroke in contracting muscle," *Nature*, vol. 355, no. 6361, pp. 638–641, 1992.

[204] A. Mansson, "Changes in force and stiffness during stretch of skeletal muscle fibers, effects of hypertonicity," *Biophysical Journal*, vol. 56, no. 2, pp. 429–433, 1989.

[205] K. A. P. Edman, G. Elzinga, and M. I. M. Noble, "Enhancement of mechanical performance by stretch during tetanic contractions of vertebrate skeletal muscle fibres," *Journal of Physiology*, vol. 281, pp. 139–155, 1978.

[206] B. Colombini, M. A. Bagni, G. Romano, and G. Cecchi, "Characterization of actomyosin bond properties in intact skeletal muscle by force spectroscopy," *Proceedings of the National Academy of Sciences of the United States of America*, vol. 104, no. 22, pp. 9284–9289, 2007.

[207] D. E. Rassier, "Pre-power stroke cross bridges contribute to force during stretch of skeletal muscle myofibrils," *Proceedings of the Royal Society B: Biological Sciences*, vol. 275, no. 1651, pp. 2577–2586, 2008.

[208] M. Chinn, E. B. Getz, R. Cooke, and S. L. Lehman, "Force enhancement by PEG during ramp stretches of skeletal muscle," *Journal of Muscle Research and Cell Motility*, vol. 24, no. 8, pp. 571–578, 2003.

[209] K. W. Ranatunga, "Force and power generating mechanism(s) in active muscle as revealed from temperature perturbation studies," *Journal of Physiology*, vol. 588, no. 19, pp. 3657–3670, 2010.

[210] D. E. Rassier and W. Herzog, "Active force inhibition and stretch-induced force enhancement in frog muscle treated with BDM," *Journal of Applied Physiology*, vol. 97, no. 4, pp. 1395–1400, 2004.

[211] G. Piazzesi, M. Reconditi, N. Koubassova et al., "Temperature dependence of the force-generating process in single fibres from frog skeletal muscle," *The Journal of Physiology*, vol. 549, no. 1, pp. 93–106, 2003.

[212] L. E. Ford, A. F. Huxley, and R. M. Simmons, "Tension responses to sudden length change in stimulated frog muscle fibres near slack length," *Journal of Physiology*, vol. 269, no. 2, pp. 441–515, 1977.

[213] L. E. Ford, A. F. Huxley, and R. M. Simmons, "The relation between stiffness and filament overlap in stimulated frog muscle fibres," *The Journal of Physiology*, vol. 311, pp. 219–249, 1981.

[214] L. E. Ford, A. F. Huxley, and R. M. Simmons, "Tension transients during steady shortening of frog muscle fibres," *Journal of Physiology*, vol. 361, pp. 131–150, 1985.

[215] L. E. Ford, A. F. Huxley, and R. M. Simmons, "Tension transients during the rise of tetanic tension in frog muscle fibres," *Journal of Physiology*, vol. 372, pp. 595–609, 1986.

[216] C. J. Barclay, R. C. Woledge, and N. A. Curtin, "Inferring crossbridge properties from skeletal muscle energetics," *Progress in Biophysics and Molecular Biology*, vol. 102, no. 1, pp. 53–71, 2010.

[217] S. Y. Bershitsky, A. K. Tsaturyan, O. N. Bershitskaya et al., "Muscle force is generated by myosin heads stereospecifically attached to action," *Nature*, vol. 388, no. 6638, pp. 186–190, 1997.

[218] B. Seebohm, F. Matinmehr, J. Köhler et al., "Cardiomyopathy mutations reveal variable region of myosin converter as major element of cross-bridge compliance," *Biophysical Journal*, vol. 97, no. 3, pp. 806–824, 2009.

[219] K. Pant, J. Watt, M. Greenberg, M. Jones, D. Szczesna-Cordary, and J. R. Moore, "Removal of the cardiac myosin regulatory light chain increases isometric force production," *The FASEB Journal*, vol. 23, no. 10, pp. 3571–3580, 2009.

[220] I. Dobbie, M. Linari, G. Piazzesi et al., "Elastic bending and active tilting of myosin heads during muscle contraction," *Nature*, vol. 396, no. 6709, pp. 383–387, 1998.

[221] A. Lewalle, W. Steffen, O. Stevenson, Z. Ouyang, and J. Sleep, "Single-molecule measurement of the stiffness of the rigor myosin head," *Biophysical Journal*, vol. 94, no. 6, pp. 2160–2169, 2008.

[222] G. Offer and K. W. Ranatunga, "Crossbridge and filament compliance in muscle: implications for tension generation and lever arm swing," *Journal of Muscle Research and Cell Motility*, vol. 31, no. 4, pp. 245–265, 2010.

[223] S. Highsmith, "Electrostatic contributions to the binding of myosin and myosin-MgADP to F-actin in solution," *Biochemistry*, vol. 29, no. 47, pp. 10690–10694, 1990.

[224] Y. Zhao and M. Kawai, "The hydrophobic interaction between actin and myosin underlies the mechanism of force generation by cross-bridges," *Biophysical Journal*, vol. 68, no. 4, supplement, p. 332s, 1995.

[225] K. W. Ranatunga, M. E. Coupland, and G. Mutungi, "An asymmetry in the phosphate dependence of tension transients induced by length perturbation in mammalian (rabbit psoas) muscle fibres," *The Journal of Physiology*, vol. 542, no. 3, pp. 899–910, 2002.

[226] Y. E. Goldman, J. A. McCray, and K. W. Ranatunga, "Transient tension changes initiated by laser temperature jumps in rabbit psoas muscle fibres," *The Journal of Physiology*, vol. 392, pp. 71–95, 1987.

[227] J. S. Davis and W. F. Harrington, "Force generation by muscle fibers in rigor: a laser temperature-jump study," *Proceedings of the National Academy of Sciences of the United States of America*, vol. 84, no. 4, pp. 975–979, 1987.

[228] K. W. Ranatunga, "Endothermic force generation in fast and slow mammalian (rabbit) muscle fibers," *Biophysical Journal*, vol. 71, no. 4, pp. 1905–1913, 1996.

[229] J. S. Davis and M. E. Rodgers, "Force generation and temperature-jump and length-jump tension transients in muscle fibers," *Biophysical Journal*, vol. 68, no. 5, pp. 2032–2040, 1995.

[230] J. S. Davis and N. D. Epstein, "Mechanistic role of movement and strain sensitivity in muscle contraction," *Proceedings of the National Academy of Sciences of the United States of America*, vol. 106, no. 15, pp. 6140–6145, 2009.

[231] S. Y. Bershitsky and A. K. Tsaturyan, "Effect of joule temperature jump on tension and stiffness of skinned rabbit muscle fibers," *Biophysical Journal*, vol. 56, no. 5, pp. 809–816, 1989.

[232] N. S. Fortune, M. A. Geeves, and K. W. Ranatunga, "Tension responses to rapid pressure release in glycerinated rabbit muscle fibers," *Proceedings of the National Academy of Sciences of the United States of America*, vol. 88, no. 16, pp. 7323–7327, 1991.

[233] J. A. Dantzig, Y. E. Goldman, N. C. Millar, J. Lacktis, and E. Homsher, "Reversal of the cross-bridge force-generating transition by photogeneration of phosphate in rabbit psoas muscle fibres," *The Journal of Physiology*, vol. 451, pp. 247–278, 1992.

[234] E. Homsher, J. Lacktis, and M. Regnier, "Strain-dependent modulation of phosphate transients in rabbit skeletal muscle fibers," *Biophysical Journal*, vol. 72, no. 4, pp. 1780–1791, 1997.

[235] C. Tesi, F. Colomo, S. Nencini, N. Piroddi, and C. Poggesi, "The effect of inorganic phosphate on force generation in single myofibrils from rabbit skeletal muscle," *Biophysical Journal*, vol. 78, no. 6, pp. 3081–3092, 2000.

[236] M. Caremani, J. Dantzig, Y. E. Goldman, V. Lombardi, and M. Linari, "Effect of inorganic phosphate on the force and number of myosin cross-bridges during the isometric contraction of permeabilized muscle fibers from rabbit psoas," *Biophysical Journal*, vol. 95, no. 12, pp. 5798–5808, 2008.

[237] U. A. van der Heide, M. Ketelaars, B. W. Treijtel, E. L. de Beer, and T. Blangé, "Strain dependence of the elastic properties of force-producing cross- bridges in rigor skeletal muscle," *Biophysical Journal*, vol. 72, no. 2, part 1, pp. 814–821, 1997.

[238] H. E. Huxley, A. Stewart, H. Sosa, and T. Irving, "X-ray diffraction measurements of the extensibility of actin and myosin filaments in contracting muscle," *Biophysical Journal*, vol. 67, no. 6, pp. 2411–2421, 1994.

[239] K. Wakabayashi, Y. Sugimoto, H. Tanaka, Y. Ueno, Y. Takezawa, and Y. Amemiya, "X-ray diffraction evidence for the extensibility of actin and myosin filaments during muscle contraction," *Biophysical Journal*, vol. 67, no. 6, pp. 2422–2435, 1994.

[240] H. Higuchi, T. Yanagida, and Y. E. Goldman, "Compliance of thin filaments in skinned fibers of rabbit skeletal muscle," *Biophysical Journal*, vol. 69, no. 3, pp. 1000–1010, 1995.

[241] A. Månsson, "Significant impact on muscle mechanics of small nonlinearities in myofilament elasticity," *Biophysical Journal*, vol. 99, no. 6, pp. 1869–1875, 2010.

[242] K. A. P. Edman, "Non-linear myofilament elasticity in frog intact muscle fibres," *Journal of Experimental Biology*, vol. 212, no. 8, pp. 1115–1119, 2009.

[243] B. Colombina, M. Nocella, M. A. Bagni, P. J. Griffiths, and G. Cecchi, "Is the cross-bridge stiffness proportional to tension during muscle fiber activation?" *Biophysical Journal*, vol. 98, no. 11, pp. 2582–2590, 2010.

[244] G. Piazzesi, M. Dolfi, E. Brunello et al., "The myofilament elasticity and its effect on kinetics of force generation by the myosin motor," *Archives of Biochemistry and Biophysics*, vol. 552-553, pp. 108–116, 2014.

[245] H. E. Huxley, R. M. Simmons, A. R. Faruqi, M. Kress, J. Bordas, and M. H. J. Koch, "Changes in the X-ray reflections from contracting muscle during rapid mechanical transients and their structural implications," *Journal of Molecular Biology*, vol. 169, no. 2, pp. 469–506, 1983.

[246] C. Knupp, G. Offer, K. W. Ranatunga, and J. M. Squire, "Probing muscle myosin motor action: x-ray (m3 and m6) interference measurements report motor domain not lever arm movement," *Journal of Molecular Biology*, vol. 390, no. 2, pp. 168–181, 2009.

[247] H. E. Huxley, "Recent X-ray diffraction studies of muscle contraction and their implications," *Philosophical Transactions of the Royal Society B: Biological Sciences*, vol. 359, no. 1452, pp. 1879–1882, 2004.

[248] J. M. Squire and C. Knupp, "X-ray diffraction studies of muscle and the crossbridge cycle," *Advances in Protein Chemistry*, vol. 71, pp. 195–255, 2005.

[249] S. Y. Bershitsky, M. A. Ferenczi, N. A. Koubassova, and A. K. Tsaturyan, "Insight into the actin-myosin motor from x-ray diffraction on muscle," *Frontiers in Bioscience*, vol. 14, no. 8, pp. 3188–3213, 2009.

[250] S. G. Campbell, P. C. Hatfield, and K. S. Campbell, "A mathematical model of muscle containing heterogeneous half-sarcomeres exhibits residual force enhancement," *PLoS Computational Biology*, vol. 7, no. 9, Article ID e1002156, 2011.

[251] K. A. P. Edman, C. Reggiani, S. Schiaffino, and G. Te Kronnie, "Maximum velocity of shortening related to myosin isoform composition in frog skeletal muscle fibres," *The Journal of Physiology*, vol. 395, pp. 679–694, 1988.

[252] K. A. P. Edman and C. Reggiani, "Redistribution of sarcomere length during isometric contraction of frog muscle fibres and its relation to tension creep," *Journal of Physiology*, vol. 351, pp. 169–198, 1984.

[253] D. Cleworth and K. A. P. Edman, "Laser diffraction studies on single skeletal muscle fibers," *Science*, vol. 163, no. 3864, pp. 296–298, 1969.

[254] B. W. C. Rosser and E. Bandman, "Heterogeneity of protein expression within muscle fibers," *Journal of Animal Science*, vol. 81, pp. E94–E101, 2003.

[255] C. Poggesi, C. Tesi, and R. Stehle, "Sarcomeric determinants of striated muscle relaxation kinetics," *Pflügers Archiv*, vol. 449, no. 6, pp. 505–517, 2005.

[256] R. Stehle, M. Krüger, and G. Pfitzer, "Force kinetics and individual sarcomere dynamics in cardiac myofibrils after rapid Ca^{2+} changes," *Biophysical Journal*, vol. 83, no. 4, pp. 2152–2161, 2002.

[257] I. A. Telley, R. Stehle, K. W. Ranatunga, G. Pfitzer, E. Stüssi, and J. Denoth, "Dynamic behaviour of half-sarcomeres during and after stretch in activated rabbit psoas myofibrils: sarcomere asymmetry but no "sarcomere popping"," *The Journal of Physiology*, vol. 573, no. 1, pp. 173–185, 2006.

[258] S. Weiss, R. Rossi, M.-A. Pellegrino, R. Bottinelli, and M. A. Geeves, "Differing ADP release rates from myosin heavy chain isoforms define the shortening velocity of skeletal muscle fibers," *Journal of Biological Chemistry*, vol. 276, no. 49, pp. 45902–45908, 2001.

[259] P. Hook and L. Larsson, "Actomyosin interactions in a novel single muscle fiber in vitro motility assay," *Journal of Muscle Research and Cell Motility*, vol. 21, no. 4, pp. 357–365, 2000.

[260] M. Canepari, R. Rossi, M. A. Pellegrino, C. Reggiani, and R. Bottinelli, "Speeds of actin translocation in vitro by myosins extracted from single rat muscle fibres of different types," *Experimental Physiology*, vol. 84, no. 4, pp. 803–806, 1999.

[261] M. Sata, S. Sugiura, H. Yamashita, S.-I. Momomura, and T. Serizawa, "Dynamic interaction between cardiac myosin isoforms modifies velocity of actomyosin sliding in vitro," *Circulation Research*, vol. 73, no. 4, pp. 696–704, 1993.

[262] D. E. Harris and D. M. Warshaw, "Smooth and skeletal muscle actin are mechanically indistinguishable in the in vitro motility assay," *Circulation Research*, vol. 72, no. 1, pp. 219–224, 1993.

[263] E. Homsher, D. M. Lee, C. Morris, D. Pavlov, and L. S. Tobacman, "Regulation of force and unloaded sliding speed in single thin filaments: effects of regulatory proteins and calcium," *The Journal of Physiology*, vol. 524, no. 1, pp. 233–243, 2000.

[264] M. Stewart, K. Franks-Skiba, and R. Cooke, "Myosin regulatory light chain phosphorylation inhibits shortening velocities of skeletal muscle fibers in the presence of the myosin inhibitor blebbistatin," *Journal of Muscle Research and Cell Motility*, vol. 30, no. 1-2, pp. 17–27, 2009.

[265] C. Tesi, F. Colomo, N. Piroddi, and C. Poggesi, "Characterization of the cross-bridge force-generating step using inorganic phosphate and BDM in myofibrils from rabbit skeletal muscles," *Journal of Physiology*, vol. 541, no. 1, pp. 187–199, 2002.

[266] C. Pun, A. Syed, and D. E. Rassier, "History-dependent properties of skeletal muscle myofibrils contracting along the ascending limb of the force-length relationship," *Proceedings of the Royal Society B: Biological Sciences*, vol. 277, no. 1680, pp. 475–484, 2010.

[267] B. Brenner and E. Eisenberg, "Rate of force generation in muscle: correlation with actomyosin ATPase activity in solution," *Proceedings of the National Academy of Sciences of the United States of America*, vol. 83, no. 10, pp. 3542–3546, 1986.

[268] A. Belus, N. Piroddi, B. Scellini et al., "The familial hypertrophic cardiomyopathy-associated myosin mutation R403Q accelerates tension generation and relaxation of human cardiac myofibrils," *The Journal of Physiology*, vol. 586, no. 15, pp. 3639–3644, 2008.

[269] S. Kurosaka, N. A. Leu, I. Pavlov et al., "Arginylation regulates myofibrils to maintain heart function and prevent dilated cardiomyopathy," *Journal of Molecular and Cellular Cardiology*, vol. 53, no. 3, pp. 333–341, 2012.

[270] P. A. B. Ribeiro, J. P. Ribeiro, F. C. Minozzo et al., "Contractility of myofibrils from the heart and diaphragm muscles measured with atomic force cantilevers: effects of heart-specific deletion of arginyl-tRNA-protein transferase," *International Journal of Cardiology*, vol. 168, no. 4, pp. 3564–3571, 2013.

[271] D. E. Rassier and I. Pavlov, "Force produced by isolated sarcomeres and half-sarcomeres after an imposed stretch," *The American Journal of Physiology—Cell Physiology*, vol. 302, no. 1, pp. C240–C248, 2012.

[272] F. C. Minozzo, B. M. Baroni, J. A. Correa, M. A. Vaz, and D. E. Rassier, "Force produced after stretch in sarcomeres and half-sarcomeres isolated from skeletal muscles," *Scientific Reports*, vol. 3, article 2320, 2013.

[273] R. R. Schroder, D. J. Manstein, W. Jahn et al., "Three-dimensional atomic model of F-actin decorated with *Dictyostelium* myosin S1," *Nature*, vol. 364, no. 6433, pp. 171–174, 1993.

[274] M. Lorenz and K. C. Holmes, "The actin-myosin interface," *Proceedings of the National Academy of Sciences of the United States of America*, vol. 107, no. 28, pp. 12529–12534, 2010.

[275] S. Fischer, B. Windshügel, D. Horak, K. C. Holmes, and J. C. Smith, "Structural mechanism of the recovery stroke in the myosin molecular motor," *Proceedings of the National Academy of Sciences of the United States of America*, vol. 102, no. 19, pp. 6873–6878, 2005.

[276] C. A. Smith and I. Rayment, "X-ray structure of the magnesium(II)-pyrophosphate complex of the truncated head of Dictyostelium discoideum myosin to 2.7 A resolution," *Biochemistry*, vol. 34, no. 28, pp. 8973–8981, 1995.

[277] R. Dominguez, Y. Freyzon, K. M. Trybus, and C. Cohen, "Crystal structure of a vertebrate smooth muscle myosin motor domain and its complex with the essential light chain: visualization of the pre-power stroke state," *Cell*, vol. 94, no. 5, pp. 559–571, 1998.

[278] S. Gourinath, D. M. Himmel, J. H. Brown, L. Reshetnikova, A. G. Szent-Györgyi, and C. Cohen, "Crystal structure of scallop Myosin s1 in the pre-power stroke state to 2.6 Å resolution: flexibility and function in the head," *Structure*, vol. 11, no. 12, pp. 1621–1627, 2003.

[279] A. Houdusse, A. G. Szent-Györgyi, and C. Cohen, "Three conformational states of scallop myosin S1," *Proceedings of the National Academy of Sciences of the United States of America*, vol. 97, no. 21, pp. 11238–11243, 2000.

[280] C. B. Bauer, H. M. Holden, J. B. Thoden, R. Smith, and I. Rayment, "X-ray structures of the Apo and MgATP-bound states of *Dictyostelium discoideum* myosin motor domain," *The Journal of Biological Chemistry*, vol. 275, no. 49, pp. 38494–38499, 2000.

[281] A. M. Gulick, C. B. Bauer, J. B. Thoden, and I. Rayment, "X-ray structures of the MgADP, MgATPγS, and MgAMPPNP complexes of the *Dictyostelium discoideum* myosin motor domain," *Biochemistry*, vol. 36, no. 39, pp. 11619–11628, 1997.

[282] J. Ménétrey, P. Llinas, J. Cicolari et al., "The post-rigor structure of myosin VI and implications for the recovery stroke," *The EMBO Journal*, vol. 27, no. 1, pp. 244–252, 2008.

[283] D. A. Winkelmann, T. S. Baker, and I. Rayment, "Three-dimensional structure of myosin subfragment-1 from electron microscopy of sectioned crystals," *The Journal of Cell Biology*, vol. 114, no. 4, pp. 701–713, 1991.

[284] P.-D. Coureux, H. L. Sweeney, and A. Houdusse, "Three myosin V structures delineate essential features of chemo-mechanical transduction," *The EMBO Journal*, vol. 23, no. 23, pp. 4527–4537, 2004.

[285] J. Menetrey, A. Bahloul, A. L. Wells et al., "The structure of the myosin VI motor reveals the mechanism of directionality reversal," *Nature*, vol. 435, no. 7043, pp. 779–785, 2005.

[286] P.-D. Coureux, A. L. Wells, J. Ménétrey et al., "A structural state of the myosin V motor without bound nucleotide," *Nature*, vol. 425, no. 6956, pp. 419–423, 2003.

[287] T. F. Reubold, S. Eschenburg, A. Becker, F. J. Kull, and D. J. Manstein, "A structural model for actin-induced nucleotide release in myosin," *Nature Structural Biology*, vol. 10, no. 10, pp. 826–830, 2003.

[288] Y. Yang, S. Gourinath, M. Kovács et al., "Rigor-like structures from muscle myosins reveal key mechanical elements in the transduction pathways of this allosteric motor," *Structure*, vol. 15, no. 5, pp. 553–564, 2007.

[289] B. Takács, E. O'Neall-Hennessey, C. Hetényi, J. Kardos, A. G. Szent-Györgyi, and M. Kovács, "Myosin cleft closure determines the energetics of the actomyosin interaction," *The FASEB Journal*, vol. 25, no. 1, pp. 111–121, 2011.

[290] K. C. Holmes, I. Angert, F. J. Kull, W. Jahn, and R. R. Schröder, "Elechron cryo-microscopy shows how strong binding of myosin to actin releases nucleotide," *Nature*, vol. 425, no. 6956, pp. 423–427, 2003.

[291] E. Behrmann, M. Müller, P. A. Penczek, H. G. Mannherz, D. J. Manstein, and S. Raunser, "Structure of the rigor actin-tropomyosin-myosin complex," *Cell*, vol. 150, no. 2, pp. 327–338, 2012.

[292] M. A. Geeves, T. E. Jeffries, and N. C. Millar, "ATP-induced dissociation of rabbit skeletal actomyosin subfragment 1. Characterization of an isomerization of the ternary Acto-S1-ATP complex," *Biochemistry*, vol. 25, no. 26, pp. 8454–8458, 1986.

[293] M. Furch, S. Fujita-Becker, M. A. Geeves, K. C. Holmes, and D. J. Manstein, "Role of the salt-bridge between switch-1 and switch-2 of *Dictyostelium* myosin," *Journal of Molecular Biology*, vol. 290, no. 3, pp. 797–809, 1999.

[294] H. Onishi, M. F. Morales, S.-I. Kojima, K. Katoh, and K. Fujiwara, "Functional transitions in myosin: role of highly conserved Gly and Glu residues in the active site," *Biochemistry*, vol. 36, no. 13, pp. 3767–3772, 1997.

[295] N. Sasaki and K. Sutoh, "Structure-mutation analysis of the ATPase site of Dictyostelium discoideum myosin II," *Advances in Biophysics*, vol. 35, pp. 1–24, 1998.

[296] N. Sasaki, T. Shimada, and K. Sutoh, "Mutational analysis of the switch II loop of Dictyostelium myosin II," *Journal of Biological Chemistry*, vol. 273, no. 32, pp. 20334–20340, 1998.

[297] P. B. Conibear, C. R. Bagshaw, P. G. Fajer, M. Kovács, and A. Málnási-Csizmadia, "Myosin cleft movement and its coupling to actomyosin dissociation," *Nature Structural Biology*, vol. 10, no. 10, pp. 831–835, 2003.

[298] H. Onishi, N. Mochizuki, and M. F. Morales, "On the myosin catalysis of ATP hydrolysis," *Biochemistry*, vol. 43, no. 13, pp. 3757–3763, 2004.

[299] T. Ohki, S. V. Mikhailenko, M. F. Morales, H. Onishi, and N. Mochizuki, "Transmission of force and displacement within the myosin molecule," *Biochemistry*, vol. 43, no. 43, pp. 13707–13714, 2004.

[300] A. J. Fisher, C. A. Smith, J. B. Thoden et al., "X-ray structures of the myosin motor domain of Dictyostelium discoideum complexed with MgADP·BeFx and MgADP·AlF4-," *Biochemistry*, vol. 34, no. 28, pp. 8960–8972, 1995.

[301] A. J. Fisher, C. A. Smith, J. Thoden et al., "Structural studies of myosin:nucleotide complexes: a revised model for the molecular basis of muscle contraction," *Biophysical Journal*, vol. 68, no. 4, supplement, pp. 19S–28S, 1995.

[302] G. Tsiavaliaris, S. Fujita-Becker, R. Batra et al., "Mutations in the relay loop region result in dominant-negative inhibition of myosin II function in dictyostelium," *EMBO Reports*, vol. 3, no. 11, pp. 1099–1105, 2002.

[303] S. Mesentean, S. Koppole, J. C. Smith, and S. Fischer, "The principal motions involved in the coupling mechanism of the recovery stroke of the myosin motor," *Journal of Molecular Biology*, vol. 367, no. 2, pp. 591–602, 2007.

[304] A. Málnási-Csizmadia, J. Tóth, D. S. Pearson et al., "Selective perturbation of the myosin recovery stroke by point mutations at the base of the lever arm affects ATP hydrolysis and phosphate release," *The Journal of Biological Chemistry*, vol. 282, no. 24, pp. 17658–17664, 2007.

[305] S. Koppole, J. C. Smith, and S. Fischer, "The structural coupling between ATPase activation and recovery stroke in the myosin II motor," *Structure*, vol. 15, no. 7, pp. 825–837, 2007.

[306] S. Koppole, J. C. Smith, and S. Fischer, "Simulations of the myosin II motor reveal a nucleotide-state sensing element that controls the recovery stroke," *Journal of Molecular Biology*, vol. 361, no. 3, pp. 604–616, 2006.

[307] M. Gyimesi, B. Kintses, A. Bodor et al., "The mechanism of the reverse recovery step, phosphate release, and actin activation of *Dictyostelium myosin* II," *The Journal of Biological Chemistry*, vol. 283, no. 13, pp. 8153–8163, 2008.

[308] A. Baumketner, "The mechanism of the converter domain rotation in the recovery stroke of myosin motor protein," *Proteins*, vol. 80, no. 12, pp. 2701–2710, 2012.

[309] A. Baumketner and Y. Nesmelov, "Early stages of the recovery stroke in myosin II studied by molecular dynamics simulations," *Protein Science*, vol. 20, no. 12, pp. 2013–2022, 2011.

[310] C. M. Yengo and H. L. Sweeney, "Functional role of loop 2 in myosin V," *Biochemistry*, vol. 43, no. 9, pp. 2605–2612, 2004.

[311] A. Lieto-Trivedi, S. Dash, and L. M. Coluccio, "Myosin surface loop 4 modulates inhibition of actomyosin 1b atpase activity by tropomyosin," *Biochemistry*, vol. 46, no. 10, pp. 2779–2786, 2007.

[312] D. Funabara, R. Osawa, M. Ueda, S. Kanoh, D. J. Hartshorne, and S. Watabe, "Myosin loop 2 is involved in the formation of a trimeric complex of twitchin, actin, and myosin," *The Journal of Biological Chemistry*, vol. 284, no. 27, pp. 18015–18020, 2009.

[313] A. M. Clobes and W. H. Guilford, "Loop 2 of myosin is a force-dependent inhibitor of the rigor bond," *Journal of Muscle Research and Cell Motility*, vol. 35, no. 2, pp. 143–152, 2014.

[314] B. H. Várkuti, Z. Yang, B. Kintses et al., "A novel actin binding site of myosin required for effective muscle contraction," *Nature Structural & Molecular Biology*, vol. 19, no. 3, pp. 299–306, 2012.

[315] H. Onishi, S. V. Mikhailenko, and M. F. Morales, "Toward understanding actin activation of myosin ATPase: the role of myosin surface loops," *Proceedings of the National Academy of Sciences of the United States of America*, vol. 103, no. 16, pp. 6136–6141, 2006.

[316] F. G. Díaz Baños, J. Bordas, J. Lowy, and A. Svensson, "Small segmental rearrangements in the myosin head can explain force generation in muscle," *Biophysical Journal*, vol. 71, no. 2, pp. 576–589, 1996.

[317] D. D. Thomas, E. Prochniewicz, and O. Roopnarine, "Changes in actin and myosin structural dynamics due to their weak and strong interactions," *Results and Problems in Cell Differentiation*, vol. 36, pp. 7–19, 2002.

[318] M. Preller and K. C. Holmes, "The myosin start-of-power stroke state and how actin binding drives the power stroke," *Cytoskeleton*, vol. 70, no. 10, pp. 651–660, 2013.

[319] B. Kintses, M. Gyimesi, D. S. Pearson et al., "Reversible movement of switch 1 loop of myosin determines actin interaction," *The EMBO Journal*, vol. 26, no. 1, pp. 265–274, 2007.

[320] W. Zeng, P. B. Conibear, J. L. Dickens et al., "Dynamics of actomyosin interactions in relation to the cross-bridge cycle," *Philosophical Transactions of the Royal Society B: Biological Sciences*, vol. 359, no. 1452, pp. 1843–1855, 2004.

[321] J. Sleep, M. Irving, and K. Burton, "The ATP hydrolysis and phosphate release steps control the time course of force development in rabbit skeletal muscle," *The Journal of Physiology*, vol. 563, part 3, pp. 671–687, 2005.

[322] Z.-H. He, R. K. Chillingworth, M. Brune et al., "ATPase kinetics on activation of rabbit and frog permeabilized isometric muscle fibres: a real time phosphate assay," *The Journal of Physiology*, vol. 501, no. 1, pp. 125–148, 1997.

[323] J. M. Muretta, K. J. Petersen, and D. D. Thomas, "Direct real-time detection of the actin-activated power stroke within the myosin catalytic domain," *Proceedings of the National Academy of Sciences of the United States of America*, vol. 110, no. 18, pp. 7211–7216, 2013.

[324] D. A. Smith and J. Sleep, "Mechanokinetics of rapid tension recovery in muscle: the myosin working stroke is followed by a slower release of phosphate," *Biophysical Journal*, vol. 87, no. 1, pp. 442–456, 2004.

[325] C. Lionne, M. Brune, M. R. Webb, F. Travers, and T. Barman, "Time resolved measurements show that phosphate release is the rate limiting step on myofibrillar ATPases," *FEBS Letters*, vol. 364, no. 1, pp. 59–62, 1995.

[326] R. F. Siemankowski, M. O. Wiseman, and H. D. White, "ADP dissociation from actomyosin subfragment 1 is sufficiently slow to limit the unloaded shortening velocity in vertebrate muscle," *Proceedings of the National Academy of Sciences of the United States of America*, vol. 82, no. 3, pp. 658–662, 1985.

[327] R. Elangovan, M. Capitanio, L. Melli, F. S. Pavone, V. Lombardi, and G. Piazzesi, "An integrated in vitro and in situ study of kinetics of myosin II from frog skeletal muscle," *The Journal of Physiology*, vol. 590, no. 5, pp. 1227–1242, 2012.

[328] R. Bowater and J. Sleep, "Demembranated muscle fibers catalyze a more rapid exchange between phosphate and adenosine triphosphate than actomyosin subfragment," *Biochemistry*, vol. 27, no. 14, pp. 5314–5323, 1988.

[329] C. Mansfield, T. G. West, N. A. Curtin, and M. A. Ferenczi, "Stretch of contracting cardiac muscle abruptly decreases the rate of phosphate release at high and low calcium," *The Journal of Biological Chemistry*, vol. 287, no. 31, pp. 25696–25705, 2012.

[330] Y. Takagi, H. Shuman, and Y. E. Goldman, "Coupling between phosphate release and force generation in muscle actomyosin," *Philosophical Transactions of the Royal Society B: Biological Sciences*, vol. 359, no. 1452, pp. 1913–1920, 2004.

[331] E. Pate and R. Cooke, "A model of crossbridge action: the effects of ATP, ADP and Pi," *Journal of Muscle Research and Cell Motility*, vol. 10, no. 3, pp. 181–196, 1989.

[332] J. Liu, T. Wendt, D. Taylor, and K. Taylor, "Refined model of the 10S conformation of smooth muscle myosin by cryo-electron microscopy 3D image reconstruction," *Journal of Molecular Biology*, vol. 329, no. 5, pp. 963–972, 2003.

[333] J. W. Shriver, "Energy transduction in myosin," *Trends in Biochemical Sciences*, vol. 9, no. 7, pp. 322–328, 1984.

[334] S. Xu, H. D. White, G. W. Offer, and L. C. Yu, "Stabilization of helical order in the thick filaments by blebbistatin: further evidence of coexisting multiple conformations of myosin," *Biophysical Journal*, vol. 96, no. 9, pp. 3673–3681, 2009.

[335] M. F. Norstrom, P. A. Smithback, and R. S. Rock, "Unconventional processive mechanics of non-muscle myosin IIB," *The Journal of Biological Chemistry*, vol. 285, no. 34, pp. 26326–26334, 2010.

[336] D. D. Hackney and P. K. Clark, "Catalytic consequences of oligometric organization: Kinetic evidence for "tethered" acto-heavy meromyosin at low ATP concentrations," *Proceedings of the National Academy of Sciences of the United States of America*, vol. 81, no. 17, pp. 5345–5349, 1984.

[337] S. Ishiwata, Y. Shimamoto, D. Sasaki, and M. Suzuki, "Molecular synchronization in actomyosin motors—from single molecule to muscle fiber via nanomuscle," *Advances in Experimental Medicine and Biology*, vol. 565, pp. 25–36, 2005.

[338] K. Ito, X. Liu, E. Katayama, and T. Q. P. Uyeda, "Cooperativity between two heads of Dictyostelium myosin II in in vitro

motility and ATP hydrolysis," *Biophysical Journal*, vol. 76, no. 2, pp. 985–992, 1999.

[339] J. E. Molloy, "Muscle contraction: actin filaments enter the fray," *Biophysical Journal*, vol. 89, no. 1, pp. 1–2, 2005.

[340] D. S. Lidke and D. D. Thomas, "Coordination of the two heads of myosin during muscle contraction," *Proceedings of the National Academy of Sciences of the United States of America*, vol. 99, no. 23, pp. 14801–14806, 2002.

[341] N. M. Kad, A. S. Rovner, P. M. Fagnant et al., "A mutant heterodimeric myosin with one inactive head generates maximal displacement," *The Journal of Cell Biology*, vol. 162, no. 3, pp. 481–488, 2003.

[342] R. D. Vale and R. A. Milligan, "The way things move: looking under the hood of molecular motor proteins," *Science*, vol. 288, no. 5463, pp. 88–95, 2000.

[343] F. Oosawa, Y. Maeda, S. Fujime, S. Ishiwata, T. Yanagida, and M. Taniguchi, "Dynamic characteristics of F-actin and thin filaments in vivo and in vitro," *Journal of Mechanochemistry & Cell Motility*, vol. 4, no. 1, pp. 63–78, 1977.

[344] A. K. Tsaturyan, N. Koubassova, M. A. Ferenczi, T. Narayanan, M. Roessle, and S. Y. Bershitsky, "Strong binding of myosin heads stretches and twists the actin helix," *Biophysical Journal*, vol. 88, no. 3, pp. 1902–1910, 2005.

[345] E. H. Egelman, "New angles on actin dynamics," *Structure*, vol. 5, no. 9, pp. 1135–1137, 1997.

[346] C. E. Schutt and U. Lindberg, "Actin as the generator of tension during muscle contraction," *Proceedings of the National Academy of Sciences of the United States of America*, vol. 89, no. 1, pp. 319–323, 1992.

[347] B. C. W. Tanner, T. L. Daniel, and M. Regnier, "Sarcomere lattice geometry influences cooperative myosin binding in muscle," *PLoS Computational Biology*, vol. 3, no. 7, article e115, 2007.

[348] F. Bai, L. Wang, and M. Kawai, "A study of tropomyosin's role in cardiac function and disease using thin-filament reconstituted myocardium," *Journal of Muscle Research and Cell Motility*, vol. 34, no. 3-4, pp. 295–310, 2013.

[349] A. S. Cornachione and D. E. Rassier, "A non-cross-bridge, static tension is present in permeabilized skeletal muscle fibers after active force inhibition or actin extraction," *American Journal of Physiology: Cell Physiology*, vol. 302, no. 3, pp. C566–C574, 2012.

[350] J. E. Baker, C. Brosseau, P. B. Joel, and D. M. Warshaw, "The biochemical kinetics underlying actin movement generated by one and many skeletal muscle myosin molecules," *Biophysical Journal*, vol. 82, no. 4, pp. 2134–2147, 2002.

[351] M. W. Elting and J. A. Spudich, "Future challenges in single-molecule fluorescence and laser trap approaches to studies of molecular motors," *Developmental Cell*, vol. 23, no. 6, pp. 1084–1091, 2012.

[352] M. Lard, L. Ten Siethoff, A. Mansson, and H. Linke, "Molecular motor transport through hollow nanowires," *Nano Letters*, vol. 14, no. 6, pp. 3041–3046, 2014.

[353] G. Tsiavaliaris, S. Fujita-Becker, and D. J. Manstein, "Molecular engineering of a backwards-moving myosin motor," *Nature*, vol. 427, no. 6974, pp. 558–561, 2004.

[354] T. D. Schindler, L. Chen, P. Lebel, M. Nakamura, and Z. Bryant, "Engineering myosins for long-range transport on actin filaments," *Nature Nanotechnology*, vol. 9, no. 1, pp. 33–38, 2014.

[355] M. Amrute-Nayak, R. P. Diensthuber, W. Steffen et al., "Targeted optimization of a protein nanomachine for operation in biohybrid devices," *Angewandte Chemie International Edition*, vol. 49, no. 2, pp. 312–316, 2010.

[356] S. S. Margossian and S. Lowey, "Preparation of myosin and its subfragments from rabbit skeletal muscle," *Methods in Enzymology*, vol. 85, pp. 55–71, 1982.

[357] S. J. Kron, Y. Y. Toyoshima, T. Q. P. Uyeda, and J. A. Spudich, "Assays for actin sliding movement over myosin-coated surfaces," *Methods in Enzymology*, vol. 196, pp. 399–416, 1991.

[358] W. Kliche, S. Fujita-Becker, M. Kollmar, D. J. Manstein, and F. J. Kull, "Structure of a genetically engineered molecular motor," *The EMBO Journal*, vol. 20, no. 1-2, pp. 40–46, 2001.

[359] P. B. Conibear, A. Málnási-Csizmadia, and C. R. Bagshaw, "The effect of F-actin on the relay helix position of myosin II, as revealed by tryptophan fluorescence, and its implications for mechanochemical coupling," *Biochemistry*, vol. 43, no. 49, pp. 15404–15417, 2004.

Hindawi Publishing Corporation
BioMed Research International
Volume 2015, Article ID 816019, 12 pages
http://dx.doi.org/10.1155/2015/816019

Research Article

A Kinase Anchoring Protein 9 Is a Novel Myosin VI Binding Partner That Links Myosin VI with the PKA Pathway in Myogenic Cells

Justyna Karolczak,[1] Magdalena Sobczak,[1] Krzysztof Skowronek,[2] and Maria Jolanta Rędowicz[1]

[1]*Department of Biochemistry, Nencki Institute of Experimental Biology, Polish Academy of Sciences, 3 Pasteur Street, 02-093 Warsaw, Poland*
[2]*International Institute of Molecular and Cell Biology, 4 Trojden Street, 02-109 Warsaw, Poland*

Correspondence should be addressed to Justyna Karolczak; j.karolczak@nencki.gov.pl and Maria Jolanta Rędowicz; j.redowicz@nencki.gov.pl

Received 20 August 2014; Revised 5 November 2014; Accepted 12 November 2014

Academic Editor: Danuta Szczesna-Cordary

Myosin VI (MVI) is a unique motor protein moving towards the minus end of actin filaments unlike other known myosins. Its important role has recently been postulated for striated muscle and myogenic cells. Since MVI functions through interactions of C-terminal globular tail (GT) domain with tissue specific partners, we performed a search for MVI partners in myoblasts and myotubes using affinity chromatography with GST-tagged MVI-GT domain as a bait. A kinase anchoring protein 9 (AKAP9), a regulator of PKA activity, was identified by means of mass spectrometry as a possible MVI interacting partner both in undifferentiated and differentiating myoblasts and in myotubes. Coimmunoprecipitation and proximity ligation assay confirmed that both proteins could interact. MVI and AKAP9 colocalized at Rab5 containing early endosomes. Similarly to MVI, the amount of AKAP9 decreased during myoblast differentiation. However, in MVI-depleted cells, both cAMP and PKA levels were increased and a change in the MVI motor-dependent AKAP9 distribution was observed. Moreover, we found that PKA phosphorylated MVI-GT domain, thus implying functional relevance of MVI-AKAP9 interaction. We postulate that this novel interaction linking MVI with the PKA pathway could be important for targeting AKAP9-PKA complex within cells and/or providing PKA to phosphorylate MVI tail domain.

1. Introduction

Myosin VI (MVI) is a unique unconventional actin-based motor that unlike other known myosins moves towards the minus end (i.e., backwards) of actin filaments [1, 2]. MVI belongs to a large myosin superfamily and has a domain organization similar to other known myosins; that is, it contains a motor, neck, and tail domain [3]. Its ~140 kDa heavy chain is composed of the N-terminal motor domain (with the actin and ATP binding sites), a neck, to which two calmodulin molecules are bound, and a tail domain [1, 2, 4]. MVI exists as a monomer or a dimer, and it is believed that several factors such as cargo binding, monomer availability, and/or phosphorylation within the tail domain determine MVI heavy chain dimerization, which occurs by a helical region within the tail [5, 6]. MVI functions in numerous cellular processes through its interaction with actin (via its N-terminal motor domain) and tissue specific partner proteins (via its C-terminal globular domain, also termed a cargo domain). Two regions of the MVI cargo domain were found to be involved in partner recognition: a positively charged RRL region and a hydrophobic WWY region. Also, a positively charged cluster located within the cargo tail was shown to bind to PIP_2-containing liposomes, possibly aiding in partner binding [2, 4]. Several tissue specific MVI binding partners have been already identified in mammals; among them are proteins engaged in the regulation of cytoskeleton dynamics, proteins associated with the Golgi apparatus and

the endoplasmic reticulum, and proteins involved in endocytosis and cell adhesion as well as proteins with enzymatic activities [2, 4].

All the known mutations within *MYO6* cause sensorineural deafness [7]. Defects were also observed in the brain [8, 9], intestines [10], and kidney [11]. One of the mutations, a H246R mutation within the human MVI motor domain, was also found to be associated with hypertrophic cardiomyopathy [12] suggesting important role(s) of this motor in striated muscle. Indeed, our recent work has shown that in striated muscle as well as in myogenic cells MVI could be involved in the organization/maintenance of the sarcoplasmic reticulum, Golgi apparatus, adhesive structures (and intercalated discs in case of cardiac muscle), nuclei, and the neuromuscular junction [13–15]. We found that in skeletal muscles MVI might interact with TOM1 (target of myb1 homolog isoform 1, a protein involved in intracellular transport and autophagy), FMRP (fragile X mental retardation autosomal homolog 1, a protein involved in mRNA transport), and hnRNP proteins (involved in the RNA transport and maturation) [13].

To further understand the role of MVI in myogenic cells, we performed a search for its interaction partners in myoblasts and myotubes. It resulted in identification of AKAP9 as a novel MVI interaction partner. This ~230 kDa coiled-coil protein (also termed as yotiao) is highly expressed in cardiac and skeletal muscle, placenta, pancreas, and the brain [16]. It belongs to A kinase anchoring proteins (AKAPs) that create a compartmentalized environment inside the cell to bring various signaling molecules to their targets [17]. For example, in the heart, AKAP9 was shown to form a complex with a slowly activating potassium channel (I_{Ks}), important for cardiac repolarization and with other enzymes, which are responsible for channel regulation such as PKA, phosphatase, adenylyl cyclase, and phosphodiesterase [18]. AKAP9 mutations cause long-QT syndrome manifested by cardiac arrhythmia [18, 19]. AKAP9 was also shown to link NMDA with the inositol 1,4,5-trisphosphate receptor type 1 [18]. There are also reports that AKAP9 could play an important role in cytoskeleton dynamics and organization by targeting the PKA kinase to the cytoskeleton, thus affecting cell motility, proliferation, and adhesion [20]. Several data indicate that AKAP9 is involved in striated muscle and synapse functioning, in development of breast and thyroid cancers, and in spermatogenesis [18, 21].

In the presented work we characterize a novel MVI-AKAP9 interaction and postulate that it could be important for linking MVI with the PKA signaling.

2. Materials and Methods

2.1. Cell Culture. C2C12 mouse myoblasts (American Type Culture Collection, USA), kindly provided by Prof. Krzysztof Zablocki from the Nencki Institute, were maintained in DMEM containing 4.5 g/L glucose and supplemented with 10% heat-inactivated fetal bovine serum (FBS), antibiotics (1000 IU/mL penicillin and 1000 UI/mL), and 4 mM L-glutamine at 37°C in humidified air containing 5% CO_2. Differentiation was initiated upon reaching confluence (considered as day 0) by transferring to medium containing 2% horse serum (HS) instead of 10% FBS, and the culture was continued for up to the next 7–10 days. To observe acetylcholine-rich clusters, cells were differentiating in 8-well Permanox chamber slides (Sigma-Aldrich, USA) coated with laminin (Invitrogen, USA) as described by [22].

2.2. siRNA Knockdown of MVI. A MVI-KD stable cell line was generated based on the pSilencer 2.1-U6 hygro vector system (Ambion Inc., USA) essentially as described by [23]. 5′-AACTACGCGATACAATCAATA-3′ siRNA sequence against a coding region of mouse MVI mRNA was used with the corresponding scrambled sequence as a negative control (5′-ATAACATACCGTACGAATAAC-3′). Notably, the chosen shRNA targeted a different MVI region than the ones used for the protein depletion in PC12 cells but evoked similar changes in the cell motility, Golgi organization, and cytoskeleton organization [23]. C2C12 cells were transfected using Lipofectamine 2000 and then selected on hygromycin B (Sigma-Aldrich, USA). MVI expression level was assessed by Western blot as well as RT-PCR.

2.3. C2C12 Cell Transfection. C2C12 myoblasts cultured on coverslips were transfected using Lipofectamine 2000 (Life Technologies, USA) with plasmids encoding GFP-fused human full length MVI (GFP-MVI) and its globular tail domain (GFP-MVI-GT), kindly provided by Dr. Tama Hasson from University of California, Los Angeles [24]. Also, the cells were transfected with plasmids encoding markers of vesicular organelles fused with GFP, kindly provided by Dr. S. Havrylov (McGill University, Canada). The following proteins were overexpressed: Rab5-GFP (found on clathrin-coated vesicles and early endosomes), Rab7-GFP (present on late endosomes), Rab11-GFP (present on early and recycling endosomes as well as the Golgi apparatus), and LAMP1-GFP (present on lysosomes). After 36 h of transfection, cells were fixed and stained with anti-AKAP9 and/or anti-MVI antibodies as described in Section 2.5.

2.4. Immunoblotting. Cells were lysed in an ice-cold buffer containing 50 mM Tris-HCl pH 7.5, 150 mM NaCl, 0,1% Triton X-100, 1 mM DTT, 1 mM EGTA, 1 mM PMSF, and complete protease inhibitor cocktail (Roche). Cell lysates (10–20 μg of protein per well) were separated using 10% or 12% polyacrylamide SDS-gels and then transferred to a nitrocellulose membrane. Protein concentration was determined by Bio-Rad protein assay reagent (Bio-Rad, USA). MVI was detected with a rabbit polyclonal antibody raised against porcine MVI heavy chain (Proteus, USA) at 1 : 500 dilution. AKAP9 and DOCK7 were detected with goat polyclonal anti-AKAP9 (Abcam, UK) and anti-DOCK7 (Santa Cruz, USA) antibodies, both at 1 : 100 dilution. PKA and phospho-PKA (pPKA) were detected with mouse anti-PKA and rabbit anti-pPKA antibodies, respectively (both from Santa Cruz), at 1 : 500 dilutions. Mouse monoclonal antibody against β-actin (from Sigma-Aldrich, USA) at 1 : 1000 dilution was used to detect β-actin. γ-actin and GAPDH (glyceraldehyde 3-phosphodehydrogenase) were detected with sheep polyclonal anti-γ-actin and mouse monoclonal anti-GAPDH antibodies (both from Merck Millipore, USA), at 1 : 500 and 1 : 10,000

dilutions, respectively. Anti-mouse, anti-sheep, and anti-rabbit antibodies conjugated with horse radish peroxidase (all diluted at 1 : 10,000) were applied for detection of primary antibodies using the ECL system (Pierce, USA). Western blot was performed and followed by densitometric analysis. Student's t-test was used to evaluate the quantitative data.

2.5. Immunolocalization Studies. Cells on cover slips were fixed in 4% formaldehyde in phosphate-buffered saline pH 7.4 (PBS) for 20 min at room temperature, washed with PBS, blocked in 2% horse serum, and permeabilized with 0.02% Triton X-100 in PBS for 30 min at room temperature. Cover slips were then incubated for 2 h at room temperature or overnight at 4°C with anti-MVI (Proteus, USA) antibody diluted at 1 : 50 and anti-AKAP9 antibody (Abcam, UK) diluted at 1 : 200 and washed with PBS, followed by cell incubation with 1 μg/mL Alexa Flour 488-conjugated goat anti-rabbit IgG or Alexa Fluor 555-conjugated donkey anti-goat IgG (both from Molecular Probes, Invitrogen, USA). Vectashield mounting medium (Vector Labs, USA) was used to mount the slides. Alexa488-conjugated bungarotoxin (BTX, from Invitrogen, USA) was used to stain acetylcholine-rich clusters. For negative controls, the primary antibodies were omitted. Images were collected as described in [13]. Unless stated otherwise, the images represent the confocal 0.3-μm sections of the cell center. MetaMorph software (Leica MM AF Basis Offline Version 1.4.0) was used for the quantification studies.

2.6. Proximity Ligation Assay (PLA). The assay was performed according to the manufacturer's instructions (Olink Bioscience, Sweden). Briefly, myoblasts and mature myotubes after fixation were blocked in Duolink blocking solution in a humidity chamber for 30 min at 37°C and incubated with primary antibodies: polyclonal anti-MVI (1 : 50) and anti-AKAP (1 : 200) in Duolink antibody diluent solution for 3 h at 37°C. Cells were next washed twice in a wash buffer for 5 min at room temperature. For secondary antibodies conjugated with oligonucleotides, PLA probe anti-goat MINUS and PLA probe anti-rabbit PLUS were applied in Duolink antibody diluent solution for 1 h at 37°C and washed twice with a wash buffer for 5 min. Duolink assay was further performed strictly according to the manufacturer's instructions. For negative controls, the primary antibodies were omitted. Also, a control assay was performed on the scrambled and MVI-KD cells, which revealed about 30% reduction of the positive signals in the knockdown cells that notably express several times more AKAP9 than the scrambled cells (not shown).

2.7. Coimmunoprecipitation. To perform coimmunoprecipitation, HEK 293 cells transiently transfected with pEGFP-C3-MVI FL+S+ construct (encoding full length human MVI, a gift from Dr. Tama Hasson from University of California, Los Angeles) were lysed in a buffer containing 50 mM Tris (pH 7.5), 150 mM NaCl, 2 mM EDTA, 0.2% Triton X-100, 2 mM $MgCl_2$, 2 mM MgATP, 50 mM NaF, and 1 mM Na_3VO_4 and supplemented with the complete protease inhibitor cocktail. The lysates were precleared with A/G magnetic beads (Pierce, USA) for 2 h at 4°C and subsequently incubated with 10 μg of the anti-MVI antibody or normal rabbit serum as a control overnight at 4°C. The beads were extensively washed with lysis buffer and then subjected to SDS-PAGE. Western blot was performed using anti-AKAP9 (1 : 200) or anti-DOCK7 (1 : 200) antibodies to detect the coimmunoprecipitated MVI-AKAP9 or MVI-DOCK7 complexes.

2.8. GST Pull-Down. A fusion protein composed of GST and the MVI C-terminal globular tail domain (GST-MVI-GT) as well as GST alone was purified as described in [13]. Cells were lysed at three time points during differentiation (days 0, 3, and 7) in ice-cold buffer containing 50 mM Tris (pH 7.5), 150 mM NaCl, 0.5% Triton X-100, 1 mM DTT, 5 mM EGTA, 50 mM NaF, 1 mM Na_3VO_4, and 0.5 mM PMSF and supplemented with the complete protease inhibitor cocktail. Samples were precleared with GST-bound Glutathione Sepharose 4B beads for 2 hours at 4°C to remove proteins nonspecifically binding to Glutathione Sepharose 4B or to GST and subsequently incubated with Glutathione Sepharose 4B beads bound with GST-MVI fusion protein or GST alone. The beads were exhaustively washed in the ice-cold buffer described above. Myoblast (and myotube) proteins associated with GST-MVI-GT or with GST were subjected to SDS-PAGE electrophoresis.

2.9. Sample Preparation and Protein Identification by LC-MS/MS. After the electrophoretic separation of samples obtained in the pull-down assay, the gel was stained with Coomassie R-250 and equal pieces were cut from the experimental (GST-fused MVI globular tail, GST-MVI-GT) and control (GST alone) gel lanes. Proteins from gel slices were subjected to the standard procedure of in-gel digestion with trypsin (Thermo, USA) and extraction according to manufacturer recommendations. Eluted peptides were loaded on an EASY-nLC II nano-LC system equipped with Acclaim PepMap100 Nano Trap Column 2 cm × 200 μm C-18 precolumn and EASY Column 10 cm × 75 μm C-18. The solvent system consisted of 0.1% formic acid in water (solvent A) and 0.1% formic acid in acetonitrile (solvent B). Samples were chromatographed using a flow rate of 300 nl/min with a two-step linear gradient of 1–40% B from 0–20 min, 40–100% B from 20–30 min, and 100% B from 30–35 min. The chromatographic eluent was directly conducted into the amaZone ion trap mass spectrometer (Bruker) working in the regime of data-dependent MS to MS/MS switch. The raw data preprocessing with Data Analysis software (version 2.1.1, Bruker) resulted in peak lists which were used to search the Swiss Prot protein database using the Mascot search engine (version 2.3.01, Matrix Science, London, UK) with the following search parameters: taxonomy restriction: Mus musculus (mouse), enzyme specificity: trypsin, permitted number of missed cleavages: 2, fixed modification: carbamidomethylation (C), variable modifications: phosphorylation (S,T,Y) and oxidation (M), protein mass: unrestricted, peptide mass tolerance: ±0.6 Da, and fragment mass tolerance: ±0.6 Da. Only the proteins that met our criteria (i.e., (i) present only in the GST-MVI-GT sample but not in the control sample, (ii) identified by at least three distinct peptide spectra, and (iii) with Mascot score ≥50) were considered the potential

MVI-binding partners. MVI peptides detected in the sample were excluded from the analysis.

2.10. Estimation of cAMP Levels. For estimation of cAMP levels, the untreated scrambled and MVI-KD cells were cultured for 48 h and then washed twice with PBS, dissolved in sample diluent of total cAMP enzyme immunoassay kit (Biotrend, Germany), and the further procedure followed the supplier protocol. The experiment was performed twice in duplicate.

2.11. PKA Phosphorylation of the MVI Globular Tail Domain. Exogenous catalytic subunit of PKA (from Sigma-Aldrich, USA) was used to phosphorylate the GST-MVI-GT domain. After dialysis against 50 mM Tris, pH 7.4, 50 mM KCl, 5 mM $MgCl_2$, and 1 mM DTT, GST-MVI-GT (1 μg) and GST (1 μg) were then incubated for 1 h at 30°C with the kinase domain (2 units per sample), which prior to the experiment was equilibrated as recommended by the supplier in the presence of 5 mM ^{32}P-γATP (10 mCi/mL, Hartmann Analytic GmbH, Germany). The reaction was stopped with the addition of 4x SDS sample buffer (0.25 mM Tris-HCl, pH 6.8, 5% β-mercaptoethanol, 5% SDS, 40% glycerol, and 0.08% bromophenol blue) followed by incubation at 100°C for 3 min. The samples were then subjected to 10% polyacrylamide SDS gel electrophoresis followed by autoradiography.

2.12. Statistical Analysis. Data are presented as mean ± SD; all P values were calculated by two-sided Student's t-test. The difference was considered to be statistically significant at the level of $P < 0.05$.

3. Results

3.1. AKAP9 Was Identified as a Potential MVI Binding Partner. We have previously shown that MVI plays important roles both in skeletal and cardiac muscle [13, 15] and in C2C12 myoblasts [14]. To further explore MVI function in myogenic cells, we performed a search for its binding partners by means of an affinity chromatography with the GST-tagged globular tail domain of MVI (GST-MVI-GT) used as a bait. The eluates were subjected to tandem mass spectrometry. The analysis was performed in undifferentiated (day 0) and differentiating (day 3 and day 7) myoblasts. Samples from the GST-bound resin served as the control. It should be emphasized that with this method one cannot discriminate whether the identified proteins bind directly or indirectly to the MVI cargo domain.

We obtained a total list of ~250 potential novel MVI interaction partners. There were proteins found only in proliferating myoblasts (77), only in 3-day myoblasts (55), and only in myotubes (51). Only nine proteins were found in all three examined samples, among them were A kinase anchoring protein (AKAP9) and talin (the constituent of adhesive complexes). Interaction of MVI and talin is to be described elsewhere (Karolczak et al., unpublished). The identified proteins for each examined sample were grouped based on their known functions depicted by the Uniprot database (Figure 1). For all three samples, the most abundant were proteins involved in transcription (30 proteins), in signal transduction (42 proteins), and in the organization of the cytoskeleton (16 proteins). However, all groups varied both quantitatively and qualitatively depending on the differentiation stage. The number of the detected proteins involved in the numerous cellular functions in three differentiation stages has been presented in Table 1.

Table 1: The number of MVI interaction partners involved in different cellular functions during myoblast differentiation.

Number	Function	Day 0	Day 3	Day 7
1	Replication and DNA repair	8	4	5
2	Transcription	22	8	9
3	RNA processing	7	1	6
4	Protein biosynthesis	7	5	9
5	Protein modifications and transport	5	5	3
6	Protein degradation	1	3	4
7	Ion transport	2	1	2
8	Cytoskeleton	10	4	4
9	Signal transduction	16	18	16
10	Metabolism	6	7	3
11	Cellular respiration	0	1	0
12	Peroxisomes	0	2	0
13	Endocytosis	2	0	2
14	Exocytosis	3	0	0
15	Stress	2	0	1
16	Autophagy	3	1	1
17	Apoptosis	3	2	0
18	Adhesion	4	1	3
19	Cell junctions	3	1	1
20	Cell movement/migration	2	2	0
21	Cell division	3	1	4
22	Unknown function	13	12	13

As it was mentioned above, AKAP9, a regulator of the PKA kinase activity, was found in all three examined samples. In day 0 myoblasts, three AKAP9 peptides were detected, seven in day 3 myoblasts, and four in the myotubes.

3.2. AKAP9 Is Expressed in Undifferentiated and Differentiating Myoblasts. The presence of AKAP9 in all three samples was confirmed by Western blotting with an antibody against the C-terminal region of the protein. As shown in Figure 2(a), the protein was detected in samples from the GST-GT-MVI resin but not from the GST resin. Interestingly, the amount of AKAP9 decreased during myoblast differentiation (similarly to MVI) as revealed by the immunoblot analysis (Figure 2(b)). We also checked that the AKAP9 level in MVI-KD myoblasts with MVI expression decreased down to <10%. Western blotting followed by densitometric analysis revealed that the level of AKAP9 was increased severalfold in MVI-KD cells (Figure 2(c)).

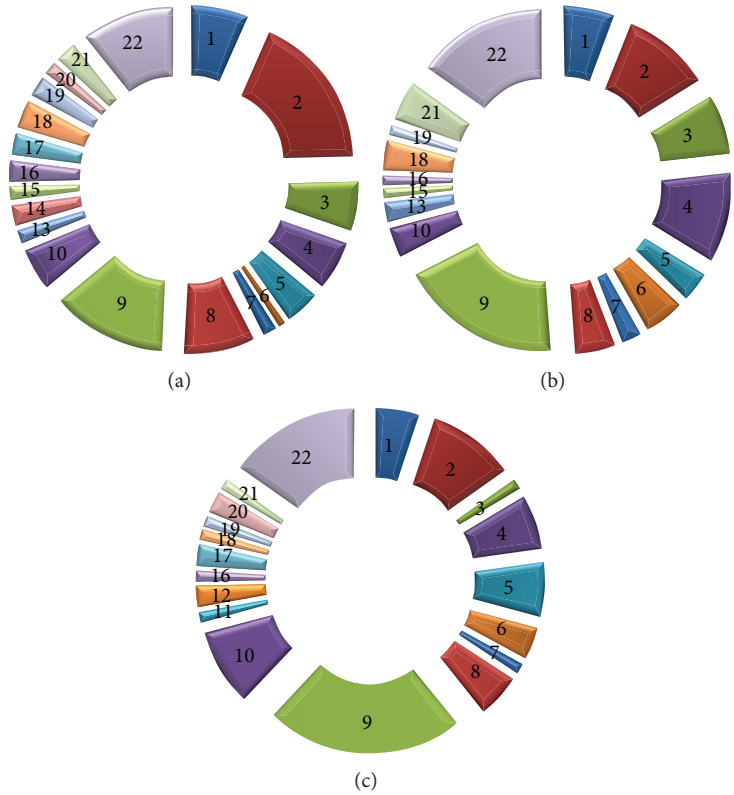

Figure 1: Potential binding partners of MVI identified by pull-down assay and mass spectrometry. (a) Protein groups identified in day 0 myoblasts, (b) proteins identified in the intermediate stage (day 3 myoblasts), and (c) proteins identified in day 7 myotubes. (1) Replication and DNA repair. (2) Transcription. (3) RNA processing. (4) Protein biosynthesis. (5) Protein modifications and transport. (6) Protein degradation. (7) Ion transport. (8) Cytoskeleton. (9) Signal transduction. (10) Metabolism. (11) Cellular respiration. (12) Peroxisome. (13) Endocytosis. (14) Exocytosis. (15) Stress. (16) Autophagy. (17) Apoptosis. (18) Adhesion. (19) Cell junctions. (20) Cell movement/migration. (21) Cell division. (22) Unknown function.

3.3. AKAP9 and MVI Colocalize in Myoblasts and Myotubes. MVI and AKAP9 colocalized in undifferentiated control and scrambled myoblasts in numerous puncti scattered throughout the cytoplasm (Figures 3(a) and 3(b), insets). To identify the MVI and AKAP9 containing puncti, we overexpressed GFP-fused constructs encoding proteins markers of endocytic and lysosomal compartments such as Rab5, Rab7, Rab11, and LAMP11. Out of them, AKAP9 localized only to Rab5-GFP containing vesicles that were also associated with MVI-stained puncti (Figure 3(a′)) and not with the other vesicle markers (not shown). These data indicate that MVI and AKAP9 colocalization is on clathrin-coated pits and early endosomes [25].

In MVI-KD cells, the protein was also visible throughout the cytoplasm with increased signal at the cell edges (Figure 3(c)). Noticeably, AKAP9-associated fluorescence intensity was evidently higher in MVI-KD cells, confirming the Western blot analysis (see Figure 2(c)) and indicating that MVI knockdown upregulated its expression.

MVI and AKAP9 colocalization was also visible in mature myotubes (Figure 3(d)). AKAP9-associated staining was evidently weaker due to its lower amount in the myotubes (see Figure 2(b)) but most of AKAP9 puncti were associated with MVI (Figure 3(d), inset).

To confirm that enhanced AKAP9 synthesis was indeed associated with less MVI, we performed a rescue experiment, in which the MVI-KD cells were transfected with a plasmid encoding GFP-fused full length MVI (GFP-MVI). In the cells expressing GFP-MVI (marked with arrows), AKAP9-associated staining was substantially lower in comparison with nontransfected MVI-KD cells (Figure 3(e), inset).

To check whether AKAP9 localization depends on MVI motor activity, we transfected MVI-KD myoblasts with a plasmid encoding the MVI globular tail domain fused with GFP (GFP-MVI-GT). As shown in Figure 3(f), unlike expression of the full length MVI, expression of the tail domain did not affect AKAP9 localization. Also, this MVI domain lacking motor activity was present in the perinuclear region in large aggregate-like puncti not associated with AKAP9 staining (Figure 3(f), inset).

3.4. Assessment of an AKAP9-MVI Interaction. Since the data presented above indicate that MVI and AKAP9 may interact with each other, we decided to further assess this association by means of coimmunoprecipitation as well as by the proximity ligation assay (PLA), which allows for *in situ* detection of two proteins that exist within close intracellular proximity (within the 20–40 nm range). The positive PLA

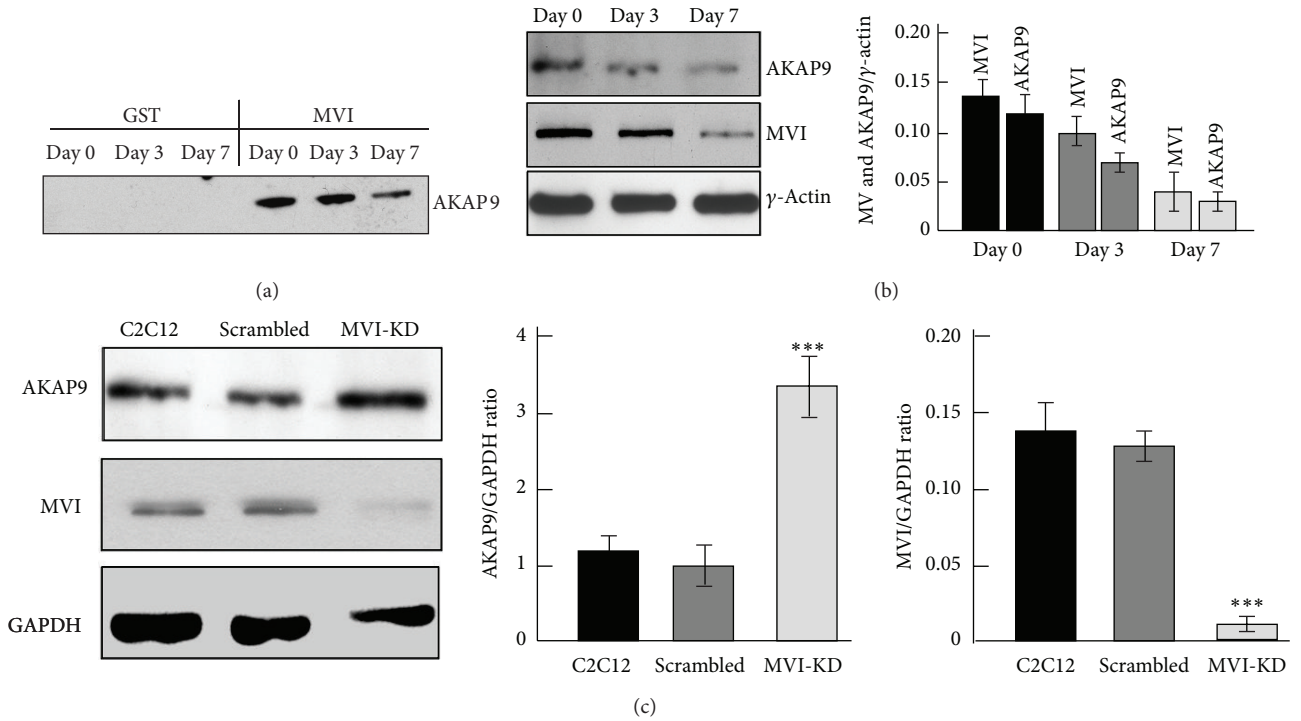

Figure 2: AKAP9 expression in myogenic cells probed by immunodetection. (a) AKAP9 was found in the pull-downs of the day 0, day 3, and day 7 myoblast samples. (b) AKAP9 expression is decreasing during myoblast differentiation into myotubes. Right panel: quantitative analysis of the AKAP9 and MVI content with respect to the level of γ-actin. (c) The level of AKAP9 expression is substantially elevated in MVI-KD cells when compared with untreated C2C12 and scrambled myoblasts. Right panels: quantitative analyses of the AKAP9 and MVI content with respect to the level of glyceraldehyde-3-phosphate dehydrogenase (GAPDH). The results in (b) and (c) are presented as means ± SD from two experiments; $^{***}P < 0.001$.

signal is considered an evidence for interaction of two given proteins (and/or their domains) [26].

Coimmunoprecipitation with the anti-MVI antibody revealed the presence of AKAP9 in the precipitate from lysates of HEK293 cells overexpressing GFP-tagged MVI construct, thus confirming the presence of both proteins in the precipitate (Figure 4(a), left panel). As a positive control, the precipitate was also probed with anti-DOCK7 antibody (Figure 4(a), right panel) as we previously showed DOCK7-MVI interaction in PC12 cells [27].

MVI-AKAP9 interaction was further visualized *in situ* by the PLA assay which revealed the presence of numerous puncti (in red) resembling the interaction sites (Figures 4(b) and 4(c)). Both proteins were in very close proximity not only in undifferentiated myoblasts (Figure 4(b)) but also in mature myotubes (Figure 4(c)). Moreover, in myotubes, this interaction was detected in the vicinity of nascent acetylcholine-rich clusters as well (Figure 4(c), arrowheads).

The control PLA assay performed on the scrambled and MVI-KD myoblasts revealed that significantly more positive PLA signals were detected in the scrambled cells than in the knockdown cells (~60% reduction) despite the fact that in MVI-KD cells the amount of AKAP9 was substantially elevated (not shown).

3.5. Depletion of MVI Affects cAMP Level. A substantial increase of AKAP9 expression and a change in its distribution in MVI-KD myoblasts imply that there could be a link between the AKAP9-MVI complex and PKA kinase activity which is dependent on the intracellular level of cyclic AMP (cAMP). It is noteworthy that a decrease in the level of cAMP is required for initiation of myoblast differentiation into myotubes and acetylcholinesterase expression [28]. In order to understand the mechanism of the MVI-AKAP9 interaction, we checked whether MVI depletion could affect the intracellular level of cAMP. With the use of a total cAMP enzyme immunoassay, we found that in MVI-KD myoblasts the level of cAMP was substantially elevated with respect to both untreated (increase by about 40%) and scrambled (increase by about 30%) cells, suggesting a MVI-dependent change in cAMP metabolism. This increase was accompanied by a threefold increase of PKA expression as assessed with an anti-PKA antibody, detecting the total amount of kinase regardless of its phosphorylated state (Figure 5(b)). However, when the same samples were probed with an anti-phospho-PKA antibody detecting (auto)phosphorylated kinase, the intensity of the band corresponding to phosphorylated kinase was ~50% decreased with respect to the untreated and scrambled cells (Figure 5(b)). Thus MVI depletion is associated with an increase in PKA level; however, a smaller kinase fraction is phosphorylated.

3.6. MVI Globular Tail Is a Substrate for PKA. MVI harbors a putative PKA phosphorylation site at threonine residue

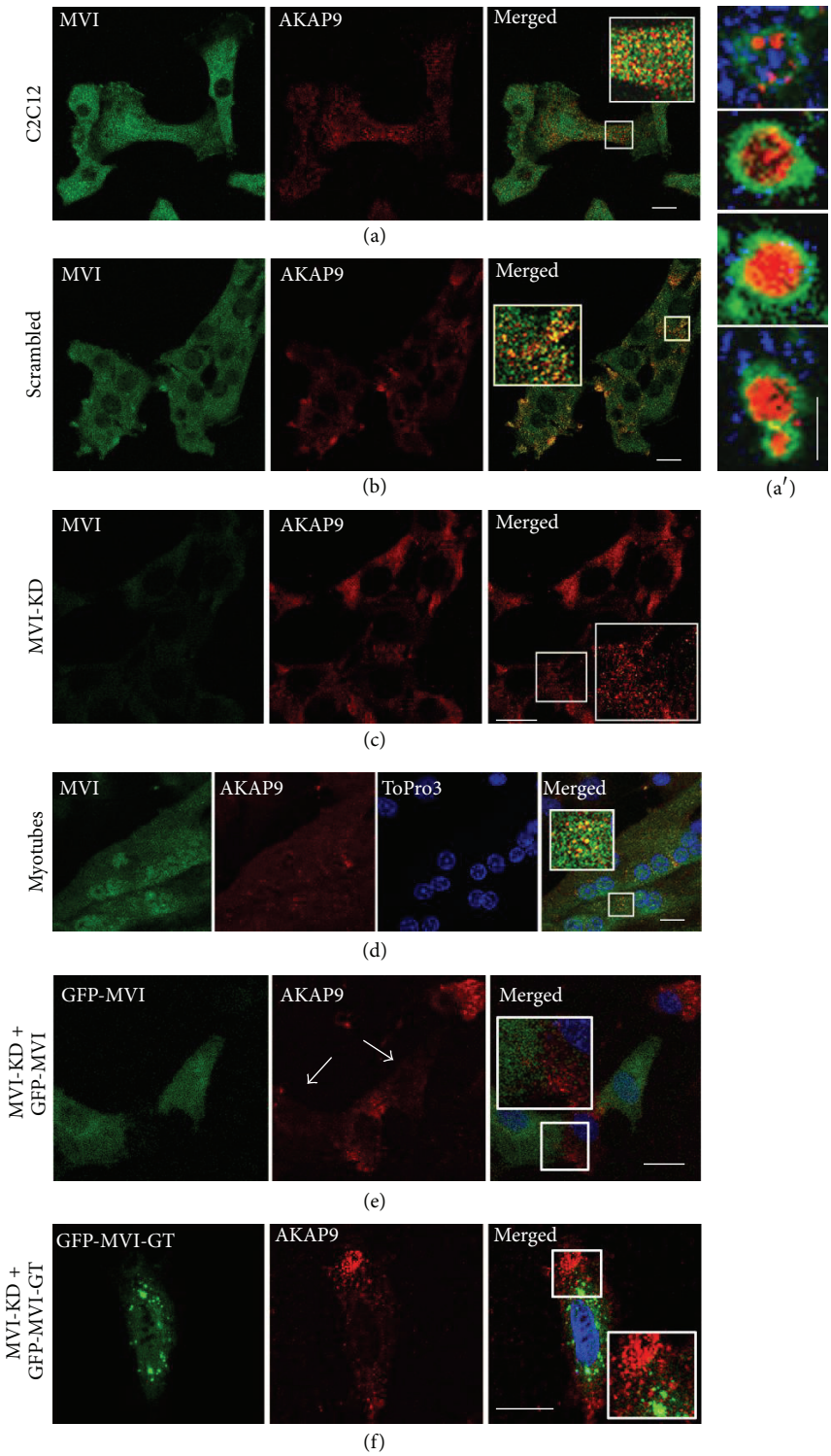

Figure 3: AKAP9 and MVI colocalization in undifferentiated myoblasts and in myotubes by means of confocal microscopy. (a) Untreated C2C12 myoblasts (C2C12), (b) scrambled cells, (c) MVI-depleted cells (MVI-KD), and (d) day 7 myotubes. (e) MVI-KD cells expressing GFP-MVI and (f) MVI-KD cells expressing GFP-tagged MVI globular tail domain (GFP-MVI-GT). MVI in (a)–(d) was visualized with anti-MVI antibody (in green) and in (e)-(f) by the GFP fluorescence and AKAP9 with anti-AKAP9 antibody (in red) and nuclei (in (d)) with ToPro3 (in blue). Insets, 2-3x magnification of the areas marked in the merged panels. (a′) AKAP9 (stained with anti-AKAP9 antibody, in red) and MVI (stained with anti-MVI antibody in blue) were associated with early endosomes containing overexpressed Rab5-GFP (in green). Images of the central cell section ($z = 0.3\ \mu$m) were obtained with a Leica confocal microscope. Bars: in (a)–(f), 20 μm and in (a′), 2 μm.

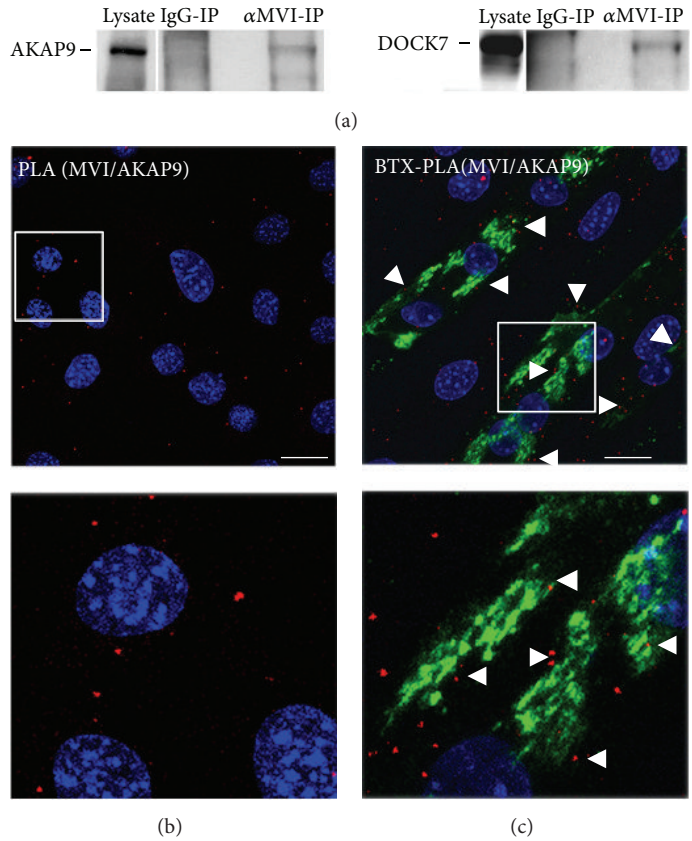

Figure 4: Validating the AKAP9 and MVI interaction. (a) Coimmunoprecipitation of AKAP9 (left panel) and DOCK7 (right panel) with anti-MVI antibody from HEK 293 cells overexpressing GFP-tagged full length human MVI heavy chain. Left lanes: cell lysate (lysate), middle lanes: samples precipitated with a normal rabbit serum (IgG-IP), and right lanes: αMVI-IP. Samples precipitated with anti-MVI antibody were probed with either anti-AKAP9 or anti-DOCK7 antibodies as marked on the figure. PLA assay probing MVI and AKAP9 interactions (in red) in undifferentiated myoblasts (b) and in myotubes (c). In blue, nuclei stained with DAPI. (c) MVI-AKAP9 possible interactions are also seen close to bungarotoxin- (BTX-) stained acetylcholine-rich clusters (in green) marked by arrowheads. The lower panels in (b) and (c) are ~3x magnifications of the areas marked in (b) and (c). Images in (b) and (c) of the cell central sections ($z = 0.3\,\mu$m) were obtained with a Leica confocal microscope. Bars: 20 μm.

1104 for mouse, 1100 for rat, and 1134 for human myosin as depicted with the NetPhos bioinformatic tool [29]. This residue is located in a very conserved region of the globular tail domain of numerous MVI heavy chains (Figure 6(a)) raising a possibility that MVI could be a substrate for PKA. Thus the interaction described above could be important not only for targeting the AKAP9-PKA complex but also for providing the kinase for MVI phosphorylation.

We addressed this hypothesis by performing an *in vitro* phosphorylation assay using GST-tagged MVI cargo domain and commercially available PKA catalytic subunit; GST alone was used as a control (Figure 6(b)). As shown in Figure 6(b), a ~52-kDa band corresponding to the recombinant GST-MVI tail domain incorporated radioactive ^{32}P resulting from the kinase assisted hydrolysis of [γ^{32}P]ATP. No incorporation was observed in a ~20-kDa band corresponding to GST indicating that it was the MVI but not the GST moiety that was phosphorylated by the PKA kinase subunit. The bands corresponding to the kinase catalytic subunit also incorporated radioactive ^{32}P due to its autophosphorylation. Noticeably, kinase autophosphorylation was higher in the presence of GST and the MVI globular tail.

4. Discussion

In the study on myogenic cells presented herein, we identified AKAP9, a regulator of PKA kinase activity, as a novel MVI binding partner and showed that this interaction could be functionally relevant.

AKAP9 was found in pull-down samples of undifferentiated and differentiating myoblasts and mature myotubes but its amount—similarly to MVI—was decreasing during myoblast differentiation into myotubes. Noticeably, the protein is also present in mature skeletal and cardiac muscle where it is termed yotiao [16]. In skeletal muscle AKAP9 is predominantly localized subjacent to acetylcholine receptors in the neuromuscular junction and was seen within the Z-line [16], and in cardiac muscle it has been recently identified as a gene associated with long-QT syndrome (LQTS), manifested by cardiac arrhythmia [18]. Interestingly, in patients with the

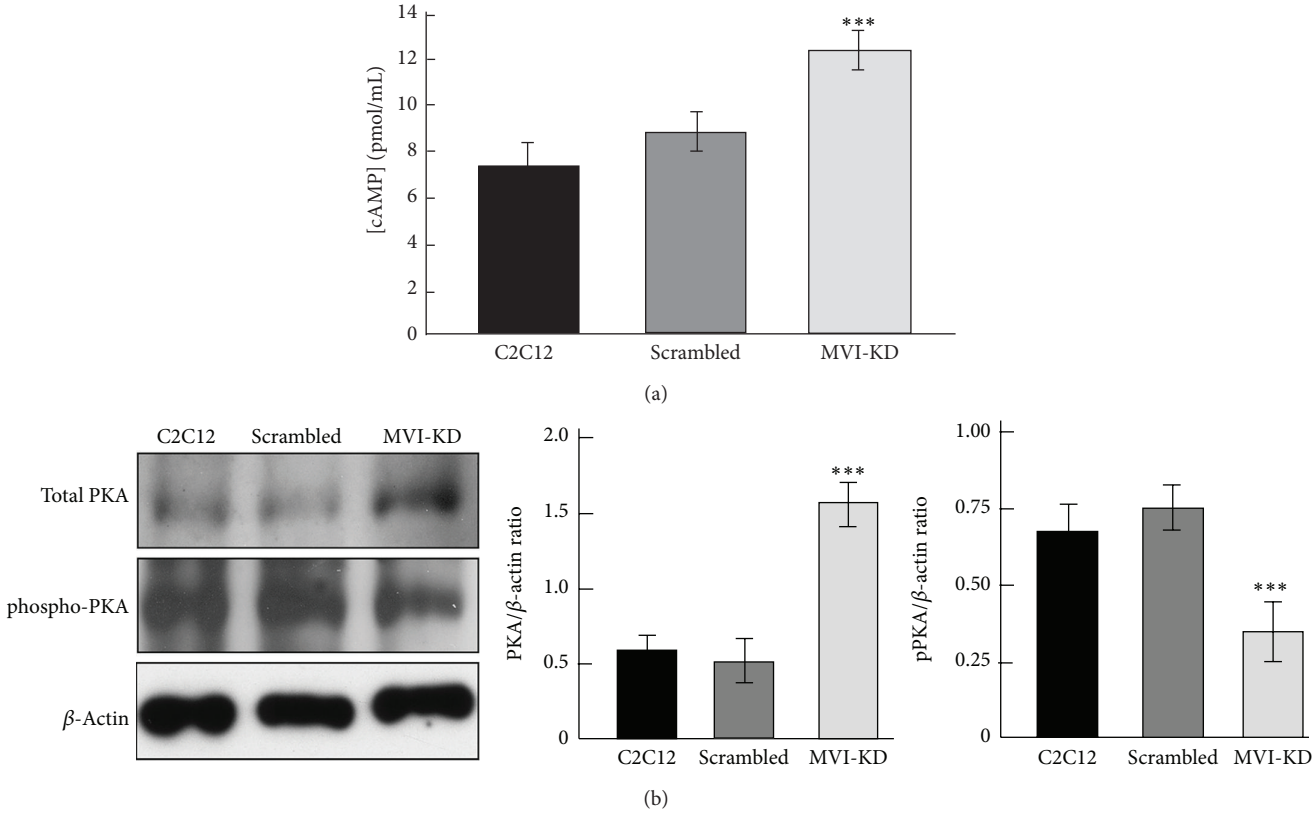

Figure 5: MVI depletion affects cAMP and PKA levels in C2C12 myoblasts. (a) The amount of cAMP (presented as pmol/mL) in untreated C2C12, scrambled and MVI-KD myoblasts was estimated as described in Section 2. (b) Probing the levels of total (upper panel) and phosphorylated (lower panel) PKA in untreated C2C12, scrambled and MVI-KD myoblasts by means of Western blot technique with the respective antibodies. Right panels: quantitative analysis of the PKA and phospho-PKA content with respect to the level of β-actin. The results in (a) and (b) are presented as a mean ± SD from two experiments (for (a) run in duplicate); $^{***}P < 0.001$.

H246R mutation in MVI that presented symptoms of dilated cardiomyopathy, a prolonged QT interval was also observed in their ECG pattern [12].

The question arises of the functional relevance of the MVI-AKAP9 interaction taking into consideration that the main role of AKAP9 (and other members of the AKAP family) is to regulate PKA kinase activity and to ensure that the activated PKA acts only on substrates that reside close to the AKAPs [30]. At least two main complementary mechanisms could be proposed to understand this novel interaction. First MVI motor activity could be necessary to target the AKAP9-PKA complex to its final destination(s). The second one assumes that the MVI-AKAP9 interaction is required to bring PKA into the vicinity of MVI so the kinase could phosphorylate the MVI tail.

MVI binding partners interact with one out of two partner recognition sites (one charged and one hydrophobic) and this binding is believed to be important for cargo transport or its anchoring to the actin cytoskeleton (see [4]). We do not know yet which of the MVI binding regions is involved in the association with AKAP9, but certainly this interaction is functional because depletion of MVI causes not only an increase of AKAP9 and PKA kinase expression levels but also a substantial increase in the cAMP level. Moreover, MVI motor-dependent changes in the distribution of AKAP9 were observed, indicating the importance of MVI motor activity for AKAP9 targeting. Interestingly, a wild-type phenotype regarding the AKAP9 localization and expression was rescued by overexpression of full length MVI and not by the globular tail domain lacking the motor domain. In our opinion, impaired AKAP9 targeting resulting from MVI depletion could be compensated by an increase of the AKAP9-PKA complex expression. For example, a compensatory effect was shown in *Saccharomyces cerevisiae*, in which increased chitin synthesis compensated a "stress response" mechanism induced by abnormal cell wall assembly due to class II myosin deficiency [31].

Several potential phosphorylation sites within the MVI cargo domain as well as a number of serine/threonine kinases that might be able to phosphorylate the MVI tail (including PKC and PKA) have been depicted by the NetPhosK 1.0 bioinformatic server [29]. It has been postulated that phosphorylation of the cargo domain could affect MVI heavy chain dimerization and cargo binding but so far no biochemical data confirming this putative phosphorylation have been reported [4, 32]. The server found one putative PKA phosphorylation threonine residue (see Figure 6(a), marked in green) located within a very conserved region of the MVI tail and is also

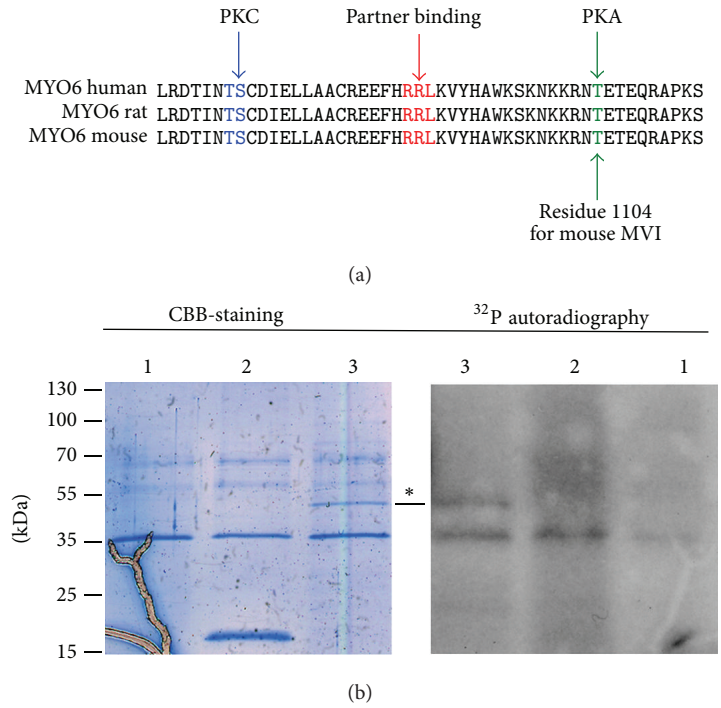

Figure 6: Myosin VI is a target of PKA. (a) A putative PKA phosphorylation site (threonine residue 1104 in the mouse MVI heavy chain, in green) is located in the vicinity of a very conserved region within the RRL partner recognition cluster (in red). In blue, the putative PKC phosphorylation sites. The kinase specific phosphorylation sites were depicted with a NetPhosK 1.0 Server (http://www.cbs.dtu.dk/services/NetPhosK/). The MVI sequences used for analyses are human (Q9UM54), rat (D4A5I9), and mouse (Q64331). (b) *In vitro* PKA phosphorylation assay. Left panel: Coomassie brilliant blue stained gel (CBB-staining), right panel: ^{32}P autoradiogram. Lane 1: the catalytic kinase domain; lane 2: GST; lane 3: GST-tagged MVI globular tail domain. ∗ Points to the ~52-kDa band of interest (GST-MVI domain).

evolutionarily conserved. For the purpose of this study, the human, rat, and mouse regions were shown (Figure 6(a)). This potentially phosphorylatable threonine residue is only 14 residues apart (towards C-terminus) from the charged RRL region involved in partner recognition. Moreover, there is also a putative conserved PKC recognition site(s) on the N-terminal flank of the RRL region (Figure 6(a)). It is therefore possible that phosphorylation of either of these sites could affect a net charge value and have impact on binding of a given cargo. Thus it could be employed by a cell to regulate the cargo binding, dependent on cargo, myosin, and kinase availability. Neither PKA nor PKC have been detected in the examined eluates though there is a report in which tyrosine LMTK-2 kinase (lemur tyrosine kinase 2) binds to MVI in HeLa cells [33]. However, unlike for MVI and PKA, there are no reports on MVI phosphorylation by LMTK-2 kinase. Noticeably, a direct interaction between the myosin V (MV) tail and CaMKII kinase associated with phosphorylation of MV Ser1650 was shown to be important for cargo dissociation and MV translocation to the nucleus [34, 35].

The observation that the MVI-AKAP9 complex was also present in myotubes at acetylcholine-rich clusters further confirms our earlier suggestion that MVI (by interaction with its muscle specific partners, e.g., with AKAP9) could play important roles in neuromuscular junction development as both MVI and AKAP9 were shown to be important for brain and muscle synapse functioning [13, 16]. It is noteworthy that PKA-associated involvement of another unconventional myosin V in the neuromuscular junction has been already shown [36, 37].

5. Conclusion

The newly identified interaction between MVI and AKAP9 seems to have functional relevance in myotube formation and neuromuscular junction development and may link MVI with cAMP-dependent PKA signaling, which is crucial for myoblast differentiation. The observation that the highest concentration of AKAP9 (and MVI) was shown in undifferentiated myoblasts and the lowest in mature myotubes is consistent with the data showing that the level of cAMP and the activities of its downstream signaling molecules decrease during myotube formation [28]. Also, it could explain why we experienced difficulties with myotube formation by MVI-depleted myoblasts [14], which—as we found out now—showed substantially higher cAMP levels than the control cells. Also, the question arises as of whether and how AKAP9 regulates MVI phosphorylation by PKA as well as whether and how PKA affects interaction between AKAP9 and MVI. We postulate that the novel MVI-AKAP9 interaction could also be important in cardiac muscle since, on one hand, AKAP9 was shown to play a crucial role in the proper

functioning of the heart [18] and, on the other hand, mutated MVI was shown to be associated with hypertrophic cardiomyopathy [12]. Pharmacological targeting of this interaction could be considered as a potential antiarrhythmia or antihypertrophy therapy.

Conflict of Interests

The authors declare that there is no conflict of interests regarding the publication of this paper.

Acknowledgments

The authors would like to thank the members of Dr. Tomasz Proszynski's Lab at the Nencki Institute for providing laminin-cultured myotubes and Ms. Jagoda Mika, an intern from Lodz University of Technology, for her excellent technical assistance. The authors also thank Dr. Elisabeth Ehler from King's College London for English improvement. This work has been supported by Grant N303 3593 35 and the statutory funds of the Nencki Institute from the Ministry of Science and Higher Education and partly by Grant 2012/05/B/NZ3/01996 from the National Science Center, Poland.

References

[1] H. L. Sweeney and A. Houdusse, "Myosin VI rewrites the rules for myosin motors," *Cell*, vol. 141, no. 4, pp. 573–582, 2010.

[2] M. V. Chibalina, C. Puri, J. Kendrick-Jones, and F. Buss, "Potential roles of myosin VI in cell motility," *Biochemical Society Transactions*, vol. 37, no. 5, pp. 966–970, 2009.

[3] F. Odronitz and M. Kollmar, "Drawing the tree of eukaryotic life based on the analysis of 2,269 manually annotated myosins from 328 species," *Genome Biology*, vol. 8, no. 9, article R196, 2007.

[4] D. A. Tumbarello, J. Kendrick-Jones, and F. Buss, "Myosin VI and its cargo adaptors—linking endocytosis and autophagy," *Journal of Cell Science*, vol. 126, no. 12, pp. 2561–2570, 2013.

[5] I. Lister, R. Roberts, S. Schmitz et al., "Myosin VI: a multifunctional motor," *Biochemical Society Transactions*, vol. 32, no. 5, pp. 685–688, 2004.

[6] S. Sivaramakrishnan and J. A. Spudich, "Coupled myosin VI motors facilitate unidirectional movement on an F-actin network," *The Journal of Cell Biology*, vol. 187, no. 1, pp. 53–60, 2009.

[7] M. J. Rędowicz, "Myosins and pathology: genetics and biology," *Acta Biochimica Polonica*, vol. 49, no. 4, pp. 789–804, 2002.

[8] E. Osterweil, D. G. Wells, and M. S. Mooseker, "A role for myosin VI in postsynaptic structure and glutamate receptor endocytosis," *The Journal of Cell Biology*, vol. 168, no. 2, pp. 329–338, 2005.

[9] H. Yano, I. Ninan, H. Zhang, T. A. Milner, O. Arancio, and M. V. Chao, "BDNF-mediated neurotransmission relies upon a myosin VI motor complex," *Nature Neuroscience*, vol. 9, no. 8, pp. 1009–1018, 2006.

[10] N. Ameen and G. Apodaca, "Defective CFTR apical endocytosis and enterocyte brush border in myosin VI-deficient mice," *Traffic*, vol. 8, no. 8, pp. 998–1006, 2007.

[11] N. Gotoh, Q. Yan, Z. Du et al., "Altered renal proximal tubular endocytosis and histology in mice lacking myosin-VI," *Cytoskeleton*, vol. 67, no. 3, pp. 178–192, 2010.

[12] S. A. Mohiddin, Z. M. Ahmed, A. J. Griffith et al., "Novel association of hypertrophic cardiomyopathy, sensorineural deafness, and a mutation in unconventional myosin VI (MYO6)," *Journal of Medical Genetics*, vol. 41, no. 4, pp. 309–314, 2004.

[13] J. Karolczak, M. Sobczak, Ł. Majewski et al., "Myosin VI in skeletal muscle: its localization in the sarcoplasmic reticulum, neuromuscular junction and muscle nuclei," *Histochemistry and Cell Biology*, vol. 139, no. 6, pp. 873–885, 2013.

[14] M. J. Redowicz, K. Justyna, and M. Lukasz, "Myosin VI in myoblasts: its possible involvement in muscle differentiation," *Journal of Muscle Research and Cell Motility*, vol. 33, p. 263, 2012.

[15] J. Karolczak, S. Weis, E. Ehler et al., "Myosin VI localization and expression in striated muscle pathology," *The Anatomical Record*, vol. 297, pp. 1706–1713, 2014.

[16] J. W. Lin, M. Wyszynski, R. Madhavan, R. Sealock, J. U. Kim, and M. Sheng, "Yotiao, a novel protein of neuromuscular junction and brain that interacts with specific splice variants of NMDA receptor subunit NR1," *The Journal of Neuroscience*, vol. 18, no. 6, pp. 2017–2027, 1998.

[17] A. S. Edwards and J. D. Scott, "A-kinase anchoring proteins: protein kinase A and beyond," *Current Opinion in Cell Biology*, vol. 12, no. 2, pp. 217–221, 2000.

[18] L. Chen and R. S. Kass, "A-Kinase anchoring protein 9 and IKs channel regulation," *Journal of Cardiovascular Pharmacology*, vol. 58, no. 5, pp. 459–461, 2011.

[19] C. P. de Villiers, L. van der, L. Merwe et al., "AKAP9 is a genetic modifier of congenital long-QT syndrome type 1," *Circulation. Cardiovascular Genetics*, 2014.

[20] D. Diviani and J. D. Scott, "AKAP signaling complexes at the cytoskeleton," *Journal of Cell Science*, vol. 114, no. 8, pp. 1431–1437, 2001.

[21] J. M. Redden and K. L. Dodge-Kafka, "AKAP phosphatase complexes in the heart," *Journal of Cardiovascular Pharmacology*, vol. 58, no. 4, pp. 354–362, 2011.

[22] T. J. Proszynski, J. Gingras, G. Valdez, K. Krzewski, and J. R. Sanes, "Podosomes are present in a postsynaptic apparatus and participate in its maturation," *Proceedings of the National Academy of Sciences of the United States of America*, vol. 106, no. 43, pp. 18373–18378, 2009.

[23] Ł. Majewski, M. Sobczak, A. Wasik, K. Skowronek, and M. J. Rędowicz, "Myosin VI in PC12 cells plays important roles in cell migration and proliferation but not in catecholamine secretion," *Journal of Muscle Research and Cell Motility*, vol. 32, no. 4-5, pp. 291–302, 2011.

[24] A. L. Dance, M. Miller, S. Seragaki et al., "Regulation of myosin-VI targeting to endocytic compartments," *Traffic*, vol. 5, no. 10, pp. 798–813, 2004.

[25] R. L. Roberts, M. A. Barbieri, K. M. Pryse, M. Chua, J. H. Morisaki, and P. D. Stahl, "Endosome fusion in living cells overexpressing GFP-rab5," *Journal of Cell Science*, vol. 112, pp. 3667–3375, 1999.

[26] O. Söderberg, M. Gullberg, M. Jarvius et al., "Direct observation of individual endogenous protein complexes in situ by proximity ligation," *Nature Methods*, vol. 3, no. 12, pp. 995–1000, 2006.

[27] Ł. Majewski, M. Sobczak, S. Havrylov, J. Jóźwiak, and M. J. Rędowicz, "Dock7: a GEF for Rho-family GTPases and a novel myosin VI-binding partner in neuronal PC12 cells," *Biochemistry and Cell Biology*, vol. 90, no. 4, pp. 565–574, 2012.

[28] N. L. Siow, R. C. Y. Choi, A. W. M. Cheng et al., "A cyclic AMP-dependent pathway regulates the expression of acetylcholinesterase during myogenic differentiation of C2C12 cells," *The Journal of Biological Chemistry*, vol. 277, no. 39, pp. 36129–36136, 2002.

[29] N. Blom, T. Sicheritz-Pontén, R. Gupta, S. Gammeltoft, and S. Brunak, "Prediction of post-translational glycosylation and phosphorylation of proteins from the amino acid sequence," *Proteomics*, vol. 4, no. 6, pp. 1633–1649, 2004.

[30] W. Wong and J. D. Scott, "AKAP signalling complexes: focal points in space and time," *Nature Reviews Molecular Cell Biology*, vol. 5, no. 12, pp. 959–970, 2004.

[31] J. A. Cruz, R. Garcia, J. F. Rodriguez-Orengo, and J. R. Rodriguez-Medina, "Increased chitin synthesis in response to type II myosin deficiency in Saccharomyces cerevisiae," *Molecular Cell Biology Research Communications*, vol. 3, no. 1, pp. 20–25, 2000.

[32] F. Buss and J. Kendrick-Jones, "How are the cellular functions of myosin VI regulated within the cell?" *Biochemical and Biophysical Research Communications*, vol. 369, no. 1, pp. 165–175, 2008.

[33] M. V. Chibalina, M. N. J. Seaman, C. C. Miller, J. Kendrick-Jones, and F. Buss, "Myosin VI and its interacting protein LMTK2 regulate tubule formation and transport to the endocytic recycling compartment," *Journal of Cell Science*, vol. 120, no. 24, pp. 4278–4288, 2007.

[34] R. L. Karcher, J. T. Roland, F. Zappacosta et al., "Cell cycle regulation of myosin-V by calcium/calmodulin—dependent protein kinase II," *Science*, vol. 293, no. 5533, pp. 1317–1320, 2001.

[35] M. C. S. Pranchevicius, M. M. A. Baqui, H. C. Ishikawa-Ankerhold et al., "Myosin Va phosphorylated on Ser^{1650} is found in nuclear speckles and redistributes to nucleoli upon inhibition of transcription," *Cell Motility and the Cytoskeleton*, vol. 65, no. 6, pp. 441–456, 2008.

[36] I. V. Röder, S. Strack, M. Reischl et al., "Participation of Myosin Va and Pka type I in the regeneration of neuromuscular junctions," *PLoS ONE*, vol. 7, no. 7, Article ID e40860, 2012.

[37] I. V. Röder, Y. Petersen, K. R. Choi, V. Witzemann, J. A. Hammer III, and R. Rudolf, "Role of myosin Va in the plasticity of the vertebrate neuromuscular junction *in vivo*," *PLoS ONE*, vol. 3, no. 12, Article ID e3871, 2008.

Hindawi Publishing Corporation
BioMed Research International
Volume 2015, Article ID 273936, 9 pages
http://dx.doi.org/10.1155/2015/273936

Research Article

Induction of Ankrd1 in Dilated Cardiomyopathy Correlates with the Heart Failure Progression

Julius Bogomolovas,[1,2] Kathrin Brohm,[1] Jelena Čelutkienė,[3] Giedrė Balčiūnaitė,[3] Daiva Bironaitė,[4] Virginija Bukelskienė,[5] Dainius Daunoravičus,[2] Christian C. Witt,[1] Jens Fielitz,[6] Virginija Grabauskienė,[2] and Siegfried Labeit[1]

[1] *Department of Integrative Pathophysiology, Medical Faculty Mannheim, Theodor-Kutzer-Ufer 1-3, 68167 Mannheim, Germany*
[2] *Department of Pathology, Forensic Medicine and Pharmacology, Faculty of Medicine, Vilnius University, M. K. Ciurlionio g. 21, LT-03101 Vilnius, Lithuania*
[3] *Vilnius University Hospital Santariskiu Klinikos, Santariškiu g. 2, LT-08661 Vilnius, Lithuania*
[4] *State Research Institute, Center for Innovative Medicine, Department of Stem Cell Biology, Žygimantu g. 9, LT-01102 Vilnius, Lithuania*
[5] *Vilnius University Institute of Biochemistry, Mokslininku g. 12, LT-08660 Vilnius, Lithuania*
[6] *Experimental and Clinical Research Center (ECRC), Max-Delbrueck Center for Molecular Medicine (MDC), Robert-Rössle-Straße 10, Buch, 13125 Berlin, Germany*

Correspondence should be addressed to Siegfried Labeit; labeit@medma.de

Received 19 August 2014; Accepted 8 October 2014

Academic Editor: Olga Mayans

Progression of idiopathic dilated cardiomyopathy (IDCM) is marked with extensive left ventricular remodeling whose clinical manifestations and molecular basis are poorly understood. We aimed to evaluate the clinical potential of titin ligands in monitoring progression of cardiac remodeling associated with end-stage IDCM. Expression patterns of 8 mechanoptotic machinery-associated titin ligands (*ANKRD1*, *ANKRD2*, *TRIM63*, *TRIM55*, *NBR1*, *MLP*, *FHL2*, and *TCAP*) were quantitated in endomyocardial biopsies from 25 patients with advanced IDCM. When comparing NYHA disease stages, elevated *ANKRD1* expression levels marked transition from NYHA < IV to NYHA IV. *ANKRD1* expression levels closely correlated with systolic strain depression and short E wave deceleration time, as determined by echocardiography. On molecular level, myocardial *ANKRD1* and serum adiponectin correlated with low *BAX/BCL-2* ratios, indicative of antiapoptotic tissue propensity observed during the worsening of heart failure. ANKRD1 is a potential marker for cardiac remodeling and disease progression in IDCM. *ANKRD1* expression correlated with reduced cardiac contractility and compliance. The association of *ANKRD1* with antiapoptotic response suggests its role as myocyte survival factor during late stage heart disease, warranting further studies on ANKRD1 during end-stage heart failure.

1. Introduction

Despite intensive search for therapeutic interventions, idiopathic dilated cardiomyopathy (IDCM) remains the major cause of heart failure eventually leading to heart transplantation. Limited availability of donor hearts results in long waiting times before transplantation can be performed. Many patients with end-stage heart failure perish before a donor heart becomes available. Management of patients awaiting transplantation is demanding, because some of them remain stable while others deteriorate quickly [1]. However, transplantation specialists do not have reliable tools to differentiate between these two disease courses. Therefore, there is a pressing need for markers predicting the prognosis and disease course of end-stage heart failure caused by IDCM in order to prioritize patient listing for transplantation.

Myocyte apoptosis was shown to be a contributor to the development of heart failure (HF) [2], whereas experimental studies on mouse models have suggested that this process might at least be mediated trough the titin filament and its ligands [3]. However, this hypothesis has not been tested so far in clinical settings. Here, we have evaluated expression

levels of 8 titin ligands in endomyocardial biopsies (EMB). Differences in *ANKRD1* expression pattern were found to be most informative: *ANKRD1* levels were associated with decreased cardiac contractility and compliance. *ANKRD1* gene encodes an ankyrin repeat-domain containing protein 1 (Ankrd1, known as well as CARP-cardiac ankyrin repeat protein). Ankrd1 belongs to a family muscle ankyrin repeat proteins, interacting with titin in a stretch-dependent manner: upon mechanical stretch it translocates to the nucleus, where it acts as transcription cofactor [4]. Ventricular *ANKRD1* upregulation was observed in increased stretch states such as experimental pressure overload [5] or clinical heart failure due to dilated [6] and arrhythmogenic right ventricular cardiomyopathy [7]. Moreover, mutations in *ANKRD1* were found to be associated with dilated [8] and hypertrophic cardiomyopathy [9]. Functionally, myocardial ANKRD1 acts as an antiapoptotic survival factor after ischemia-reperfusion injury [10] and hypoxia [11] and is downregulated in apoptosis-driven [12, 13] anthracycline cardiomyopathy [14]. In this work, we present data indicating that ANKRD1 together with adiponectin might act as myocyte survival factors, associated with antiapoptotic response in the terminal stage of IDCM.

2. Materials and Methods

2.1. Patients. Our study cohort was composed of patients admitted to the Vilnius University Hospital during 2011–2013 with suspected diagnosis of IDCM. All patients underwent a careful history and physical examination, as well as routine laboratory studies, including B-type natriuretic peptide (BNP), adiponectin, and cardiac troponin T (hsTnT). 23 patients were selected because of a reduced left ventricular ejection fraction (LVEF < 45%) in the absence of significant coronary artery disease (stenosis of coronary arteries of less than 50%), a history of myocardial infarction, and other specific heart muscle diseases (primary valvular heart disease, toxic cardiomyopathy, arterial hypertension, renal failure, and abuse of alcohol or illicit drugs), all consistent with primary IDCM. IDCM diagnosis was confirmed by histological analysis of endomyocardial biopsies (EMB). Patients who were diagnosed as having acute myocarditis according to histological evidence were excluded from the present study. NYHA class was assigned by a clinician unaware of patient echocardiographic investigation. All patients received maximal pharmacological heart failure therapy according to European Society of Cardiology guidelines: ACE inhibitors or angiotensin receptors blockers, β-blockers, mineralocorticoid receptors blockers, digitalis (in case of atrial fibrillation), diuretics, anticoagulant (in case of atrial fibrillation, EF < 40%), and antiarrhythmics (class III: amiodarone) (see Supplementary Table 1 in Supplementary Material available online at http://dx.doi.org/10.1155/2015/273936). Clinical decision about possible treatment with cardiac resynchronization therapy, radiofrequency ablation, or implantation of a left ventricular assist device or implantable cardioverter-defibrillator was made after coronary angiography and EMB. All patients gave written informed consent to this study, including cardiac catheterisation and EMB. The study was approved by Lithuanian Bioethics Committee (Protocol number 158200-2011/09) and conducted in compliance with the Declaration of Helsinki.

2.2. Echocardiography and Cardiac Catheterisation. Echocardiographic evaluation was performed 1 day before cardiac catheterisation by GE Vivid 7 and 9 ultrasound system by an investigator blinded for the study objectives. The standard LV apical (apical 4, apical 2, and apical 3) views and parasternal short axis views at mid-papillary level were acquired at 70–90 frames/s. Conventional echocardiographic parameters such as left ventricular ejection fraction (LVEF), left ventricular end-diastolic dimension (LVEDD), left ventricular end-systolic dimension (LVESD), velocities of E and A waves (E and A) and their ratio (E/A), and E deceleration time (DcT) were obtained. All images were stored digitally for subsequent offline analysis. Quantification of myocardial deformation values was performed by 2D speckle tracking using Echopac PCBT08 (GE Healthcare) software. After the manual selection, speckles were assumed automatically and then confirmed by the investigator. By the semiautomatic postprocessing longitudinal (in 4 chamber-4C, two-chamber-2C, and three chamber-3C views), circumferential, and radial strain (RS) and strain rate parameters were extracted. Mean pulmonary artery (PA) pressure, pulmonary capillary wedge pressure (PCWP), and pulmonary vascular resistance (PVR) were measured and EMB was taken during right heart catheterization. Biopsy specimens were immediately placed to −70°C until further processing.

2.3. Quantitative RT-PCR. RNA from EMB samples was extracted using RNeasy fibrous tissue minikit according to provided protocol (Qiagen). Tissue was directly homogenized in lysis buffer using Ultra-Turrax device. RNA was reverse transcribed using High Capacity RNA-to-cDNA Kit primed with mixture of random and poly-dT primers (Invitrogen). Transcripts were quantified using TaqMan Gene Expression assay on Real-Time Stratagene MX 3005P machine following manufacturer recommendations. Amplification efficiency validated TaqMan probes (Supplementary Table 2) used in this work are presented in Table 2. 18S rRNA was used for standardization. As this study did not contain a reference group and was based on individual EMB samples, C_t method could not be used for quantification of transcript levels. Therefore relative transcript abundances were quantified using C_t method ($C_{t\ \text{gene of interest}} - C_{t\ \text{S18 rRNA}}$). Transcript levels in this work are expressed as negative C_t values; thus higher $-C_t$ values denote higher mRNA levels whereas negative C_t values represent genes that are less abundant compared with the reference gene. Bax/Bcl-2 ratios were calculated as $C_t((C_{t\ \text{Bax}} - C_{t\ \text{S18 rRNA}}) - (C_{t\ \text{Bcl-2}} - C_{t\ \text{S18 rRNA}}))$ corresponding to relative expression ratio [15].

2.4. Measurement of Activated Caspase-3. Levels of activated caspase-3 in EMB samples were determined using ELISA, specific for the activated protein form (Invitrogen, Paisley, UK). Tissue samples were lysed by sonification in RIPA

Table 1: Patient characteristics.

	NYHA class	
	<IV	IV
Age (years)	44.2 ± 14.2	43.5 ± 13.9
Sex		
Female	4	1
Male	15	5
BMI (kg/m^2)	24.7 ± 4.7	28.7 ± 5.1
NYHA class		
II	1	
III	16	
III-IV	2	
IV		6
BNP (pg/mL)	1259 ± 1180	1964 ± 1177
TnT (pg/mL)	80.9 ± 143.5	34.4 ± 13.9
Adiponectin (μg/mL)	22.9 ± 12.6	33.8 ± 17.5
LVEF (%)	24.1 ± 7.4	20.1 ± 6.2
LVESD (mm)	58.2 ± 9.9	64.3 ± 10.2
LVEDD (mm)	67.3 ± 7.4	71.1 ± 12
RAP (mmHg)	12.5 ± 7.3	16.2 ± 11
PAP (mmHg)	32.2 ± 12.1	43.2 ± 15.8
PCWP (mmHg)	23 ± 9.1	31.8 ± 14.2
PVR (Wood units)	2.5 ± 1.7	3.2 ± 0.8
E wave (m/s)	0.9 ± 0.2	1 ± 0.3
A wave (m/s)	0.5 ± 0.2	0.4 ± 0.1
E/A	1.8 ± 1.1	2.3 ± 0.4
E wave T_{dec} (ms)	140.1 ± 35.2	109 ± 45.4

lysis buffer (Thermo Scientific Inc., USA) supplemented with phosphatase and protease inhibitors according to manufacturer's recommendations (Thermo Scientific Inc., USA). Protein content in clarified lysates was measured using modified Lowry protein assay using bovine serum albumin as standard according to the provided protocol (Thermo Scientific Inc., USA). Analyte concentration was expressed as ng/mg of total protein.

2.5. Statistics. Statistical analysis was performed using SPSS 17 software. Nonparametric Mann-Whitney U test was used to assess differences between two independent groups. Pearson product-moment correlation coefficient was used to evaluate linear dependence between values. If otherwise not indicated, a value of $P < 0.05$ was taken as significant (two-tailed).

3. Results

3.1. Induction of the Titin Ligands ANKRD1, ANKRD2, and TRIM63 in Patients with End-Stage IDCM in Correlation with NYHA Staging. Here, we determined the transcript levels of *ANKRD1, ANKRD2, TRIM63, TRIM55, NBR1, MLP, FHL2,* and *TCAP* in EMB biopsies from end-stage IDCM patient cohort to test their potential roles in titin-based cellular stress transmission. Clinically, we surveyed patients with significantly reduced LVEF, elevated BNP and TnT values, elevated intracardiac pressures, and impaired relaxation (Table 1). Patients were divided into two groups according to the severity of HF symptoms based on NYHA functional class: Group IV (symptomatically Severe HF) and Group <IV (mainly class III; symptomatically moderate HF), and the expression levels of mechanoptotic machinery members were compared (Table 2). Out of 8 studied transcripts, *ANKRD1, ANKRD2,* and *TRIM63* were significantly higher in NYHA class IV than <IV NYHA class group (Figure 1, $P = 0.01$ for *ANKRD1* and $P = 0.03$ for *ANKRD2* and *TRIM63*). *ANKRD1* had the highest expression levels compared to other titin

Table 2: Differences in myocardial expression patterns of titin ligands according to NYHA functional class <IV ($n = 19$) and NYHA IV ($n = 6$).

Transcript level ($-\Delta C_t$)	NYHA class		P value
	<IV	IV	
ANKRD1*	−9.42 ± 0.7	−6.83 ± 0.7	0.01
ANKRD2*	−16.79 ± 0.7	−14.5 ± 0.8	0.03
TRIM63*	−13.81 ± 0.6	−11.82 ± 0.5	0.03
TRIM55	−14.23 ± 0.8	−13.11 ± 0.7	0.25
NBR1	−11.97 ± 0.7	−11.73 ± 0.9	0.44
MLP	−10.39 ± 1.0	−9.15 ± 0.9	0.20
FHL2	−10.07 ± 0.8	−9.75 ± 0.6	0.56
TCAP	−7.08 ± 0.9	−6.16 ± 0.8	0.30
BCL-2*	−17.81 ± 0.4	−16.25 ± 0.7	0.02
BAX	−15.71 ± 0.3	−14.39 ± 0.9	0.22

Significant differences (P value < 0.05 of the Mann-Whitney U test) marked with $*$.

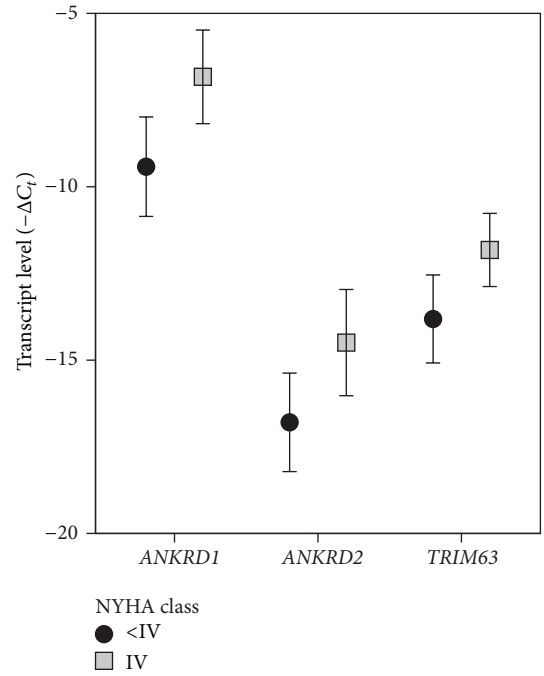

Figure 1: Myocardial titin ligand expression patterns associate with disease progression in IDCM patients. Statistically significant titin ligand expression differences represented as bar graph. Data are presented as mean ± 2 s.e.m. Note the highest expression level and the most pronounced difference between groups in *ANKRD1* expression pattern.

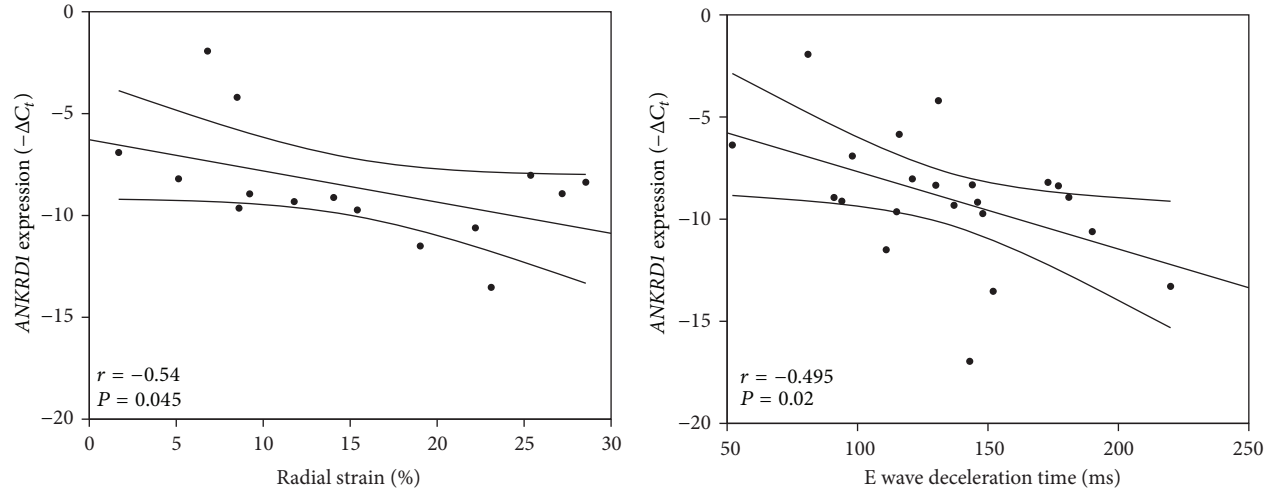

Figure 2: Increased *ANKRD1* expression marks left ventricular remodeling. (a) Linear correlation between *ANKRD1* expression and radial stain. Regression line is represented within 95% confidence interval for the mean value. A negative correlation between *ANKRD1* expression ($-C_t$) and radial strain (RS; %) was found ($n = 14$, $r = -0.54$, $P < 0.05$). (b) Linear correlation between *ANKRD1* expression and E wave deceleration time. Regression line is represented within 95% confidence interval for the mean value. A negative correlation between *ANKRD1* expression ($-C_t$) and E wave deceleration time (ms) was detected ($n = 21$, $r = -0.495$, $P < 0.05$).

ligands and the most profound 6-fold induction (calculated as $2^{C_t\ \text{IV NYHA}-C_t<\text{IV NYHA}}$) in NYHA IV patients as compared to NYHA <IV patients. Therefore, *ANKRD1* expression pattern was the most sensitive to the disease progression and was chosen for the further analysis.

3.2. ANKRD1 Expression Correlates with LV Remodeling in End-Stage IDCM Patients. In order to investigate clinical correlates of *ANKRD1* expression we looked for further clinical parameters different between NYHA class >IV and <IV. Statistically significant differences between NYHA <IV and NYHA IV groups were only detected for parameters of systolic strain (Table 3). Strain measurements quantify magnitudes and velocities of myocardial deformation estimating myocardial contractility [16]. Radial and longitudinal strain in 3C projection showed marked reduction in severe HF patients (NYHA IV) when compared to symptomatically moderate HF patients (NYHA <IV) (Table 3). Correlation analysis confirmed that reduced cardiac contractility correlated with *ANKRD1* expression independently from NYHA functional class (Figure 2(a)). Further, we found that *ANKRD1* expression correlated with the E wave deceleration time shortening, which is an index for LV stiffness [17] (Figure 2(b)). Taken together, *ANKRD1* expression is associated with LV remodeling resulting in reduced cardiac contractility and compliance.

3.3. Deteriorating Cardiac Contractility Is Associated with Blunted Myocardial Vulnerability to Apoptosis. Because myocyte apoptosis is associated with contractile dysfunction in HF [18, 19] and ANKRD1 acts as antiapoptotic [10, 11], we hypothesized that decreased cardiac contractility in end-stage IDCM patients is associated with proteins involved in mechanoptosis. As presented above, the most pronounced deterioration of cardiac contractility upon IDCM progression was observed in radial direction by echocardiography, referred to as radial strain (RS). Thus, for further analysis we used RS to monitor worsening of cardiac contractility. Patients were subdivided into two groups according to the median value of RS. The above median RS group displayed normal radial cardiac contractility as mean RS was still within a healthy population reference range [20]. In contrast, patients with RS values below the median RS had severely impaired cardiac contractility (Table 4). Further strain parameters, RS rate and 3C longitudinal

Table 3: Differences in strain parameters between NYHA <IV and NYHA IV groups.

Strain parameter	NYHA class		*P* value
	<IV	IV	
4C strain (%)	−7.4 ± 1	−4 ± 0.8	0.10
4C strain rate (s^{-1})	−0.4 ± 0	−0.2 ± 0	0.10
2C strain (%)	−6.7 ± 0.9	−5.1 ± 0.9	0.25
2C strain rate (s^{-1})	−0.3 ± 0	−0.3 ± 0	0.34
3C strain (%)*	−8.1 ± 0.8	−3.9 ± 1.1	0.01
3C strain rate (s^{-1})	−0.8 ± 0.4	−0.2 ± 0	0.11
Circumferential strain (%)	−5.5 ± 0.5	−4.3 ± 1.2	0.51
Circumferential strain rate (s^{-1})	−0.4 ± 0	−0.2 ± 0	0.20
Radial strain (%)*	17.4 ± 2.3	6.1 ± 1.7	0.01
Radial strain rate (s^{-1})	1.3 ± 0.1	0.8 ± 0.2	0.11

Note further reduction of systolic strain parameters along disease progression.
Significant differences (*P* value < 0.05 of the Mann-Whitney *U* test) marked with ∗.

Table 4: Clinical characteristics of patients ($n = 14$) with high radial strain (RS, above median) and low RS (below median).

	Radial strain	
	Below median	Above median
Age (years)	48 ± 6.51	44 ± 3.3
Sex		
Female	2	3
Male	5	4
BMI (kg/m^2)	25.6 ± 2.0	27.03 ± 2.13
NYHA class		
III	3	5
III-IV	0	2
IV	4	0
BNP (pg/mL)*	1824 ± 461	525 ± 197
TnT (pg/mL)	31.17 ± 6.1	157 ± 136.4
Adiponectin (μg/mL)*	35 ± 5.4	8.5 ± 1.8
LVEF (%)	21.29 ± 1.1	25.29 ± 3.34
LVESD (mm)	61 ± 2.1	55.5 ± 2.1
LVEDD (mm)	71.3 ± 2.1	65.6 ± 1.7
RAP (mmHg)	12.33 ± 3.9	9.33 ± 1.28
PAP (mmHg)	32.6 ± 4.7	25.3 ± 1.91
PCWP (mmHg)	23.14 ± 3.8	18.17 ± 1.51
PVR (Wood units)	2.5 ± 0.44	2.025 ± 0.55
E wave (m/s)	1 ± 0.11	0.92 ± 0.06
A wave (m/s)	0.398 ± 0.05	0.63 ± 0.095
E/A	2.71 ± 0.36	1.86 ± 0.48
E wave T_{dec} (ms)	118 ± 12	146 ± 15.42
3C strain (%)*	−5.07 ± 0.96	−8.75 ± 0.98
Radial strain (%)*	7.39 ± 1.23	21.1 ± 1.95
Radial strain rate (s^{-1})*	0.88 ± 0.19	1.55 ± 0.13
ANKRD1 ($-\Delta C_t$)*	−7.02 ± 1.1	−10.26 ± 0.68
BCL-2 ($-\Delta C_t$)†	−16.36 ± 1.0	−18.67 ± 0.22
BAX ($-\Delta C_t$)	−14.60 ± 1.0	−16.02 ± 0.17
BAX/*BCL-2* ratio ($\Delta\Delta C_t$)*	1.76 ± 0.27	2.65 ± 0.19
Active caspase-3 (ng/mg)†	0.19 ± 0.06	0.45 ± 0.11

* $P_{\text{two-sided}} < 0.05$; † $P_{\text{one-sided}} < 0.05$ (Mann-Whitney U test).

strain, indicated better cardiac contractility in above median RS group. None of the echocardiographic parameters or cardiac chamber pressure values reached statistically significant differences. However, the group with severe loss of radial deformation (below RS median) showed a tendency towards worse cardiac function. *ANKRD1* and stretch-marker BNP levels were higher in the group with impaired radial contractility. Next, we evaluated transcript levels of proapoptotic *BAX* and antiapoptotic *BCL-2* whose ratio defines tissue propensity to apoptosis [21] and amount of active caspase-3, a major apoptosis executer [22] that corresponds to intensity of ongoing apoptosis. Better contractility correlated with lower antiapoptotic *BCL-2* levels and thus corresponded to a group more prone to apoptosis (Figures 3(a) and 3(b)). Consequently, higher levels of ongoing apoptosis, as measured by levels of active caspase-3, were detected in higher RS group (Figure 3(c)). Low *BAX*/*BCL-2* ratios and therefore myocardial insensitivity to apoptosis correlated well with *ANKRD1* transcript levels (Figure 4(a)). In addition, *BAX*/*BCL-2* ratios inversely correlated with serum adiponectin levels (Figure 4(b)). Taken together our data imply that *ANKRD1* might be involved in antiapoptotic response observed in end-stage DCM [23].

4. Discussion

Genes coding for titin binding proteins has been suggested to act as members of a titin filament based stress sensing mechanoptotic machinery in previous mouse work [3]. Here, we tested for a potential clinical significance of titin ligands for LV remodeling in IDCM patients. Out of 8 studied transcripts we found that *ANKRD1* expression levels showed the most significant increase in symptomatically severe HF (NYHA class IV) compared to moderate HF (NYHA < IV) patients. Clinically, severe HF patients had notably poorer systolic strain rates indicating reduced cardiac contractility. Our data indicate that myocardial strain parameters are superior to LV ejection fraction and chamber diameter, intracardiac pressure, and relaxation measures in detecting the severity of heart failure as estimated by NYHA functional class. Our findings are in line with previous studies where myocardial strain predicted rapid HF progression in end-stage IDCM patients [1]. We found a significant reduction of longitudinal strain in 4C and 3C projections, but the major difference was observed for radial strain measurements. These findings are in line with a study on hypertensive patients with heart failure, where a reduction in radial strain was only seen in NYHA classes III-IV, whereas longitudinal strain was decreased as early as NYHA class II [24]. Moreover we found that *ANKRD1* expression correlated not only with reduced LV contractility, but also with increased cardiac stiffness; *ANKRD1* expression positively correlated with shortening of E wave deceleration time, marking restrictive filling pattern—the most powerful independent prognostic indicator of poor outcome or transplantation in DCM patients [25]. Taken together our data indicate that ventricular *ANKRD1* levels in IDCM patients are associated with progression of LV remodeling, resulting in reduced cardiac contractility and compliance. In DCM, myocyte apoptosis is related to LV dysfunction [26] and appears to directly affect cardiac contractility [18, 19]. Finally, myocardial ANKRD1 functions as an antiapoptotic survival factor after ischemia-reperfusion injury [10] and hypoxia [11]. Therefore, we investigated the relation between *ANKRD1* expression and apoptotic status in the myocardium. We found that tissue samples more susceptible to apoptosis (high *BAX*/*BCL-2* ratio) had lower *ANKRD1* levels than apoptosis-resistant samples (low *BAX*/*BCL-2* ratio) implying that *ANKRD1* could act as myocyte survival factor. However, counterintuitively the group with less impaired cardiac contractility (above median RS) was more prone to apoptosis than low RS group. In addition, impaired contractility was associated with higher *BAX*/*BCL-2* ratios and elevated levels of key apoptosis-executing enzyme [22] and active caspase-3, indicating that

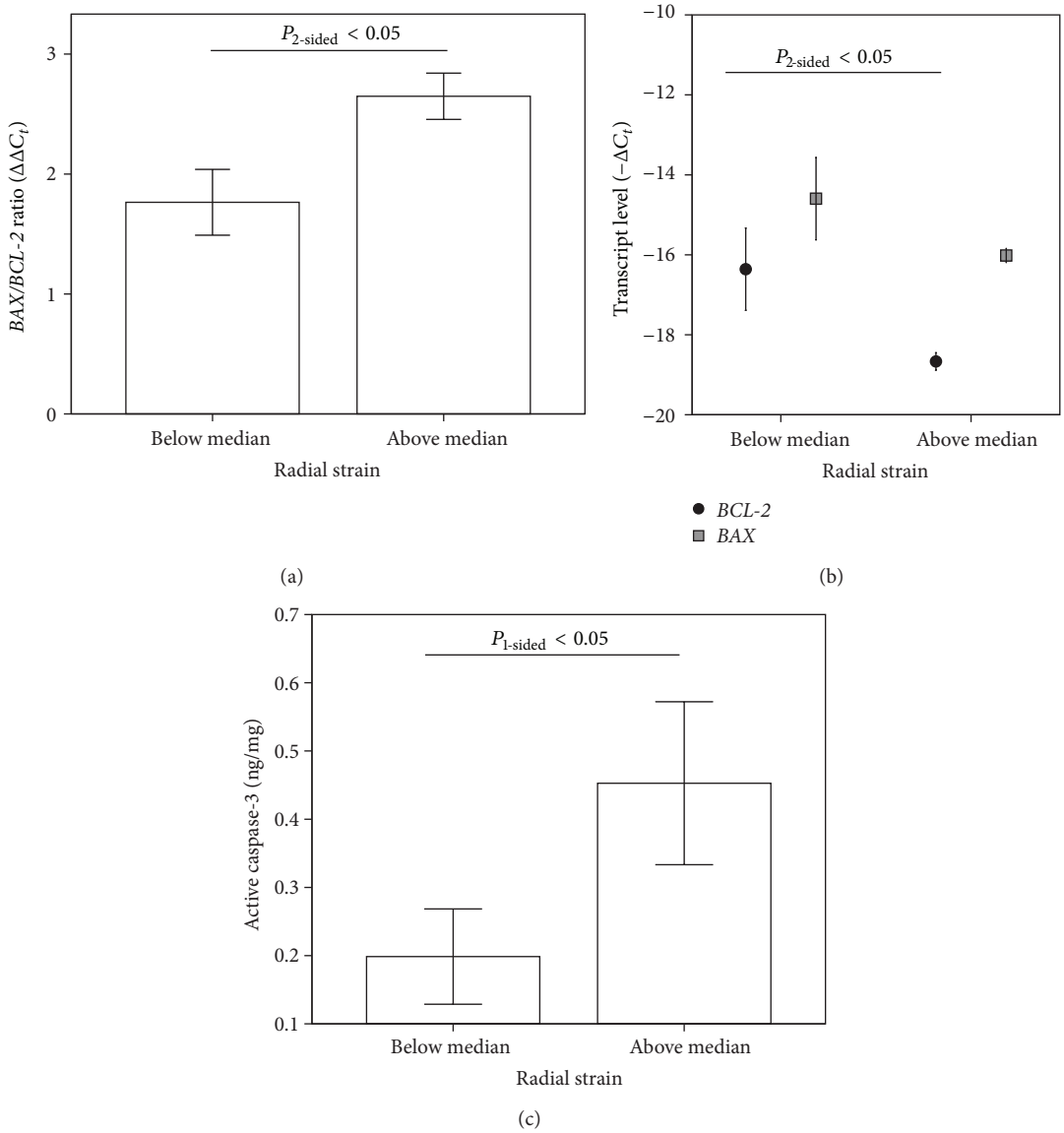

Figure 3: *ANKRD1* and adiponectin upregulation are associated with antiapoptotic response in progression of IDCM. (a) Difference in *BAX/BCL-2* ratio between high and low RS groups. Data are presented as mean ± 2 s.e.m; P value < 0.05 (Mann-Whitney U test). (b) Relative expression levels of *BAX* and *BCL-2*. Data are presented as mean ± 2 s.e.m. $P_{\text{one-sided}}$ value < 0.05 (Mann-Whitney U test). (c) Difference in active caspase-3 levels between high and low RS groups. Data are presented as mean ± 2 s.e.m; $P_{\text{one-sided}}$ value < 0.05 (Mann-Whitney U test); $n = 6$ (lower RS); $n = 5$ (higher RS).

better contractility was marked with higher levels of ongoing apoptosis. These findings correspond to previous observations that terminal IDCM stage is associated with marked antiapoptotic response [23]. In agreement with previous data on end-stage HF [27], we found that a decreased *BAX*/*BCL-2* ratio in hearts with severely impaired contractility was mainly due to increased levels of the survival factor Bcl-2. Moreover, insensitivity to apoptosis was associated with increased serum adiponectin levels, a predictor for mortality in patients with chronic HF [28]. Possibly, adiponectin could account for the reduced *BAX*/*BCL-2* ratio in end-stage IDCM patients, as it has antiapoptotic effects in myocardium [29].

Speculatively, stretch-sensing and prosurvival properties of Ankrd1 could be responsible for the observed antiapoptotic response in terminal IDCM stages (Figure 5). LV remodeling in IDCM leading to the wall thickening and chamber dilation is accompanied by myocyte overstretch and slippage [30] which in vicious cycle provokes myocyte mechanoptosis [31]. Subsequently stretch would directly upregulate *ANKRD1* transcript and launch Ankrd1-mediated survival cascades. Hypothetically, *ANKRD1* and adiponectin or their agonists could be used as heart-specific antiapoptotic agents in treatment of IDCM.

This study has some limitations which have to be pointed out. The study cohort consisted of patients with advanced

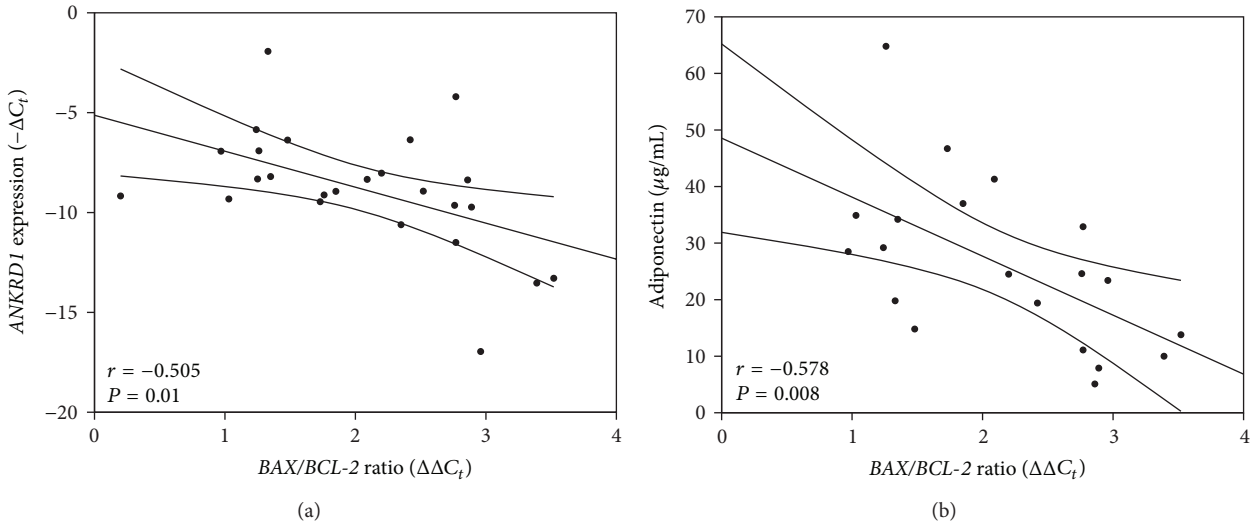

FIGURE 4: *ANKRD1* and adiponectin correlate with tissue propensity to apoptosis. (a) Linear correlation between *ANKRD1* expression and *BAX/BCL-2* ratio. Regression line is represented within 95% confidence interval for the mean value. A negative correlation between *ANKRD1* expression ($-C_t$) and *BAX/BCL-2* ratio (C_t) was found ($n = 25$, $r = -0.505$, $P = 0.01$). (b) Linear correlation between adiponectin levels and *BAX/BCL-2* ratio. Regression line is represented within 95% confidence interval for the mean value. A negative correlation between serum adiponectin levels (μg/mL) and cardiac *BAX/BCL-2* ratio (C_t) was observed ($n = 20$, $r = -0.578$, $P < 0.01$).

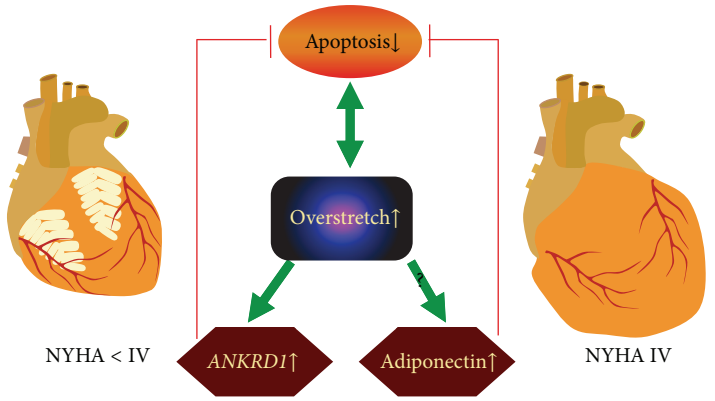

FIGURE 5: Antiapoptotic response in end-stage IDCM. Speculatively, ongoing apoptosis and myocyte overstretch in vicious cycle mediate the LV remodeling, whereas myocyte stretch induces Ankrd1 expression and increases adiponectin levels by unknown mechanism that in turn inhibit apoptotic signaling. Arrows indicate process dynamics in NYHA <IV to NYHA IV transition.

HF (NYHA classes III-IV); thus future research would be needed to confirm the validity of observed clinical correlations in patients with mild HF (NYHA I-II). Recent studies have demonstrated that genetic alterations of titin [32] and *ANKRD1* [33, 34] are associated with DCM and result in poorer prognosis [32]. Thus, it is not excluded that genetic alterations of titin-ligand network might be present in studied patients. However, observed upregulation of *ANKRD1* is very likely to be universal pathophysiological as it was described in controlled increased stretch states such as experimental pressure overload [5] and not due to genetic alterations. This study was based on patients with advanced stages of HF (mostly NYHA classes III-IV); thus future research would be needed to evaluate the validity of observed clinical correlations in early HF (NYHA I-II).

Although transcript levels do not always represent changes in protein concentration, our data suggest that *ANKRD1* transcript quantification is sensitive test for monitoring progression of advanced IDCM stages. Moreover, quantitative RT-PCR might be method of choice to quantify *ANKRD1* levels, when using minute EMB samples.

In conclusion, expression profiling of selected mechanoptotic machinery members revealed association between increased *ANKRD1* expression and deterioration of cardiac contractility and compliance in IDCM patients. Therefore, elevated *ANKRD1* expression could serve as potential clinical marker to uncover a coming need to plan heart transplantation in end-stage HF patients. Further research is warranted on the functional roles of *ANKRD1* induction in IDCM associated apoptosis.

Conflict of Interests

The authors declare that there is no conflict of interests regarding the publication of this paper.

Acknowledgments

Virginija Grabauskienė and Dainius Daunoravičus are funded by a grant (no. MIP-086/2012); Julius Bogomolovas, Virginija Grabauskienė, Daiva Bironaitė, and Virginija Bukelskienė are funded by a grant (MIP-011/2014) from the Research Council of Lithuania. Siegfried Labeit is supported by DFG (La668/11-2 and La668/15-1) and EU-FP7 (SarcoSi). Christian C. Witt is grateful for the generous support of DFG (La668/15-1 and Wi3278/2-2).

References

[1] R. Jasaityte, M. Dandel, H. Lehmkuhl, and R. Hetzer, "rediction of short-term outcomes in patients with idiopathic dilated cardiomyopathy referred for transplantation using standard echocardiography and strain imaging," *Transplantation Proceedings*, vol. 41, no. 1, pp. 277–280, 2009.

[2] P. M. Kang and S. Izumo, "Apoptosis and heart failure: a critical review of the literature," *Circulation Research*, vol. 86, no. 11, pp. 1107–1113, 2000.

[3] R. Knöll and B. Buyandelger, "Z-disc transcriptional coupling, sarcomeroptosis and mechanoptosis," *Cell Biochemistry and Biophysics*, vol. 66, no. 1, pp. 65–71, 2013.

[4] M. K. Miller, M.-L. Bang, C. C. Witt et al., "The muscle ankyrin repeat proteins: CARP, ankrd2/Arpp and DARP as a family of titin filament-based stress response molecules," *Journal of Molecular Biology*, vol. 333, no. 5, pp. 951–964, 2003.

[5] Y. Aihara, M. Kurabayashi, Y. Saito et al., "Cardiac ankyrin repeat protein is a novel marker of cardiac hypertrophy: role of M-CAT element within the promoter," *Hypertension*, vol. 36, no. 1, pp. 48–53, 2000.

[6] S. F. Nagueh, G. Shah, Y. Wu et al., "Altered titin expression, myocardial stiffness, and left ventricular function in patients with dilated cardiomyopathy," *Circulation*, vol. 110, no. 2, pp. 155–162, 2004.

[7] Y.-J. Wei, C.-J. Cui, Y.-X. Huang, X.-L. Zhang, H. Zhang, and S.-S. Hu, "Upregulated expression of cardiac ankyrin repeat protein in human failing hearts due to arrhythmogenic right ventricular cardiomyopathy," *European Journal of Heart Failure*, vol. 11, no. 6, pp. 559–566, 2009.

[8] M. Moulik, M. Vatta, S. H. Witt et al., "*ANKRD1*, the gene encoding cardiac ankyrin repeat protein, is a novel dilated cardiomyopathy gene," *Journal of the American College of Cardiology*, vol. 54, no. 4, pp. 325–333, 2009.

[9] T. Arimura, J. M. Bos, A. Sato et al., "Cardiac ankyrin repeat protein gene (*ANKRD1*) mutations in hypertrophic cardiomyopathy," *Journal of the American College of Cardiology*, vol. 54, no. 4, pp. 334–342, 2009.

[10] M.-J. Lee, Y.-K. Kwak, K.-R. You, B.-H. Lee, and D.-G. Kim, "Involvement of GADD153 and cardiac ankyrin repeat protein in cardiac ischemia-reperfusion injury," *Experimental and Molecular Medicine*, vol. 41, no. 4, pp. 243–252, 2009.

[11] X.-J. Han, J.-K. Chae, M.-J. Lee, K.-R. You, B.-H. Lee, and D.-G. Kim, "Involvement of GADD153 and cardiac ankyrin repeat protein in hypoxia-induced apoptosis of H9c2 cells," *The Journal of Biological Chemistry*, vol. 280, no. 24, pp. 23122–23129, 2005.

[12] P. J. Lee, D. Rudenko, M. A. Kuliszewski et al., "Survivin gene therapy attenuates left ventricular systolic dysfunction in doxorubicin cardiomyopathy by reducing apoptosis and fibrosis," *Cardiovascular Research*, vol. 101, no. 3, pp. 423–433, 2014.

[13] T. Nakamura, Y. Ueda, Y. Juan, S. Katsuda, H. Takahashi, and E. Koh, "Fas-mediated apoptosis in Adriamycin-induced cardiomyopathy in rats: in vivo study," *Circulation*, vol. 102, no. 5, pp. 572–578, 2000.

[14] B. Chen, L. Zhong, S. F. Roush et al., "Disruption of a GATA4/Ankrd1 signaling axis in cardiomyocytes leads to sarcomere disarray: implications for anthracycline cardiomyopathy," *PLoS ONE*, vol. 7, no. 4, Article ID e35743, 2012.

[15] J. S. Yuan, A. Reed, F. Chen, and C. N. Stewart Jr., "Statistical analysis of real-time PCR data," *BMC Bioinformatics*, vol. 7, article 85, 2006.

[16] N. L. Greenberg, M. S. Firstenberg, P. L. Castro et al., "Doppler-derived myocardial systolic strain rate is a strong index of left ventricular contractility," *Circulation*, vol. 105, no. 1, pp. 99–105, 2002.

[17] W. C. Little, M. Ohno, D. W. Kitzman, J. D. Thomas, and C.-P. Cheng, "Determination of left ventricular chamber stiffness from the time for deceleration of early left ventricular filling," *Circulation*, vol. 92, no. 7, pp. 1933–1939, 1995.

[18] D. Wencker, M. Chandra, K. Nguyen et al., "A mechanistic role for cardiac myocyte apoptosis in heart failure," *The Journal of Clinical Investigation*, vol. 111, no. 10, pp. 1497–1504, 2003.

[19] K.-L. Laugwitz, A. Schömig, M. Ungerer et al., "Blocking caspase-activated apoptosis improves contractility in failing myocardium," *Human Gene Therapy*, vol. 12, no. 17, pp. 2051–2063, 2001.

[20] S. Cheng, M. G. Larson, E. L. McCabe et al., "Age- and sex-based reference limits and clinical correlates of myocardial strain and synchrony: the framingham heart study," *Circulation: Cardiovascular Imaging*, vol. 6, no. 5, pp. 692–699, 2013.

[21] Z. N. Oltvai, C. L. Milliman, and S. J. Korsmeyer, "Bcl-2 heterodimerizes in vivo with a conserved homolog, Bax, that accelerates programed cell death," *Cell*, vol. 74, no. 4, pp. 609–619, 1993.

[22] G. M. Cohen, "Caspases: the executioners of apoptosis," *The Biochemical Journal*, vol. 326, no. 1, pp. 1–16, 1997.

[23] Ö. Akyürek, N. Akyürek, T. Sayin et al., "Association between the severity of heart failure and the susceptibility of myocytes to apoptosis in patients with idiopathic dilated cardiomyopathy," *International Journal of Cardiology*, vol. 80, no. 1, pp. 29–36, 2001.

[24] W. Kosmala, R. Plaksej, J. M. Strotmann et al., "Progression of left ventricular functional abnormalities in hypertensive patients with heart failure: an ultrasonic two-dimensional speckle tracking study," *Journal of the American Society of Echocardiography*, vol. 21, no. 12, pp. 1309–1317, 2008.

[25] C. S. Rihal, R. A. Nishimura, L. K. Hatle, K. R. Bailey, and A. J. Tajik, "Systolic and diastolic dysfunction in patients with clinical diagnosis of dilated cardiomyopathy: relation to symptoms and prognosis," *Circulation*, vol. 90, no. 6, pp. 2772–2779, 1994.

[26] W. Ibe, A. Saraste, S. Lindemann et al., "Cardiomyocyte apoptosis is related to left ventricular dysfunction and remodelling in dilated cardiomyopathy, but is not affected by growth hormone

treatment," *European Journal of Heart Failure*, vol. 9, no. 2, pp. 160–167, 2007.

[27] N. Latif, M. A. Khan, E. Birks et al., "Upregulation of the Bcl-2 family of proteins in end stage heart failure," *Journal of the American College of Cardiology*, vol. 35, no. 7, pp. 1769–1777, 2000.

[28] C. Kistorp, J. Faber, S. Galatius et al., "Plasma adiponectin, body mass index, and mortality in patients with chronic heart failure," *Circulation*, vol. 112, no. 12, pp. 1756–1762, 2005.

[29] Y. Zhang, X.-L. Wang, J. Zhao et al., "Adiponectin inhibits oxidative/nitrative stress during myocardial ischemia and reperfusion via PKA signaling," *American Journal of Physiology—Endocrinology and Metabolism*, vol. 305, no. 12, pp. E1436–E1443, 2013.

[30] C. A. Beltrami, N. Finato, M. Rocco et al., "Structural basis of end-stage failure in ischemic cardiomyopathy in humans," *Circulation*, vol. 89, no. 1, pp. 151–163, 1994.

[31] W. Cheng, B. Li, J. Kajstura et al., "Stretch-induced programmed myocyte cell death," *The Journal of Clinical Investigation*, vol. 96, no. 5, pp. 2247–2259, 1995.

[32] D. S. Herman, L. Lam, M. R. G. Taylor et al., "Truncations of titin causing dilated cardiomyopathy," *The New England Journal of Medicine*, vol. 366, no. 7, pp. 619–628, 2012.

[33] M. Moulik, M. Vatta, S. H. Witt et al., "ANKRD1, the gene encoding cardiac ankyrin repeat protein, is a novel dilated cardiomyopathy gene," *Journal of the American College of Cardiology*, vol. 54, no. 4, pp. 325–333, 2009.

[34] L. Duboscq-Bidot, P. Charron, V. Ruppert et al., "Mutations in the *ANKRD1* gene encoding CARP are responsible for human dilated cardiomyopathy," *European Heart Journal*, vol. 30, no. 17, pp. 2128–2136, 2009.

Hindawi Publishing Corporation
BioMed Research International
Volume 2015, Article ID 396593, 7 pages
http://dx.doi.org/10.1155/2015/396593

Research Article

Low Frequency Electromagnetic Field Conditioning Protects against I/R Injury and Contractile Dysfunction in the Isolated Rat Heart

Dariusz Bialy,[1] Magdalena Wawrzynska,[2] Iwona Bil-Lula,[3] Anna Krzywonos-Zawadzka,[3] Mieczyslaw Wozniak,[3,4] Virgilio J. J. Cadete,[5] and Grzegorz Sawicki[3,4]

[1]*Department and Clinic of Cardiology, Medical University of Wroclaw, 50-556 Wroclaw, Poland*
[2]*Department of Medical Emergency, Medical University of Wroclaw, 51-616 Wroclaw, Poland*
[3]*Department of Clinical Chemistry, Medical University of Wroclaw, 50-556 Wroclaw, Poland*
[4]*Department of Pharmacology, College of Medicine, University of Saskatchewan, 107 Wiggins Road, Saskatoon, SK, Canada S7N 5E5*
[5]*Faculty of Pharmacy, University of Montreal, Montreal, QC, Canada H3T 1J4*

Correspondence should be addressed to Grzegorz Sawicki; greg.sawicki@usask.ca

Received 23 October 2014; Accepted 17 December 2014

Academic Editor: Danuta Szczesna-Cordary

Low frequency electromagnetic field (LF-EMF) decreases the formation of reactive oxygen species, which are key mediators of ischemia/reperfusion (I/R) injury. Therefore, we hypothesized that the LF-EMF protects contractility of hearts subjected to I/R injury. Isolated rat hearts were subjected to 20 min of global no-flow ischemia, followed by 30 min reperfusion, in the presence or absence of LF-EMF. Coronary flow, heart rate, left ventricular developed pressure (LVDP), and rate pressure product (RPP) were determined for evaluation of heart mechanical function. The activity of cardiac matrix metalloproteinase-2 (MMP-2) and the contents of coronary effluent troponin I (TnI) and interleukin-6 (IL-6) were measured as markers of heart injury. LF-EMF prevented decreased RPP in I/R hearts, while having no effect on coronary flow. In addition, hearts subjected to I/R exhibited significantly increased LVDP when subjected to LF-EMF. Although TnI and IL-6 levels were increased in I/R hearts, their levels returned to baseline aerobic levels in I/R hearts subjected to LF-EMF. The reduced activity of MMP-2 in I/R hearts was reversed in hearts subjected to LF-EMF. The data presented here indicate that acute exposure to LF-EMF protects mechanical function of I/R hearts and reduces I/R injury.

1. Introduction

Low frequency electromagnetic fields (LF-EMFs) have been used for over 30 years in orthopaedics to enhance bone healing [1–4] and also in skin lesion repair [5] and neoangiogenesis [6]. Several biological systems have been studied, with particular focus on the cardiovascular and central nervous systems as primary targets of LF-EMF. This is primarily due to shared common characteristics between these two systems, such as high electrical activity and sensitivity to induced electrical currents, which make these systems potential targets of electromagnetic fields. Although several human studies have evaluated the effects of long- and short-term exposure to LF-EMF on the cardiovascular system, the contradictory results reported (ranging from increased cardiovascular risk to increased cardioprotection and the absence of any effect) further add to the controversial discussion on the effects of LF-EMF on biological systems.

Despite the numerous studies, the underlying mechanisms regarding the interaction between electromagnetic fields and biological systems remain unknown. Little is also known about the acute effects of LF-EMF. The study of the effects of LF-EMF on the cardiovascular system demonstrated protection against myocardial infarction (MI) [7]. Similarly, data from Ma and colleagues [8] suggest that LF-EMFs inhibit the generation of reactive oxygen species, such as nitric oxide and peroxynitrite, thereby protecting cardiomyocytes from I/R and oxidative damage. The protective

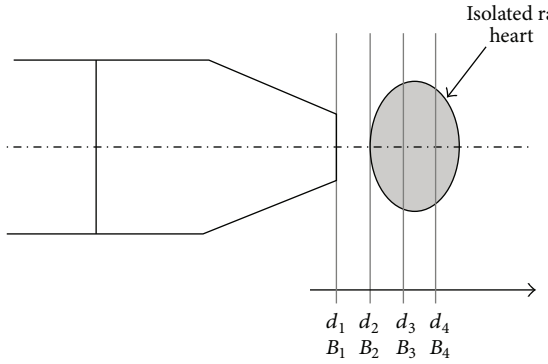

Figure 1: Diagram of dependence of the electromagnetic field to distance (d_{1-4}) from the head of applicator to the isolated heart. Different electromagnetic fields are represented by B_{1-4}. The arrow indicates increased distance and decreased electromagnetic field from the head. The estimated values of electromagnetic induction (B) in relation to distance (d) from the head of the applicator are showed in Table 1.

effects of LF-EMF are further supported by a study examining the effects of LF-EMF on skin wound healing which suggests that LF-EMF stimulates endogenous antioxidant systems. A recent study by Kim and colleagues [9], involving both teenaged and adult subjects, suggests that acute exposure to LF-EMF has no physiological effects. Taken together, these observations strongly suggest a potential protective role of LF-EMF against cardiac injury, with minimal physiological alterations.

The purpose of this study was to evaluate the protective effects of LF-EMF in a model of *ex vivo* cardiac I/R. We demonstrate that LF-EMF alone, when applied prior to, during, and after the ischemic insult, protects the heart against I/R-induced cardiac contractile dysfunction and heart injury.

2. Materials and Methods

All procedures were performed in conformity with "Guidelines and Authorization for the Use of Laboratory Animals" (Polish Government, Ministry of Health).

2.1. Retrograde Isolated Rat Heart Perfusions. Male Wistar rats (300 g to 350 g) were anaesthetized with sodium pentobarbital (60 mg/kg i.p.). Once surgical plane was achieved, hearts were rapidly excised and rinsed by immersion in ice-cold Krebs-Henseleit buffer, followed by cannulation of the aorta and beginning of the retrograde perfusion at constant flow (10 mL/min). Spontaneously beating hearts were perfused in the Langendorff mode at a constant pressure of 60 mmHg in a water-jacketed chamber at 37°C (EMKA Technologies, Paris, France). Krebs-Henseleit buffer at 37°C containing (in mM) NaCl (118), KCl (4.7), KH_2PO_4 (1.2), $MgSO_4$ (1.2), $CaCl_2$ (3.0), $NaHCO_3$ (25), glucose (11), and EDTA (0.5) and gassed continuously with 95% O_2/5% CO_2 (pH 7.4) was used throughout the perfusion period.

Left ventricular pressures and heart rate were measured with the help of a water-filled latex balloon connected to a pressure transducer and inserted through an incision in the left atrium into the left ventricle through the mitral valve. The volume was adjusted at the beginning of the perfusion period to achieve an end-diastolic pressure of 10 mmHg. Coronary flow, heart rate, and left ventricular pressure were monitored using an EMKA recording system with IOX2 software (EMKA Technologies, Paris, France). Left ventricular developed pressure (LVDP) was calculated as the difference between peak systolic and diastolic pressures. The rate pressure product (RPP) was calculated as the product of heart rate and LVDP.

Table 1: Estimated values of magnetic induction in relation to distance from the head of the applicator.

Value of magnetic induction in relation to distance from the head of applicator:	Induction at value "12"	Induction at value "10"
$d_1 = 0$ mm $\rightarrow$ $B_1 = 100\%$	13,440 μT	11,200 μT
$d_2 = 3$ mm $\rightarrow$ $B_2 = 50\%$	6,720 μT	5,600 μT
$d_3 = 6$ mm $\rightarrow$ $B_3 = 18\%$	2,419 μT	2,016 μT
$d_4 = 9$ mm $\rightarrow$ $B_4 = 3\%$	403 μT	336 μT

The max values are indicated in the table for control unit levels 10 and 12.
d_{1-4}: distance to the head of the applicator.
B_{1-4}: magnetic field.

2.2. Ischemia/Reperfusion Protocol and Low Frequency Electromagnetic Field Exposure. Control hearts (aerobic control, $n = 9$) were perfused aerobically for 75 minutes. Ischemic hearts (I/R, $n = 9$), after 25 min of aerobic perfusion, were subjected to 20 minutes global no-flow ischemia (by closing of the aortic inflow line), followed by 30 minutes of aerobic reperfusion.

Low frequency electromagnetic fields (LF-EMF) were applied to a subset of hearts perfused either aerobically ($n = 9$) or subjected to I/R ($n = 9$). LF-EMF was generated by a point applicator Z connected to a Viofor JPS classic control unit (Viofor JPS, Poland). Magnetic field induction (B) varied, depending on the distance (d), from the inducing point applicator Z and averaged 500 μT. Figure 1 schematizes the dependence of the field on distance. Table 1 summarizes the field variations (B_{1-4}) with respect to distance (d_{1-4}).

The scheme of the experimental protocol is shown in Figure 2. After 20 min of aerobic perfusions (control hearts) or at the first minutes of reperfusion (from I/R hearts) samples of perfusates were collected for measurement of interleukin-6 (IL-6) and tropoponin I (TnI). At the end of perfusion the hearts were freeze-clamped in liquid nitrogen and used for measurement of activity of matrix metalloproteinase-2 (MMP-2).

2.3. Measurement Interleukin-6 and Troponin I Levels. IL-6 from coronary perfusate was measured by ELISA method using Quantikine Rat IL-6 Immunoassay (R&D Systems, USA). TnI from coronary effluent was measured by ELISA method using Rat TnI, fast cardiac muscle ELISA kit from Wuhan EIAaB Science Co. (Wuhan, China). Before

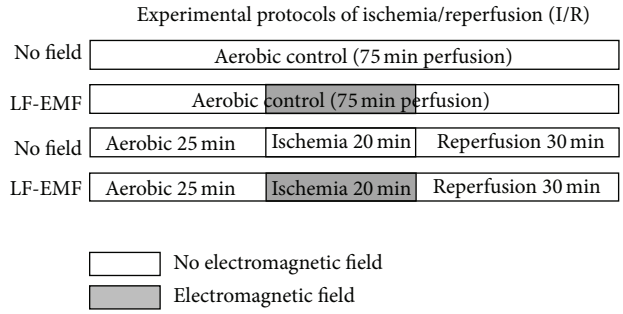

Figure 2: Schematic representation of the perfusion protocol for isolated rat hearts subjected to global no-flow ischemia and protected with low frequency electromagnetic field (LF-EMF).

biochemical analysis all perfusates were concentrated in Amicon Ultra concentrating vessels (EMD Millipore, Billerica, MA, USA). The final volume of concentrate was measured by gravimetry and adjusted to the same final volume for each sample (500 μL).

2.4. Measurement of MMP-2 Activity. Gelatin zymography was performed as previously described [4, 10, 11]. Briefly, homogenates from heart preparations containing 10 μg of protein were applied to 8% polyacrylamide gel copolymerized with 2 mg/mL gelatin. After electrophoresis, gels were rinsed three times for 20 minutes in 2.5% Triton X-100 to remove SDS. The gels were then washed twice in incubation buffer (50 mM Tris-HCl, 5 mM $CaCl_2$, 150 mM NaCl, and 0.05% NaN_3) for 20 minutes at room temperature and incubated in incubation buffer at 37°C for 24 hours. The gels were stained using 0.05% Coomassie Brilliant Blue G-250 in a mixture of methanol : acetic acid : water (2.5 : 1 : 6.5, v : v : v) and destained in aqueous solution of 4% methanol : 8% acetic acid (v : v). Developed gels were scanned with GS-800 calibrated densitometer and MMP-2 activity was measured using Quantity One 4.6 software (Bio-Rad, Hercules, CA, USA).

2.5. Statistical Analysis. Data from contractility measurements and biochemical studies were analyzed with ANOVA and Kruskal-Wallis post hoc analysis or Student's t-tests. A $P < 0.05$ indicated statistical significance. Data are presented as the mean ± SEM.

3. Results

3.1. Effect of Low Frequency Electromagnetic Field on Cardiac Hemodynamic Parameters. In order to evaluate the effect of LF-EMF on isolated perfused rat hearts subjected to no-flow ischemia followed by reperfusion, hemodynamic parameters measured during and at the end of the perfusion protocol were analyzed (Figure 3). As previously reported [12], subjecting hearts to an ischemia/reperfusion (I/R) protocol results in a significant decrease in coronary flow (Figure 3(a)) concomitant with decreases in heart rate (Figure 3(b)) and left ventricular developed pressure (LVDP) (Figure 3(c)), in comparison to aerobically perfused hearts. Subjecting aerobically perfused hearts to an induced LF-EMF did not affect any of the measured parameters (Figures 3(a)–3(c)). However, when hearts were subjected to I/R, while having no effect on coronary flow (Figure 3(a)), LF-EMF prevented the I/R-induced decrease in heart rate and LVDP (Figures 3(b) and 3(c), resp.).

3.2. Effect of LF-EMF on Cardiac Contractility and Markers of Cardiac Tissue Injury and Outcome. Cardiac contractility was evaluated by rate pressure product (RPP) at the end of the perfusion protocol (Figure 4). As expected (taking into account that RPP is the product of heart rate and LVDP), LF-EMF did not alter RPP in aerobically perfused hearts but prevented the reduction of RPP in I/R hearts (Figure 4).

The levels of TnI (marker of heart cardiac damage in acute coronary syndromes [13]) and IL-6 (marker of inflammation [14]) were measured in perfusates to determine cardiac tissue injury. Similar to what is observed clinically, the levels of both TnI and IL-6 were significantly increased in the perfusates of hearts subjected to I/R (Figure 5). When hearts were subjected to I/R in the presence of LF-EMF the levels of TnI and IL-6 in the perfusates were significantly decreased in comparison to I/R hearts but not significantly different from LF-EMF aerobic hearts (Figure 5).

3.3. Effect of LF-EMF on MMP-2 Activity in I/R Hearts. MMP-2 significantly contributes to heart I/R injury by degrading cardiac contractile proteins [15–18]. Further, MMP-2 contributes to the damage of endothelium in I/R hearts and consequent increase in protein release [19, 20], including MMP-2 itself.

MMP-2 activity was significantly decreased in I/R hearts, in comparison to aerobic controls (Figure 6), likely due to endothelial damage and increased protein release. LF-EMF did not affect MMP-2 activity in aerobically perfused hearts and reduced the decrease in MMP-2 tissue activity induced by I/R (Figure 6).

4. Discussion

Despite significant technological and pharmacological advances in the management of heart disease, novel therapeutic alternatives are desired to prevent cardiac tissue damage. Although still controversial, the use of low frequency electromagnetic field (LF-EMF) as a nonpharmacological, noninvasive protective intervention against ischemia/reperfusion-(I/R-) induced cardiac injury is a promising technique that deserves further attention to establish the mechanisms underlying potential cardioprotective effects. This study demonstrates that LF-EMFs protect against cellular damage and preserve mechanical function in hearts subjected to I/R. In addition, this study provides additional support to earlier studies demonstrating LF-EMFs could be of particular clinical relevance in situations in which onset of ischemia and/or reperfusion are controlled, such as CABG surgery and reperfusion therapy.

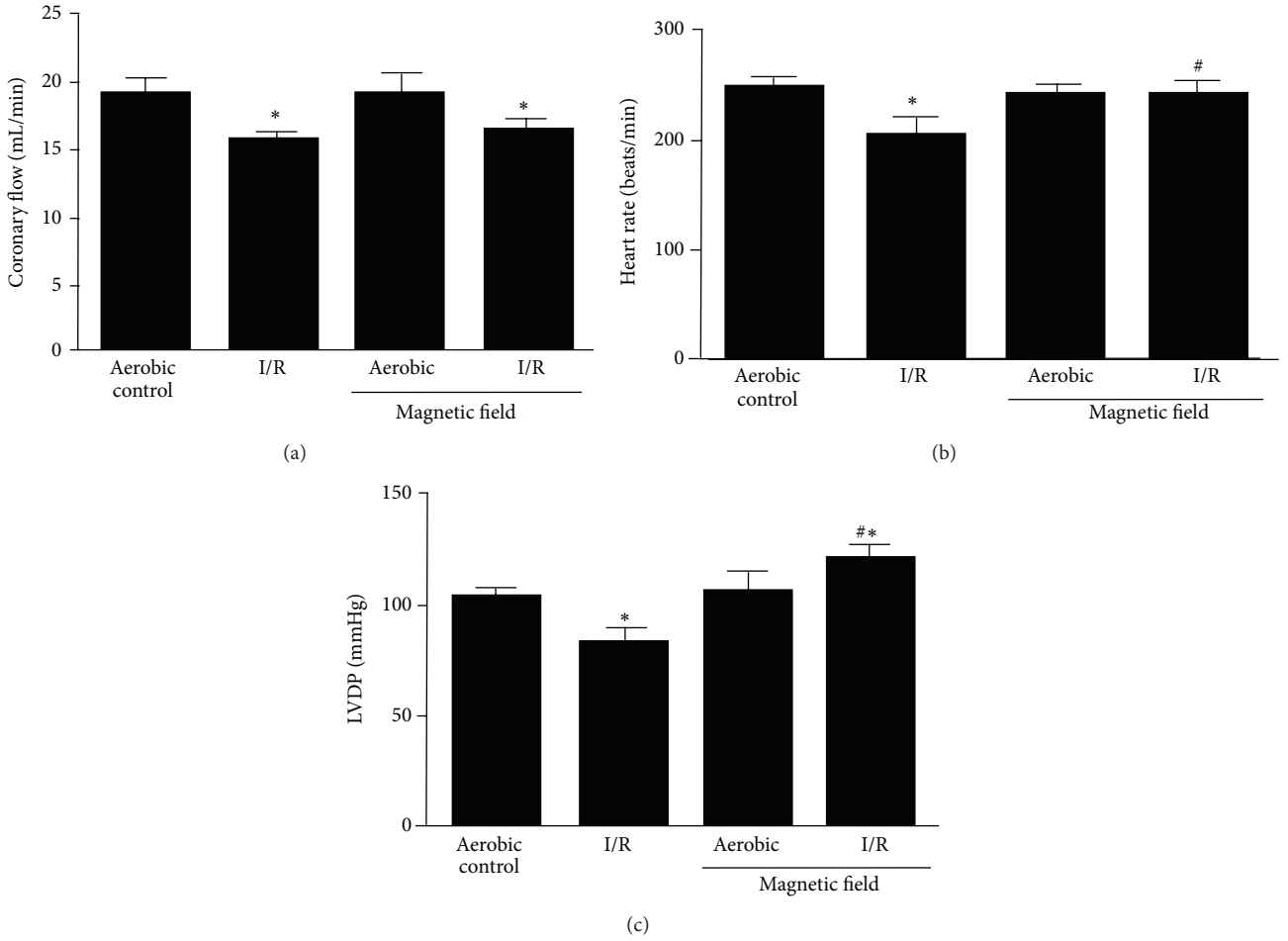

Figure 3: Effect of low frequency electromagnetic field (LF-EMF) on hemodynamic parameters on hearts subjected to global no-flow ischemia and reperfusion. Effect of LF-EMF on (a) coronary flow, (b) heart rate, and (c) LVDP. $n = 9$ heart preparations per group; $^{*}P < 0.05$ versus aerobic control; $^{\#}P < 0.05$ versus I/R alone.

A number of health concerns have been raised relating to chronic environmental LF-EMF exposure. Several studies, including human studies, have reported contradictory observations regarding the relationship between LF-EMF and oxidative stress [21]. Goraca and colleagues [22] reported a decrease in antioxidant capacity in hearts of rats subjected to chronic LF-EMF exposure. Similarly, prolonged exposure to LF-EMF enhanced free radical generation in the brain and retina of rats leading to the reduced antioxidant defense capacity and increased lipid peroxidation [23–25]. Recently, it has been shown that the exposure of blood samples to LF-EMF induced changes in ROS production in both stimulated and nonstimulated neutrophils [25]. Taken together, these observations support the growing concerns regarding chronic exposure to LF-EMFs. Indeed, it appears that chronic exposure to LF-EMF can have a negative impact on the antioxidant capacity.

Despite the potential deleterious effects of chronic exposure to LF-EMF, the evidence suggests short-term exposure to LF-EMF has little or no effect on healthy subjects [9]. Raggi and colleagues demonstrated a significant reduction of blood malondialdehyde levels (free radicals marker) following LF-EMF exposure [21]. LM-EMFs were also found to induce an increase of glutathione peroxidase activity and a decrease in malondialdehyde concentration in liver and serum [26]. Such evidence suggests an effect of LM-EMF on the development of protective antioxidant activity.

Since short-term exposure to LF-EMF has no effect on healthy subjects, or if any, potentially protective, the use of acute LF-EMF as a therapeutic tool to protect against injury is currently being explored. Ma and colleagues demonstrated acute exposure to LF-EMF protects isolated cardiomyocytes from I/R-induced cell death by mediating ROS production and maintaining the $NO/ONOO^{-}$ balance [8]. Although Ma and colleagues did not examine cardiomyocyte contractility, their data suggests a possible mechanism behind the observed LF-EMF cardioprotection. ROS generation can lead to protein and lipid oxidation. At the level of contractile proteins, we have previously demonstrated that cardiac contractile protein nitration and nitrosylation in response to I/R increase its degradation [27]. Consequently, a reduction in ROS production (as described by Ma and colleagues) would result in decreased contractile protein degradation and preservation of cardiac function as previously shown [27–31]. In addition,

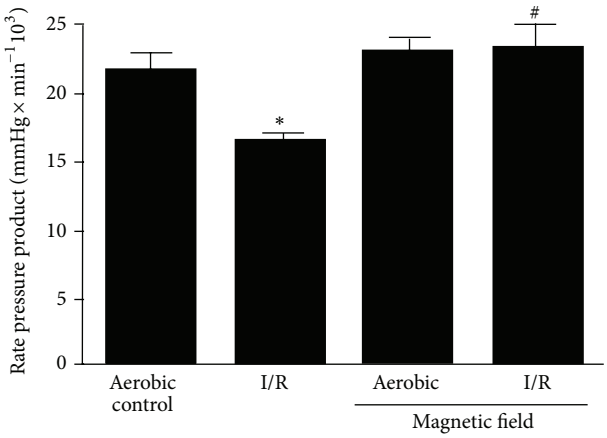

Figure 4: Effect of low frequency electromagnetic field (LF-EMF) on heart contractility subjected to ischemia/reperfusion (I/R) injury. $n = 9$ heart preparations per group; $^*P < 0.05$ versus aerobic control; $^\#P < 0.05$ versus I/R alone.

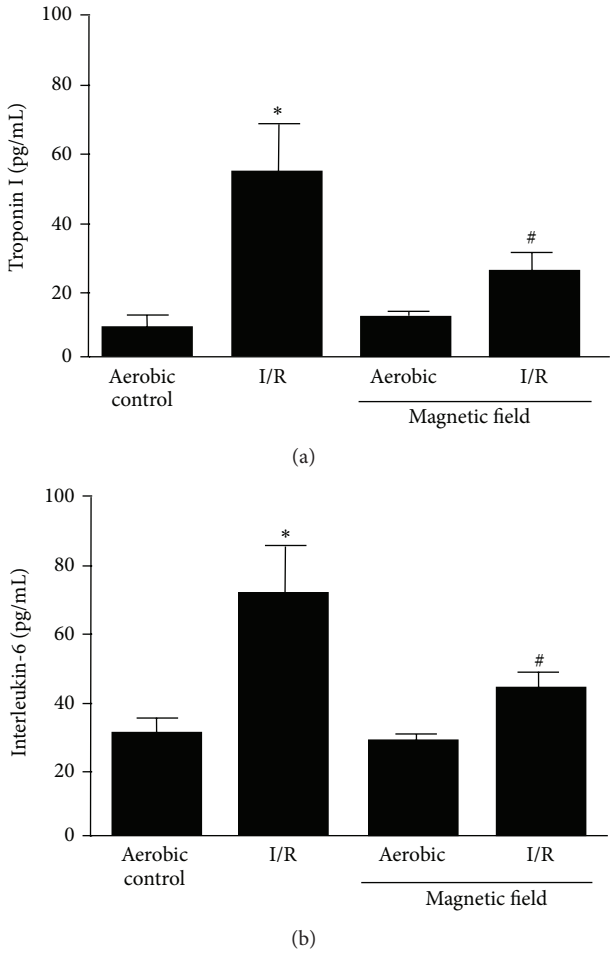

Figure 5: The effect of low frequency electromagnetic field (LF-EMF) on release of troponin I (TnI) (a) and interleukin-6 (IL-6) from hearts subjected to ischemia/reperfusion (I/R) injury. $n = 9$ heart preparations per group; $^*P < 0.05$ versus aerobic control; $^\#P < 0.05$ versus I/R alone.

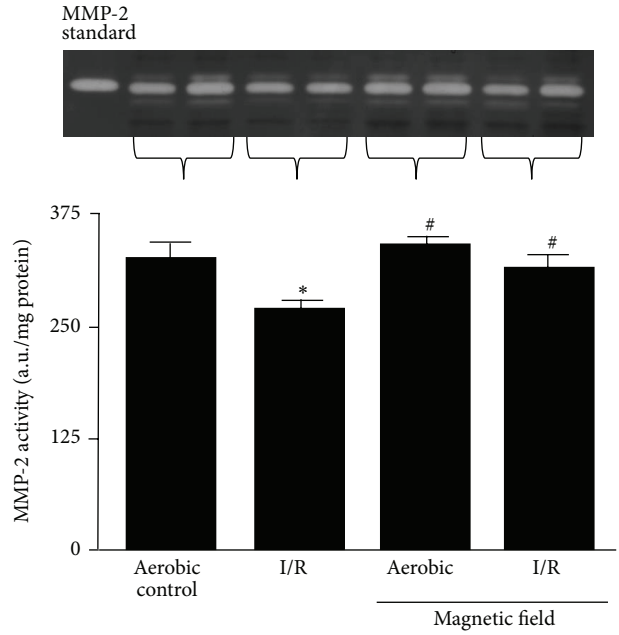

Figure 6: The effect of low frequency electromagnetic field (LF-EMF) on matrix metalloproteinase-2 (MMP-2) activity in hearts subjected to ischemia/reperfusion (I/R) injury. $n = 9$ heart preparations per group; $^*P < 0.05$ versus aerobic control; $^\#P < 0.05$ versus I/R alone.

since MMP-2 can be activated by ROS, a reduction in ROS production would attenuate MMP-2 activation, contribute to the preservation of endothelial integrity [30], and further reduce cardiac contractile protein degradation and consequent cardiac contractile dysfunction induced by I/R injury. These effects would explain our observations relating to MMP-2 activity in response to I/R. Under conditions of acute stress, such as I/R, endothelial integrity can be compromised leading to increased protein release [19, 20]. In our model we observed decreased MMP-2 tissue activity in the I/R group indicating that endothelial integrity was compromised and MMP-2 was released. When I/R hearts were exposed to LF-EMF, MMP-2 activity was similar to that of controls suggesting that a consequence of LF-EMF cardioprotection is the preservation of endothelial integrity.

The regulation of calcium homeostasis is another potential mechanism modulating the observed cardioprotective effects of LF-EMF. Increased Ca^{2+} levels have been observed in cardiac ventricular cells in response to LF-EMF exposure [32]. LF-EMF can induce depolarization of the cell membrane followed by an increase of Ca^{2+} and expression of neurofilament protein [33]. In addition, LF-EMF stimulates the differentiation of embryonic stem cells into cardiomyocytes. The modulation of proliferation and cardiac differentiation observed in LF-EMF/Ca^{2+} exposed cells correlates with induced changes in intracellular Ca^{2+} accumulation and stimulation of signaling cascade pathways [10]. In our model of I/R, calcium deregulation is a relevant mechanism contributing to the development of I/R injury. LF-EMF can have distinct effects on calcium homeostasis, either protective

or deleterious, which appear to be cell specific (for review see [11]). Although the dissection of the effects of LF-EMF on calcium homeostasis was not the focus of this study, it is possible that part of the cardioprotective effect that we observed was due to LF-EMF-induced alterations on calcium homeostasis and signaling.

In addition, we observed a significant protection of cardiac function in hearts exposed to short exposure of LF-EMF. It is known that isolated rat hearts subjected to ischemia exhibit decreased maximal force generation, as well as increased troponin I (TnI) degradation and sensitivity to Ca^{2+} [34]. Moreover, this protection of cardiac function is associated with decreased release of TnI (a clinical marker of myocardial tissue damage).

Taken together, our results further support the literature suggesting that, contrary to chronic LF-EMF exposure, acute exposure to LF-EMFs can have beneficial effects and important cardioprotective actions, namely, by conferring mechanical and cellular protection against I/R. Although further studies are required to elucidate the molecular mechanisms behind cardioprotection by LF-EMFs, the data gathered thus far validates its safety and usefulness, rendering it of possible clinical importance.

Conflict of Interests

The authors declare that there is no conflict of interests regarding the publication of this paper.

Authors' Contribution

Dariusz Bialy was responsible for hypothesis generation, experimental design, experimental work, and paper writing. Magdalena Wawrzynska was responsible for experimental design, experimental work, and paper writing. Iwona Bil-Lula was responsible for experimental work. Anna Krzywonos-Zawadzka was responsible for experimental work. Mieczyslaw Wozniak was responsible for experimental design and paper writing. Virgilio J. J. Cadete was responsible for experimental design and paper writing. Grzegorz Sawicki was responsible for hypothesis generation, experimental design, and paper writing.

References

[1] C. A. L. Bassett, A. A. Pilla, and R. J. Pawluk, "A non operative salvage of surgically resistant pseudarthroses and non unions by pulsing electromagnetic fields. A preliminary report," *Clinical Orthopaedics and Related Research*, vol. 124, pp. 128–143, 1977.

[2] G. C. Traina, R. Cadossi, G. Ceccherelli et al., "La modulazione elettrica della osteogenesi," *Giornale Italiano di Ortopedia*, vol. 12, pp. 165–176, 1986.

[3] G. Borsalino, M. Bagnacani, E. Bettati et al., "Electrical stimulation of human femoral intertrochanteric osteotomies: double-blind study," *Clinical Orthopaedics and Related Research*, no. 237, pp. 256–263, 1988.

[4] W. J. W. Sharrard, "A double-blind trial of pulsed electromagnetic fields for delayed union of tibial fractures," *The Journal of Bone & Joint Surgery B*, vol. 72, no. 3, pp. 347–355, 1990.

[5] M. Ieran, S. Zaffuto, M. Bagnacani, M. Annovi, A. Moratti, and R. Cadossi, "Effect of low frequency pulsing electromagnetic fields on skin ulcers of venous origin in humans: a double-blind study," *Journal of Orthopaedic Research*, vol. 8, no. 2, pp. 276–282, 1990.

[6] G. P. A. Yen-Patton, W. F. Patton, D. M. Beer, and B. S. Jacobson, "Endothelial cell response to pulsed electromagnetic fields: stimulation of growth rate and angiogenesis in vitro," *Journal of Cellular Physiology*, vol. 134, no. 1, pp. 37–46, 1988.

[7] A. Albertini, P. Zucchini, G. Noera, R. Cadossi, C. P. Napoleone, and A. Pierangeli, "Protective effect of low frequency low energy pulsing electromagnetic fields on acute experimental myocardial infarcts in rats," *Bioelectromagnetics*, vol. 20, no. 6, pp. 372–377, 1999.

[8] S. Ma, Z. Zhang, F. Yi et al., "Protective effects of low-frequency magnetic fields on cardiomyocytes from ischemia reperfusion injury via ros and $NO/ONOO^-$," *Oxidative Medicine and Cellular Longevity*, vol. 2013, Article ID 529173, 9 pages, 2013.

[9] S. K. Kim, J. L. Choi, M. K. Kwon, J. Y. Choi, and D. W. Kim, "Effects of 60 Hz magnetic fields on teenagers and adults," *Environmental Health*, vol. 12, article 42, 2013.

[10] R. Gaetani, M. Ledda, L. Barile et al., "Differentiation of human adult cardiac stem cells exposed to extremely low-frequency electromagnetic fields," *Cardiovascular Research*, vol. 82, no. 3, pp. 411–420, 2009.

[11] M. L. Pall, "Electromagnetic fields act via activation of voltage-gated calcium channels to produce beneficial or adverse effects," *Journal of Cellular and Molecular Medicine*, vol. 17, no. 8, pp. 958–965, 2013.

[12] V. J. J. Cadete, J. Sawicka, D. Polewicz, A. Doroszko, M. Wozniak, and G. Sawicki, "Effect of the Rho kinase inhibitor Y-27632 on the proteome of hearts with ischemia-reperfusion injury," *Proteomics*, vol. 10, no. 24, pp. 4377–4385, 2010.

[13] S. J. Maynard, I. B. A. Menown, and A. A. J. Adgey, "Troponin T or troponin I as cardiac markers in ischaemic heart disease," *Heart*, vol. 83, no. 4, pp. 371–373, 2000.

[14] T. A. Pearson, G. A. Mensah, R. W. Alexander et al., "Markers of inflammation and cardiovascular disease: application to clinical and public health practice: A statement for healthcare professionals from the centers for disease control and prevention and the American Heart Association," *Circulation*, vol. 107, no. 3, pp. 499–511, 2003.

[15] P. Y. Cheung, G. Sawicki, M. Wozniak, W. Wang, M. W. Radomski, and R. Schulz, "Matrix metalloproteinase-2 contributes to ischemia-reperfusion injury in the heart," *Circulation*, vol. 101, no. 15, pp. 1833–1839, 2000.

[16] A. Doroszko, D. Polewicz, V. J. J. Cadete et al., "Neonatal asphyxia induces the nitration of cardiac myosin light chain 2 that is associated with cardiac systolic dysfunction," *Shock*, vol. 34, no. 6, pp. 592–600, 2010.

[17] G. Sawicki, H. Leon, J. Sawicka et al., "Degradation of myosin light chain in isolated rat hearts subjected to ischemia-reperfusion injury: a new intracellular target for matrix metalloproteinase-2," *Circulation*, vol. 112, no. 4, pp. 544–552, 2005.

[18] W. Wang, C. J. Schulze, W. L. Suarez-Pinzon, J. R. B. Dyck, G. Sawicki, and R. Schulz, "Intracellular action of matrix metalloproteinase-2 accounts for acute myocardial ischemia and reperfusion injury," *Circulation*, vol. 106, no. 12, pp. 1543–1549, 2002.

[19] J. Fert-Bober, H. Leon, J. Sawicka et al., "Inhibiting matrix metalloproteinase-2 reduces protein release into coronary effluent from isolated rat hearts during ischemia-reperfusion," *Basic Research in Cardiology*, vol. 103, no. 5, pp. 431–443, 2008.

[20] J. Fert-Bober, R. S. Basran, J. Sawicka, and G. Sawicki, "Effect of duration of ischemia on myocardial proteome in ischemia/reperfusion injury," *Proteomics*, vol. 8, no. 12, pp. 2543–2555, 2008.

[21] F. Raggi, G. Vallesi, S. Rufini, S. Gizzi, E. Ercolani, and R. Rossi, "ELF magnetic therapy and oxidative balance," *Electromagnetic Biology and Medicine*, vol. 27, no. 4, pp. 325–339, 2008.

[22] A. Goraca, E. Ciejka, and A. Piechota, "Effects of extremely low frequency magnetic field on the parameters of oxidative stress in heart," *Journal of Physiology and Pharmacology*, vol. 61, no. 3, pp. 333–338, 2010.

[23] S. Falone, A. Mirabilio, M. C. Carbone et al., "Chronic exposure to 50 Hz magnetic fields causes a significant weakening of antioxidant defence systems in aged rat brain," *The International Journal of Biochemistry & Cell Biology*, vol. 40, no. 12, pp. 2762–2770, 2008.

[24] D. Akpinar, N. Ozturk, S. Ozen, A. Agar, and P. Yargicoglu, "The effect of different strengths of extremely low-frequency electric fields on antioxidant status, lipid peroxidation, and visual evoked potentials," *Electromagnetic Biology and Medicine*, vol. 31, no. 4, pp. 436–448, 2012.

[25] B. Poniedziałek, P. Rzymski, J. Karczewski, F. Jaroszyk, and K. Wiktorowicz, "Reactive oxygen species (ROS) production in human peripheral blood neutrophils exposed in vitro to static magnetic field," *Electromagnetic Biology and Medicine*, vol. 32, no. 4, pp. 560–568, 2013.

[26] M. Glinka, A. Sieroń, E. Birkner, and G. Cieślar, "Influence of extremely low-frequency magnetic field on the activity of antioxidant enzymes during skin wound healing in rats," *Electromagnetic Biology and Medicine*, vol. 32, no. 4, pp. 463–470, 2013.

[27] D. Polewicz, V. J. J. Cadete, A. Doroszko et al., "Ischemia induced peroxynitrite dependent modifications of cardiomyocyte MLC1 increases its degradation by MMP-2 leading to contractile dysfunction," *Journal of Cellular and Molecular Medicine*, vol. 15, no. 5, pp. 1136–1147, 2011.

[28] V. J. J. Cadete, S. A. Arcand, H.-B. Lin, and G. Sawicki, "Synergistic protection of MLC 1 against cardiac ischemia/reperfusion-induced degradation: a novel therapeutic concept for the future," *Future Medicinal Chemistry*, vol. 5, no. 4, pp. 389–398, 2013.

[29] M. M. Sung, C. G. Schulz, W. Wang, G. Sawicki, N. L. Bautista-López, and R. Schulz, "Matrix metalloproteinase-2 degrades the cytoskeletal protein alpha-actinin in peroxynitrite mediated myocardial injury," *Journal of Molecular and Cellular Cardiology*, vol. 43, no. 4, pp. 429–436, 2007.

[30] S. Viappiani, A. C. Nicolescu, A. Holt et al., "Activation and modulation of 72 kDa matrix metalloproteinase-2 by peroxynitrite and glutathione," *Biochemical Pharmacology*, vol. 77, no. 5, pp. 826–834, 2009.

[31] W. Wang, G. Sawicki, and R. Schulz, "Peroxynitrite-induced myocardial injury is mediated through matrix metalloproteinase-2," *Cardiovascular Research*, vol. 53, no. 1, pp. 165–174, 2002.

[32] C. Sert, S. Söker, M. Deniz, and Y. Nergiz, "Intracellular Ca^{2+} levels in rat ventricle cells exposed to extremely low frequency magnetic field," *Electromagnetic Biology and Medicine*, vol. 30, no. 1, pp. 14–20, 2011.

[33] A. Foletti, S. Grimaldi, A. Lisi, M. Ledda, and A. R. Liboff, "Bioelectromagnetic medicine: the role of resonance signaling," *Electromagnetic Biology and Medicine*, vol. 32, no. 4, pp. 484–499, 2013.

[34] J. E. van Eyk, F. Powers, W. Law, C. Larue, R. S. Hodges, and R. J. Solaro, "Breakdown and release of myofilament proteins during ischemia and ischemia/reperfusion in rat hearts: identification of degradation products and effects on the pCa-force relation," *Circulation Research*, vol. 82, no. 2, pp. 261–271, 1998.

Hindawi Publishing Corporation
BioMed Research International
Volume 2015, Article ID 714197, 25 pages
http://dx.doi.org/10.1155/2015/714197

Review Article

The Sarcomeric M-Region: A Molecular Command Center for Diverse Cellular Processes

Li-Yen R. Hu, Maegen A. Ackermann, and Aikaterini Kontrogianni-Konstantopoulos

Department of Biochemistry and Molecular Biology, School of Medicine, University of Maryland, 108 N Greene Street, Baltimore, MD 21201, USA

Correspondence should be addressed to Aikaterini Kontrogianni-Konstantopoulos; akons001@umaryland.edu

Received 17 November 2014; Accepted 8 February 2015

Academic Editor: Oleg S. Matusovsky

The sarcomeric M-region anchors thick filaments and withstands the mechanical stress of contractions by deformation, thus enabling distribution of physiological forces along the length of thick filaments. While the role of the M-region in supporting myofibrillar structure and contractility is well established, its role in mediating additional cellular processes has only recently started to emerge. As such, M-region is the hub of key protein players contributing to cytoskeletal remodeling, signal transduction, mechanosensing, metabolism, and proteasomal degradation. Mutations in genes encoding M-region related proteins lead to development of severe and lethal cardiac and skeletal myopathies affecting mankind. Herein, we describe the main cellular processes taking place at the M-region, other than thick filament assembly, and discuss human myopathies associated with mutant or truncated M-region proteins.

1. Introduction

The M-band is a dense protein-packed structure at the center of the A-band of cardiac and skeletal muscle cells (Figure 1 and Table 1). Under the electron microscope, M-band appears as a series of dark transverse lines spanning ~500–750 Å, depending on fiber type and species [1]. Named for the German word "mittelscheibe," which means "central disc," the M-band lies at the center of the bare zone, which is devoid of myosin heads and cross-bridges [2] but encompasses overlapping arrays of antiparallel myosin rods [3]. Adjacent myosin rods are connected via M-bridges, forming a regular hexagonal lattice [4]. The M-bridges are necessary to maintain thick filament alignment and aid in the controlled distribution of mechanical stress across the sarcomere during active contraction [5].

In addition to the rod region of myosin, the M-band is "home" to several other proteins (Figure 1 and Table 1). As such, the COOH-termini of titin molecules from half sarcomeres converge in an antiparallel fashion at the M-band [6]. Composed of immunoglobulin (Ig) domains and unique sequences, the COOH-terminus of titin is located downstream of its kinase domain, which is found at the junction of A- and M-bands.

The M-band also contains myomesin, M-protein, and myomesin-3, which share similar domain architectures and are primarily composed of Ig and fibronectin type III (FnIII) domains, but contain distinct NH_2-terminal heads [7, 8]. These proteins are the principal components of M-bridges forming the backbone of the M-band filamentous system, which cross-links neighboring thick filaments [6, 8].

Also localizing at the level of the M-region are additional sarcomeric and membrane associated proteins, including obscurins, select variants of Myosin Binding Protein-C Slow, ankyrins, and spectrins [9–12]. These contribute to the assembly and stabilization of the M-region and its linkage with the sarcomeric cytoskeleton, the sarcoplasmic reticulum (SR), and the sarcolemma [13].

Within the last decade, our knowledge of the sarcomeric M-region has steadily expanded. To date, there are several excellent reviews on protein complexes mediating the assembly and organization of the entire M-region encompassing the M-band core as well as its periphery, and its role in thick filament assembly and integration into A-bands [5, 14].

Table 1: Properties of M-region proteins.

	Protein	Localization	Muscle specificity	Residency	PDB ID
			M-band organization		
Complex 1	Obscurins (ABD)	Periphery	Cardiac/skeletal	Permanent	NA
	Ankyrin-B (Exon 43′)	Periphery	Cardiac	Permanent	NA
	PP2A (B56α)	Periphery	Cardiac/skeletal	Permanent	NA
Complex 2	Titin (Mis4)	Periphery/interior	Cardiac/skeletal	Permanent	NA
	Bin-1	Interior	Cardiac/skeletal (developmental)	Transient	1MV3
	Cdc2 Kinase	Interior	Cardiac/skeletal (developmental)	Transient	NA
	Myomesin	Periphery/interior	Cardiac/skeletal	Permanent	3RBS, 2Y23, 2R15, 2Y25
	SmyD1	Periphery	Cardiac/fast skeletal	Permanent	3N71
	FHLs	Periphery	Cardiac/skeletal	Permanent	2EGQ, 2D8Z
			Cytoskeletal remodeling		
	Obscurins (RhoGEF)	Periphery	Cardiac/skeletal	Permanent	NA
	RhoA	Periphery	Cardiac/skeletal	Transient	1LB1, 3KZ1
	CRIK	Periphery	Cardiac/skeletal	Transient	NA
	Active ROCK1	Periphery	Cardiac/skeletal	Transient	2ETR
			Mechanosensing		
	Titin (Titin Kinase)	Periphery/interior	Cardiac/skeletal	Permanent	4JNW, 1TKI
	NBR1	Periphery	Cardiac/skeletal	Permanent	4OLE
	P62	Periphery	Cardiac/skeletal	Permanent	2KTR, 3B0F, 2MGW
	MuRFs	Periphery	Cardiac/skeletal	Permanent	4M3L, 3Q1D
			Metabolism		
	PFK	Periphery	Cardiac/skeletal	Permanent	4OMT
	M-CK	Periphery	Cardiac/skeletal	Permanent	1I0E
	AK	Periphery	Cardiac/skeletal	Permanent	2C95
	Enolases	Periphery	Cardiac/skeletal	Permanent	3B97, 2XSX
	AMPD	Periphery	Cardiac/skeletal	Permanent	2Y2C
			Proteasomal degradation		
	MuRFs	Periphery	Cardiac/skeletal	Permanent	4M3L, 3Q1D

Note: protein domains mediating complex formation or participating in cellular processes are shown in parenthesis when known. Acronyms of proteins are described in the text; ABD: ankyrin binding domain; NA: not available. The PDB files of proteins in Complex 1 and Complex 2, as well as obscurins (RhoGEF) and titin (titin kinase), are associated with the specific domains that mediate binding within the complex; in all other cases, the available PDB files for the entire protein are provided.

Herein, we focus on key protein mediators of additional cellular processes occurring at the M-region. In addition, we highlight skeletal and cardiac myopathies that are linked to mutations in genes encoding M-region related proteins.

2. Cellular Processes at the M-Region

M-region is the hub for multiple cellular processes including signal transduction, metabolism, mechanosensing, and proteasomal degradation. Such processes support cellular homeostasis, myofibrillar organization, and contractile activity by maintaining sarcomeric integrity, meeting the energy demand during active contraction, and enabling adaptation to different biochemical and biomechanical stimuli. Below we will address these important processes occurring at the M-region and discuss key proteins.

2.1. Signal Transduction via Posttranslational Modifications. Two main types of posttranslational modifications, phosphorylation and sumoylation, have been described at the M-region. These mediate proper protein localization, regulate protein-protein interactions, and relay signals in response to biochemical or biomechanical stimuli.

2.1.1. Phosphorylation. Several M-region proteins possess active kinase domains and/or are regulated by phosphorylation. Below we discuss such proteins.

Titin (~3-4 MDa). The giant protein titin extends longitudinally across a half-sarcomere, with its NH_2-terminus anchored to the Z-disc, and its COOH-terminus localized at the center of the M-band [15]. The M-band portion of titin (~200 kDa) is composed of ten Ig CII type domains, which are interspersed with unique nonmodular segments, termed

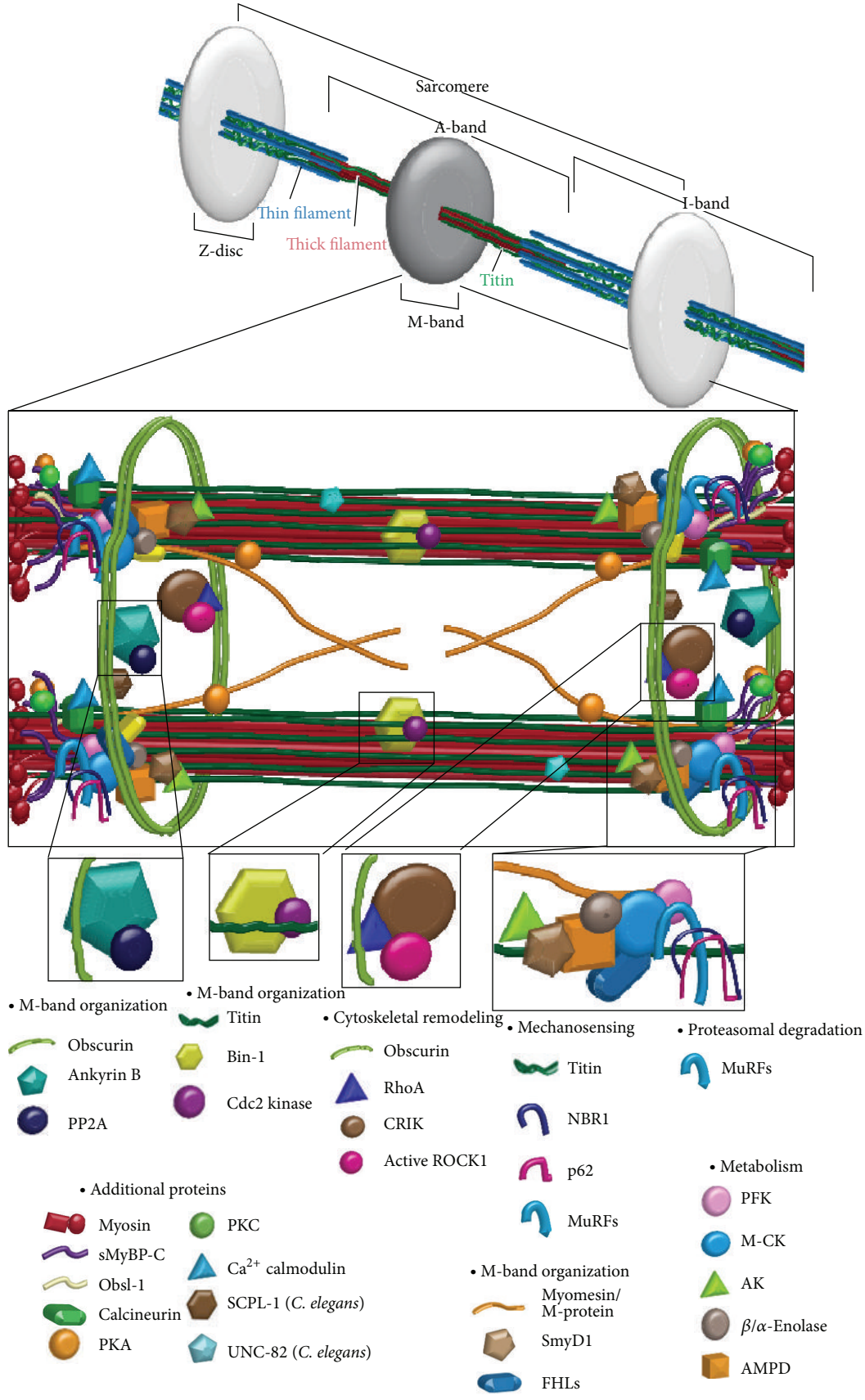

Figure 1: Sarcomeric M-region road map and cellular processes. Schematic representation of the sarcomeric M-region depicting key proteins and highlighting cellular processes.

M-insertions [13, 16, 17]. The insertion between Ig CII-5 and Ig CII-6 contains tandem lysine-serine-proline (KSP) repeats, which are heavily phosphorylated by Cdc2 kinase in developing, but not in differentiated muscle cells [16]. The phosphorylated KSP repeats interact *in vitro* with the SH3 domain of the tumor suppressor bridging integrator protein 1 (Bin1) [18]. Bin1 is a negative regulator of c-Myc activation that is preferentially expressed in differentiating, but not mature, myotubes [18]. Transgenic mice overexpressing the SH3 domain of Bin1 exhibit dramatic disarray in myofiber size and structure [18]. Conversely, mouse C2C12 skeletal myoblasts fail to differentiate following downregulation of Bin1 [19, 20], and Bin1 homozygous knock-out mice develop hypertrophic cardiomyopathy leading to perinatal lethality, although skeletal muscles do not exhibit any apparent abnormalities at this stage [21]. It is therefore possible that disruption of the interaction between the phosphorylated KSP repeats of titin and Bin1 at the M-band may result in deregulated myofibrillar assembly, loss of differentiation, and aberrant fiber size.

In addition to being phosphorylated within its M-band portion, titin may regulate different sarcomeric processes via its kinase domain, residing at the periphery of the M-band [6, 13, 22, 23]; one of these processes is mechanosensing, which will be discussed in a later section of this review.

Obscurin (720–890 kDa). Incorporated early during development into the periphery of the sarcomeric M-band, obscurin is an important player of thick filament assembly and stabilization [24]. Downregulation of obscurin using siRNA technology leads to selective disorganization of M- and A-bands in developing skeletal and cardiac myocytes, indicating its scaffolding role [24–26]. Importantly, recent studies have demonstrated that the two Ser/Thr kinase domains, which are present at the COOH-terminus of giant obscurin-B are catalytically active and can directly bind major components of the M-band, including titin and four and a half LIM domains 2 (FHL2) protein [27, 28]. Examining if these proteins are catalytic substrates of the obscurin kinase domains at the M-band will be the next challenge.

Obscurin is also involved in dephosphorylation events at the M-band. Ankyrin-B (Ank-B), fulfilling its role as an anchoring protein, binds directly to both obscurin and the regulatory subunit, B56α, of protein phosphatase 2A (PP2A) at the M-band [29, 30]. Overexpression of the obscurin-binding region of Ank-B in isolated adult cardiomyocytes results in displacement of B56α from the M-band [29]. Moreover, UNC-89, the obscurin homologue in *C. elegans*, directly binds to small C-terminal domain (CTD) phosphatase-like 1 (SCPL-1) at the M-band [28, 31]. However, the cellular processes that PP2A and SCPL-1 mediate at the M-band are still unknown.

Myomesin (178–188 kDa). Spanning the entire M-region by residing in the interior yet extending to the periphery of the M-band, myomesin serves as a cross-linker between myosin, titin, and obscurin [32, 33]. It consists of tandem Ig and FnIII domains, along with a nonmodular NH_2-terminus [32–35]. While the NH_2-terminus of myomesin interacts with sarcomeric myosin [36], the region encompassing Ig domains 4 and 5 (My4-My5) directly interacts with titin Ig4 within its M-band portion (MIg4) [32, 34]. Phosphorylation of the linker region between myomesin domains My4 and My5 by protein kinase A (PKA) abolishes its binding to titin MIg4 [32]. Importantly, the linker region also interacts with two other M-band proteins, obscurin, and obscurin-like 1, but these interactions are not modulated by phosphorylation [33]. Thus, a ternary complex of regulated and potentially constitutive interactions between myomesin and titin, and myomesin and obscurin, or obsl-1 occurs at the M-band [33].

M-Protein (~165 kDa). Similar to myomesin, M-protein also consists of tandem Ig and FnIII domains, which are preceded by a unique NH_2-terminus [6, 37, 38]. Unlike myomesin though, which is expressed ubiquitously in all striated muscles, M-protein is only expressed in cardiac and fast-twitch skeletal muscles [39–41]. Phosphorylation at S76, present in the nonmodular NH_2-terminus of M-protein, by PKA abolishes its binding to myosin [42].

Thus, the PKA-mediated phosphorylation of both myomesin and M-protein may modulate thick filament integration, organization, and stability at the M-band during myofibrillogenesis or myofilament turnover.

Myomesin-3 (~162 kDa), also composed of a nonmodular NH_2-terminus and tandem Ig and FnIII domains, is present at the M-band, too [8]. Unlike myomesin, which is ubiquitously present in all striated muscles and M-protein that is preferentially expressed in cardiac and fast-twitch skeletal muscles, myomesin-3 is selectively expressed in slow-twitch skeletal muscles [8, 43]. Whether myomesin-3 is subjected to posttranslational modifications, however, remains to be investigated. Along the same lines, select variants of Myosin binding protein-C slow (MyBP-C slow), FHL1, and FHL2 and obscurin-like 1 also localize at the M-region [10, 33, 44–48]. Out of these proteins, at least MyBP-C slow is modulated via phosphorylation mediated by PKA and PKC [49]. Moreover, the Ca^{2+}/calmodulin-dependent serine/threonine phosphatase, calcineurin (also known as protein phosphatase 2B, PP2B), is also present at the M-band and may mediate dephosphorylation events of M-band proteins [47]. At this time though, the physiological significance of the phosphorylation and dephosphorylation events involving these proteins remains speculative.

In addition to the phosphorylation events discussed above, which have been mainly studied in mammalian striated muscles, additional protein players involved in post-translational modification events within the M-region have been reported in *C. elegans*. Unlike the cross-striated muscles of mammals, myofilaments of body muscles in *C. elegans* are arranged in oblique striations. Therefore, both the protein composition and the functional role(s) of individual proteins at the M-region of body muscles of *C. elegans* may differ from those of mammalian striated muscles. Below, we provide such an example.

UNC-82 (33–203 kDa). Recently identified as a Ser/Thr kinase that localizes at or near the M-band in *C. elegans*, UNC-82 is closely related to mammalian proteins AMPK-related protein

kinase 5 (ARK5) and sucrose nonfermenting AMPK-related kinase (SNARK) (also known as NUAK1 and NUAK2, resp.), which are members of the AMP-activated protein kinase (AMPK) family of Ser/Thr kinases [50]. While the enzymatic activity and substrates of UNC-82 remain to be determined, mutant *C. elegans* embryos containing either a missense mutation presumably abolishing its kinase activity or a nonsense mutation resulting in truncated UNC-82 exhibit disorganized A- and M-bands [50]. Interestingly, its closely related mammalian counterparts, ARK5 and SNARK, have been implicated in glucose metabolism in skeletal muscle [51, 52]; however the localization of ARK5 and SNARK has yet to be examined.

2.1.2. SUMOylation. In addition to phosphorylation, proteins at the M-region undergo sumoylation. While less studied compared to phosphorylation, sumoylation has been implicated as a possible mechanism for targeting proteins to the M-region.

Myomesin (178–188 kDa). In addition to being regulated via phosphorylation, myomesin is also subjected to sumoylation, possibly at K228, in adult rat cardiomyocytes [53]. Moreover, in neonatal rat ventricular myocytes (NRVM), where myomesin is localized to the nucleus, overexpression of the SUMO peptide mediates its translocation to the cytoplasm and promotes sarcomeric organization [54]. Sumoylation of myomesin is mediated by myofibrillogenesis regulator-1 (MR-1), which is highly expressed in both skeletal and cardiac muscles [54, 55]. While overexpression of MR-1 in mice enhances cardiac hypertrophy stimulated by angiotensin II, overexpression of MR-1 in NRVM induces sarcomeric organization and translocation of myomesin from the nucleus to the cytoplasm, similar to SUMO overexpression [54, 56]. Consistent with this, downregulation of MR-1 abolishes SUMO-induced translocation of myomesin to the cytoplasm and sarcomeric organization [54].

SET and MYND Domain Containing-1 (SmyD1) (~54–56 kDa). SmyD1 is another M-band protein whose localization is modulated by sumoylation [57, 58]. Also known as Bop, SmyD1 is a histone methyltransferase that is abundantly expressed in striated muscles with its methyl transferase activity attributed to its Su(var)3-9, enhancer-of-zeste, and trithorax (SET) domain [59–63]. In mouse, the *smyd1* locus encodes two alternatively spliced isoforms, SmyD1_tv1, and SmyD1_tv2 (also known as skm-Bop1 and skm-Bop2, resp.) [60, 61, 63]. SmyD1_tv1 and SmyD1_tv2 localize at the M-band and the nucleus in both cardiac and skeletal muscles [57, 60]. Homozygous deletion of *smyd1* in mice results in embryonic lethality at E10.5 due to disrupted ventricular formation, which is accompanied by loss of right ventricles [61]. Recently, skeletal muscle- and heart-specific α nascent polypeptide-associated complex, skNAC, was shown to mediate the sumoylation of SmyD1 proteins and thus regulate their nuclear export and translocation to the M-band during sarcomerogenesis [58, 64]. Thus, sumoylation mediates SmyD1 targeting to the M-band, where it potentially regulates the activities of major M-band proteins, such as myosin and muscle-type creatine kinase, via its methyl transferase activity.

Proteins at the M-region undergo additional posttranslational modifications, such as acetylation, methylation, and neddylation. For instance, small ankyrin 1.5 (sAnk1.5) is subjected to acetylation and neddylation [65, 66], while muscle-type creatine kinase and myosin are subjected to acetylation and methylation [66, 67]. However, the functional significance and the identity of the relevant enzymes carrying out these posttranslational modifications at the M-band remain to be further investigated.

2.2. Cytoskeletal Remodeling via Small GTPases. Small GTPases play important roles in diverse cellular and developmental processes, including cytoskeletal remodeling, actomyosin contractility, vesicle transport, growth, and proliferation [68–72]. Small GTPases are regulated via repeating cycles of GTP binding and hydrolysis. Three accessory proteins contribute to their regulation: (i) GTPase activating proteins (GAP), which hydrolyze GTP to GDP, inactivating small GTPases, (ii) guanine nucleotide exchange factors (GEF), which mediate the exchange of GDP to GTP activating small GTPases, and (iii) guanosine nucleotide dissociation inhibitors (GDI), which prevent the exchange of GDP for GTP by sequestering GTPases and preventing them from binding to downstream effectors [73, 74]. Ras homolog gene family, member A protein, RhoA, localizes at the M-band in adult skeletal and cardiac muscles [66, 75]. While RhoA mediates several cellular processes, the discussion below will mainly focus on its roles in cytoskeletal remodeling at the M-band.

2.2.1. RhoA Signaling in Skeletal Muscle. Inactive RhoA preferentially localizes to the M-band of adult skeletal myofibers, whereas active RhoA exhibits a dual distribution, at both M-bands and Z-disks [75]. RhoA activity is significantly increased following overexpression of the obscurin RhoGEF motif in adult rat tibialis anterior (TA) muscle and after injury induced by large-strain lengthening contractions [75]. Consistent with this, the RhoGEF/Pleckstrin homology cassette of Unc-89, the *C. elegans* obscurin homologue, activates Rho-1, the RhoA *C. elegans* homologue [76]. In mammalian skeletal muscle, active RhoA leads to loss of citron rho-interacting kinase (CRIK), which is involved in the regulation of cytokinesis in proliferating cells, from M- and A-bands [75, 77, 78]. Moreover, active RhoA leads to translocation of Rho-associated protein kinase 1 (ROCK1) from the Z-disk to the I-band, the Z/I junction, and the M-band [75]. Although the functional ramifications of the concurrent loss of CRIK from the M-band and the translocation of ROCK1 to the M-band are still elusive, it is likely that they mediate the activation of stretch-response genes leading to cytoskeletal remodeling or the development of hypertrophy following injury. Consistent with this, activation of the RhoA/ROCK pathway in dystrophin/utrophin double knockout mice has been implicated with heterotopic ossification, while inhibition of the RhoA/ROCK pathway has been associated with improved myogenic potential [79, 80].

RhoA localizes at both M-bands and Z-disks in cardiac muscle, too, although its distribution has not been correlated with its state of activation [66]. Extensive studies have focused on the diverse processes that RhoA mediates in the developing and adult myocardium, emphasizing its roles in the regulation of actin filament assembly and stress fiber formation, sarcomeric organization, induction of a hypertrophic response, tolerance to ischemia/reperfusion, survival, and apoptosis [81–88]. Given that it is currently unknown whether RhoA contributes to these processes through its interactions at the Z-disk or the M-band, we will refrain from presenting such studies in detail.

2.3. Mechanosensing. In addition to biochemical stimuli, muscle cells respond to biomechanical stimuli by modulating protein expression through activation of signaling pathways [89, 90]. Consistent with this, both the Z-disk [91, 92] and the M-band [92] contain mechanosensors that may transform biomechanical stimuli to biochemical signals. At the M-band, the kinase domain of titin is a major player mediating cell responses to mechanical stress.

2.3.1. Titin Kinase. Use of atomic force microscopy (AFM) has demonstrated that the kinase domain of titin is activated upon exertion of mechanical force, leading to unfolding of its regulatory autoinhibitory tail and phosphorylation of Y170, allowing ATP binding to the catalytic aspartate [93]. It is therefore likely that activation of the titin kinase via mechanical force may result in regulation of its proximal substrates via phosphorylation. This is exemplified in the case of the direct interaction between the titin kinase domain and the muscle-specific ring finger (MuRF) complex, consisting of NBR1 (neighbor of BRCA1 gene 1 protein)/p62/MURF-2, which has been suggested to regulate protein turnover in response to mechanical force [23]. Both NBR1 and p62 are substrates of titin kinase [23] and are required in autophagosome-mediated protein degradation by serving as receptors for ubiquitinated proteins [94–96]. Since NBR1 can only bind to the semiopened conformation of the titin kinase that is likely induced by exertion of mechanical force during stretching, it is possible that MuRF-2 is anchored to the M-band via the interaction of NBR1 with the kinase domain of titin [23]. Consistent with this, denervation of skeletal myofibers or mechanical arrest of neonatal cardiomyocytes leads to dissociation of the MuRF-2/NBR1/p62 complex, with MuRF-2 translocating to the nucleus in both skeletal and cardiac cells where it suppresses serum response factor- (SRF-) mediated expression of hypertrophic genes, and p62 accumulating at intercalated disks in cardiac cells [23]. It is noteworthy to mention, however, that a recent study indicated that the kinase domain of titin is not enzymatically active but serves as a scaffold for other proteins that localize to the M-region [97]. Additional studies are warranted to resolve these opposing results.

2.4. Metabolism. Sarcomeric M-band is strategically located in close proximity to where significant amounts of energy are consumed during repeating cycles of actomyosin contractility [98–100]. Maintaining the ATP and ADP levels at optimal concentrations in the sarcoplasm is essential in sustaining muscle activity, as depletion of ATP or accumulation of ADP would attenuate contractility [101]. Below we discuss several proteins localized at the M-band, which play key roles in metabolism by maintaining the ATP/ADP ratio at optimal levels within the sarcoplasm.

2.4.1. Muscle-Type Creatine Kinase (M-CK). Creatine kinase (CK) catalyzes the phosphate transfer from phosphocreatine to ADP, generating ATP and creatine ($\text{Phosphocreatine}^{2-} + \text{MgADP}^{-} + \text{H}^{+} \leftrightarrow \text{MgATP}^{2-} + \text{creatine}$) [102]. In the mammalian genome, there are four gene loci encoding the different CK isoenzymes: muscle-type CK (M-CK), brain-type CK (B-CK), ubiquitous mitochondrial CK (uMtCK), and sarcomeric mitochondrial CK (sMtCK) [103]. While both M-CK and sMtCK are readily expressed in striated muscles, only M-CK is present within the sarcomere [103–105]. M-CK functions as a dimer and localizes at the M-band by interacting with myomesin, M-protein, and FHL-2 [46, 106]. Homozygous null M-CK mice exhibit decreased voluntary running capability, which is accompanied by a significant reduction in force production during initial contractions due to inadequate supply of local ATP [105, 107–109]. Interestingly, malignant transformation of skeletal muscle to sarcoma results in reduction of M-CK levels, indicating that M-CK supports the specific metabolic needs of skeletal myofibers, which gradually lose their differentiation status and contractile properties during sarcoma development [110].

2.4.2. Adenylate Kinase (AK). Similar to M-CK, AK is also present at the M-band [46]. AK catalyzes the transfer of a phosphate from ADP to another ADP to generate AMP and ATP and *vice versa* ($\text{MgADP}^{-} + \text{ADP}^{2-} \leftrightarrow \text{MgATP}^{2-} + \text{AMP}^{-}$), thus maintaining myofibrillar ATP and ADP concentrations at optimal levels [111, 112]. There are nine AK isoenzymes in mammals, referred to as AK1-AK9 [113]. While the majority of AKs localize to mitochondria, AK1 and AK7 are primarily present in the sarcoplasm [113]. At rest, skeletal muscles of homozygous AK1 knockout mice contain increased levels of AMP, without any other pathological phenotype [112]. However, upon induction of high frequency (90–120 *tetani*/min) contractions, gastrocnemius, plantaris, and soleus AK1 null muscles exhibit increased levels of ADP, accompanied by slower relaxation rate, although the magnitude of the generated force is unaltered [112, 114, 115]. The slower relaxation rate is likely due to reduced Gibbs-free energy in response of the increased ADP : ATP ratio, resulting in compromised sarco/endoplasmic reticulum Ca^{2+}-ATPase (SERCA) activity and decreased Ca^{2+} uptake by the SR [112]. Moreover, exposure of AK1 deficient mice to ischemia/reperfusion results in accelerated loss of cardiac contractility and reduced ATP and ADP levels during reperfusion, underscoring the importance of AK1 in supporting myocardial function by regulating energy metabolism [116]. The presence of AK in the sarcomere is therefore essential for meeting the high-energy demands of muscle cells and protecting them from insults.

2.4.3. Adenosine Monophosphate Deaminase (AMPD). Three genes encoding AMPD proteins have been identified: *AMPD1*, *AMPD2*, and *AMPD3* (reviewed in [117]). *AMPD1* encodes an AMPD form that is preferentially expressed in striated muscles, M-AMPD [118, 119]. M-AMPD at the M-band is coupled with M-CK and AK to modulate the ATP, ADP, and AMP levels [101, 120]. AMPD catalyzes the removal of an amine group from AMP, giving rise to ammonia and IMP ($AMP^- \rightarrow IMP^- + NH_3$) [101]. In conjunction with AK, AMPD maintains constant intracellular ADP levels, therefore preventing AMP accumulation and favoring the formation of ATP by AK [101].

2.4.4. Phosphofructokinase (PFK). The fourth metabolic enzyme residing at the M-band, PFK, mediates the transfer of a phosphate group from ATP to fructose-6-phosphate to yield fructose-1, 6-bisphosphate (Fructose-6-P^- + $MgATP^{2-}$ → Fructose-1,6-$P_2{}^{2-}$ + $MgADP^-$), and is a rate-limiting enzyme of the glycolytic pathway [121, 122]. There are three PFK isoenzymes in mammals, PFK-M (muscle), PFK-L (liver), and PFK-P (platelet). Skeletal muscles express exclusively PFK-M, whereas cardiac muscle expresses all three isoenzymes, with PFK-M being the predominant one [123]. Fully activated PFK exists in tetrameric or a more complex oligomeric form, while dimeric PFK confers minimal activity [124]. PFK's activity is modulated by allosteric regulators (e.g., adenosine phosphates and fructose-2, 6-bisphosphate), interacting partners (e.g., F-actin and calmodulin), or posttranslational modifications (e.g., acylation and phosphorylation) [122, 124–126]. Thus, AMP and ADP stabilize PFK in a tetrameric conformation, whereas ATP and citrate stabilize PFK in a dimeric conformation [121, 124, 127–132]. Enhanced binding to F-actin in response to insulin stimulation also stabilizes the tetrameric form of PFK and maintains it in an active conformation [133–135]. Alternatively, PFK may be regulated by a complex mechanism in response to calcium fluctuation in the sarcoplasm [136]. Given the presence of two calmodulin binding sites in PFK, it has been proposed that PFK activity is strongly inhibited when both sites are occupied [124, 137]. However, occupation of only one calmodulin site may abrogate the inhibitory effect mediated by ATP- and citrate-binding via induction of a dimeric conformation that is fully active [124, 138]. Intriguingly, phosphorylation mediated by calmodulin-dependent kinase (CaMK) results in increased sensitivity to ATP inhibition [129]. Since calmodulin binding is modulated by Ca^{2+}, the activity of PFK may be modulated by the Ca^{2+} levels in the sarcoplasm, especially during contractions. PFK-M homozygous null mice ($PFKM^{-/-}$) exhibit high mortality at weaning (60%), reduced life-span (~3–6 months), and decreased ATP concentration in skeletal muscles, accompanied by increased glycogen content and exercise intolerance [139]. Notably, the small number of PFKM null animals that survive beyond 6 months of age develops cardiac hypertrophy by year one [139]. The reduced viability of the PFKM deficient mice is consistent with PFK being the rate-limiting enzyme in the glycolytic pathway and underscores its key role in energy production.

2.4.5. Enolase. In addition to PFK, enolase is another glycolytic enzyme that resides at the M-band [140, 141]. Three gene loci encode the three known enolase isozymes, which are expressed in different tissues: nonneuronal enolase, α *(NNE)*, muscle-specific enolase, β *(MSE)*, and neuronal-specific enolase, γ *(NSE)* [142, 143]. Both α- and β-isozymes are expressed in cardiac and skeletal muscles, localize at the M-band, and may form homo- or heterodimers [140, 141, 144, 145]. Dimeric enolase converts the glycolytic intermediate 2-phospho-D-glycerate to phosphoenolpyruvate (2-phospho-D-glycerate^{2-} ↔ phosphoenolpyruvate^{2-} + H_2O) [146]. While $\beta\beta$-enolase homodimers are predominantly expressed in skeletal muscle, especially in Type II muscle fibers [141, 147, 148], $\alpha\alpha$-, $\alpha\beta$-, and $\beta\beta$-dimers are present in cardiac muscle [145, 148, 149]. The relative expression of α and β isozymes in the heart is important in fine-tuning metabolic activity. Consistent with this, in a rat hypertrophy model induced by aortic stenosis, where the rate of glycolysis is increased [150], the ratio of the α- to β-isozymes is increased in the heart, due to reduced expression of β-enolase, although the levels of α-enolase are unaltered [149]. Conversely, in the spontaneous hypertensive (SHR) rat model, the hypertrophied heart expresses increased levels of the α-isozyme, which is also hyperphosphorylated [149, 151, 152]. While the α- and β-enolases exhibit comparable enzymatic kinetics, the hyperphosphorylated α-isozyme performs slower catalysis [152, 153]. Overexpression of α-enolase in response to ischemia/reperfusion in a rat model confers improved contractility of affected cardiomyocytes [154]. Consistent with its protective role in the heart, α-enolase is significantly upregulated in mouse skeletal muscle, which predominately expresses β-enolase, in response to muscle injury induced by cardiotoxin; interestingly, the expression of β-enolase is drastically decreased after the first day but recovers a week later [155]. Similarly, in rat skeletal muscles subjected to denervation, the levels of the $\alpha\alpha$ dimer are modestly increased, while the levels of the $\beta\beta$-dimer are decreased [148]. It is noteworthy to mention that since α-enolase may also serve as a heat-shock protein or a plasminogen receptor involved in cardiac remodeling and muscle regeneration, it is possible that the protective role of α-enolase may not only be related to its glycolytic activity [152, 156].

Regulation of energy metabolism may also be mediated through proteasomal degradation. Muscle-specific RING finger proteins (MuRFs) present at the M-band ubiquitinate metabolic enzymes, which are subsequently targeted for proteasomal degradation [157–159]. Along these lines, oxidized muscle-type creatine kinase is rapidly ubiquitinated by MuRF-1 and subsequently targeted to the proteasome [159, 160]. In addition, MuRF-1 also interacts with adenylate kinase [157], although the effects of this interaction are still elusive. The importance of MuRFs at the M-band is further discussed in the following section.

2.5. Proteasomal Degradation

MuRFs. The MuRF family consists of three members, MuRF-1, MuRF-2, and MuRF-3, which are E3 ubiquitin ligases, and preferentially expressed in striated muscles [161–163].

They contain a RING finger domain at their NH_2-terminus and transfer ubiquitin-chains to the proteins destined for proteasomal degradation [158, 162]. The poly-ubiquitinated proteins are recognized by the proteasome, subjected to deubiquitination, unfolding, and hydrolysis in its proteolysis core [164]. While MuRF-3 is ubiquitously expressed in skeletal and cardiac muscles, MuRF-1 is preferentially expressed in cardiac and fast-twitch skeletal muscles, and MuRF-2 is predominantly expressed in slow-twitch skeletal muscles, with minimal expression in cardiac and fast-twitch skeletal muscles [165, 166]. All three MuRFs localize to the M-band and the nucleus [167]. Additionally, MuRF-1 and MuRF-3 are also present at the Z-disc [167].

2.5.1. MuRF-1. MuRF-1 interacts with the Ig168/Ig169 domains within the A-band portion of titin, while the presence of the adjacent titin kinase domain enhances this interaction [97, 163]. Overexpression of MuRF-1 disrupts the organization of M- and A-bands, but not of Z-disks and I-bands, in chick cardiomyocytes [168], indicating that increased protein turnover rate at M- and A-bands results in dissolution of these structures. Interestingly, MuRF-1 deficient mice exhibit no major alterations in the levels of ubiquitination within the myocardium, suggesting redundant functionality among MuRFs in cardiac muscle [157].

2.5.2. MuRF-2. MuRF-2 anchors to the M-band via its association with p62 and NBR1 [23, 94]. Downregulation of MuRF-2 results in disrupted M-bands, in addition to perturbed intermediate filament and microtubule networks [169]. Consistent with the notion that MuRFs may have redundant functions in striated muscles, MuRF-2 deficient mice exhibit no apparent phenotype in the absence of physiological stress [157, 170]. Interestingly though, homozygous MuRF-1/MuRF-2 double knock-out mice exhibit loss of Type II fibers in soleus muscle as well as severe cardiac and modest skeletal muscle hypertrophy due to increased protein synthesis, although proteasomal degradation is unaffected [165, 171]. This suggests additional roles for MuRFs, possibly in transcriptional regulation and protein synthesis, which is consistent with their nuclear localization [23, 171].

2.5.3. MuRF-3. MuRF-3 localizes to the M-band by heterodimerizing with MuRF-1 or MuRF-2 [163]. Homozygous deletion of MuRF-3 in mice reveals its role in sarcomeric organization, as evidenced by increased sarcomeric length and upregulation of select proteins, including FHL-2 [172]. In spite of the increased sarcomeric length, MuRF-3 null mice do not exhibit cardiac hypertrophy in the absence of stress [172]. However, MuRF-3 null hearts are more prone to rupture following myocardial infarction [172]. Moreover, double knock-out mice of MuRF-1 and MuRF-3 exhibit skeletal myopathy and hypertrophic cardiomyopathy, as shown by accumulation of myosin at the subsarcolemma region, myofiber fragmentation, and reduced muscle contractility [158]. Interestingly, Z-disks, but not M-bands, are disrupted in the MuRF-1/MuRF-3 double knock-out mice [158]. Since MuRF-2 is present at M-bands, but not Z-disks, it is possible that it may compensate for the loss of MuRF-1 and MuRF-3 with regards to protein turnover, thus contributing to the maintenance of M-band organization. This is consistent with MuRF proteins having redundant functions, at least partially, and highlights the importance of regulated proteasomal degradation in myofilament organization and contractility.

In addition to the MuRF family, another E3 ubiquitin ligase, cullin-3, is involved in the proteasomal degradation of small Ankyrin 1 (sAnk1), an integral membrane protein of the network sarcoplasmic reticulum that overlies M-bands and Z-disks [66]. However, since cullin-3 is localized at Z-disks rather than M-bands [66], it is highly possible that this process takes place at the former rather than the latter structure.

3. Cardiac and Skeletal Myopathies Associated with M-Band Proteins

A significant percentage of skeletal and cardiac myopathies are linked to genetic mutations in genes encoding sarcomeric, metabolic, and enzymatic proteins [173–176], many of which are localized to the M-region (Figure 2). Herein, we present a comprehensive overview of mutations associated with sarcomeric proteins of the M-region. In particular, we summarize early and current literature on genes encoding M-region related proteins that are heavily mutated (referring the reader to focused reviews) (Tables 2 and 3) and emphasize the emerging roles of genes recently implicated in the development of skeletal and cardiac myopathies.

3.1. Cytoskeletal Proteins and M-Band Myopathies

3.1.1. Light Meromyosin. Hereditary myosin myopathies are a group of diseases caused by mutations in the heavy chain of myosin (MyHC) [259]. Mutations have been reported in the genes encoding three muscle-specific MyHC isoforms, including *MYH7*, which is expressed in slow-twitch skeletal and cardiac muscles, *MYH3*, which is abundantly expressed in embryonic skeletal muscles, and *MYH6*, which is selectively expressed in cardiac muscle [98]. Although multiple mutations have been identified along the entire length of MyHC [174, 214, 259], we only note those associated with the light meromyosin (LMM) portion of myosin that localizes to the M-band (Table 2). Over 86 disease-causing LMM mutations have been linked to the development of different skeletal and cardiac myopathies. Of those mutations, 78 map to *MYH7* with 68 being missense mutations, 9 being insertions and/or deletions, and 1 being a nonsense mutation. Currently, the molecular alterations underlying the majority of these mutations are elusive.

3.1.2. Titin. Due to the development of next-generation sequencing, routine analysis of the giant titin gene *(TTN)* has been made possible. Consequently, *TTN* has emerged as a "hot spot" for inherited skeletal and cardiac myopathies affecting mankind [175]. Over 120 disease-causing titin mutations have been reported in patients with different skeletal and cardiac myopathies [175]. Of those mutations, 23 map

Table 2: Disease-causing mutations in genes encoding structural proteins of the M-region.

Protein	Mutation	Region on protein	Effect	Disease	Reference
FHL-1	K45SfsX1	LIM domain 1	Unknown	HCM	[177]
FHL-1	R95W	Linker region between LIM domain 1 and 2	Unknown	RBM	[178]
FHL-1	C101F	LIM domain 2	Unknown	RBM	[179]
FHL-1	102–104 del KFC	LIM domain 2	Unknown	RBM	[179]
FHL-1	C104R/Y	LIM domain 2	Unknown	RBM	[179, 180]
FHL-1	111–229 del ins G	LIM domain 2	Unknown	EDMD	[181]
FHL-1	N112FfsX51	LIM domain 2	Unknown	EDMD	[181]
FHL-1	W122S/C	LIM domain 2	Unknown	SPM	[182, 183]
FHL-1	H123Y/Q/L/R	LIM domain 2	Unknown	RBM	[178, 184–186]
FHL-1	K124RfsX6	LIM domain 2	Unknown	EDMD	[181]
FHL-1	F127 ins 128I	LIM domain 2	Unknown	XMPMA	[187]
FHL-1	C132F	LIM domain 2	Unknown	RBM	[186]
FHL-1	C150Y/R/S	LIM domain 2	Unknown	RBM	[179, 185, 188]
FHL-1	151–153 del VTC	LIM domain 2	Unknown	RSS	[179]
FHL-1	C153Y/R/S/W	LIM domain 2	Unknown	RBM	[186]
FHL-1	153Stop	LIM domain 2	Unknown	HCM	[177]
FHL-1	Delete exon 6 ins 84 bp	LIM domain 3	Loss of full length FHL-1A, increase in FHL-1C	EDMD	[189]
FHL-1	K157VfsX36	LIM domain 3	Unknown	EDMD	[181]
FHL-1	A168GfsX195	LIM domain 3	Unknown	XMPMA	[187]
FHL-1	194Stop	LIM domain 3	Premature stop codon and truncated protein corresponding to FHL-1C	XMPMA	[190]
FHL-1	198Stop	LIM domain 3	Unknown	HCM	[191]
FHL-1	F200fs32X	LIM domain 3	Unknown	HCM	[192]
FHL-1	C209R	LIM domain 3	Unknown	EDMD/HCM	[181, 193]
FHL-1	C224W	LIM domain 4	Unknown	XMPMA	[187]
FHL-1	H246Y	LIM domain 4	Unknown	XMPMA	[190]
FHL-1	C273LfsX11	LIM domain 4	Unknown	EDMD	[181]
FHL-1	C276Y	LIM domain 4	Unknown	EDMD	[181]
FHL-1	C276S	LIM domain 4	Unknown	HCM	[177]
FHL-1	V280M	NLS of FHL-1B	Unknown	XMPMA	[190]
FHL-1	E281Stop	Extreme COOH-terminus	Unknown	EDMD	[181]
FHL-2	G48S	LIM domain 1	Loss of titin binding	DCM	[194]
sMyBP-C	W236R	M-motif	Loss of actin and myosin binding	DA-1	[195]
sMyBP-C	R318Stop	IgC2	Premature stop codon and truncated protein	LCCS4	[196]
sMyBP-C	Y856H	IgC8	Loss of myosin binding	DA-1	[195]
MyH 3	841-841 del L	LMM	Reduced catalytic activity	DA Sheldon-Hall syndrome	[197]
MyH 6	A1004S E1457K	LMM	Unknown	DCM	[198]
MyH 6	Q1065H	LMM	Unknown	HCM	[198]
MyH 6	R1116S A1366D A1443D R1865Q	LMM	Unknown	CHD	[199]

Table 2: Continued.

Protein	Mutation	Region on protein	Effect	Disease	Reference
MyH 7	847-847 del K	LMM	Unknown	HCM	[200]
MyH 7	M852T	LMM	Unknown	HCM	[201]
MyH 7	R858C	LMM	Unknown	HCM	[200]
MyH 7	R869G	LMM	Unknown	HCM	[201]
MyH 7	R870H	LMM	Unknown	HCM	[202]
MyH 7	883-883 del E	LMM	Unknown	HCM	[201]
MyH 7	E894G	LMM	Unknown	HCM	[200]
MyH 7	D906G	LMM	Unknown	HCM	[203]
MyH 7	L908V	LMM	Unknown	HCM with CCD	[204]
MyH 7	E921K	LMM	Unknown	HCM	[200]
MyH 7	E924K E949K	LMM	Unknown	HCM	[205]
MyH 7	D928V	LMM	Unknown	HCM	[206]
MyH 7	E931K	LMM	Unknown	HCM	[200]
MyH 7	E935K	LMM	Unknown	HCM	[207]
MyH 7	D953H	LMM	Unknown	HCM	[200]
MyH 7	T1019N	LMM	Unknown	DCM	[208]
MyH 7	R1053Q	LMM	Unknown	HCM	[209]
MyH 7	G1057S	LMM	Unknown	HCM	[200]
MyH 7	L1135R	LMM	Unknown	HCM	[201]
MyH 7	R1193S	LMM	Unknown	DCM	[208]
MyH 7	E1218Q	LMM	Unknown	HCM	[201]
MyH 7	N1327K	LMM	Reduced α-helical content of the rod domain	HCM	[210]
MyH 7	E1356K	LMM	Reduced α-helical content of the rod domain	HCM	[211]
MyH 7	E1377M A1379T R1382W	LMM	Unknown	HCM	[201]
MyH 7	R1420W	LMM	Unknown	HCM	[200]
MyH 7	E1426K	LMM	Unknown	DCM	[208]
MyH 7	A1439P	LMM	Unknown	MPD1	[212]
MyH 7	K1459N	LMM	Unknown	HCM	[200]
MyH 7	L1467V	LMM	Unknown	Congenital myopathy	[213]
MyH 7	L1481P	LMM	Unknown	MPD1	[214]
MyH 7	R1500W	LMM	Reduced α-helical content of the rod domain	DCM	[215]
MyH 7	R1500P 1617-1617 del K	LMM	Unknown	Laing distal myopathy	[216]
MyH 7	1508-1508 del E	LMM	Unknown	MPD1	[217]
MyH 7	T1513S	LMM	Unknown	HCM	[200]
MyH 7	Q1541P	LMM	Unknown	MPD1	[214]
MyH 7	E1555K	LMM	Reduced α-helical content of the rod domain	HCM	[218]
MyH 7	R1588P	LMM	Unknown	MPD1	[213]
MyH 7	L1591P	LMM	Unknown	MPD1	[219]
MyH 7	L1597R	LMM	Unknown	Axial myopathy, contractual myopathy	[220]
MyH 7	T1599P	LMM	Unknown	MPD1	[214]
MyH 7	A1603P	LMM	Unknown	MPD1	[217]

Table 2: Continued.

Protein	Mutation	Region on protein	Effect	Disease	Reference
MyH 7	R1608P	LMM	Unknown	Congenital myopathy, HCM	[214]
MyH 7	L1612P	LMM	Unknown	MPD1	[214]
MyH 7	1617-1617 del K	LMM	Unknown	MPD1, DCM	[214, 216]
MyH 7	R1634S	LMM	Unknown	DCM	[208]
MyH 7	A1636P L1646P R1662P	LMM	Unknown	MPD1	[214]
MyH 7	A1663P	LMM	Unknown	MPD1	[216]
MyH 7	1669-1669 del E	LMM	Unknown	MPD1	[214]
MyH 7	V1691M	LMM	Unknown	HCM	[201]
MyH 7	L1706P	LMM	Unknown	MPD1	[216]
MyH 7	R1712W	LMM	Unknown	HCM	[210]
MyH 7	L1723P	LMM	Unknown	CCD	[221]
MyH 7	1729-1729 del K	LMM	Unknown	Laing distal myopathy	[216]
MyH 7	E1753K	LMM	Unknown	HCM	[210]
MyH 7	A1766T	LMM	Unknown	LVNC	[222]
MyH 7	E1768K	LMM	Increased α-helical content of the rod domain	HCM	[200]
MyH 7	S1776G	LMM	Unknown	HCM	[223]
MyH 7	A1777T	LMM	Unknown	HCM	[201]
MyH 7	1784-1784 del K	LMM	Unknown	MPD1, MSM	[219, 224]
MyH 7	L1793P	LMM	Destabilization of the thick filaments	HCM with MSD	[225, 226]
MyH 7	1793-1793 del L	LMM	Unknown	MPD1	[214]
MyH 7	E1801K	LMM	Unknown	MPD1, DCM, HCM	[214, 217]
MyH 7	T1834M	LMM	Unknown	HCM	[200]
MyH 7	R1845W	LMM	Alters interactions between filaments	MSM	[227]
MyH 7	E1856K	LMM	Unknown	Late onset myopathy with cardiac involvement	[228]
MyH 7	E1883K	LMM	Destabilization of the thick filaments	HCM	[226, 229]
MyH 7	H1901L	LMM	Alters interactions between filaments	MSM	[230]
MyH 7	E1914K	LMM	Unknown	DCM	[214]
MyH 7	N1918K	LMM	Unknown	LVNC	[231]
MyH 7	T1929M	LMM	Unknown	HCM	[200]
MyH 7	Stop1936W	LMM	Unknown	MSM	[232]
Myomesin	Aberrant splicing of exon 17a	EH-motif	Premature stop codon and truncated protein	MD1	[233]
Myomesin	V1490I	Ig12	Reduced dimerization	HCM	[234]
Obscurin	R4344Q	Ig58	Loss of titin binding	HCM	[235]
Titin	S33705LfsX4	TK	Unknown	LGMD2J	[236]
Titin	N34020TfsX9	TK	Increased structural stability of TK, loss of interactions with proteins partners of TK	MmD-HD	[175]
Titin	R34091W	TK	Unknown	HMERF	[23]
Titin	R34175Stop	MIg1	Unknown	MmD-HD	[175]

Table 2: Continued.

Protein	Mutation	Region on protein	Effect	Disease	Reference
Titin	32664-32665 del ins K	MIg2	Unknown	HCM	[237]
Titin	P34617QinsX3	MIs2	Unknown	CNM	[238]
Titin	R34637Q	MIg4	Unknown	DCM	[239]
Titin	A32606fsX7	MIg5	Unknown	DCM	[240]
Titin	Q35176HfsX9	MIg5	Truncated titin	MmD-HD (EOMFC)	[241]
Titin	Q35278Stop	MIs4	Unknown	MmD-HD	[175]
Titin	G35340VfsX65	MIg6	Unknown	CNM	[238]
Titin	33710-33711 del ins K	MIg6	Unknown	HCM	[237]
Titin	S35469SfsX11	MIg7	Unknown	MmD-HD	[175]
Titin	K35524RfsX22	MIs6	Unknown	MmD-HD (EOMFC)	[241]
Titin	32986-32987 del ins K	MIg8	Unknown	DCM	[240]
Titin	M35859T	MIs7	Unknown	ARVC	[242]
Titin	S35883QfsX10	MIs7	Unknown	TMD	[243]
Titin	Q35927–35931W del ins VKQK	MIg10	Truncated titin	TMD, LGMD2J, MD	[236, 244, 245]
Titin	H35946P	MIg10	Unknown	TMD	[246]
Titin	I35947N	MIg10	Unknown	TMD	[247]
Titin	L35956P	MIg10	Unknown	TMD	[244]
Titin	K35963NfsX9	MIg10	Unknown	TMD, CNM	[238, 243]
Titin	Q35964Stop	MIg10	Truncated titin	TMD	[243]

Note: nomenclature refers to the canonical full-length human isoforms; FHL-1, NP_001153174.1, sMyBP-C, AAI43503.1, MyH 3, NP_002461.2, MyH 6, NP_002462.2, MyH 7, NP_000248.2, myomesin, CAF18565.1, obscurin, CAC44768.1, titin, NP_001254479.2. HCM: hypertrophic cardiomyopathy, RBM: reducing body myopathy, XMPMA: X-linked myopathy with postural muscle atrophy, SPM: scapuloperoneal myopathy, RSS: rigid spine syndrome, EDMD: Emery-Dreifuss muscular dystrophy, DCM: dilated cardiomyopathy, DA-1: distal arthrogryposis type 1, LCCS4: lethal congenital contracture syndrome type 4, MPD1: Laing distal myopathy, CHD: congenital heart defect, CCD: central core disease, MSM: myosin storage myopathy, LVNC: left ventricular noncompaction, MD1: myotonic dystrophy type 1, LGMD2J: limb-girdle muscular dystrophy type 2J, MmD-HD: multiminicore disease with heart disease, HMERF: hereditary myopathy with early respiratory failure, CNM: centronuclear myopathy, EOMFC: early-onset myopathy with fatal cardiomyopathy, ARVC: arrhythmogenic right ventricular cardiomyopathy, TMD: tibial muscular dystrophy, MD: muscle disease, NLS: nuclear localization sequence, TK: titin kinase, MIgX: titin M-band IgX, MyH: myosin heavy chain, and LMM: light meromyosin.

to the M-band region of titin, a significant percentage given the relatively small size of titin's M-band region (~200 kDa) compared to the rest of the molecule (~2-3 MDa). Of these 23 mutations, 9 are frameshift, 3 are nonsense, 6 are missense, and 5 are insertions and/or deletions (Table 2). While the mutations associated with the development of cardiomyopathies affect several domains throughout the M-band portion of titin, the ones that are linked to skeletal myopathies are mainly contained within the last Ig domain of titin, MIg10 [260].

3.1.3. Obscurin. Mutations in *OBSCN*, the gene encoding giant obscurins, have been linked to the development of hypertrophic cardiomyopathy (HCM) [13, 261]. Specifically, the presence of a missense mutation results in an R4344Q substitution within the Ig58 domain of obscurin [235]. *In vitro* studies have shown that the R4344Q mutation results in decreased binding of obscurin Ig58/Ig59 domains to the titin Ig9/Ig10 domains, which localize at the Z/I junction. However, the pathological effects of this mutation on sarcomeric assembly or Ca^{2+} homeostasis are still unknown.

3.1.4. Myosin Binding Protein-C Slow. *MYBPC1* encodes the slow isoform of MyBP-C and has been directly implicated in the development of severe and lethal skeletal myopathies [10, 195, 196]. Two autosomal dominant missense mutations have been identified to date, W236R and Y856H, which are linked to the development of distal arthrogryposis type-1 (DA1), a severe skeletal myopathy selectively affecting distal muscles [195]. Recent work from our group has demonstrated that the W236R and Y856H mutations abolish the ability of the NH_2 and COOH termini, respectively, to bind native actin and/or myosin and to regulate the formation of actomyosin cross-bridges *in vitro* [262]. Moreover, *MYBC1* has been causally associated with the development of lethal congenital contractual syndrome type-4 (LCCS4), a neonatal lethal form of arthrogryposis myopathy [196] that most likely results in a null phenotype. A homozygous nonsense mutation in the C2 domain of sMyBP-C (R318Stop) consists of the molecular basis of LCCS4. Given that all three mutations are encoded by exons that are constitutively expressed, they are present in all sMyBP-C variants, including those that carry a unique COOH-terminal insertion and preferentially localize to the periphery of the M-band [10, 263].

Table 3: Proteins with enzymatic activity at the M-region and related diseases.

Protein	Mutation	Effect	Disease	Reference
β-Enolase	G156N G374E	Unknown	GSD XIII	[248]
MuRF1	S5L	Unknown	HCM	[249]
MuRF1	F73S	Unknown	HCM	[249]
MuRF1	R86C/H	Unknown	HCM	[249]
MuRF1	I101F	Unknown	HCM	[249]
MuRF1	T232M	Unknown	HCM	[249]
MuRF1	E299Stop	Unknown	HCM	[249]
MuRF1	M305I	Unknown	HCM	[249]
MuRF1	A318D	Unknown	HCM	[249]
MuRF2	C50Y	Unknown	HCM	[249]
MuRF2	P79A	Unknown	HCM	[249]
MuRF2	Q187fs	Unknown	HCM	[249]
MuRF2	L241M	Unknown	HCM	[249]
MuRF2	S252F	Unknown	HCM	[249]
MuRF2	E371fs	Unknown	HCM	[249]
MuRF2	P392T	Unknown	HCM	[249]
MuRF2	K425N	Unknown	HCM	[249]
MuRF2	A488T	Unknown	HCM	[249]
MuRF2	T506S	Unknown	HCM	[249]
MuRF2	H523W	Unknown	HCM	[249]
MuRF2	F538fs	Unknown	HCM	[249]
MuRF3	P9L	Unknown	HCM	[249]
MuRF3	G94C	Unknown	HCM	[249]
MuRF3	P115S	Unknown	HCM	[249]
MuRF3	L163P	Unknown	HCM	[249]
MuRF3	A221V	Unknown	HCM	[249]
MuRF3	R249Q	Unknown	HCM	[249]
MuRF3	R269H	Unknown	HCM	[249]
MuRF3	K270N	Unknown	HCM	[249]
MuRF3	P346T	Unknown	HCM	[249]
MuRF3	G373D	Unknown	HCM	[249]
PFK	R39P/L	Unknown	GSD VII	[250, 251]
PFK	G57V	Unknown	GSD VII	[252]
PFK	G80fs4X	Unknown	GSD VII	[252]
PFK	R95Stop	Unknown	GSD VII	[253]
PFK	R100Q	Unknown	GSD VII	[254]
PFK	S108C	Unknown	GSD VII	[252]
PFK	G209D	Unknown	GSD VII	[254]
PFK	N309G	Unknown	GSD VII	[255]
PFK	D543A	Unknown	GSD VII	[250]
PFK	D591A	Unknown	GSD VII	[252]
PFK	P668Q	Unknown	GSD VII	[251]
PFK	W686C	Unknown	GSD VII	[254]
PFK	R696H	Unknown	GSD VII	[251]
PFK	78 bp del exon 5	Unknown	GSD VII	[254]
PFK	5 or 12 bp del exon 7	Unknown	GSD VII	[250]

Table 3: Continued.

Protein	Mutation	Effect	Disease	Reference
PFK	75 bp del exon 15	Unknown	GSD VII	[256]
PFK	Retention of intron 13, truncated protein	Unknown	GSD VII	[257]
PFK	Retention of intron 16, truncated protein	Unknown	GSD VII	[257]
PFK	169 bp del exon 19	Unknown	GSD VII	[258]

Note: nomenclature refers to the canonical full-length human isoforms; beta-enolase, NP_001967.3, MuRF1, NP_115977.2, MuRF2, Q9BYV6.2, MuRF3, NP_912730.2, PFK, and NP_000280.1. HCM: hypertrophic cardiomyopathy; GSD: glycogen storage disease.

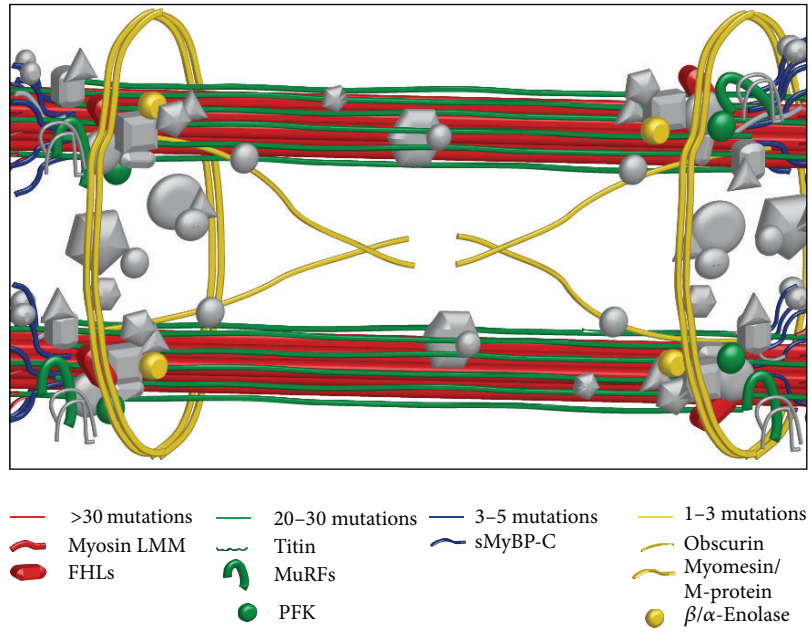

Figure 2: M-region proteins associated with skeletal and cardiac myopathies. Schematic representation of sarcomeric M-region proteins linked to the development of skeletal and cardiac myopathies. Proteins exhibiting no known disease-linked mutations are shown in grey color.

3.1.5. Myomesin. The gene that encodes myomesin, *MYOM1,* has been directly linked to the development of HCM [234]. Specifically, a missense mutation resulting in V1490I substitution within the COOH-terminal Ig12 domain reduces the ability of myomesin to homodimerize (Table 2). Although the molecular etiology of HCM due to the V1490I substitution is still unknown, it is likely that mutant myomesin fails to cross-link myosin thick filaments at the M-band [234].

In addition, myomesin has been associated with myotonic dystrophy type 1 (DM1), a multisystem disease characterized by myotonia, muscle weakness, cardiac conduction defects, insulin resistance, and mental retardation. DM1 is caused by expansion of a CTG repeat present in the 3′ UTR region of dystrophia myotonica-protein kinase, DMPK [264], resulting in aggregation of muscle blind-like (MBNL) protein. MBNL is an RNA binding protein that regulates the alternative splicing of the *MYOM1* gene [233]. Specifically, exon 17a encoding the EH-motif that links the third and fourth FnIII domains of myomesin is developmentally regulated. In normalcy, exon 17a is expressed in embryonic heart, while in heart failure it is also expressed in adult myocardium, as a compensatory mechanism to render the heart muscle more compliant [265, 266]. In the case of DM1 patients, loss of MBNL function leads to inclusion of exon 17a in adult cardiac muscle resulting in expression of a myomesin form that compromises the ability of the afflicted muscles to withstand stress and generate force [233].

3.1.6. Four and a Half LIM (FHL) Domain Proteins. FHL-1 and FHL-2 have been directly linked to the development of skeletal and cardiac myopathies [176, 267]. Mutations in the *FHL1* gene, encoding FHL-1, have been linked to the development of five distinct skeletal muscle diseases, including reducing body myopathy (RBM), X-linked myopathy with postural muscle atrophy (XMPMA), scapuloperoneal myopathy (SPM), rigid spine syndrome (RSS), and Emery-Dreifuss muscular dystrophy (EDMD) [176]. Since a number of thorough reviews on FHL-1 associated myopathies have

been published prior to 2011 [176, 184, 267], we will focus our discussion on new information, originating after 2011. For consistency purposes, a complete listing of all known FHL-1 mutations to date is listed in Table 2.

Since 2011, six additional mutations in *FHL-1* have been linked to the development of RBM and EDMD, increasing the total number of FHL-1 skeletal myopathy linked mutations from 29 prior to 2011 to 35 after 2011. Specifically, RBM linked mutation R95W is located within the linker region between LIM domains 1 and 2, while C104Y, H123R, C126Y, and C153S/W substitutions are present in LIM domain 2 [178, 180, 268]. Moreover, deletion of exon 6 resulting in loss of full length FHL-1 was linked to the development of EDMD [189]. Recently, Binder et al. demonstrated that patients, who presented with XMPMA due to mutations in the *FHL1* gene, also suffer from reduced cardiac function [269]. This was observed in hemizygote males as well as heterozygote females carrying one of the following mutations, C224W, H246Y, V280M, and A168fsX195 [269].

Furthermore, six novel mutations in *FHL-1* have been directly linked with the development of HCM, by generating truncated or deleterious FHL-1 proteins. These include 2 frameshift mutations at residues 45 and 200 within LIM domains 1 and 3, respectively, 2 nonsense mutations generating premature termination codons at residues 153 and 198 within LIM domains 2 and 3, respectively, and 2 missense mutations, C209R and C276S, both located within LIM domain 3 [177, 191, 192]. In addition to the expression of truncated or poisonous forms of FHL-1, the levels of FHL-1 are also altered in cardiomyopathies. In particular, patients with HCM exhibit ~2-fold increased expression of *FHL1,* with a subsequent increase in protein levels of FHL-1 [270], while patients diagnosed with end-stage dilated cardiomyopathy (DCM) show a ~3.5-fold decrease in the levels of FHL-1 transcripts resulting in reduced protein expression [271].

Although mutations in FHL-1 protein are commonly linked to the development of skeletal and cardiac myopathies, we are just beginning to unravel the molecular mechanisms underlying the pathogenesis of these myopathies. Recently, Wilding et al. showed that select RBM (H123Y, C132F, and C153Y), SPM (W122S), and XMPMA (F127 ins 128I and C224W) FHL-1 mutants accumulate in reducing bodies or protein aggregates when overexpressed in C2C12 cells [272]. These reducing bodies are phenotypically similar to those found in patients suffering from the corresponding diseases. In addition, these same mutations result in impaired myoblast differentiation when overexpressed in C2C12 cells, consistent with the loss of normal FHL-1 function [272]. Conversely, select EDMD (K157VfsX36, C273LfsX11, C276Y, and E281Stop) and EDMD/HCM (C209R) FHL-1 mutations result in reduced protein expression when overexpressed in C2C12 cells, suggesting impaired transcriptional regulation and/or protein stability and degradation [272]. Thus, these studies are the first to suggest potential molecular alterations that underlie the different FHL-1 linked myopathies.

FHL-2 has also been associated with heart failure progression and the development of DCM. A missense mutation, G48S, in the first LIM domain of FHL-2 has been identified in a patient with familial DCM [194] (Table 2). The presence of this mutation reduces the ability of mutant FHL-2 protein to bind titin, suggesting a structural role for FHL-2 at the M-band.

3.2. Metabolic Enzymes and M-Band Myopathies. In addition to alterations in genes encoding cytoskeletal proteins, mutations in the metabolic enzymes PFK, β-enolase, and AMPD that localize at the M-band have been linked to the development of skeletal and cardiac myopathies; this group of diseases is collectively classified as "metabolic myopathies." Affected individuals present with muscle weakness, occasionally triggered by exercise, chronic respiratory failure, muscle rigidity, and decreased voluntary contractions [273]. Tarui disease, also referred to as glycogen storage disease (GSD) type VII, is a rare disorder involving impaired glycogen metabolism due to PFK deficiency and is characterized by exercise intolerance, myalgias, muscle cramps, and episodic myoglobinuria [252]. To date, 21 mutations in the *PFK* gene have been linked to the development of Tarui/GSD type VII disease (Table 3) [252, 255] (for a thorough discussion on Tarui disease and the molecular details of the identified mutations, please see [252]). Another form of GSD, referred to as GSD type XIII, is linked to defects in β-enolase. Two missense mutations (G156N and G374E) in the β-enolase gene have been linked to the development of GSD type XIII. These mutations result in decreased protein levels leading to a dramatic reduction (~95%) in cellular enolase activity [248] (Table 3).

Lastly, missense and truncation mutations in the human *AMPD1* gene have been linked with AMPD deficiency in skeletal muscle [274–277]. Specifically, the Q12X nonsense mutation gives rise to a premature stop codon leading to the generation of truncated mRNA and loss of AMPD-1 protein [275]. In addition, the P48L, Q156H, K287I, R388W, and R425H missense mutations result in expression of mutant AMPD-1 proteins with negligible enzymatic activity [274, 276, 277], while a deletion mutation (IVS2 del CTTT) leads to expression of multiple inactive spliced forms of the protein [277]. While loss of AMPD-1 may be partially compensated by isoforms encoded by *AMPD3* [278], the importance of AMPD-1 in maintaining optimal AMP levels is underscored by the severe effects of many of these disease-linked mutations.

3.3. Ubiquitin Ligases and M-Band Myopathies

3.3.1. MuRFs. It is only very recently that mutations in members of the MuRF family have been linked to the development of hypertrophic cardiomyopathies. Su et al. recently identified 8, 12, and 10 mutations in MuRF-1, MuRF-2, and MuRF-3 genes, respectively (Table 3) [249]. Interestingly, these mutations are suggested to modify the severity of the HCM phenotype but not cause it *per se*. Moreover, select HCM linked MuRF-1 and MuRF-2 mutations cosegregate with mutations in genes encoding sarcomeric proteins, that is, *MYH7, MYBPC3, MYC2*, and *MYL3*. However, the contribution of these MuRF-1 and MuRF-2 mutations in the pathogenesis of HCM is still unknown.

In addition, the expression profile of MuRF-1 is differentially regulated in response to pathophysiological processes, such as aging, atrophy, and senescence. Specifically, the levels of MuRF-1 are significantly increased in the initial phases of muscle disuse and atrophy in humans; this is consistent with a decrease in muscle fiber size [279]. Conversely, in aged skeletal muscle, the levels of MuRF-1 are decreased, coinciding with slowing of muscle atrophy [279]. Moreover, muscle loss is often associated with chronic diseases, such as cirrhosis and heart failure. Muscle biopsies obtained from malnourished cirrhotic patients exhibiting muscle atrophy contain increased amounts of MuRF-1 [280]. Similarly, MuRF-1's expression is upregulated in skeletal muscles of patients with chronic heart failure [281]. However, this trend is reversed in the same patients following exercise training [281].

Although the molecular etiologies underlying the differential expression of the MuRF proteins in skeletal and cardiac myopathies are yet to be defined, it is apparent that they play key roles in regulating muscle fiber size and muscle loss [282].

4. Perspectives and Future Directions

Throughout the last decade, it has become clear that in addition to its structural role, the M-region also acts as a mechanosensor, signal transduction center, and metabolic hub (Figure 1 and Table 1). Distinct mutations or alterations in the expression levels of M-band proteins have been implicated in the development of skeletal and cardiac muscle diseases. To date, more than 210 distinct mutations affect proteins that localize to the M-region. Notably, a striking 163 missense and nonsense mutations, 21 frameshift mutations, and 26 deletions/insertions within genes encoding M-region related proteins (Figure 2 and Tables 2 and 3) have been associated with the development of different forms of skeletal and cardiac myopathies. The severity of these diseases can vary dramatically, depending on the nature of the mutation and the role of the affected protein. Our current understanding of the molecular pathophysiology of individual mutations is still incomplete and only just emerging in most cases. Deciphering how these mutations alter M-band structure, contractile activity, signaling networks, posttranslational modifications, and energy production will aid in improving clinical diagnosis and developing individualized therapeutic approaches for affected individuals.

Conflict of Interests

The authors declare that there is no conflict of interests regarding the publication of this paper.

Acknowledgments

This work was supported by grants to Li-Yen R. Hu (NIH, 5 T32AR7592), Maegen A. Ackermann (NIH, K99 KHL116778A), and Aikaterini Kontrogianni-Konstantopoulos (AHA, 14GRNT20380360).

References

[1] H. M. Eppenberger and J.-C. Perriard, *Developmental Processes in Normal and Diseased Muscle*, S. Karger AG, Basel, Switzerland, 1984.

[2] M. Sjöström and J. M. Squire, "Cryo-ultramicrotomy and myofibrillar fine structure: a review," *Journal of Microscopy*, vol. 111, no. 3, pp. 239–278, 1977.

[3] H. A. AL-Khayat, R. W. Kensler, E. P. Morris, and J. M. Squire, "Three-dimensional structure of the M-region (bare zone) of vertebrate striated muscle myosin filaments by single-particle analysis," *Journal of Molecular Biology*, vol. 403, no. 5, pp. 763–776, 2010.

[4] P. Luther and J. Squire, "Three dimensional structure of the vertebrate muscle M region," *Journal of Molecular Biology*, vol. 125, no. 3, pp. 313–324, 1978.

[5] I. Agarkova, E. Ehler, S. Lange, R. Schoenauer, and J.-C. Perriard, "M-band: a safeguard for sarcomere stability?" *Journal of Muscle Research and Cell Motility*, vol. 24, no. 2-3, pp. 191–203, 2003.

[6] W. M. J. Obermann, M. Gautel, F. Steiner, P. F. M. van der Ven, K. Weber, and D. O. Fürst, "The structure of the sarcomeric M band: localization of defined domains of myomesin, M-protein, and the 250-kD carboxy-terminal region of titin by immunoelectron microscopy," *The Journal of Cell Biology*, vol. 134, no. 6, pp. 1441–1453, 1996.

[7] P. A. Kenny, E. M. Liston, and D. G. Higgins, "Molecular evolution of immunoglobulin and fibronectin domains in titin and related muscle proteins," *Gene*, vol. 232, no. 1, pp. 11–23, 1999.

[8] R. Schoenauer, S. Lange, A. Hirschy, E. Ehler, J.-C. Perriard, and I. Agarkova, "Myomesin 3, a novel structural component of the M-band in striated muscle," *Journal of Molecular Biology*, vol. 376, no. 2, pp. 338–351, 2008.

[9] A. Kontrogianni-Konstantopoulos, E. M. Jones, D. B. van Rossum, and R. J. Bloch, "Obscurin is a ligand for small ankyrin 1 in skeletal muscle," *Molecular Biology of the Cell*, vol. 14, no. 3, pp. 1138–1148, 2003.

[10] M. A. Ackermann, L.-Y. R. Hu, A. L. Bowman, R. J. Bloch, and A. Kontrogianni-Konstantopoulos, "Obscurin interacts with a novel isoform of MyBP-C slow at the periphery of the sarcomeric M-band and regulates thick filament assembly," *Molecular Biology of the Cell*, vol. 20, no. 12, pp. 2963–2978, 2009.

[11] P. Bagnato, V. Barone, E. Giacomello, D. Rossi, and V. Sorrentino, "Binding of an ankyrin-1 isoform to obscurin suggests a molecular link between the sarcoplasmic reticulum and myofibrils in striated muscles," *Journal of Cell Biology*, vol. 160, no. 2, pp. 245–253, 2003.

[12] M. J. Flick and S. F. Konieczny, "The muscle regulatory and structural protein MLP is a cytoskeletal binding partner of betaI-spectrin," *Journal of Cell Science*, vol. 113, part 9, pp. 1553–1564, 2000.

[13] A. Kontrogianni-Konstantopoulos, M. A. Ackermann, A. L. Bowman, S. V. Yap, and R. J. Bloch, "Muscle giants: molecular scaffolds in sarcomerogenesis," *Physiological Reviews*, vol. 89, no. 4, pp. 1217–1267, 2009.

[14] I. Agarkova and J.-C. Perriard, "The M-band: an elastic web that crosslinks thick filaments in the center of the sarcomere," *Trends in Cell Biology*, vol. 15, no. 9, pp. 477–485, 2005.

[15] D. O. Fürst, M. Osborn, R. Nave, and K. Weber, "The organization of titin filaments in the half-sarcomere revealed by monoclonal antibodies in immunoelectron microscopy: a map of ten nonrepetitive epitopes starting at the Z line extends close

to the M line," *The Journal of Cell Biology*, vol. 106, no. 5, pp. 1563–1572, 1988.

[16] M. Gautel, K. Leonard, and S. Labeit, "Phosphorylation of KSP motifs in the C-terminal region of titin in differentiating myoblasts," *The EMBO Journal*, vol. 12, no. 10, pp. 3827–3834, 1993.

[17] S. Labeit, B. Kolmerer, and W. A. Linke, "The giant protein titin: emerging roles in physiology and pathophysiology," *Circulation Research*, vol. 80, no. 2, pp. 290–294, 1997.

[18] P. Fernando, J. S. Sandoz, W. Ding et al., "Bin 1 Src homology 3 domain acts as a scaffold for myofiber sarcomere assembly," *The Journal of Biological Chemistry*, vol. 284, no. 40, pp. 27674–27686, 2009.

[19] R. J. Wechsler-Reya, K. J. Elliott, and G. C. Prendergast, "A role for the putative tumor suppressor Bin1 in muscle cell differentiation," *Molecular and Cellular Biology*, vol. 18, no. 1, pp. 566–575, 1998.

[20] N.-C. Mao, E. Steingrimsson, J. Duhadaway et al., "The murine Bin1 gene functions early in myogenesis and defines a new region of synteny between mouse chromosome 18 and human chromosome 2," *Genomics*, vol. 56, no. 1, pp. 51–58, 1999.

[21] A. J. Muller, J. F. Baker, J. B. DuHadaway et al., "Targeted disruption of the murine Bin1/Amphiphysin II gene does not disable endocytosis but results in embryonic cardiomyopathy with aberrant myofibril formation," *Molecular and Cellular Biology*, vol. 23, no. 12, pp. 4295–4306, 2003.

[22] S. Labeit, M. Gautel, A. Lakey, and J. Trinick, "Towards a molecular understanding of titin," *The EMBO Journal*, vol. 11, no. 5, pp. 1711–1716, 1992.

[23] S. Lange, F. Xiang, A. Yakovenko et al., "Cell biology: the kinase domain of titin controls muscle gene expression and protein turnover," *Science*, vol. 308, no. 5728, pp. 1599–1603, 2005.

[24] A. Kontrogianni-Konstantopoulos, D. H. Catino, J. C. Strong et al., "Obscurin modulates the assembly and organization of sarcomeres and the sarcoplasmic reticulum," *The FASEB Journal*, vol. 20, no. 12, pp. 2102–2111, 2006.

[25] A. Kontrogianni-Konstantopoulos, D. H. Catino, J. C. Strong, W. R. Randall, and R. J. Bloch, "Obscurin regulates the organization of myosin into A bands," *American Journal of Physiology—Cell Physiology*, vol. 287, no. 1, pp. C209–C217, 2004.

[26] A. B. Borisov, S. B. Sutter, A. Kontrogianni-Konstantopoulos, R. J. Bloch, M. V. Westfall, and M. W. Russell, "Essential role of obscurin in cardiac myofibrillogenesis and hypertrophic response: evidence from small interfering RNA-mediated gene silencing," *Histochemistry and Cell Biology*, vol. 125, no. 3, pp. 227–238, 2006.

[27] L.-Y. R. Hu and A. Kontrogianni-Konstantopoulos, "The kinase domains of obscurin interact with intercellular adhesion proteins," *The FASEB Journal*, vol. 27, no. 5, pp. 2001–2012, 2013.

[28] G. Xiong, H. Qadota, K. B. Mercer, L. A. McGaha, A. F. Oberhauser, and G. M. Benian, "A LIM-9 (FHL)/SCPL-1 (SCP) complex interacts with the C-terminal protein kinase regions of UNC-89 (obscurin) in *Caenorhabditis elegans* muscle," *Journal of Molecular Biology*, vol. 386, no. 4, pp. 976–988, 2009.

[29] S. R. Cunha and P. J. Mohler, "Obscurin targets ankyrin-B and protein phosphatase 2A to the cardiac M-line," *The Journal of Biological Chemistry*, vol. 283, no. 46, pp. 31968–31980, 2008.

[30] N. Bhasin, S. R. Cunha, M. Mudannayake, M. S. Gigena, T. B. Rogers, and P. J. Mohler, "Molecular basis for PP2A regulatory subunit B56alpha targeting in cardiomyocytes," *The American Journal of Physiology—Heart and Circulatory Physiology*, vol. 293, no. 1, pp. H109–H119, 2007.

[31] H. Qadota, L. A. McGaha, K. B. Mercer, T. J. Stark, T. M. Ferrara, and G. M. Benian, "A novel protein phosphatase is a binding partner for the protein kinase domains of UNC-89 (obscurin) in *Caenorhabditis elegans*," *Molecular Biology of the Cell*, vol. 19, no. 6, pp. 2424–2432, 2008.

[32] W. M. J. Obermann, M. Gautel, K. Weber, and D. O. Fürst, "Molecular structure of the sarcomeric M band: mapping of titin and myosin binding domains in myomesin and the identification of a potential regulatory phosphorylation site in myomesin," *The EMBO Journal*, vol. 16, no. 2, pp. 211–220, 1997.

[33] A. Fukuzawa, S. Lange, M. Holt et al., "Interactions with titin and myomesin target obscurin and obscurin-like 1 to the M-band-Implications for hereditary myopathies," *Journal of Cell Science*, vol. 121, no. 11, pp. 1841–1851, 2008.

[34] D. Auerbach, S. Bantle, S. Keller et al., "Different domains of the M-band protein myomesin are involved in myosin binding and M-band targeting," *Molecular Biology of the Cell*, vol. 10, no. 5, pp. 1297–1308, 1999.

[35] L. Tskhovrebova and J. Trinick, "Making muscle elastic: the structural basis of myomesin stretching," *PLoS Biology*, vol. 10, no. 2, Article ID e1001264, 2012.

[36] W. M. J. Obermann, U. Plessmann, K. Weber, and D. O. Furst, "Purification and biochemical characterization of myomesin, a myosin-binding and titin-binding protein, from bovine skeletal muscle," *European Journal of Biochemistry*, vol. 233, no. 1, pp. 110–115, 1995.

[37] J. Noguchi, M. Yanagisawa, M. Imamura et al., "Complete primary structure and tissue expression of chicken pectoralis M-protein," *The Journal of Biological Chemistry*, vol. 267, no. 28, pp. 20302–20310, 1992.

[38] F. Steiner, K. Weber, and D. O. Fürst, "Structure and expression of the gene encoding murine M-protein, a sarcomere-specific member of the immunoglobulin superfamily," *Genomics*, vol. 49, no. 1, pp. 83–95, 1998.

[39] B. K. Grove, L. Cerny, J. C. Perriard, and H. M. Eppenberger, "Myomesin and M-protein: expression of two M-band proteins in pectoral muscle and heart during development," *Journal of Cell Biology*, vol. 101, no. 4, pp. 1413–1421, 1985.

[40] B. K. Grove, B. Holmbom, and L. E. Thornell, "Myomesin and M protein: differential expression in embryonic fibers during pectoral muscle development," *Differentiation*, vol. 34, no. 2, pp. 106–114, 1987.

[41] E. Carlsson, B. K. Grove, T. Wallimann, H. M. Eppenberger, and L.-E. Thornell, "Myofibrillar M-band proteins in rat skeletal muscles during development," *Histochemistry*, vol. 95, no. 1, pp. 27–35, 1990.

[42] W. M. J. Obermann, P. P. M. van der Ven, F. Steiner, K. Weber, and D. O. Fürst, "Mapping of a myosin-binding domain and a regulatory phosphorylation site in M-protein, a structural protein of the sarcomeric M band," *Molecular Biology of the Cell*, vol. 9, no. 4, pp. 829–840, 1998.

[43] H. C. A. Drexler, A. Ruhs, A. Konzer et al., "On marathons and Sprints: an integrated quantitative proteomics and transcriptomics analysis of differences between slow and fast muscle fibers," *Molecular & Cellular Proteomics*, vol. 11, no. 6, Article ID M111.010801, 2012.

[44] M. A. Ackermann and A. Kontrogianni-Konstantopoulos, "Myosin binding protein-C slow: an intricate subfamily of proteins," *Journal of Biomedicine and Biotechnology*, vol. 2010, Article ID 652065, 10 pages, 2010.

[45] M. J. McGrath, D. L. Cottle, M.-A. Nguyen et al., "Four and a half LIM protein 1 binds myosin-binding protein C and

regulates myosin filament formation and sarcomere assembly," *The Journal of Biological Chemistry*, vol. 281, no. 11, pp. 7666–7683, 2006.

[46] S. Lange, D. Auerbach, P. McLoughlin et al., "Subcellular targeting of metabolic enzymes to titin in heart muscle may be mediated by DRAL/FHL-2," *Journal of Cell Science*, vol. 115, no. 24, pp. 4925–4936, 2002.

[47] C. E. Torgan and M. P. Daniels, "Calcineurin localization in skeletal muscle offers insights into potential new targets," *Journal of Histochemistry and Cytochemistry*, vol. 54, no. 1, pp. 119–128, 2006.

[48] S. B. Geisler, D. Robinson, M. Hauringa et al., "Obscurin-like 1, OBSL1, is a novel cytoskeletal protein related to obscurin," *Genomics*, vol. 89, no. 4, pp. 521–531, 2007.

[49] M. A. Ackermann and A. Kontrogianni-Konstantopoulos, "Myosin binding protein-C slow is a novel substrate for protein kinase A (PKA) and C (PKC) in skeletal muscle," *Journal of Proteome Research*, vol. 10, no. 10, pp. 4547–4555, 2011.

[50] P. E. Hoppe, J. Chau, K. A. Flanagan, A. R. Reedy, and L. A. Schriefer, "Caenorhabditis elegans unc-82 encodes a serine/threonine kinase important for myosin filament organization in muscle during growth," *Genetics*, vol. 184, no. 1, pp. 79–90, 2010.

[51] H. J. Koh, T. Toyoda, N. Fujii et al., "Sucrose nonfermenting AMPK-related kinase (SNARK) mediates contraction-stimulated glucose transport in mouse skeletal muscle," *Proceedings of the National Academy of Sciences of the United States of America*, vol. 107, no. 35, pp. 15541–15546, 2010.

[52] F. Inazuka, N. Sugiyama, M. Tomita, T. Abe, G. Shioi, and H. Esumi, "Muscle-specific knock-out of NUAK family SNF1-like kinase 1 (NUAK1) prevents high fat diet-induced glucose intolerance," *The Journal of Biological Chemistry*, vol. 287, no. 20, pp. 16379–16389, 2012.

[53] K. B. Reddy, J. E. B. Fox, M. G. Price et al., "Nuclear localization of myomesin-1: possible functions," *Journal of Muscle Research and Cell Motility*, vol. 29, no. 1, pp. 1–8, 2008.

[54] X. Wang, X. Liu, S. Wang, and K. Luan, "Myofibrillogenesis regulator 1 induces hypertrophy by promoting sarcomere organization in neonatal rat cardiomyocytes," *Hypertension Research*, vol. 35, no. 6, pp. 597–603, 2012.

[55] T. B. Li, X. H. Liu, S. Feng et al., "Characterization of MR-1, a novel myofibrillogenesis regulator in human muscle," *Acta Biochimica et Biophysica Sinica (Shanghai)*, vol. 36, no. 6, pp. 412–418, 2004.

[56] H. L. Li, Z. G. She, T. B. Li et al., "Overexpression of myofibrillogenesis regulator-1 aggravates cardiac hypertrophy induced by angiotensin II in mice," *Hypertension*, vol. 49, no. 6, pp. 1399–1408, 2007.

[57] S. Just, B. Meder, I. M. Berger et al., "The myosin-interacting protein SMYD1 is essential for sarcomere organization," *Journal of Cell Science*, vol. 124, no. 18, pp. 3127–3136, 2011.

[58] J. Berkholz, L. Michalick, and B. Munz, "The E3 SUMO ligase Nse2 regulates sumoylation and nuclear-to-cytoplasmic translocation of skNAC-Smyd1 in myogenesis," *Journal of Cell Science*, vol. 127, part 17, pp. 3794–3804, 2014.

[59] I. Hwang and P. D. Gottlieb, "Bop: A new T-cell-restricted gene located upstream of and opposite to mouse CD8b," *Immunogenetics*, vol. 42, no. 5, pp. 353–361, 1995.

[60] I. Hwang and P. D. Gottlieb, "The Bop gene adjacent to the mouse CD8b gene encodes distinct zinc-finger proteins expressed in CTLs and in muscle," *Journal of Immunology*, vol. 158, no. 3, pp. 1165–1174, 1997.

[61] P. D. Gottlieb, S. A. Pierce, R. J. Sims III et al., "Bop encodes a muscle-restricted protein containing MYND and SET domains and is essential for cardiac differentiation and morphogenesis," *Nature Genetics*, vol. 31, no. 1, pp. 25–32, 2002.

[62] X. Tan, J. Rotllant, H. Li, P. DeDeyne, and S. J. Du, "SmyD1, a histone methyltransferase, is required for myofibril organization and muscle contraction in zebrafish embryos," *Proceedings of the National Academy of Sciences of the United States of America*, vol. 103, no. 8, pp. 2713–2718, 2006.

[63] S. J. Du, X. Tan, and J. Zhang, "SMYD proteins: key regulators in skeletal and cardiac muscle development and function," *The Anatomical Record*, vol. 297, no. 9, pp. 1650–1662, 2014.

[64] R. J. Sims III, E. K. Weihe, L. Zhu, S. O'Malley, J. V. Harriss, and P. D. Gottlieb, "m-Bop, a repressor protein essential for cardiogenesis, interacts with skNAC, a heart- and muscle-specific transcription factor," *The Journal of Biological Chemistry*, vol. 277, no. 29, pp. 26524–26529, 2002.

[65] S. Lange, K. Ouyang, G. Meyer et al., "Obscurin determines the architecture of the longitudinal sarcoplasmic reticulum," *Journal of Cell Science*, vol. 122, no. 15, pp. 2640–2650, 2009.

[66] S. Lange, S. Perera, P. Teh, and J. Chen, "Obscurin and KCTD6 regulate cullin-dependent small ankyrin-1 (sAnk1.5) protein turnover," *Molecular Biology of the Cell*, vol. 23, no. 13, pp. 2490–2504, 2012.

[67] H. Iwabata, M. Yoshida, and Y. Komatsu, "Proteomic analysis of organ-specific post-translational lysine-acetylation and -methylation in mice by use of anti-acetyllysine and -methyllysine mouse monoclonal antibodies," *Proteomics*, vol. 5, no. 18, pp. 4653–4664, 2005.

[68] S. Etienne-Manneville and A. Hall, "Rho GTPases in cell biology," *Nature*, vol. 420, no. 6916, pp. 629–635, 2002.

[69] I. de Curtis and J. Meldolesi, "Cell surface dynamics—how Rho GTPases orchestrate the interplay between the plasma membrane and the cortical cytoskeleton," *Journal of Cell Science*, vol. 125, no. 19, pp. 4435–4444, 2012.

[70] C. Bucci, P. Alifano, and L. Cogli, "The role of rab proteins in neuronal cells and in the trafficking of neurotrophin receptors," *Membranes*, vol. 4, no. 4, pp. 642–677, 2014.

[71] F. Nakamura, "FilGAP and its close relatives: a mediator of Rho-Rac antagonism that regulates cell morphology and migration," *Biochemical Journal*, vol. 453, no. 1, pp. 17–25, 2013.

[72] K. F. Wilson, J. W. Erickson, M. A. Antonyak, and R. A. Cerione, "Rho GTPases and their roles in cancer metabolism," *Trends in Molecular Medicine*, vol. 19, no. 2, pp. 74–82, 2013.

[73] R. García-Mata and K. Burridge, "Catching a GEF by its tail," *Trends in Cell Biology*, vol. 17, no. 1, pp. 36–43, 2007.

[74] G. Lazer and S. Katzav, "Guanine nucleotide exchange factors for RhoGTPases: good therapeutic targets for cancer therapy?" *Cellular Signalling*, vol. 23, no. 6, pp. 969–979, 2011.

[75] D. L. Ford-Speelman, J. A. Roche, A. L. Bowman, and R. J. Bloch, "The rho-guanine nucleotide exchange factor domain of obscurin activates rhoA signaling in skeletal muscle," *Molecular Biology of the Cell*, vol. 20, no. 17, pp. 3905–3917, 2009.

[76] H. Qadota, A. Blangy, G. Xiong, and G. M. Benian, "The DH-PH region of the giant protein UNC-89 activates RHO-1 GTPase in Caenorhabditis elegans body wall muscle," *Journal of Molecular Biology*, vol. 383, no. 4, pp. 747–752, 2008.

[77] P. Madaule, T. Furuyashiki, T. Reid et al., "A novel partner for the GTP-bound forms of rho and rac," *FEBS Letters*, vol. 377, no. 2, pp. 243–248, 1995.

[78] P. Madaule, M. Eda, N. Watanabe et al., "Role of citron kinase as a target of the small GTPase Rho in cytokinesis," *Nature*, vol. 394, no. 6692, pp. 491–494, 1998.

[79] X. Mu, A. Usas, Y. Tang et al., "RhoA mediates defective stem cell function and heterotopic ossification in dystrophic muscle of mice," *The FASEB Journal*, vol. 27, no. 9, pp. 3619–3631, 2013.

[80] M. Bowerman, L. M. Murray, J. G. Boyer, C. L. Anderson, and R. Kothary, "Fasudil improves survival and promotes skeletal muscle development in a mouse model of spinal muscular atrophy," *BMC Medicine*, vol. 10, article 24, 2012.

[81] H. Aoki, S. Izumo, and J. Sadoshima, "Angiotensin II activates RhoA in cardiac myocytes: a critical role of RhoA in angiotensin II-induced premyofibril formation," *Circulation Research*, vol. 82, no. 6, pp. 666–676, 1998.

[82] M. Hoshijima, V. P. Sah, Y. Wang, K. R. Chien, and J. H. Brown, "The low molecular weight GTPase Rho regulates myofibril formation and organization in neonatal rat ventricular myocytes: Involvement of Rho kinase," *The Journal of Biological Chemistry*, vol. 273, no. 13, pp. 7725–7730, 1998.

[83] J. H. Brown, D. P. Del Re, and M. A. Sussman, "The Rac and Rho hall of fame: a decade of hypertrophic signaling hits," *Circulation Research*, vol. 98, no. 6, pp. 730–742, 2006.

[84] S. Miyamoto, D. P. del Re, S. Y. Xiang, X. Zhao, G. Florholmen, and J. H. Brown, "Revisited and revised: is RhoA always a villain in cardiac pathophysiology?" *Journal of Cardiovascular Translational Research*, vol. 3, no. 4, pp. 330–343, 2010.

[85] S. Y. Xiang, D. Vanhoutte, D. P. del Re et al., "RhoA protects the mouse heart against ischemia/reperfusion injury," *The Journal of Clinical Investigation*, vol. 121, no. 8, pp. 3269–3276, 2011.

[86] D. P. del Re, S. Miyamoto, and J. H. Brown, "RhoA/Rho kinase up-regulate Bax to activate a mitochondrial death pathway and induce cardiomyocyte apoptosis," *The Journal of Biological Chemistry*, vol. 282, no. 11, pp. 8069–8078, 2007.

[87] D. P. del Re, S. Miyamoto, and J. H. Brown, "Focal adhesion kinase as a RhoA-activable signaling scaffold mediating akt activation and cardiomyocyte protection," *The Journal of Biological Chemistry*, vol. 283, no. 51, pp. 35622–35629, 2008.

[88] A. Zeidan, X. T. Gan, A. Thomas, and M. Karmazyn, "Prevention of RhoA activation and cofilin-mediated actin polymerization mediates the antihypertrophic effect of adenosine receptor agonists in angiotensin II- and endothelin-1-treated cardiomyocytes," *Molecular and Cellular Biochemistry*, vol. 385, no. 1-2, pp. 239–248, 2014.

[89] D. Frank, C. Kuhn, B. Brors et al., "Gene expression pattern in biomechanically stretched cardiomyocytes: evidence for a stretch-specific gene program," *Hypertension*, vol. 51, no. 2, pp. 309–318, 2008.

[90] A. M. de Jong, A. H. Maass, S. U. Oberdorf-Maass, R. A. de Boer, W. H. van Gilst, and I. C. van Gelder, "Cyclical stretch induces structural changes in atrial myocytes," *Journal of Cellular and Molecular Medicine*, vol. 17, no. 6, pp. 743–753, 2013.

[91] M. Hoshijima, "Mechanical stress-strain sensors embedded in cardiac cytoskeleton: Z disk, titin, and associated structures," *The American Journal of Physiology—Heart and Circulatory Physiology*, vol. 290, no. 4, pp. H1313–H1325, 2006.

[92] R. Knöll and S. Marston, "On mechanosensation, acto/myosin interaction, and hypertrophy," *Trends in Cardiovascular Medicine*, vol. 22, no. 1, pp. 17–22, 2012.

[93] E. M. Puchner, A. Alexandrovich, L. K. Ay et al., "Mechanoenzymatics of titin kinase," *Proceedings of the National Academy of Sciences of the United States of America*, vol. 105, no. 36, pp. 13385–13390, 2008.

[94] V. Kirkin, T. Lamark, Y. S. Sou et al., "A role for NBR1 in autophagosomal degradation of ubiquitinated substrates," *Molecular Cell*, vol. 33, no. 4, pp. 505–516, 2009.

[95] V. I. Korolchuk, A. Mansilla, F. M. Menzies, and D. C. Rubinsztein, "Autophagy inhibition compromises degradation of ubiquitin-proteasome pathway substrates," *Molecular Cell*, vol. 33, no. 4, pp. 517–527, 2009.

[96] N. Myeku and M. E. Figueiredo-Pereira, "Dynamics of the degradation of ubiquitinated proteins by proteasomes and autophagy: association with sequestosome 1/p62," *The Journal of Biological Chemistry*, vol. 286, no. 25, pp. 22426–22440, 2011.

[97] J. Bogomolovas, A. Gasch, F. Simkovic, D. J. Rigden, S. Labeit, and O. Mayans, "Titin kinase is an inactive pseudokinase scaffold that supports MuRF1 recruitment to the sarcomeric M-line," *Open Biology*, vol. 4, no. 5, Article ID 140041, 2014.

[98] C. Batters, C. Veigel, E. Homsher, and J. R. Sellers, "To understand muscle you must take it apart," *Frontiers in Physiology*, vol. 5, no. 90, 2014.

[99] T. Clausen, "Quantification of Na^+,K^+ pumps and their transport rate in skeletal muscle: functional significance," *Journal of General Physiology*, vol. 142, no. 4, pp. 327–345, 2013.

[100] A. R. Marks, "Calcium cycling proteins and heart failure: mechanisms and therapeutics," *The Journal of Clinical Investigation*, vol. 123, no. 1, pp. 46–52, 2013.

[101] C. R. Hancock, J. J. Brault, and R. L. Terjung, "Protecting the cellular energy state during contractions: role of AMP deaminase," *Journal of Physiology and Pharmacology*, vol. 57, no. 10, pp. 17–29, 2006.

[102] T. Wallimann, M. Tokarska-Schlattner, and U. Schlattner, "The creatine kinase system and pleiotropic effects of creatine.," *Amino Acids*, vol. 40, no. 5, pp. 1271–1296, 2011.

[103] R. M. Payne, R. C. Haas, and A. W. Strauss, "Structural characterization and tissue-specific expression of the mRNAs encoding isoenzymes from two rat mitochondrial creatine kinase genes," *Biochim Biophys Acta*, vol. 1089, no. 3, pp. 352–361, 1991.

[104] T. Wallimann and H. M. Eppenberger, "Localization and function of M-line-bound creatine kinase. M-band model and creatine phosphate shuttle," *Cell and Muscle Motility*, vol. 6, pp. 239–285, 1985.

[105] R. Ventura-Clapier, A. Kaasik, and V. Veksler, "Structural and functional adaptations of striated muscles to CK deficiency," *Molecular and Cellular Biochemistry*, vol. 256-257, no. 1-2, pp. 29–41, 2004.

[106] T. Hornemann, S. Kempa, M. Himmel, K. Hayeß, D. O. Fürst, and T. Wallimann, "Muscle-type creatine kinase interacts with central domains of the M-band proteins myomesin and M-protein," *Journal of Molecular Biology*, vol. 332, no. 4, pp. 877–887, 2003.

[107] J. van Deursen, A. Heerschap, F. Oerlemans et al., "Skeletal muscles of mice deficient in muscle creatine kinase lack burst activity," *Cell*, vol. 74, no. 4, pp. 621–631, 1993.

[108] J. van Deursen, W. Ruitenbeek, A. Heerschap, P. Jap, H. Ter Laak, and B. Wieringa, "Creatine kinase (CK) in skeletal muscle energy metabolism: a study of mouse mutants with graded reduction in muscle CK expression," *Proceedings of the National Academy of Sciences of the United States of America*, vol. 91, no. 19, pp. 9091–9095, 1994.

[109] I. Momken, P. Lechêne, N. Koulmann et al., "Impaired voluntary running capacity of creatine kinase-deficient mice," *Journal of Physiology*, vol. 565, no. 3, pp. 951–964, 2005.

[110] S. Patra, S. Bera, S. SinhaRoy et al., "Progressive decrease of phosphocreatine, creatine and creatine kinase in skeletal muscle upon transformation to sarcoma," *FEBS Journal*, vol. 275, no. 12, pp. 3236–3247, 2008.

[111] D. G. Hardie, "Metabolic control: a new solution to an old problem," *Current Biology*, vol. 10, no. 20, pp. R757–R759, 2000.

[112] C. R. Hancock, E. Janssen, and R. L. Terjung, "Skeletal muscle contractile performance and ADP accumulation in adenylate kinase-deficient mice," *The American Journal of Physiology—Cell Physiology*, vol. 288, no. 6, pp. C1287–C1297, 2005.

[113] C. Panayiotou, N. Solaroli, and A. Karlsson, "The many isoforms of human adenylate kinases," *International Journal of Biochemistry and Cell Biology*, vol. 49, no. 1, pp. 75–83, 2014.

[114] E. Janssen, P. P. Dzeja, F. Oerlemans et al., "Adenylate kinase 1 gene deletion disrupts muscle energetic economy despite metabolic rearrangement," *The EMBO Journal*, vol. 19, no. 23, pp. 6371–6381, 2000.

[115] D. Pucar, E. Janssen, P. P. Dzeja et al., "Compromised energetics in the adenylate kinase AK1 gene knockout heart under metabolic stress," *The Journal of Biological Chemistry*, vol. 275, no. 52, pp. 41424–41429, 2000.

[116] D. Pucar, P. Bast, R. J. Gumina et al., "Adenylate kinase AK1 knockout heart: energetics and functional performance under ischemia-reperfusion," *The American Journal of Physiology—Heart and Circulatory Physiology*, vol. 283, no. 2, pp. H776–H782, 2002.

[117] R. L. Sabina and D. K. Mahnke-Zizelman, "Towards an understanding of the functional significance of N-terminal domain divergence in human AMP deaminase isoforms," *Pharmacology and Therapeutics*, vol. 87, no. 2-3, pp. 279–283, 2000.

[118] N. Ogasawara, H. Goto, Y. Yamada, and T. Watanabe, "Distribution of AMP-deaminase isozymes in rat tissues," *European Journal of Biochemistry*, vol. 87, no. 2, pp. 297–304, 1978.

[119] N. Ogasawara, H. Goto, Y. Yamada, T. Watanabe, and T. Asano, "AMP deaminase isozymes in human tissues," *Biochim Biophys Acta: General Subjects*, vol. 714, no. 2, pp. 298–306, 1982.

[120] T. H. van Kuppevelt, J. H. Veerkamp, W. N. Fishbein, N. Ogasawara, and R. L. Sabina, "Immunolocalization of AMP-deaminase isozymes in human skeletal muscle and cultured muscle cells: Concentration of isoform M at the neuromuscular junction," *Journal of Histochemistry and Cytochemistry*, vol. 42, no. 7, pp. 861–868, 1994.

[121] K. Uyeda, "Phosphofructokinase," *Advances in Enzymology and Related Areas of Molecular Biology*, vol. 48, pp. 193–244, 1979.

[122] G. A. Dunaway, "A review of animal phosphofructokinase isozymes with an emphasis on their physiological role," *Molecular and Cellular Biochemistry*, vol. 52, no. 1, pp. 75–91, 1983.

[123] G. A. Dunaway, T. P. Kasten, T. Sebo, and R. Trapp, "Analysis of the phosphofructokinase subunits and isoenzymes in human tissues," *Biochemical Journal*, vol. 251, no. 3, pp. 677–683, 1988.

[124] M. Sola-Penna, D. Da Silva, W. S. Coelho, M. M. Marinho-Carvalho, and P. Zancan, "Regulation of mammalian muscle type 6-phosphofructo-1-kinase and its implication for the control of the metabolism," *IUBMB Life*, vol. 62, no. 11, pp. 791–796, 2010.

[125] E. Van Schaftingen, L. Hue, and H. G. Hers, "Fructose 2,6-bisphosphate, the probable structure of the glucose- and glucagon-sensitive stimulator of phosphofructokinase," *Biochemical Journal*, vol. 192, no. 3, pp. 897–901, 1980.

[126] T. Schöneberg, M. Kloos, A. Brüser, J. Kirchberger, and N. Sträter, "Structure and allosteric regulation of eukaryotic 6-phosphofructokinases," *Biological Chemistry*, vol. 394, no. 8, pp. 977–993, 2013.

[127] P. B. Garland, P. J. Randle, and E. A. Newsholme, "Citrate as an intermediary in the inhibition of phosphofructokinase in rat heart muscle by fatty acids, ketone bodies, pyruvate, diabetes and starvation," *Nature*, vol. 200, no. 4902, pp. 169–170, 1963.

[128] M. Y. Tsai and R. G. Kemp, "Rabbit brain phosphofructokinase. Comparison of regulatory properties with those of other phosphofructokinase isozymes," *Journal of Biological Chemistry*, vol. 249, no. 20, pp. 6590–6596, 1974.

[129] A. M. Mahrenholz, L. Lan, and T. E. Mansour, "Phosphorylation of heart phosphofructokinase by Ca^{2+}/calmodulin protein kinase," *Biochemical and Biophysical Research Communications*, vol. 174, no. 3, pp. 1255–1259, 1991.

[130] C. M. Jenkins, J. Yang, H. F. Sims, and R. W. Gross, "Reversible high affinity inhibition of phosphofructokinase-1 by Acyl-CoA: a mechanism integrating glycolytic flux with lipid metabolism," *Journal of Biological Chemistry*, vol. 286, no. 14, pp. 11937–11950, 2011.

[131] P. Zancan, F. V. R. Almeida, J. Faber-Barata, J. M. Dellias, and M. Sola-Penna, "Fructose-2,6-bisphosphate counteracts guanidinium chloride-, thermal-, and ATP-induced dissociation of skeletal muscle key glycolytic enzyme 6-phosphofructo-1-kinase: a structural mechanism for PFK allosteric regulation," *Archives of Biochemistry and Biophysics*, vol. 467, no. 2, pp. 275–282, 2007.

[132] P. Zancan, M. M. Marinho-Carvalho, J. Faber-Barata, J. M. M. Dellias, and M. Sola-Penna, "ATP and fructose-2,6-bisphosphate regulate skeletal muscle 6-phosphofructo-1-kinase by altering its quaternary structure," *IUBMB Life*, vol. 60, no. 8, pp. 526–533, 2008.

[133] R.-S. Liou and S. Anderson, "Activation of rabbit muscle phosphofructokinase by F-actin and reconstituted thin filaments," *Biochemistry*, vol. 19, no. 12, pp. 2684–2688, 1980.

[134] S. J. Roberts and G. N. Somero, "Binding of phosphofructokinase to filamentous actin," *Biochemistry*, vol. 26, no. 12, pp. 3437–3442, 1987.

[135] C.-Z. Malca, T. Livnat, and R. Beitner, "Insulin rapidly stimulates binding of phosphofructokinase and aldolase to muscle cytoskeleton," *International Journal of Biochemistry*, vol. 24, no. 5, pp. 821–826, 1992.

[136] J. P. J. Schmitz, W. Groenendaal, B. Wessels et al., "Combined in vivo and in silico investigations of activation of glycolysis in contracting skeletal muscle," *The American Journal of Physiology—Cell Physiology*, vol. 304, no. 2, pp. C180–C193, 2013.

[137] B. Buschmeier, H. E. Meyer, and G. W. Mayr, "Characterization of the calmodulin-binding sites of muscle phosphofructokinase and comparison with known calmodulin-binding domains," *Journal of Biological Chemistry*, vol. 262, no. 20, pp. 9454–9462, 1987.

[138] M. M. Marinho-Carvalho, P. V. Costa-Mattos, G. A. Spitz, P. Zancan, and M. Sola-Penna, "Calmodulin upregulates skeletal muscle 6-phosphofructo-1-kinase reversing the inhibitory effects of allosteric modulators," *Biochimica et Biophysica Acta*, vol. 1794, no. 8, pp. 1175–1180, 2009.

[139] M. García, A. Pujol, A. Ruzo et al., "Phosphofructo-1-kinase deficiency leads to a severe cardiac and hematological disorder in addition to skeletal muscle glycogenosis," *PLoS Genetics*, vol. 5, no. 8, Article ID e1000615, 2009.

[140] G. Foucault, M. Vacher, T. Merkulova, A. Keller, and M. Arrio-Dupont, "Presence of enolase in the M-band of skeletal muscle and possible indirect interaction with the cytosolic muscle isoform of creatine kinase," *Biochemical Journal*, vol. 338, no. 1, pp. 115–121, 1999.

[141] A. Keller, J. Demeurie, T. Merkulova et al., "Fibre-type distribution and subcellular localisation of α and β enolase in mouse striated muscle," *Biology of the Cell*, vol. 92, no. 7, pp. 527–535, 2000.

[142] S. P. Craig, I. N. M. Day, R. J. Thompson, and I. W. Craig, "Localisation of neurone-specific enolase (ENO2) to 12p13," *Cytogenetics and Cell Genetics*, vol. 54, no. 1-2, pp. 71–73, 1990.

[143] S. Feo, D. Oliva, G. Barbieri, W. Xu, M. Fried, and A. Giallongo, "The gene for the muscle-specific enolase is on the short arm of human chromosome 17," *Genomics*, vol. 6, no. 1, pp. 192–194, 1990.

[144] C. C. Rider and C. B. Taylor, "Enolase isoenzymes in rat tissues. Electrophoretic, chromatographic, immunological and kinetic properties," *Biochimica et Biophysica Acta*, vol. 365, no. 1, pp. 285–300, 1974.

[145] C. C. Rider and C. B. Taylor, "Enolase isoenzymes. II. Hybridization studies, developmental and phylogenetic aspects," *Biochimica et Biophysica Acta*, vol. 405, no. 1, pp. 175–187, 1975.

[146] O. F. Wolf, "Enolase," in *The Enzymes*, pp. 499–538, Academic Press, New York, NY, USA, 1971.

[147] T. Ibi, K. Sahashi, K. Kato, A. Takahashi, and I. Sobue, "Immunohistochemical demonstration of β-enolase in human skeletal muscle," *Muscle & Nerve*, vol. 6, no. 9, pp. 661–663, 1983.

[148] K. Kato, A. Shimizu, R. Semba, and T. Satoh, "Tissue distribution, developmental profiles and effect of denervation of enolase isozymes in rat muscles," *Biochimica et Biophysica Acta*, vol. 841, no. 1, pp. 50–58, 1985.

[149] A. Keller, J.-D. Rouzeau, F. Farhadian et al., "Differential expression of α- and β-enolase genes during rat heart development and hypertrophy," *The American Journal of Physiology—Heart and Circulatory Physiology*, vol. 269, no. 6, pp. H1843–H1851, 1995.

[150] H. S. Leong, M. Grist, H. Parsons et al., "Accelerated rates of glycolysis in the hypertrophied heart: are they a methodological artifact?" *American Journal of Physiology—Endocrinology and Metabolism*, vol. 282, no. 5, pp. E1039–E1045, 2002.

[151] L.-A. Zhu, N.-Y. Fang, P.-J. Gao, X. Jin, and H.-Y. Wang, "Differential expression of α-enolase in the normal and pathological cardiac growth," *Experimental and Molecular Pathology*, vol. 87, no. 1, pp. 27–31, 2009.

[152] X. Jin, L.-S. Wang, L. Xia et al., "Hyper-phosphorylation of α-enolase in hypertrophied left ventricle of spontaneously hypertensive rat," *Biochemical and Biophysical Research Communications*, vol. 371, no. 4, pp. 804–809, 2008.

[153] A. Shimizu, F. Suzuki, and K. Kato, "Characterization of $\alpha\alpha$, $\beta\beta$, $\gamma\gamma$ and $\alpha\gamma$ human enolase isozymes, and preparation of hybrid enolases ($\alpha\gamma$, $\beta\gamma$ and $\alpha\beta$) from homodimeric forms," *Biochimica et Biophysica Acta*, vol. 748, no. 2, pp. 278–284, 1983.

[154] Y. Mizukami, A. Iwamatsu, T. Aki et al., "ERK1/2 regulates intracellular ATP levels through α-enolase expression in cardiomyocytes exposed to ischemic hypoxia and reoxygenation," *The Journal of Biological Chemistry*, vol. 279, no. 48, pp. 50120–50131, 2004.

[155] T. Merkulova, M. Dehaupas, M.-C. Nevers, C. Créminon, H. Alameddine, and A. Keller, "Differential modulation of α, β and γ enolase isoforms in regenerating mouse skeletal muscle," *European Journal of Biochemistry*, vol. 267, no. 12, pp. 3735–3743, 2000.

[156] À. Díaz-Ramos, A. Roig-Borrellas, A. García-Melero, and R. López-Alemany, "α-enolase, a multifunctional protein: Its role on pathophysiological situations," *Journal of Biomedicine and Biotechnology*, vol. 2012, Article ID 156795, 12 pages, 2012.

[157] S. H. Witt, H. Granzier, C. C. Witt, and S. Labeit, "MURF-1 and MURF-2 target a specific subset of myofibrillar proteins redundantly: towards understanding MURF-dependent muscle ubiquitination," *Journal of Molecular Biology*, vol. 350, no. 4, pp. 713–722, 2005.

[158] J. Fielitz, M.-S. Kim, J. M. Shelton et al., "Myosin accumulation and striated muscle myopathy result from the loss of muscle RING finger 1 and 3," *The Journal of Clinical Investigation*, vol. 117, no. 9, pp. 2486–2495, 2007.

[159] S. Koyama, S. Hata, C. C. Witt et al., "Muscle RING-finger protein-1 (MuRF1) as a connector of muscle energy metabolism and protein synthesis," *Journal of Molecular Biology*, vol. 376, no. 5, pp. 1224–1236, 2008.

[160] T.-J. Zhao, Y.-B. Yan, Y. Liu, and H.-M. Zhou, "The generation of the oxidized form of creatine kinase is a negative regulation on muscle creatine kinase," *The Journal of Biological Chemistry*, vol. 282, no. 16, pp. 12022–12029, 2007.

[161] J. A. Spencer, S. Eliazer, R. L. Ilaria Jr., J. A. Richardson, and E. N. Olson, "Regulation of microtubule dynamics and myogenic differentiation by MURF, a striated muscle RING-finger protein," *Journal of Cell Biology*, vol. 150, no. 4, pp. 771–784, 2000.

[162] S. C. Bodine, E. Latres, S. Baumhueter et al., "Identification of ubiquitin ligases required for skeletal muscle atrophy," *Science*, vol. 294, no. 5547, pp. 1704–1708, 2001.

[163] T. Centner, J. Yano, E. Kimura et al., "Identification of muscle specific ring finger proteins as potential regulators of the titin kinase domain," *Journal of Molecular Biology*, vol. 306, no. 4, pp. 717–726, 2001.

[164] J. Callis, "The ubiquitination machinery of the ubiquitin system," *The Arabidopsis Book*, vol. 12, article e0174, 2014.

[165] A. S. Moriscot, I. L. Baptista, J. Bogomolovas et al., "MuRF1 is a muscle fiber-type II associated factor and together with MuRF2 regulates type-II fiber trophicity and maintenance," *Journal of Structural Biology*, vol. 170, no. 2, pp. 344–353, 2010.

[166] S. Perera, B. Mankoo, and M. Gautel, "Developmental regulation of MURF E3 ubiquitin ligases in skeletal muscle," *Journal of Muscle Research and Cell Motility*, vol. 33, no. 2, pp. 107–122, 2012.

[167] C. C. Gregorio, C. N. Perry, and A. S. Mcelhinny, "Functional properties of the titin/connectin-associated proteins, the muscle-specific RING finger proteins (MURFs), in striated muscle," *Journal of Muscle Research and Cell Motility*, vol. 26, no. 6-8, pp. 389–400, 2005.

[168] A. S. McElhinny, K. Kakinuma, H. Sorimachi, S. Labeit, and C. C. Gregorio, "Muscle-specific RING finger-1 interacts with titin to regulate sarcomeric M-line and thick filament structure and may have nuclear functions via its interaction with glucocorticoid modulatory element binding protein-1," *The Journal of Cell Biology*, vol. 157, no. 1, pp. 125–136, 2002.

[169] A. S. McElhinny, C. N. Perry, C. C. Witt, S. Labeit, and C. C. Gregorio, "Muscle-specific RING finger-2 (MURF-2) is important for microtubule, intermediate filament and sarcomeric M-line maintenance in striated muscle development," *Journal of Cell Science*, vol. 117, part 15, pp. 3175–3188, 2004.

[170] M. S. Willis, C. Ike, L. Li, D.-Z. Wang, D. J. Glass, and C. Patterson, "Muscle ring finger 1, but not muscle ring finger 2, regulates cardiac hypertrophy in vivo," *Circulation Research*, vol. 100, no. 4, pp. 456–459, 2007.

[171] C. C. Witt, S. H. Witt, S. Lerche, D. Labeit, W. Back, and S. Labeit, "Cooperative control of striated muscle mass and metabolism by MuRF1 and MuRF2," *The EMBO Journal*, vol. 27, no. 2, pp. 350–360, 2008.

[172] J. Fielitz, E. van Rooij, J. A. Spencer et al., "Loss of muscle-specific RING-finger 3 predisposes the heart to cardiac rupture after myocardial infarction," *Proceedings of the National Academy of Sciences of the United States of America*, vol. 104, no. 11, pp. 4377–4382, 2007.

[173] A. L. Kho, S. Perera, A. Alexandrovich, and M. Gautel, "The sarcomeric cytoskeleton as a target for pharmacological intervention," *Current Opinion in Pharmacology*, vol. 12, no. 3, pp. 347–354, 2012.

[174] E. M. McNally, J. R. Golbus, and M. J. Puckelwartz, "Genetic mutations and mechanisms in dilated cardiomyopathy," *The Journal of Clinical Investigation*, vol. 123, no. 1, pp. 19–26, 2013.

[175] C. Chauveau, C. G. Bonnemann, C. Julien et al., "Recessive TTN truncating mutations define novel forms of core myopathy with heart disease," *Human Molecular Genetics*, vol. 23, no. 4, pp. 980–991, 2014.

[176] B. S. Cowling, D. L. Cottle, B. R. Wilding, C. E. D'Arcy, C. A. Mitchell, and M. J. McGrath, "Four and a half LIM protein 1 gene mutations cause four distinct human myopathies: a comprehensive review of the clinical, histological and pathological features," *Neuromuscular Disorders*, vol. 21, no. 4, pp. 237–251, 2011.

[177] F. W. Friedrich, B. R. Wilding, S. Reischmann et al., "Evidence for FHL1 as a novel disease gene for isolated hypertrophic cardiomyopathy," *Human Molecular Genetics*, vol. 21, no. 14, pp. 3237–3254, 2012.

[178] D. Selcen, M. B. Bromberg, S. S. Chin, and A. G. Engel, "Reducing bodies and myofibrillar myopathy features in FHL1 muscular dystrophy," *Neurology*, vol. 77, no. 22, pp. 1951–1959, 2011.

[179] S. Shalaby, Y. K. Hayashi, I. Nonaka, S. Noguchi, and I. Nishino, "Novel FHL1 mutations in fatal and benign reducing body myopathy," *Neurology*, vol. 72, no. 4, pp. 375–376, 2009.

[180] L. B. Waddell, J. Tran, X. F. Zheng et al., "A study of FHL1, BAG3, MATR3, PTRF and TCAP in Australian muscular dystrophy patients," *Neuromuscular Disorders*, vol. 21, no. 11, pp. 776–781, 2011.

[181] L. Gueneau, A. T. Bertrand, J.-P. Jais et al., "Mutations of the FHL1 gene cause Emery-Dreifuss muscular dystrophy," *American Journal of Human Genetics*, vol. 85, no. 3, pp. 338–353, 2009.

[182] D.-H. Chen, W. H. Raskind, W. W. Parson et al., "A novel mutation in *FHL1* in a family with X-linked scapuloperoneal myopathy: phenotypic spectrum and structural study of *FHL1* mutations," *Journal of the Neurological Sciences*, vol. 296, no. 1-2, pp. 22–29, 2010.

[183] C. M. Quinzii, T. H. Vu, K. C. Min et al., "X-linked dominant scapuloperoneal myopathy is due to a mutation in the gene encoding four-and-a-half-LIM protein 1," *The American Journal of Human Genetics*, vol. 82, no. 1, pp. 208–213, 2008.

[184] J. Schessl, A. L. Taratuto, C. Sewry et al., "Clinical, histological and genetic characterization of reducing body myopathy caused by mutations in FHL1," *Brain*, vol. 132, no. 2, pp. 452–464, 2009.

[185] J. Schessl, A. Columbus, Y. Hu et al., "Familial reducing body myopathy with cytoplasmic bodies and rigid spine revisited: identification of a second LIM domain mutation in FHL1," *Neuropediatrics*, vol. 41, no. 1, pp. 43–46, 2010.

[186] J. Schessl, Y. Zou, M. J. McGrath et al., "Proteomic identification of FHL1 as the protein mutated in human reducing body myopathy," *Journal of Clinical Investigation*, vol. 118, no. 3, pp. 904–912, 2008.

[187] C. Windpassinger, B. Schoser, V. Straub et al., "An X-linked myopathy with postural muscle atrophy and generalized hypertrophy, termed XMPMA, is caused by mutations in FHL1," *The American Journal of Human Genetics*, vol. 82, no. 1, pp. 88–99, 2008.

[188] T. Schreckenbach, W. Henn, W. Kress et al., "Novel FHL1 mutation in a family with reducing body myopathy," *Muscle and Nerve*, vol. 47, no. 1, pp. 127–134, 2013.

[189] H. R. Tiffin, Z. A. Jenkins, M. J. Gray et al., "Dysregulation of FHL1 spliceforms due to an indel mutation produces an Emery-Dreifuss muscular dystrophy plus phenotype," *Neurogenetics*, vol. 14, no. 2, pp. 113–121, 2013.

[190] B. Schoser, H. H. Goebel, I. Janisch et al., "Consequences of mutations within the C terminus of the FHL1 gene," *Neurology*, vol. 73, no. 7, pp. 543–551, 2009.

[191] T. D. Gossios, L. R. Lopes, and P. M. Elliott, "Left ventricular hypertrophy caused by a novel nonsense mutation in FHL1," *European Journal of Medical Genetics*, vol. 56, no. 5, pp. 251–255, 2013.

[192] H. Hartmannova, M. Kubanek, M. Sramko et al., "Isolated X-linked hypertrophic cardiomyopathy caused by a novel mutation of the four-and-a-half LIM domain 1 gene," *Circulation: Cardiovascular Genetics*, vol. 6, no. 6, pp. 543–551, 2013.

[193] H. Knoblauch, C. Geier, S. Adams et al., "Contractures and hypertrophic cardiomyopathy in a novel FHL1 mutation," *Annals of Neurology*, vol. 67, no. 1, pp. 136–140, 2010.

[194] T. Arimura, T. Hayashi, Y. Matsumoto et al., "Structural analysis of four and half LIM protein-2 in dilated cardiomyopathy," *Biochemical and Biophysical Research Communications*, vol. 357, no. 1, pp. 162–167, 2007.

[195] C. A. Gurnett, D. M. Desruisseau, K. McCall et al., "Myosin binding protein C1: a novel gene for autosomal dominant distal arthrogryposis type 1," *Human Molecular Genetics*, vol. 19, no. 7, Article ID ddp587, pp. 1165–1173, 2010.

[196] B. Markus, G. Narkis, D. Landau, R. Z. Birk, I. Cohen, and O. S. Birk, "Autosomal recessive lethal congenital contractural syndrome type 4 (LCCS4) caused by a mutation in MYBPC1," *Human Mutation*, vol. 33, no. 10, pp. 1435–1438, 2012.

[197] R. M. Toydemir, A. Rutherford, F. G. Whitby, L. B. Jorde, J. C. Carey, and M. J. Bamshad, "Mutations in embryonic myosin heavy chain (MYH3) cause Freeman-Sheldon syndrome and Sheldon-Hall syndrome," *Nature Genetics*, vol. 38, no. 5, pp. 561–565, 2006.

[198] E. Carniel, M. R. G. Taylor, G. Sinagra et al., "α-myosin heavy chain: a sarcomeric gene associated with dilated and hypertrophic phenotypes of cardiomyopathy," *Circulation*, vol. 112, no. 1, pp. 54–59, 2005.

[199] J. T. Granados-Riveron, T. K. Ghosh, M. Pope et al., "α-Cardiac myosin heavy chain (MYH6) mutations affecting myofibril formation are associated with congenital heart defects," *Human Molecular Genetics*, vol. 19, no. 20, pp. 4007–4016, 2010.

[200] S. L. van Driest, M. A. Jaeger, S. R. Ommen et al., "Comprehensive analysis of the beta-myosin heavy chain gene in 389

unrelated patients with hypertrophic cardiomyopathy," *Journal of the American College of Cardiology*, vol. 44, no. 3, pp. 602–610, 2004.

[201] P. Richard, P. Charron, L. Carrier et al., "Hypertrophic cardiomyopathy: distribution of disease genes, spectrum of mutations, and implications for a molecular diagnosis strategy," *Circulation*, vol. 107, no. 17, pp. 2227–2232, 2003.

[202] R. R. Tanjore, A. D. Sikindlapuram, N. Calambur, B. Thakkar, P. G. Kerkar, and P. Nallari, "Genotype-phenotype correlation of R870H mutation in hypertrophic cardiomyopathy," *Clinical Genetics*, vol. 69, no. 5, pp. 434–436, 2006.

[203] M. Arad, M. Penas-Lado, L. Monserrat et al., "Gene mutations in apical hypertrophic cardiomyopathy," *Circulation*, vol. 112, no. 18, pp. 2805–2811, 2005.

[204] L. Fananapazir, M. C. Dalakas, F. Cyran, G. Cohn, and N. D. Epstein, "Missense mutations in the β-myosin heavy-chain gene cause central core disease in hypertrophic cardiomyopathy," *Proceedings of the National Academy of Sciences of the United States of America*, vol. 90, no. 9, pp. 3993–3997, 1993.

[205] H. Watkins, L. Thierfelder, D.-S. Hwang, W. McKenna, J. G. Seidman, and C. E. Seidman, "Sporadic hypertrophic cardiomyopathy due to de novo myosin mutations," *Journal of Clinical Investigation*, vol. 90, no. 5, pp. 1666–1671, 1992.

[206] M. Michels, O. I. I. Soliman, J. Phefferkorn et al., "Disease penetrance and risk stratification for sudden cardiac death in asymptomatic hypertrophic cardiomyopathy mutation carriers," *European Heart Journal*, vol. 30, no. 21, pp. 2593–2598, 2009.

[207] H. Nishi, A. Kimura, H. Harada et al., "Possible gene dose effect of a mutant cardiac β-myosin heavy chain gene on the clinical expression of familial hypertrophic cardiomyopathy," *Biochemical and Biophysical Research Communications*, vol. 200, no. 1, pp. 549–556, 1994.

[208] E. Villard, L. Duboscq-Bidot, P. Charron et al., "Mutation screening in dilated cardiomyopathy: prominent role of the beta myosin heavy chain gene," *European Heart Journal*, vol. 26, no. 8, pp. 794–803, 2005.

[209] P. Jääskeläinen, T. Heliö, K. Aalto-Setälä et al., "A new common mutation in the cardiac beta-myosin heavy chain gene in Finnish patients with hypertrophic cardiomyopathy," *Annals of Medicine*, vol. 46, no. 6, pp. 424–429, 2014.

[210] L. Hougs, O. Havndrup, H. Bundgaard et al., "One third of Danish hypertrophic cardiomyopathy patients with MYH7 mutations have mutations [corrected] in MYH7 rod region," *European Journal of Human Genetics*, vol. 13, no. 2, pp. 161–165, 2005.

[211] A. Perrot, H. Schmidt-Traub, B. Hoffmann et al., "Prevalence of cardiac beta-myosin heavy chain gene mutations in patients with hypertrophic cardiomyopathy," *Journal of Molecular Medicine*, vol. 83, no. 6, pp. 468–477, 2005.

[212] J.-M. Park, Y. J. Kim, J. H. Yoo et al., "A novel MYH7 mutation with prominent paraspinal and proximal muscle involvement," *Neuromuscular Disorders*, vol. 23, no. 7, pp. 580–586, 2013.

[213] T. Cullup, P. J. Lamont, S. Cirak et al., "Mutations in MYH7 cause Multi-minicore Disease (MmD) with variable cardiac involvement," *Neuromuscular Disorders*, vol. 22, no. 12, pp. 1096–1104, 2012.

[214] P. J. Lamont, W. Wallefeld, D. Hilton-Jones et al., "Novel mutations widen the phenotypic spectrum of slow skeletal/β-cardiac myosin (MYH7) distal myopathy," *Human Mutation*, vol. 35, no. 7, pp. 868–879, 2014.

[215] S. Kärkkäinen, T. Heliö, P. Jääskeläinen et al., "Two novel mutations in the β-myosin heavy chain gene associated with dilated cardiomyopathy," *European Journal of Heart Failure*, vol. 6, no. 7, pp. 861–868, 2004.

[216] C. Meredith, R. Herrmann, C. Parry et al., "Mutations in the slow skeletal muscle fiber myosin heavy chain gene (MYH7) cause Laing early-onset distal myopathy (MPD1)," *American Journal of Human Genetics*, vol. 75, no. 4, pp. 703–708, 2004.

[217] B. Udd, "Genetics and pathogenesis of distal muscular dystrophies," *Advances in Experimental Medicine and Biology*, vol. 652, pp. 23–38, 2009.

[218] S. Waldmüller, P. Freund, S. Mauch, R. Toder, and H.-P. Vosberg, "Low-density DNA microarrays are versatile tools to screen for known mutations in hypertrophic cardiomyopathy," *Human Mutation*, vol. 19, no. 5, pp. 560–569, 2002.

[219] G. Tasca, E. Ricci, S. Penttilä et al., "New phenotype and pathology features in MYH7-related distal myopathy," *Neuromuscular Disorders*, vol. 22, no. 7, pp. 640–647, 2012.

[220] N. F. Clarke, K. Amburgey, J. Teener et al., "A novel mutation expands the genetic and clinical spectrum of MYH7-related myopathies," *Neuromuscular Disorders*, vol. 23, no. 5, pp. 432–436, 2013.

[221] N. B. Romero, T. Xie, E. Malfatti et al., "Autosomal dominant eccentric core disease caused by a heterozygous mutation in the MYH7 gene," *Journal of Neurology, Neurosurgery and Psychiatry*, vol. 85, no. 10, pp. 1149–1152, 2014.

[222] S. Klaassen, S. Probst, E. Oechslin et al., "Mutations in sarcomere protein genes in left ventricular noncompaction," *Circulation*, vol. 117, no. 22, pp. 2893–2901, 2008.

[223] E. Blair, C. Redwood, M. de Jesus Oliveira et al., "Mutations of the light meromyosin domain of the beta-myosin heavy chain rod in hypertrophic cardiomyopathy," *Circulation Research*, vol. 90, no. 3, pp. 263–269, 2002.

[224] X. Stalpers, A. Verrips, J. Braakhekke, M. Lammens, A. van den Wijngaard, and A. Mostert, "Scoliosis surgery in a patient with 'de novo' myosin storage myopathy," *Neuromuscular Disorders*, vol. 21, no. 11, pp. 812–815, 2011.

[225] D. E. Dye, B. Azzarelli, H. H. Goebel, and N. G. Laing, "Novel slow-skeletal myosin (MYH7) mutation in the original myosin storage myopathy kindred," *Neuromuscular Disorders*, vol. 16, no. 6, pp. 357–360, 2006.

[226] T. Z. Armel and L. A. Leinwand, "Mutations in the β-myosin rod cause myosin storage myopathy via multiple mechanisms," *Proceedings of the National Academy of Sciences of the United States of America*, vol. 106, no. 15, pp. 6291–6296, 2009.

[227] H. Tajsharghi, L.-E. Thornell, C. Lindberg, B. Lindvall, K.-G. Henriksson, and A. Oldfors, "Myosin storage myopathy associated with a heterozygous missense mutation in MYH7," *Annals of Neurology*, vol. 54, no. 4, pp. 494–500, 2003.

[228] J. Finsterer, O. Brandau, C. Stöllberger, W. Wallefeld, N. G. Laing, and F. Laccone, "Distal myosin heavy chain-7 myopathy due to the novel transition c.5566G>A (p.E1856K) with high interfamilial cardiac variability and putative anticipation," *Neuromuscular Disorders*, vol. 24, no. 8, pp. 721–725, 2014.

[229] H. Tajsharghi, A. Oldfors, D. P. Macleod, and M. Swash, "Homozygous mutation in MYH7 in myosin storage myopathy and cardiomyopathy," *Neurology*, vol. 68, no. 12, p. 962, 2007.

[230] S. Bohlega, S. N. Abu-Amero, S. M. Wakil et al., "Mutation of the slow myosin heavy chain rod domain underlies hyaline body myopathy," *Neurology*, vol. 62, no. 9, pp. 1518–1521, 2004.

[231] A. V. Postma, K. van Engelen, J. van de Meerakker et al., "Mutations in the sarcomere gene MYH7 in Ebstein anomaly," *Circulation: Cardiovascular Genetics*, vol. 4, no. 1, pp. 43–50, 2011.

[232] S. Ortolano, R. Tarrío, P. Blanco-Arias et al., "A novel *MYH7* mutation links congenital fiber type disproportion and myosin storage myopathy," *Neuromuscular Disorders*, vol. 21, no. 4, pp. 254–262, 2011.

[233] M. Koebis, N. Ohsawa, Y. Kino, N. Sasagawa, I. Nishino, and S. Ishiura, "Alternative splicing of myomesin 1 gene is aberrantly regulated in myotonic dystrophy type 1," *Genes to Cells*, vol. 16, no. 9, pp. 961–972, 2011.

[234] R. Siegert, A. Perrot, S. Keller et al., "A myomesin mutation associated with hypertrophic cardiomyopathy deteriorates dimerisation properties," *Biochemical and Biophysical Research Communications*, vol. 405, no. 3, pp. 473–479, 2011.

[235] T. Arimura, Y. Matsumoto, O. Okazaki et al., "Structural analysis of obscurin gene in hypertrophic cardiomyopathy," *Biochemical and Biophysical Research Communications*, vol. 362, no. 2, pp. 281–287, 2007.

[236] A. Evilä, A. Vihola, J. Sarparanta et al., "Atypical phenotypes in titinopathies explained by second titin mutations," *Annals of Neurology*, vol. 75, no. 2, pp. 230–240, 2014.

[237] J. R. Golbus, M. J. Puckelwartz, J. P. Fahrenbach, L. M. Dellefave-Castillo, D. Wolfgeher, and E. M. McNally, "Population-based variation in cardiomyopathy genes," *Circulation: Cardiovascular Genetics*, vol. 5, no. 4, pp. 391–399, 2012.

[238] O. Ceyhan-Birsoy, P. B. Agrawal, C. Hidalgo et al., "Recessive truncating titin gene, TTN, mutations presenting as centronuclear myopathy," *Neurology*, vol. 81, no. 14, pp. 1205–1214, 2013.

[239] Y. Matsumoto, T. Hayashi, N. Inagaki et al., "Functional analysis of titin/connectin N2-B mutations found in cardiomyopathy," *Journal of Muscle Research & Cell Motility*, vol. 26, no. 6–8, pp. 367–374, 2005.

[240] D. S. Herman, L. Lam, M. R. Taylor et al., "Truncations of titin causing dilated cardiomyopathy," *The New England Journal of Medicine*, vol. 366, no. 7, pp. 619–628, 2012.

[241] V. Carmignac, M. A. M. Salih, S. Quijano-Roy et al., "C-terminal titin deletions cause a novel early-onset myopathy with fatal cardiomyopathy," *Annals of Neurology*, vol. 61, no. 4, pp. 340–351, 2007.

[242] M. Taylor, S. Graw, G. Sinagra et al., "Genetic variation in titin in arrhythmogenic right ventricular cardiomyopathy-overlap syndromes," *Circulation*, vol. 124, no. 8, pp. 876–885, 2011.

[243] P. Hackman, S. Marchand, J. Sarparanta et al., "Truncating mutations in C-terminal titin may cause more severe tibial muscular dystrophy (TMD)," *Neuromuscular Disorders*, vol. 18, no. 12, pp. 922–928, 2008.

[244] P. Hackman, A. Vihola, H. Haravuori et al., "Tibial muscular dystrophy is a titinopathy caused by mutations in TTN, the gene encoding the giant skeletal-muscle protein titin," *American Journal of Human Genetics*, vol. 71, no. 3, pp. 492–500, 2002.

[245] B. Udd, A. Vihola, J. Sarparanta, I. Richard, and P. Hackman, "Titinopathies and extension of the M-line mutation phenotype beyond distal myopathy and LGMD2J," *Neurology*, vol. 64, no. 4, pp. 636–642, 2005.

[246] M. Pollazzon, T. Suominen, S. Penttilä et al., "The first Italian family with tibial muscular dystrophy caused by a novel titin mutation," *Journal of Neurology*, vol. 257, no. 4, pp. 575–579, 2010.

[247] P. Y. K. van den Bergh, O. Bouquiaux, C. Verellen et al., "Tibial muscular dystrophy in a Belgian family," *Annals of Neurology*, vol. 54, no. 2, pp. 248–251, 2003.

[248] G. P. Comi, F. Fortunato, S. Lucchiari et al., "β-enolase deficiency, a new metabolic myopathy of distal glycolysis," *Annals of Neurology*, vol. 50, no. 2, pp. 202–207, 2001.

[249] M. Su, J. Wang, L. Kang et al., "Rare variants in genes encoding *MuRF1* and *MuRF2* are modifiers of hypertrophic cardiomyopathy," *International Journal of Molecular Sciences*, vol. 15, no. 6, pp. 9302–9313, 2014.

[250] S. Tsujino, S. Servidei, P. Tonin, S. Shanske, G. Azan, and S. DiMauro, "Identification of three novel mutations in non-Ashkenazi Italian patients with muscle phosphofructokinase deficiency," *American Journal of Human Genetics*, vol. 54, no. 5, pp. 812–819, 1994.

[251] J. B. Sherman, N. Raben, C. Nicastri et al., "Common mutations in the phosphofructokinase-M gene in Ashkenazi Jewish patients with glycogenesis VII—and their population frequency," *The American Journal of Human Genetics*, vol. 55, no. 2, pp. 305–313, 1994.

[252] O. Musumeci, C. Bruno, T. Mongini et al., "Clinical features and new molecular findings in muscle phosphofructokinase deficiency (GSD type VII)," *Neuromuscular Disorders*, vol. 22, no. 4, pp. 325–330, 2012.

[253] O. Vasconcelos, K. Sivakumar, M. C. Dalakas et al., "Nonsense mutation in the phosphofructokinase muscle subunit gene associated with retention of intron 10 in one of the isolated transcripts in Ashkenazi Jewish patients with Tarui disease," *Proceedings of the National Academy of Sciences of the United States of America*, vol. 92, no. 22, pp. 10322–10326, 1995.

[254] N. Raben, R. Exelbert, R. Spiegel et al., "Functional expression of human mutant phosphofructokinase in yeast: genetic defects in French Canadian and Swiss patients with phosphofructokinase deficiency," *American Journal of Human Genetics*, vol. 56, no. 1, pp. 131–141, 1995.

[255] J.-L. Vives-Corrons, P. Koralkova, J. M. Grau, M. D. M. M. Pereira, and R. Van Wijk, "First description of phosphofructokinase deficiency in spain: identification of a novel homozygous missense mutation in the PFKM gene," *Frontiers in Physiology*, vol. 4, article 393, 2013.

[256] H. Nakajima, N. Raben, T. Hamaguchi, and T. Yamasaki, "Phosphofructokinase deficiency; past, present and future," *Current Molecular Medicine*, vol. 2, no. 2, pp. 197–212, 2002.

[257] R. C. Nichols, O. Rudolphi, B. Ek, R. Exelbert, P. H. Plotz, and N. Raben, "Glycogenosis type VII (Tarui disease) in a Swedish family: two novel mutations in muscle phosphofructokinase gene (PFK-M) resulting in intron retentions," *American Journal of Human Genetics*, vol. 59, no. 1, pp. 59–65, 1996.

[258] T. Hamaguchi, H. Nakajima, T. Noguchi et al., "A new variant of muscle phosphofructokinase deficiency in a Japanese case with abnormal RNA splicing," *Biochemical and Biophysical Research Communications*, vol. 202, no. 1, pp. 444–449, 1994.

[259] H. Tajsharghi and A. Oldfors, "Myosinopathies: pathology and mechanisms," *Acta Neuropathologica*, vol. 125, no. 1, pp. 3–18, 2013.

[260] B. Udd, "Third filament diseases," *Advances in Experimental Medicine and Biology*, vol. 642, pp. 99–115, 2008.

[261] M. A. Ackermann, L. Y. Hu, and A. Kontrogianni-Konstnatopoulos, "Intercellular connections in the heart: the intercalated disc," in *Cardiomyopathies—From Basic Research to Clinical Management*, J. Veselka, Ed., InTech, 2012.

[262] M. A. Ackermann, P. D. Patel, J. Valenti et al., "Loss of actomyosin regulation in distal arthrogryposis myopathy due to mutant myosin binding protein-C slow," *The FASEB Journal*, vol. 27, no. 8, pp. 3217–3228, 2013.

[263] M. A. Ackermann and A. Kontrogianni-Konstantopoulos, "Myosin binding protein-C slow: a multifaceted family of proteins with a complex expression profile in fast and slow twitch skeletal muscles," *Frontiers in Physiology*, vol. 4, article 391, 2013.

[264] W. Piyamongkol, J. C. Harper, J. K. Sherlock et al., "A successful strategy for preimplantation genetic diagnosis of myotonic dystrophy using multiplex fluorescent PCR," *Prenatal Diagnosis*, vol. 21, no. 3, pp. 223–232, 2001.

[265] I. Agarkova, D. Auerbach, E. Ehler, and J.-C. Perriard, "A novel marker for vertebrate embryonic heart, the EH-myomesin isoform," *The Journal of Biological Chemistry*, vol. 275, no. 14, pp. 10256–10264, 2000.

[266] R. Schoenauer, M. Y. Emmert, A. Felley et al., "EH-myomesin splice isoform is a novel marker for dilated cardiomyopathy," *Basic Research in Cardiology*, vol. 106, no. 2, pp. 233–247, 2011.

[267] T. Shathasivam, T. Kislinger, and A. O. Gramolini, "Genes, proteins and complexes: the multifaceted nature of FHL family proteins in diverse tissues," *Journal of Cellular and Molecular Medicine*, vol. 14, no. 12, pp. 2702–2720, 2010.

[268] E. Malfatti, M. Olivé, A. L. Taratuto et al., "Skeletal muscle biopsy analysis in reducing body myopathy and other FHL1-related disorders," *Journal of Neuropathology & Experimental Neurology*, vol. 72, no. 9, pp. 833–845, 2013.

[269] J. S. Binder, F. Weidemann, B. Schoser et al., "Spongious hypertrophic cardiomyopathy in patients with mutations in the four-and-a-half LIM domain 1 gene," *Circulation: Cardiovascular Genetics*, vol. 5, no. 5, pp. 490–502, 2012.

[270] D.-S. Lim, R. Roberts, and A. J. Marian, "Expression profiling of cardiac genes in human hypertrophic cardiomyopathy: insight into the pathogenesis of phenotypes," *Journal of the American College of Cardiology*, vol. 38, no. 4, pp. 1175–1180, 2001.

[271] J. Yang, C. S. Moravec, M. A. Sussman et al., "Decreased SLIM1 expression and increased gelsolin expression in failing human hearts measured by high-density oligonucleotide arrays," *Circulation*, vol. 102, no. 25, pp. 3046–3052, 2000.

[272] B. R. Wilding, M. J. McGrath, G. Bonne, and C. A. Mitchell, "FHL1 mutants that cause clinically distinct human myopathies form protein aggregates and impair myoblast differentiation," *Journal of Cell Science*, vol. 127, no. 10, pp. 2269–2281, 2014.

[273] C. Angelini, "Spectrum of metabolic myopathies," *Biochimica et Biophysica Acta*, vol. 1852, no. 4, pp. 615–621, 2015.

[274] H. Morisaki, I. Higuchi, M. Abe, M. Osame, and T. Morisaki, "First missense mutations (R388W and R425H) of AMPD1 accompanied with myopathy found in a Japanese patient," *Human Mutation*, vol. 16, no. 6, pp. 467–472, 2000.

[275] T. Morisaki, M. Gross, H. Morisaki, D. Pongratz, N. Zollner, and E. W. Holmes, "Molecular basis of AMP deaminase deficiency in skeletal muscle," *Proceedings of the National Academy of Sciences of the United States of America*, vol. 89, no. 14, pp. 6457–6461, 1992.

[276] M. Gross, E. Rötzer, P. Kölle et al., "A G468-T AMPD1 mutant allele contributes to the high incidence of myoadenylate deaminase deficiency in the Caucasian population," *Neuromuscular Disorders*, vol. 12, no. 6, pp. 558–565, 2002.

[277] P. J. Isackson, H. Bujnicki, C. O. Harding, and G. D. Vladutiu, "Myoadenylate deaminase deficiency caused by alternative splicing due to a novel intronic mutation in the AMPD1 gene," *Molecular Genetics and Metabolism*, vol. 86, no. 1-2, pp. 250–256, 2005.

[278] D. K. Mahnke-Zizelman and R. L. Sabina, "Cloning of human AMP deaminase isoform E cDNAs. Evidence for a third AMPD gene exhibiting alternatively spliced 5′-exons," *Journal of Biological Chemistry*, vol. 267, no. 29, pp. 20866–20877, 1992.

[279] C. Suetta, U. Frandsen, L. Jensen et al., "Aging affects the transcriptional regulation of human skeletal muscle disuse atrophy," *PLoS ONE*, vol. 7, no. 12, Article ID e51238, 2012.

[280] M. Merli, M. Giusto, A. Molfino et al., "MuRF-1 and p-GSK3β expression in muscle atrophy of cirrhosis," *Liver International*, vol. 33, no. 5, pp. 714–721, 2013.

[281] S. Gielen, M. Sandri, I. Kozarez et al., "Exercise training attenuates MuRF-1 expression in the skeletal muscle of patients with chronic heart failure independent of age: the randomized leipzig exercise intervention in chronic heart failure and aging catabolism study," *Circulation*, vol. 125, no. 22, pp. 2716–2727, 2012.

[282] O. Mayans and S. Labeit, "MuRFs: specialized members of the TRIM/RBCC family with roles in the regulation of the trophic state of muscle and its metabolism," *Advances in Experimental Medicine and Biology*, vol. 770, pp. 119–129, 2012.

Hindawi Publishing Corporation
BioMed Research International
Volume 2015, Article ID 468548, 12 pages
http://dx.doi.org/10.1155/2015/468548

Research Article

Dissociation of Calcium Transients and Force Development following a Change in Stimulation Frequency in Isolated Rabbit Myocardium

Kaylan M. Haizlip, Nima Milani-Nejad, Lucia Brunello, Kenneth D. Varian, Jessica L. Slabaugh, Shane D. Walton, Sandor Gyorke, Jonathan P. Davis, Brandon J. Biesiadecki, and Paul M. L. Janssen

Department of Physiology and Cell Biology and D. Davis Heart Lung Institute, College of Medicine, The Ohio State University, 304 Hamilton Hall, 1645 Neil Avenue, Columbus, OH 43210-1218, USA

Correspondence should be addressed to Paul M. L. Janssen; janssen.10@osu.edu

Received 6 May 2014; Revised 1 August 2014; Accepted 19 August 2014

Academic Editor: Danuta Szczesna-Cordary

As the heart transitions from one exercise intensity to another, changes in cardiac output occur, which are modulated by alterations in force development and calcium handling. Although the steady-state force-calcium relationship at various heart rates is well investigated, regulation of these processes during transitions in heart rate is poorly understood. In isolated right ventricular muscle preparations from the rabbit, we investigated the beat-to-beat alterations in force and calcium during the transition from one stimulation frequency to another, using contractile assessments and confocal microscopy. We show that a change in steady-state conditions occurs in multiple phases: a rapid phase, which is characterized by a fast change in force production mirrored by a change in calcium transient amplitude, and a slow phase, which follows the rapid phase and occurs as the muscle proceeds to stabilize at the new frequency. This second/late phase is characterized by a quantitative dissociation between the calcium transient amplitude and developed force. Twitch timing kinetics, such as time to peak tension and 50% relaxation rate, reached steady-state well before force development and calcium transient amplitude. The dynamic relationship between force and calcium upon a switch in stimulation frequency unveils the dynamic involvement of myofilament-based properties in frequency-dependent activation.

1. Introduction

The force frequency response (FFR), or Bowditch effect, is one of the major physiological regulators governing alterations in contractile function of the heart [1, 2]. The FFR can occur in the absence of neurohumoral stimulation and is characterized by an increase in heart rate leading to an increase in contractile function [3, 4] and an acceleration of kinetics. These changes in force and kinetics result from alterations in cytosolic calcium levels as well as in the sensitivity of the myofilament to calcium [3–5]. During the FFR, increases in the frequency of pacing lead to an increase in the entry of calcium via the L-type calcium channel, subsequently increasing sarcoplasmic reticulum (SR) calcium load and release [3, 6]. A key characteristic of heart failure (HF) is a negative FFR, due to a decrease in calcium pump function and/or a decline in myofilament sensitivity [7–9]. Thus, the response in contractile function to changes in frequency is a diagnostic marker of the failing myocardium.

Although steady-state behavior of FFR is well investigated, the underlying regulatory mechanisms and the dynamic nature of this response are not fully understood. In nonfailing myocardium, changes in calcium and contractile function are known to involve multiple physical and chemical processes [2, 8]; however, the beat-to-beat variations in force and calcium homeostasis that occur during normal function are not well understood. Specifically, during the FFR there are changes in contractile function and calcium handling that happen on a timescale that does not easily lend itself to investigation as tools to assess myofilament responsiveness require

minutes and/or the presence of steady-state conditions [10]. However, by taking a closer look at the temporal processes from one point of contractile steady-state (such as during rest) to another (such as during endurance exercise), we can potentially unravel changes in the relationship between force and calcium. This will allow us to then better characterize physiological mechanisms underlying the regulation of contraction and relaxation.

It has been shown by our lab and others that an increase in the frequency of pacing induces an increase in the calcium transient amplitude and a decrease in calcium transient duration [4, 6, 7]. These alterations in calcium handling eventually lead to molecular modifications within the myocyte [6]. Increases in frequency have also been shown to lead to increases in the phosphorylation state of many calcium handling channels and proteins such as the L-type calcium channel, troponin I (TnI), myosin binding protein C (MyBP-C), and phospholamban [3, 4, 11–14]. These alterations, together or separate, have the potential to either directly or indirectly lead to a change in myofilament calcium sensitivity and thus contractile kinetics.

Although much is known about the alterations in calcium handling when the heart is paced at different steady-state frequencies, the need for further understanding of the transitions between states is growing. Typically the heart beats at least once every second, with small and large changes in interbeat duration resulting from breathing and the level of physical activity and is not functioning at steady-state. Yet, most experimental designs require contractions to occur at a set frequency [10, 13]. Here we attempt to elucidate the effects of immediate changes in frequency on contractility and calcium transients at every beat. By determining what occurs during the stabilization of contractile force in relation to calcium handling we are able to better determine the functional characteristics of the calcium and force relationship.

Our results indicate that force and calcium are not changing in parallel and neither are force amplitude and contractile kinetics. Dissociation between the developed force and calcium transient has been documented following changes in muscle length at steady-state that indicate a myofilament-based process [15]. Our study highlights a disconnect between the intracellular calcium transient and the developed force during a dynamic frequency change, indicating the involvement of a myofilament-based regulation also during a change in the cardiac contractile steady-state.

2. Materials and Methods

2.1. Muscle Excision and Preparation. Male New Zealand white rabbits (2 kg, approximately 3 months old) were anesthetized with 50 mg/kg pentobarbital sodium (IV) and injected with 5,000 units/kg heparin. The investigation conforms to the *Guide for the Care and Use of Laboratory Animals* published by the US National Institutes of Health (NIH Publication number 85-23, revised 1996) and was approved by the local animal care and use committee.

The heart was rapidly excised and perfused retrogradely through the aorta with Krebs-Henseleit (KH) solution containing the following (in mmol/L): 120 NaCl, 5 KCl, 2 $MgSO_4$, 1.2 NaH_2PO_4, 20 $NaHCO_3$, 0.25 Ca^{2+}, and 10 glucose (pH 7.4) in equilibrium with 95%O_2/5%CO_2 at 37°C. Additionally, 20 mmol/L 2,3-butanedione monoxime (BDM) was added to the dissection solution to stop the heart from beating and thus prevent cutting damage [16]. The effects of BDM after brief exposure have been found to be reversible [17]. Thin (to prevent core-hypoxia [18]) linear trabeculae from the right ventricular free wall were carefully excised and mounted between a force transducer and a micromanipulator. The muscle was bathed in a continuous flow of oxygenated 95%O_2/5%CO_2 KH solution (without BDM) at 37°C. The muscle was stimulated at 1 Hz, while calcium concentration was raised to 1.5 mM, and the muscle was stretched until maximal active force was attained. This length is comparable to maximally attained length *in vivo* at the end of diastole (around 2.2 μm sarcomere length) [19]. The following protocols were run under isometric conditions with muscle length maintained at optimal length for maximal force production.

2.2. Twitch Protocol. Muscles were stabilized at 1 Hz for at least 10 minutes then subjected a rapid FFR interval change via a custom designed LabVIEW program, as previously published [10]. Briefly, muscle contractions were recorded at 1 Hz for between 30 and 120 seconds and were subjected to changes in frequency of pacing from 1 to 4 Hz (or 4 to 1 Hz). Muscles were then allowed to restabilize at the second frequency for an additional 1–10 minutes. Long periods of stabilization were avoided to prevent muscle run-down of twitch force [20]. Twitches and alterations in contractile kinetics, including developed force (F_{dev}), time to peak force production (TTP), and 50% relaxation time (RT_{50}), were analyzed using custom LabVIEW analysis software.

2.3. Calcium Transient. Intracellular calcium transient imaging was performed using Rhod-2 acetoxymethyl (AM) dye along with Olympus Fluoview 1000 confocal microscope in line-scan or XY-mode. Cytosolic calcium measurement was performed using Rhod-2 specifically for its brightness, photostability, and clarity of resolution [21–23]. This dye allows us to determine beat-to-beat alterations that are not visible using ratiometric non-AM dyes. Rhod-2 was excited by 488 and 543 nm and fluorescence was acquired at 550–650 nm [22].

Prior to data acquistion, muscles were incubated for 40 minutes in the dark at room temperature with Rhod-2. Rhod-2 AM was prepared in 2% pluronic, 0.2% cremphor, 0.1% TPEN, and KH solution. After incubation muscles were stimulated to contract at 1 Hz for an additional 5 minutes in Rhod-2 solution to ensure dye uptake into the muscle. Rhod-2 was then washed from the bath using the KH solution at 1.5 mM [$CaCl_2$]. Fresh KH was then added and contractile force was allowed to stabilize for up to 20 minutes. After stabilization and visualization of proper dye loading, muscles were subjected to aforementioned twitch protocol.

Calcium alterations were measured at 10x magnification to determine global calcium transient and analyzed. Temporal dynamics in fluorescence of Rhod-2 was expressed as $\Delta F/F_o$, where F represents the fluorescence of Rhod-2 and F_o represents background fluorescence [22].

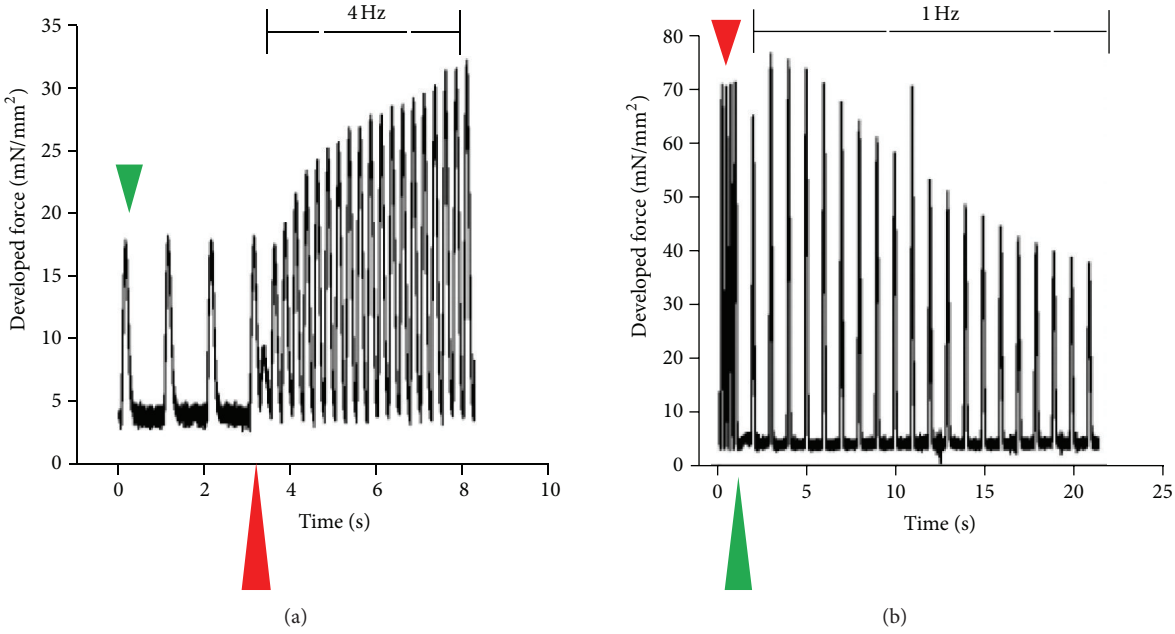

Figure 1: Beat-to-beat data output of twitches from an individual representative trabecula. Trabeculae from the New Zealand white male rabbit were excised from the right ventricular free wall and stabilized at either 1 Hz or 4 Hz. Muscles were perfused in KH with 1.5 mM $CaCl_2$ at 37°C and were subjected to jumps in frequency from either (a) 1 Hz (green arrow) to 4 Hz (red arrow) with arrow marking moment of frequency change or (b) 4 Hz (red arrow) to 1 Hz (green arrow).

2.4. Myofilament Protein Preparation. To determine alterations in myofilament proteins (troponin T, troponin I, tropomyosin, myosin light chain 2, myosin binding protein C, and actin) phosphorylation status, individual trabeculae were flash frozen (<1 second) as previously described [4, 24] at 1 Hz, 4 Hz prior to stabilization, 4 Hz after stabilization for 1 minute, and 4 Hz after stabilization for 5 minutes. Muscles were homogenized by glass mortar and pestle in a solution containing the following: 75 mM KCl, 10 mM imidazole (pH 7.2), 2 mM EGTA, 2 mM $MgCl_2$, 1 mM NaN_3, 4 mM phosphocreatine, 1 mM DTT, and 1 mM benzamidine-HCl [25]. The solution was modified with the addition of 1% Triton depending on homogenization step. After homogenization protein pellets were resuspended in sample buffer containing the following: 6% SDS, 0.3% bromophenol blue, 30% glycerol, 150 mM Tris HCl, and 15 mM BME. Prior to loading, samples were heated to 80°C, vortexed, and centrifuged.

2.5. ProQ Phosphoprotein Stain and SYPRO Total Protein Stain. To determine key myofilament protein phosphorylation levels ProQ Diamond phosphoprotein gel (Life Technologies) and SYPRO Ruby total protein gel (Life Technologies) stains were used according to the manufactures instructions and similar to that previously described [4, 25]. Briefly, muscle myofilament preparations were fractionated by electrophoresis on a 12% 200 : 1 *bis*-acrylamide Laemmli gel with a 4% 29 : 1 *bis*-acrylamide stacking gel. ProQ Diamond followed by SYPRO Ruby protein gel staining was performed in dark at room temperature. Fluorescent imaging was done using a Typhoon 9410 imager (GE Healthcare) (ProQ Diamond: 532-nm excitation/580-nm BP 40 emission; SYPRO Ruby: 457-nm excitation/610-nm BP 30 emission) at a pixel size of 50 microns [14]. Resultant gel images were quantified by ImageQuant TL (GE Healthcare). Troponin T, tropomyosin, and myosin light chain 2 phosphorylation levels were normalized to SYPRO Ruby total protein stain levels for the protein of interest in the individual muscle while troponin I and myosin binding protein C phosphorylation levels were normalized to actin.

2.6. Data Analysis and Statistics. Calcium transient analysis was preformed through the use of ImageJ and Origin 7 software. Contractile data were collected and analyzed on- and offline using custom-written software in LabVIEW (National Instruments). Data are expressed as mean ± SEM unless otherwise stated. Data were statistically analyzed using ANOVA or Student's *t*-test (paired or unpaired) where applicable. A two-tailed $P < 0.05$ was considered significant.

3. Results

Frequency-induced changes in developed force and changes in contractile kinetics occur in several phases. Figure 1 depicts a representative tracing of beat-to-beat alterations in developed force (F_{dev}). The majority of changes in F_{dev} that occur on a beat-to-beat basis during a frequency jump from 1 to 4 Hz (Figure 1(a)) and 4 to 1 Hz (Figure 1(b)) occur within 20 beats during 1 or 4 Hz stabilization frequency. As shown,

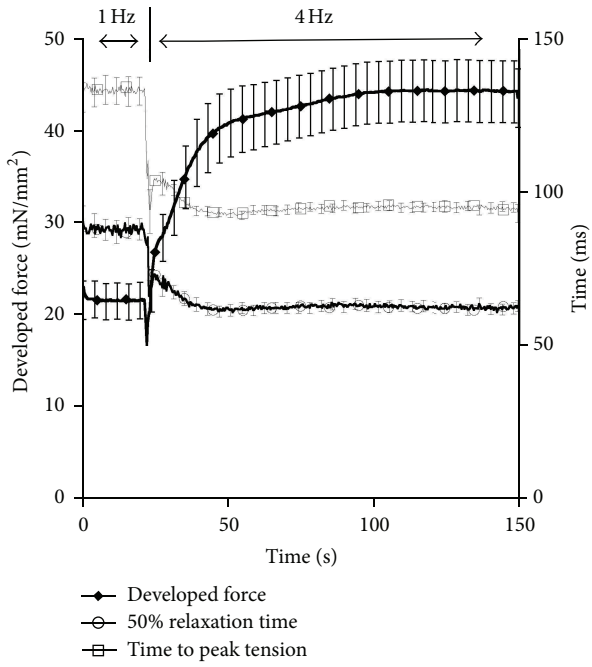

Figure 2: Kinetic tracings from muscles stimulated from 1 Hz to 4 Hz ($n = 35$). Developed force (F_{dev}) increases rapidly and then gradually following an increase in pacing frequency. The switch in frequency is marked by a rapid decline in F_{dev} at approximately 60 seconds. Time to peak tension (TTP) and time to 50% relaxation (RT_{50}) rapidly decline following an increase from 1 to 4 Hz pacing frequency and stabilize within 20 seconds of the frequency change.

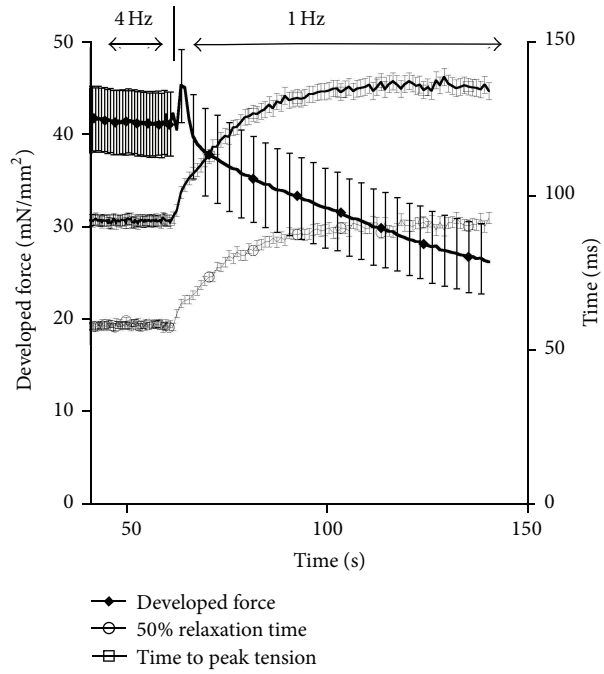

Figure 3: Kinetic response following a decrease in pacing frequency from 4 Hz to 1 Hz ($n = 26$). Developed force (F_{dev}) decreases gradually following the initial change in pacing frequency. Prior to the decline in F_{dev} there is a rapid increase in force for approximately 5 seconds. Time to peak tension (TTP) and time to 50% relaxation (RT50) both increase following an increase in pacing frequency that stabilizes in approximately 30 seconds.

developed force of the first beat drops immediately following an increase in frequency. This drop is followed by a rapid increase in force production within 20 beats of the frequency change. Decreasing frequency from 4 to 1 Hz produces a transient increase in force production followed by a rapid decline. As can be seen in Figure 1, once the frequency is increased or decreased, there is an aberrant twitch immediately following the last twitch from the previous steady-state frequency.

Figure 2 depicts the alterations in contractile force and twitch kinetics that occur during the transition from 1 to 4 Hz. As the muscle continues at a higher pacing frequency the rapid increase in force production that occurs over the first 5–10 seconds (early phase) is followed by a slower phase (~1-2 minutes) in which the developed force gradually increases (late phase) and eventually stabilizes at the new steady-state. As more clearly shown in Figure 1, during the transition to 4 Hz, there is a rapid decline in force production of the 1st beat following a change in stimulation rate followed by a slower further increase until force stabilizes. Twitch kinetics, time to peak tension (TTP), and time from peak tension to 50% relaxation (RT_{50}) measurements show a similar initial phase, but they reach the steady-state level prior to F_{dev} reaching the new steady-state.

To determine the twitch dynamics that occurs during a decrease in pacing we reversed the previous protocol and changed the frequency from 4 Hz to 1 Hz. We then allowed the muscle to stabilize at 1 Hz. As depicted in Figure 3, as the pacing is immediately decreased from 4 to 1 Hz there is a rapid increase followed by a decrease in F_{dev}. The stabilization at 1 Hz occurs much slower than the 4 Hz stabilization time previously presented. Additional studies on twitch kinetics during this drop in pacing frequency show a more gradual increase in TTP and RT_{50}. As seen with increases in frequency, the twitch kinetics change rapidly with decreases in frequency and stabilize prior to the stabilization of force. These findings suggest additional alterations at either the calcium transient level or in myofilament calcium sensitivity. Thus, we set out to determine the effects of frequency on calcium transient amplitude.

In order to ensure that under our experimental conditions, most notably at 37°C, the dye can accurately track the calcium transient, the off-rate of the dye was investigated using a stopped-flow protocol as performed previously [15]. In Figure 4 the results of this verification are depicted in absence (a) and presence (b) of myofilaments.

Confocal fluorescent microscopy line-scans of isolated trabeculae loaded with Rhod-2 AM (Figures 5(a) and 5(c)) show the changes in calcium transient in conjunction with changes in pacing frequency from 1 Hz to 4 Hz and 4 Hz to 1 Hz. Figures 5(b) and 5(d) depict these changes in a graphical representation of the microscopy line-scans. As the frequency is increased from 1 Hz to 4 Hz, the first beat is

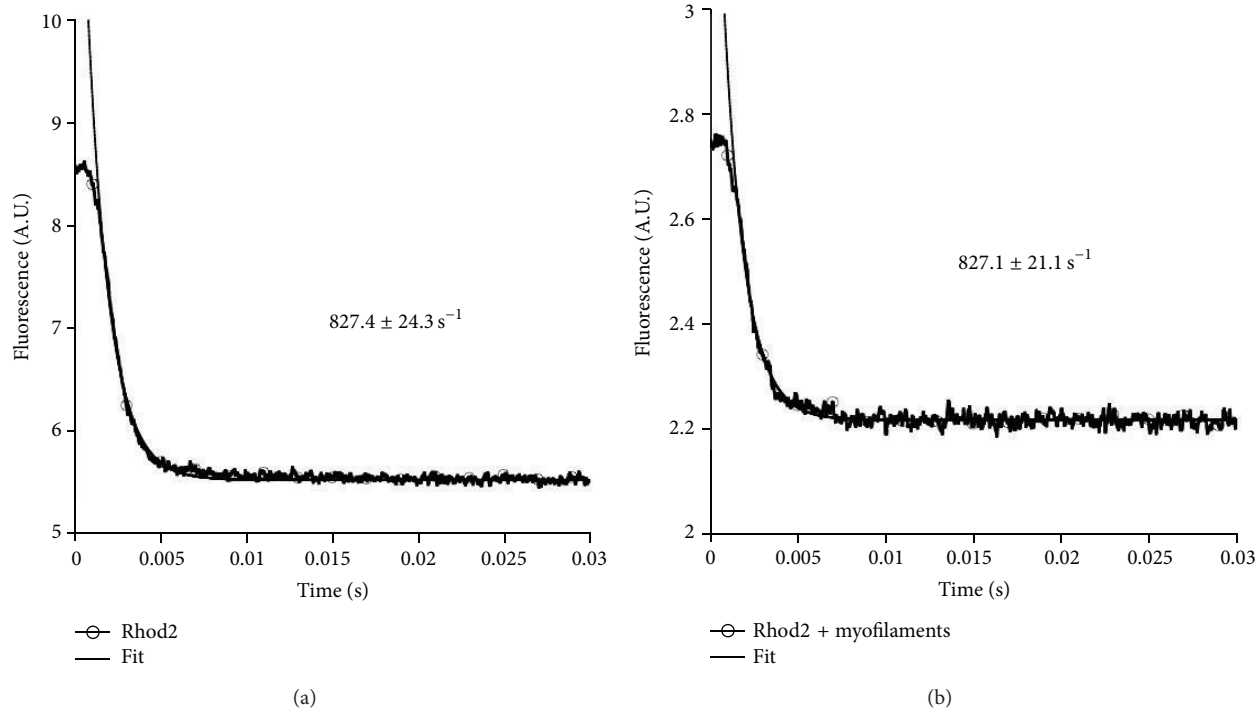

Figure 4: Stopped-flow analysis of the off-rate of Calcium from Rhod-2. Single experimental trace of determining the calcium off-rate, determined from a minimum of $n = 10$ runs in absence (a) or in presence (b) of myofilaments. Stopped-flow experiments were performed at 37°C.

characterized by a depression of calcium transient amplitude due to incomplete SR reloading, followed by a gradual increase in the amplitude of the calcium transient along with an increase in peak twitch and end twitch calcium level. Analysis of $\Delta F/F_o$ show an immediate increase in diastolic calcium levels and a gradual increase in end twitch calcium levels (Figure 5(b)). Following a decrease in the frequency of pacing (from 4 Hz to 1 Hz), there is an immediate decline in the diastolic calcium level as well as in the end twitch calcium level (Figure 5(d)).

Averages of the calcium transient alterations from 1 to 4 Hz show a drastic increase in the diastolic calcium level not necessarily due to changes in end twitch calcium levels (Figure 6(a)). The averages were taken at 5 seconds prior to the frequency change and at subsequent time points after the change in frequency. Additionally, once the muscle is stabilized (60-second time point), the end twitch and peak calcium levels are at their highest, as compared to all other earlier time points. To determine the effect of decreasing frequency on calcium transient, we examined the alterations in end twitch and peak calcium amplitude during the transition from 4 Hz to 1 Hz. In Figure 6(b), we looked at 4 beats (or 1 second) prior to the change in frequency, followed by 5, 10, 15, 20, and 60 seconds after the change to 1 Hz. During these times the functional changes during the frequency transition can be visualized and can thus be compared to the contractile function at steady-state. Once again we used the 60-second time point as a representative of the stabilized force and calcium transient amplitude. Here, we are able to show that with decreases in frequency there is a decline in end twitch and peak calcium amplitude maintained until the muscle has stabilized.

In order to determine if calcium transient amplitude and F_{dev} would parallel each other through the early and late stabilization phases, we simultaneously measured F_{dev} and calcium transient amplitude during our frequency protocols. As shown in Figures 7(a) and 7(b), with increases in frequency there is no significant dissociation between end or peak calcium and F_{dev} during the early stabilization phase. Surprisingly, when taking an expanded look at the entire stabilization period, a rise in peak and end calcium occurs during the period at which the force has already reached a plateau. This phenomenon is not seen with a decreasing frequency of pacing (Figures 7(c) and 7(d)) suggesting a pertinent role for alterations in myofilament calcium sensitivity during stabilization.

Additionally, a phase-plane plot of the force-calcium relationship at 1 Hz and at 4 Hz (Figure 8) depicts an upward and leftward shift, indicative of a desensitization of the myofilaments at higher frequency.

In order to explain this dissociation between calcium amplitude and the force response, we attempted to identify posttranslational modifications associated with alterations in myofilament calcium sensitivity. Figure 9 shows representative SYPRO Ruby total protein and ProQ Diamond phosphoprotein stained blots during 1 Hz stabilization ($n = 6$),

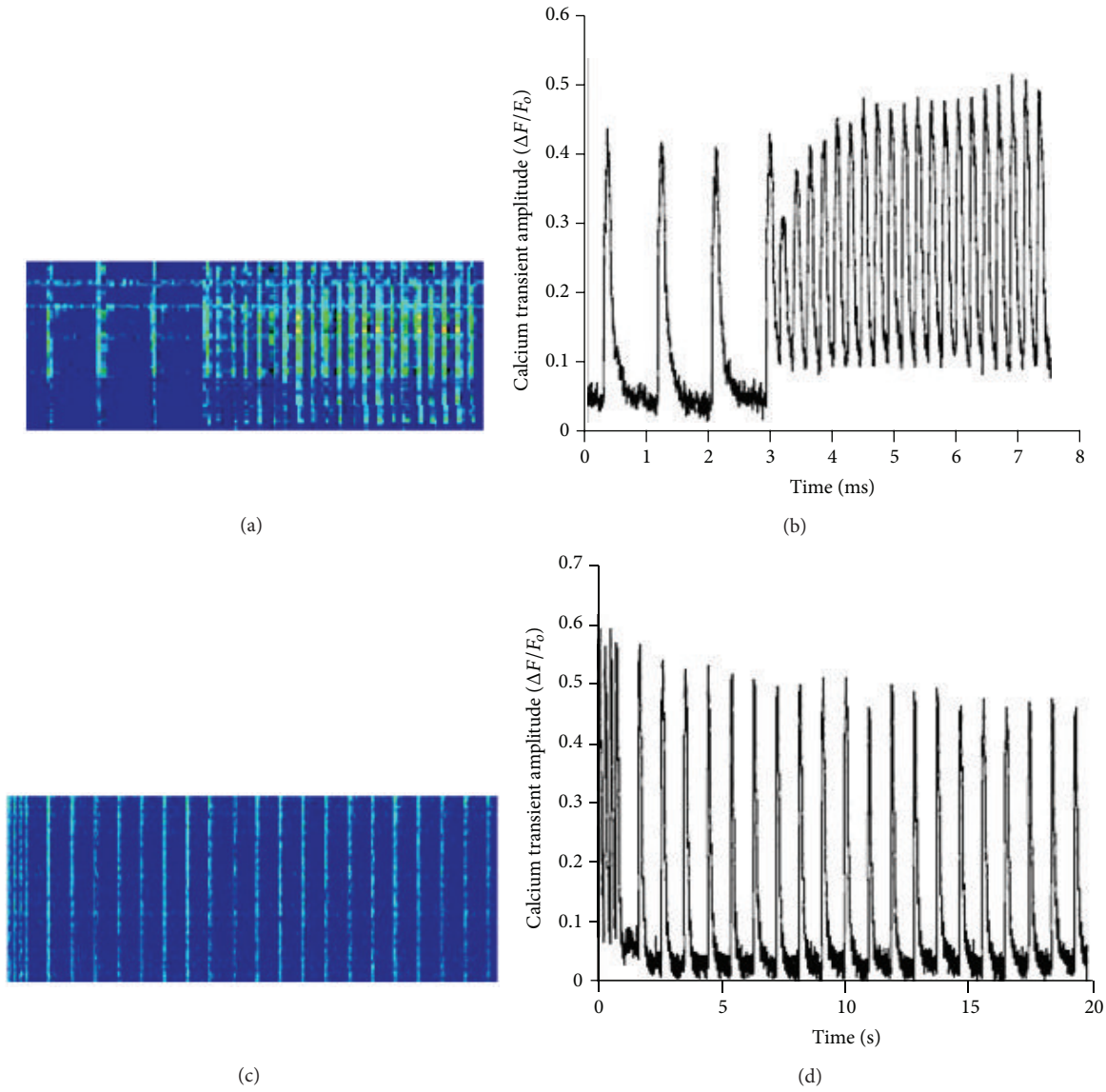

Figure 5: Line-scans of a Rhod-2 AM loaded isolated trabecula and changes in calcium amplitude during changes in pacing frequency from 1 Hz to 4 Hz and 4 Hz to 1 Hz. (a) Representative image of matrix line-scan of Rhod-2 AM loaded, isolated muscle, during frequency change from 1 Hz to 4 Hz and corresponding change (b) in calcium transient amplitude ($\Delta F/F_o$). Representative image of line-scan of Rhod-2 AM loaded isolated muscle (c) during frequency change from 4 Hz to 1 Hz and corresponding calcium transient amplitude trace (d) ($\Delta F/F_o$).

10 seconds after frequency-switch ($n = 7$), 1–4 minutes after frequency-switch ($n = 6$), 4 Hz steady-state ($n = 3$), and muscles stabilized at 1 Hz treated with 1 μm isoproterenol ($n = 2$) to serve as a positive control. Key myofilament proteins (TnI, TnT, MyBP-C, Tm, and MLC2) were analyzed to determine alterations in phosphorylation status as compared to either SYPRO total protein for the protein of interest (TnT, Tm, MLC-2, TnI, and MyBP-C) or actin. Cumulative myofilament protein phosphorylation increased over time ($P < 0.05$, ANOVA), but the assay lacked the power to detect significance in individual protein phosphorylation levels (Figure 9(c)).

4. Discussion

The FFR has been utilized as a diagnostic tool to determine cardiovascular health. The FFR is characterized by a species-dependent increase in contractile force and acceleration of contractile kinetics following increases in the frequency of stimulation [5]. Calcium plays a critical role in the regulation of contractile function, and it is the calcium and force homeostatic relationship that is a critical regulator of the response to frequency on the heart [2]. In the past decade the focus was on understanding and utilizing the moderate variability in heart rate as a clinically diagnostic tool [26]. Heart rate variability

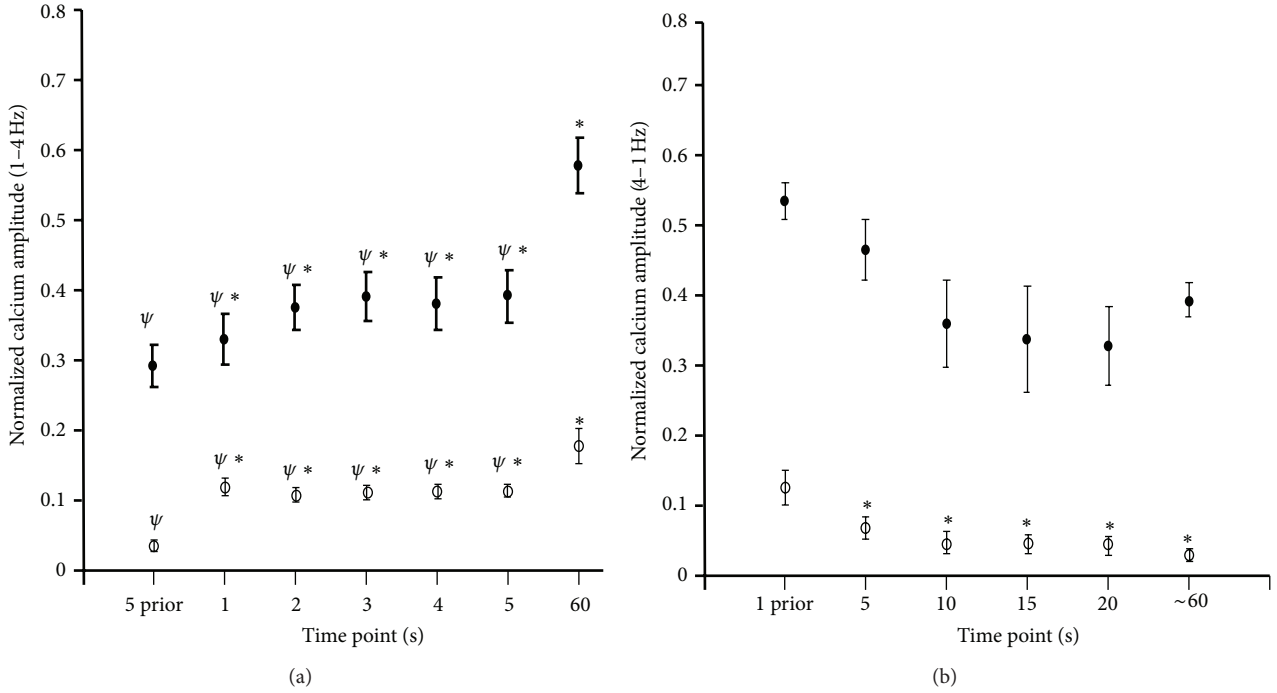

Figure 6: Normalized calcium transient amplitude during changes in pacing frequency. (a) Average relative calcium amplitude ($n = 6$) during the transition from 1 Hz to 4 Hz. Maximal and minimal calcium transient amplitudes were averaged for 5 seconds prior to the 4 Hz change in frequency, at the 1-, 2-, 3-, 4-, 5-, and 60-second time points following the frequency switch to 4 Hz. $*$ represents statistical significance from 5-second prior value and ψ represent statistical significance from 60-second value, $P < 0.05$. (b) Average relative maximal and minimal calcium transient amplitude recorded at 1 second prior to the 1 Hz frequency change and at 5, 10, 15, 20, and 60 seconds during the 1 Hz stabilization process ($n = 4$). $*$ represents a statistical significance from 1 second prior values. A $P < 0.05$ is considered significant.

(HRV) reflects the balance between the sympathetic and parasympathetic nervous systems [27]. Variability of the heart rate is intrinsic with increases in variability being considered as a positive marker of health [27, 28]. Our hope in this study is to utilize a simplified model of HRV to determine the mechanism regulating contractile stabilization from one steady-state frequency to another. Building a more in-depth understanding of the minute modifications that occur in a beat-to-beat regulated system is important to the development of potential HRV targeted therapeutic techniques.

Analyses of specific beat-to-beat force and calcium transient kinetics suggest a dissociation between the force production profile and contractile kinetics during the late phase of force stabilization. By determining the effectors that govern these alterations, we would eventually be able to stimulate or inhibit HRV in the failing myocardium. We here show that there is a disconnect between the changes in developed force and calcium amplitude in the late phase of force stabilization and that myofilament protein phosphorylation does not appear to play a significant role in the effects of early stabilization. This finding suggests a potential role for regulation at the level of cellular calcium entry and/or extrusion. In latter stages of stabilization, overall myofilament protein phosphorylation is increased, in accordance with earlier findings [4, 13, 14, 24]. The studies were performed at optimal length, where baseline phosphorylation of certain myofilament proteins may already be relatively high [29–31]. Also, note that overall phosphorylation of various sites may differentially impact function [32, 33], and further studies are needed to dissect these changes at the protein/specific site level.

Previous studies in our lab have shown that the interbeat duration can be a determinant of contractile function [24, 26]. Additionally, studies looking at the effects of previous beats have shown that interbeat duration impacts upon contractile function up to three beats prior to the beat of interest [24]. These effects have been studied in numerous species and point to a species-dependent interbeat duration relationship [34]. For this particular study we aimed to determine the difference between contractile kinetics and calcium transient on a beat-to-beat basis during alterations in frequency in the rabbit myocardium. Previously, studies have been unable to determine twitch and calcium transient characteristics following immediate changes in stimulated pacing frequency. Similar studies in isolated rat muscle have highlighted changes in peak active stress and correlated those changes to fluctuations in calcium levels [35]. However, here we are able to not only visualize the changes in maximal activation of force and calcium but also determine alterations that occur on twitch and calcium kinetics during every contraction. This technique enables the direct identification of how the characteristics of the calcium transient impact upon twitch kinetics. As shown above, when changing the frequency of pacing (from low to high), there is first an immediate and then gradual increase in force production. During decreased

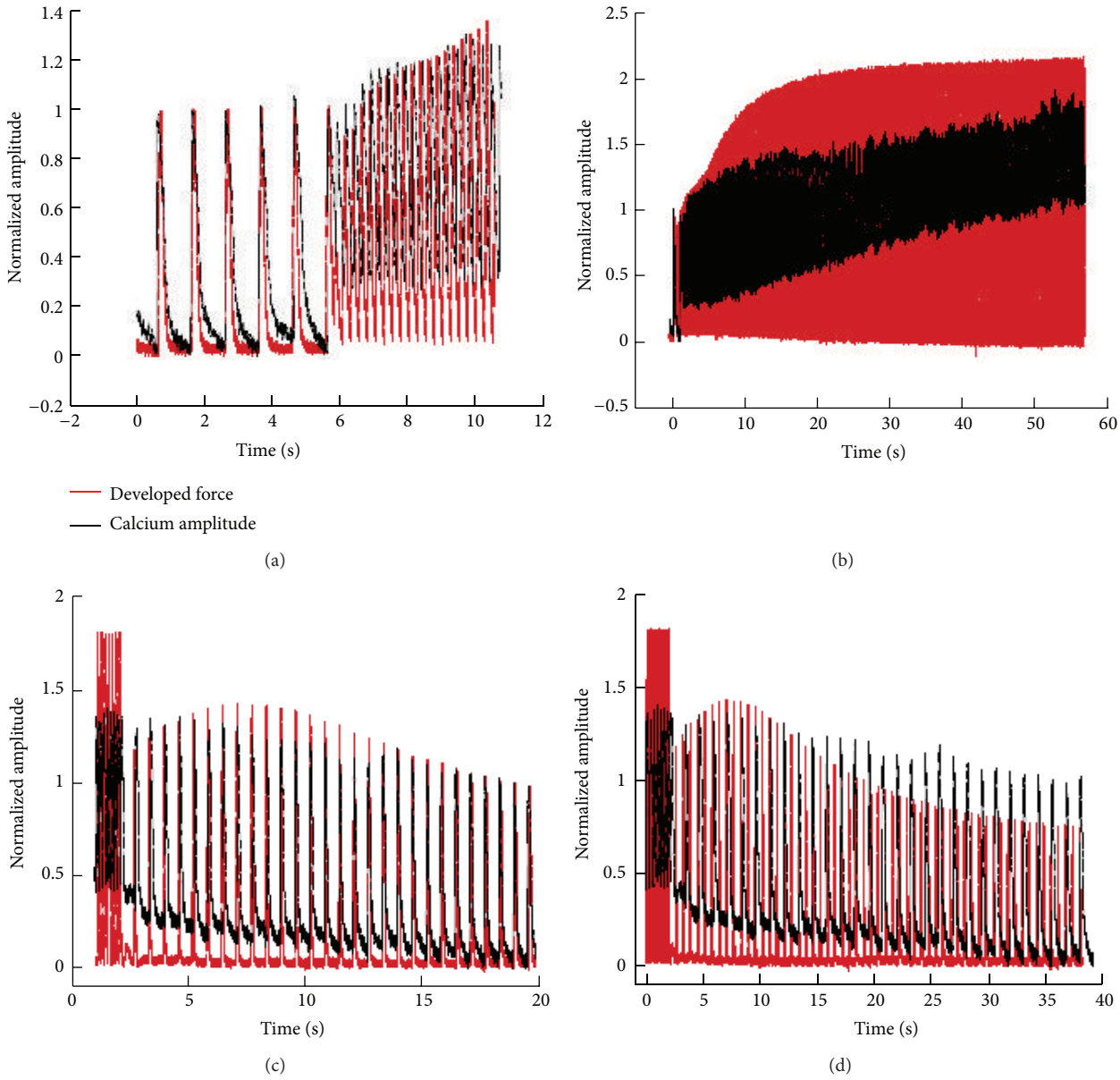

Figure 7: Force and calcium response during twitch after increases in pacing frequency. (a) Overlay of force and calcium tracings normalized to 1 Hz values during the transition from 1 Hz to 4 Hz (approximately 11 seconds). Twitch profiles and calcium transient changes are recorded for every contraction occurring in the trabecula during the brief transition from 1 Hz to 4 Hz. (b) Overlay of force and calcium tracings normalized to 1 Hz values. One twitch at 1 Hz is recorded followed by every twitch that occurs during the 4 Hz stabilization process (60 seconds total). (c) Normalized force tracings overlaid with normalized relative calcium amplitude transients of an individual isolated muscle during a frequency change from 4 Hz to 1 Hz (approximately 20 seconds). Tracings are normalized to 1 Hz stabilized values. (d) Overlay of force and calcium tracings normalized to 1 Hz values. Eight twitches at 4 Hz are recorded followed by every twitch that occurs during the 1 Hz stabilization process (40 seconds total).

stimulation frequency, there is a characteristic increase in force production followed by a rapid force decline and then a more gradual decline as the muscle stabilizes at its new pacing frequency. It was our goal to determine the role of calcium transients and myofilament protein posttranslational modifications during the early and late phases of frequency stabilization. The kinetic profile of these muscles during the transition from low to high and vice versa parallels the changes in developed force.

Because most calcium handling studies are done in either mouse or rat individual myocytes [6] we aimed to gain insight into the global calcium transient in a multicellular preparation in a mammalian model that more closely resembles human calcium handling, which is different in

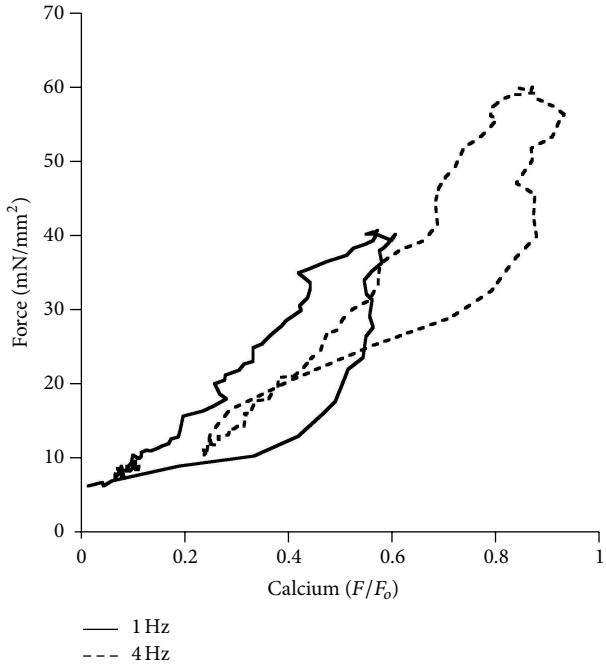

Figure 8: Phase-plane plot of force-calcium relationship. Force-calcium relationship at 1 Hz (solid line) and 4 Hz (dashed line) in a muscle paced stabilized at 1 Hz and thereafter paced and stabilized at 4 Hz.

many aspects from small mammals [36, 37]. Most calcium is circulated through the SR in rat and mouse (~90–98%) [6], thus concepts which focus mainly on SR function are valid. However, in humans the SR only accounts for ~70% of the calcium sequestering capabilities. Because of these intrinsic differences in calcium handling, mouse and rat models may progress faster through the early and latent phases during the frequency transition leading to faster stabilization. This suggests that HRV and frequency transition may not significantly affect the rodent physiology. For this study, we have utilized rabbit ventricular multicellular preparations at physiological temperature to aid in our understanding of human myocardial function and myofilament calcium sensitivity. Our study shows that during the early phase of the frequency stabilization the force response parallels the calcium response of both peak and end calcium levels. In the late phase (characterized by complete force stabilization) we observed a continual increase in end and peak calcium transient amplitude. This disconnect suggests an alteration in myofilament calcium sensitivity that is occurring late in the stabilization period. Upon a decrease in pacing frequency, there is a decrease in calcium transient amplitude followed by a more gradual decline as the muscle continues to stabilize. The peak and end calcium and force levels eventually decline in parallel as the muscle reaches steady-state. Together these findings suggest alterations in myofilament calcium sensitivity at higher frequencies that are later diminished as the muscle reaches steady-state at lower frequencies.

It was originally hypothesized that the latent stabilization phases were due to alterations in myofilament protein phosphorylation status which would account for changes in myofilament calcium sensitivity. However, proQ diamond phosphoprotein stain does not offer, with the experimental design of this study, to draw significance at least at the individual protein level, although overall the myofilaments are hyperphosphorylated at higher frequency. Our own as well as previous studies by others have highlighted the potential additive effect of myofilament protein phosphorylation [30, 33]. Additionally, changes in length have been associated with changes in myofilament protein phosphorylation [29]; thus utilizing optimal preload in the above experiments may induce phosphorylation to such a degree that differences induced by frequency are not significant. There is a clear role for the different calcium handling mechanism in the regulation of calcium transients during changing frequencies. The sodium-calcium exchanger (NCX) may be playing a role in the late phase, during which the muscle is stabilizing slowly and showing only gradual increases in contractile force [38]. NCX function has been shown to increase during the FFR [39, 40] and could account for the increases in peak and end calcium present during the late phase of frequency stabilization. Recent studies show S-glutathionylation of MyBP-C inducing a significant increase in myofilament calcium sensitivity [41]. Additionally, alterations through nitrosative and oxidative activity can also modify cytosolic calcium levels leading to changes in myofilament calcium sensitivity and force production [42]. For instance modification of the ryanodine receptor (RyR) by poly-S-nitrosylation increases calcium release potentially leading to a downstream effect of decreased calcium sensitivity at the myofilament level [43].

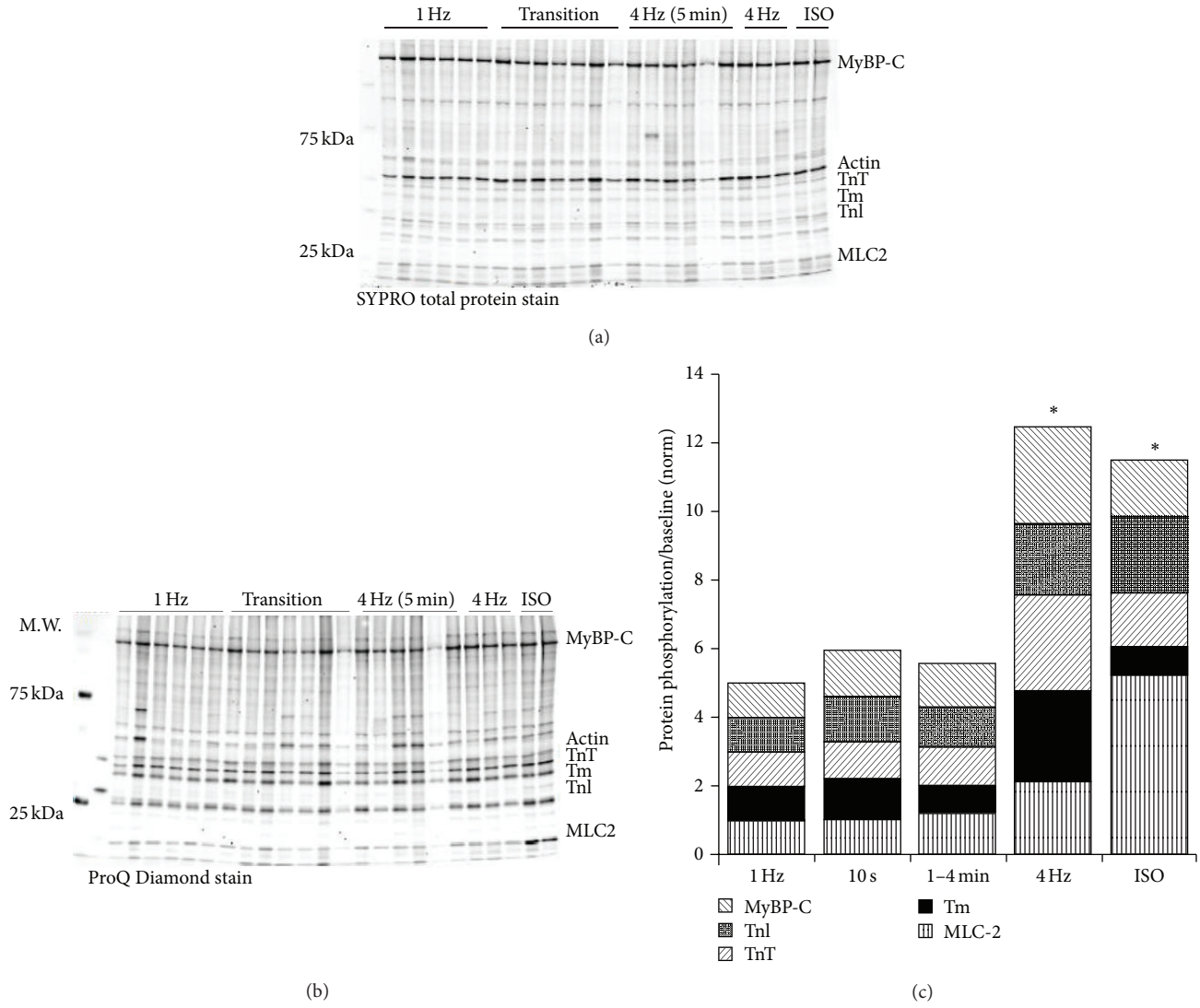

Figure 9: Alterations in phosphorylation during early and late frequency stabilization. Isolated trabeculae were frozen after stabilization at 1 Hz, up to 10 seconds following the switch from 1 Hz to 4 Hz, and 1 and 4 minutes after the switch from 1 to 4 Hz. Two trabeculae were also treated with ISO as a positive control for phosphorylation. (a) SYPRO Ruby total protein analysis of pertinent myofilament proteins. (b) ProQ Diamond analysis of key myofilament protein phosphorylation state. (c) Normalized (to 1 Hz) ratio of phosphorylated TnI and MyBP-C to total actin, and phosphorylated TnT, MLC-2, and Tm to total protein indicated a significant increase in cumulative phosphorylation at 4 Hz compared to 1 Hz but no significant changes during the early (10 seconds) and mid- (1–4 minutes) transition. $*$ represents a statistical significance from 1 Hz levels, $P < 0.05$.

This study highlights a novel technique in which multicellular contractile kinetics and the corresponding calcium transient can be analyzed in the same muscle during a dynamic contractile protocol. Taken together, our results validate the importance of calcium transient amplitude when considering the rapid changes in pacing frequency, which occur endogenously. The disconnect between amplitude of the calcium and force transients further indicates a role of regulation at the myofilament level, other than through phosphorylation in the early stages of transition, in frequency-dependent activation and HRV.

Conflict of Interests

The authors declare that there is no conflict of interests regarding the publication of this paper.

Acknowledgments

This study was supported by NIH R01HL113084 (PMLJ) and F31HL096397 (KMH) and American Heart Association Grants EIA0740040N (PMLJ), PRE0615288B (KDV), and PRE1148008 (NM).

References

[1] H. P. Bowditch, "Über die Eigenthümlichkeiten der Reizbarkeit, welche die Muskelfasern des Herzens zeigen. Berichte über die Verhandlungen der Königlich-Sächsischen Gesellschaft der Wissenschaften zu Leipzig," *Mathematisch Physische Klasse*, vol. 23, pp. 652–689, 1871.

[2] P. M. L. Janssen, "54th Bowditch Lecture: myocardial contraction-relaxation coupling," *American Journal of Physiology: Heart and Circulatory Physiology*, vol. 299, no. 6, pp. H1741–H1749, 2010.

[3] J. Palomeque, M. G. Vila Petroff, and A. Mattiazzi, "Pacing staircase phenomenon in the heart: from Bodwitch to the XXI century," *Heart, Lung and Circulation*, vol. 13, no. 4, pp. 410–420, 2004.

[4] K. D. Varian and P. M. L. Janssen, "Frequency-dependent acceleration of relaxation involves decreased myofilament calcium sensitivity," *The American Journal of Physiology—Heart and Circulatory Physiology*, vol. 292, no. 5, pp. H2212–H2219, 2007.

[5] M. Endoh, "Force-frequency relationship in intact mammalian ventricular myocardium: physiological and pathophysiological relevance," *European Journal of Pharmacology*, vol. 500, no. 1–3, pp. 73–86, 2004.

[6] D. M. Bers, *Excitation-Contraction Coupling and Cardiac Contractile Force*, Kluwer Academic, Dordrecht, The Netherlands, 2001.

[7] B. Pieske, B. Kretschmann, M. Meyer et al., "Alterations in intracellular calcium handling associated with the inverse force-frequency relation in human dilated cardiomyopathy," *Circulation*, vol. 92, no. 5, pp. 1169–1178, 1995.

[8] E. I. Rossman, R. E. Petre, K. W. Chaudhary et al., "Abnormal frequency-dependent responses represent the pathophysiologic signature of contractile failure in human myocardium," *Journal of Molecular and Cellular Cardiology*, vol. 36, no. 1, pp. 33–42, 2004.

[9] G. A. Ramirez-Correa, S. Cortassa, B. Stanley, W. D. Gao, and A. M. Murphy, "Calcium sensitivity, force frequency relationship and cardiac troponin I: critical role of PKA and PKC phosphorylation sites," *Journal of Molecular and Cellular Cardiology*, vol. 48, no. 5, pp. 943–953, 2010.

[10] K. D. Varian, S. Raman, and P. M. L. Janssen, "Measurement of myofilament calcium sensitivity at physiological temperature in intact cardiac trabeculae," *American Journal of Physiology—Heart and Circulatory Physiology*, vol. 290, no. 5, pp. H2092–H2097, 2006.

[11] R. Zhang, J. Zhao, A. Mandveno, and J. D. Potter, "Cardiac troponin I phosphorylation increases the rate of cardiac muscle relaxation," *Circulation Research*, vol. 76, no. 6, pp. 1028–1035, 1995.

[12] K. C. Bilchick, J. G. Duncan, R. Ravi et al., "Heart failure-associated alterations in troponin I phosphorylation impair ventricular relaxation-afterload and force-frequency responses and systolic function," *The American Journal of Physiology—Heart and Circulatory Physiology*, vol. 292, no. 1, pp. H318–H325, 2007.

[13] C. W. Tong, R. D. Gaffin, D. C. Zawieja, and M. Muthuchamy, "Roles of phosphorylation of myosin binding protein-C and troponin I in mouse cardiac muscle twitch dynamics," *Journal of Physiology*, vol. 558, no. 3, pp. 927–941, 2004.

[14] K. D. Varian, B. J. Biesiadecki, M. T. Ziolo, J. P. Davis, and P. M. L. Janssen, "Staurosporine inhibits frequency-dependent myofilament desensitization in intact rabbit cardiac trabeculae," *Biochemistry Research International*, vol. 2012, Article ID 290971, 10 pages, 2012.

[15] M. M. Monasky, K. D. Varian, J. P. Davis, and P. M. L. Janssen, "Dissociation of force decline from calcium decline by preload in isolated rabbit myocardium," *Pflugers Archiv European Journal of Physiology*, vol. 456, no. 2, pp. 267–276, 2008.

[16] L. A. Mulieri, G. Hasenfuss, F. Ittleman, E. M. Blanchard, and N. R. Alpert, "Protection of human left ventricular myocardium from cutting injury with 2,3-butanedione monoxime," *Circulation Research*, vol. 65, no. 5, pp. 1441–1449, 1989.

[17] N. Zimmermann, P. Boknik, E. Gams et al., "Mechanisms of the contractile effects of 2,3-butanedione-monoxime in the mammalian heart," *Naunyn-Schmiedeberg's Archives of Pharmacology*, vol. 354, no. 4, pp. 431–436, 1996.

[18] S. Raman, M. A. Kelley, and P. M. L. Janssen, "Effect of muscle dimensions on trabecular contractile performance under physiological conditions," *Pflugers Archiv European Journal of Physiology*, vol. 451, no. 5, pp. 625–630, 2006.

[19] E. K. Rodriguez, W. C. Hunter, M. J. Royce, M. K. Leppo, A. S. Douglas, and H. F. Weisman, "A method to reconstruct myocardial sarcomere lengths and orientations at transmural sites in beating canine hearts," *The American Journal of Physiology—Heart and Circulatory Physiology*, vol. 263, no. 1, part 2, pp. H293–H306, 1992.

[20] N. Milani-Nejad, L. Brunello, S. Gyorke, and P. M. L. Janssen, "Decrease in sarcoplasmic reticulum calcium content, not myofilament function, contributes to muscle twitch force decline in isolated cardiac trabeculae," *Journal of Muscle Research and Cell Motility*, 2014.

[21] A. E. Belevych, D. Terentyev, R. Terentyeva et al., "The relationship between arrhythmogenesis and impaired contractility in heart failure: role of altered ryanodine receptor function," *Cardiovascular Research*, vol. 90, no. 3, pp. 493–502, 2011.

[22] A. Belevych, Z. Kubalova, D. Terentyev, R. L. Hamlin, C. A. Carnes, and S. Györke, "Enhanced ryanodine receptor-mediated calcium leak determines reduced sarcoplasmic reticulum calcium content in chronic canine heart failure," *Biophysical Journal*, vol. 93, no. 11, pp. 4083–4092, 2007.

[23] L. Brunello, J. L. Slabaugh, P. B. Radwanski et al., "Decreased RyR2 refractoriness determines myocardial synchronization of aberrant Ca^{2+} release in a genetic model of arrhythmia," *Proceedings of the National Academy of Sciences of the United States of America*, vol. 110, no. 25, pp. 10312–10317, 2013.

[24] K. D. Varian, A. Kijtawornrat, S. C. Gupta et al., "Impairment of diastolic function by lack of frequency-dependent myofilament desensitization in rabbit right ventricular hypertrophy," *Circulation: Heart Failure*, vol. 2, no. 5, pp. 472–481, 2009.

[25] B. J. Biesiadecki, K. Tachampa, C. Yuan, J. P. Jin, P. P. de Tombe, and R. J. Solaro, "Removal of the cardiac troponin I N-terminal extension improves cardiac function in aged mice," *Journal of Biological Chemistry*, vol. 285, no. 25, pp. 19688–19698, 2010.

[26] C. A. A. Torres, K. D. Varian, and P. M. L. Janssen, "Variability in interbeat duration influences myocardial contractility in rat cardaic trabeculae," *The Open Cardiovascular Medicine Journal*, vol. 2, pp. 96–100, 2008.

[27] P. J. Counihan, L. Fei, Y. Bashir, T. G. Farrell, G. A. Haywood, and W. J. McKenna, "Assessment of heart rate variability in hypertrophic cardiomyopathy: association with clinical and prognostic features," *Circulation*, vol. 88, no. 4, pp. 1682–1690, 1993.

[28] R. E. Kleiger, J. P. Miller, J. T. Bigger Jr., and A. J. Moss, "Decreased heart rate variability and its association with increased mortality after acute myocardial infarction," *The American Journal of Cardiology*, vol. 59, no. 4, pp. 256–262, 1987.

[29] M. M. Monasky, B. J. Biesiadecki, and P. M. L. Janssen, "Increased phosphorylation of tropomyosin, troponin I, and myosin light chain-2 after stretch in rabbit ventricular myocardium under physiological conditions," *Journal of Molecular and Cellular Cardiology*, vol. 48, no. 5, pp. 1023–1028, 2010.

[30] M. M. Monasky, D. M. Taglieri, A. K. Jacobson, K. M. Haizlip, R. J. Solaro, and P. M. Janssen, "Post-translational modifications of myofilament proteins involved in length-dependent prolongation of relaxation in rabbit right ventricular myocardium," *Archives of Biochemistry and Biophysics*, vol. 535, no. 1, pp. 22–29, 2013.

[31] P. J. M. Wijnker, V. Sequeira, D. B. Foster et al., "Length-dependent activation is modulated by cardiac troponin I bisphosphorylation at Ser23 and Ser24 but not by Thr143 phosphorylation," *The American Journal of Physiology: Heart and Circulatory Physiology*, vol. 306, no. 8, pp. H1171–H1181, 2014.

[32] R. J. Solaro and J. van der Velden, "Why does troponin I have so many phosphorylation sites? Fact and fancy," *Journal of Molecular and Cellular Cardiology*, vol. 48, no. 5, pp. 810–816, 2010.

[33] B. R. Nixon, S. D. Walton, B. Zhang et al., "Combined troponin I Ser-150 and Ser-23/24 phosphorylation sustains thin filament Ca^{2+} sensitivity and accelerates deactivation in an acidic environment," *Journal of Molecular and Cellular Cardiology*, vol. 72, pp. 177–185, 2014.

[34] Y. Xu, M. M. Monasky, N. Hiranandani, K. M. Haizlip, G. E. Billman, and P. M. L. Janssen, "Effect of twitch interval duration on the contractile function of subsequent twitches in isolated rat, rabbit, and dog myocardium under physiological conditions," *Journal of Applied Physiology*, vol. 111, no. 4, pp. 1159–1167, 2011.

[35] J. Layland and J. C. Kentish, "Positive force- and [Ca2+](i)-frequency relationships in rat ventricular trabeculae at physiological frequencies," *American Journal of Physiology—Heart and Circulatory Physiology*, vol. 276, no. 1, part 2, pp. H9–H18, 1999.

[36] M. Periasamy and P. M. L. Janssen, "Molecular basis of diastolic dysfunction," *Heart Failure Clinics*, vol. 4, no. 1, pp. 13–21, 2008.

[37] N. Milani-Nejad and P. M. L. Janssen, "Small and large animal models in cardiac contraction research: advantages and disadvantages," *Pharmacology and Therapeutics*, vol. 141, no. 3, pp. 235–249, 2014.

[38] H. Schotola, S. Sossalla, T. K. Rajab et al., "Influence of mild metabolic acidosis on cardiac contractility and isoprenaline response in isolated ovine myocardium," *Artificial Organs*, vol. 35, no. 11, pp. 1065–1074, 2011.

[39] D. M. Bers, "SR Ca loading in cardiac muscle preparations based on rapid-cooling contractures," *The American Journal of Physiology—Cell Physiology*, vol. 256, no. 1, part 1, pp. C109–C120, 1989.

[40] R. A. Bassani, J. W. M. Bassani, and D. M. Bers, "Relaxation in ferret ventricular myocytes: role of the sarcolemmal Ca ATPase," *Pflügers Archiv*, vol. 430, no. 4, pp. 573–578, 1995.

[41] B. G. Patel, T. Wilder, and R. John Solaro, "Novel control of cardiac myofilament response to calcium by S-glutathionylation at specific sites of myosin binding protein C," *Frontiers in Physiology*, vol. 4, article 336, 2013.

[42] R. A. Kelly, J.-L. Balligand, and T. W. Smith, "Nitric oxide and cardiac function," *Circulation Research*, vol. 79, no. 3, pp. 363–380, 1996.

[43] L. Xu, J. P. Eu, G. Meissner, and J. S. Stamler, "Activation of the cardiac calcium release channel (Ryanodoine receptor) by poly-S-nitrosylation," *Science*, vol. 279, no. 5348, pp. 234–237, 1998.

Hindawi Publishing Corporation
BioMed Research International
Volume 2014, Article ID 810371, 11 pages
http://dx.doi.org/10.1155/2014/810371

Research Article

Inhibition of MMP-2 Expression with siRNA Increases Baseline Cardiomyocyte Contractility and Protects against Simulated Ischemic Reperfusion Injury

Han-Bin Lin,[1] Virgilio J. J. Cadete,[1,2] Bikramjit Sra,[1] Jolanta Sawicka,[1] Zhicheng Chen,[3] Lane K. Bekar,[1] Francisco Cayabyab,[3] and Grzegorz Sawicki[1,4]

[1] *Department of Pharmacology, College of Medicine, University of Saskatchewan, 107 Wiggins Road, Saskatoon, SK, Canada S7N 5E5*
[2] *Faculté de Pharmacie, Université de Montréal, Montréal, QC, Canada H3T 1J4*
[3] *Department of Physiology, University of Saskatchewan, Saskatoon, SK, Canada S7N 5E5*
[4] *Department of Clinical Chemistry, Medical University of Wroclaw, 50-556 Wroclaw, Poland*

Correspondence should be addressed to Grzegorz Sawicki; greg.sawicki@usask.ca

Received 27 May 2014; Accepted 25 June 2014; Published 24 July 2014

Academic Editor: Danuta Szczesna-Cordary

Matrix metalloproteinases (MMPs) significantly contribute to ischemia reperfusion (I/R) injury, namely, by the degradation of contractile proteins. However, due to the experimental models adopted and lack of isoform specificity of MMP inhibitors, the cellular source and identity of the MMP(s) involved in I/R injury remain to be elucidated. Using isolated adult rat cardiomyocytes, subjected to chemically induced I/R-like injury, we show that specific inhibition of MMP-2 expression and activity using MMP-2 siRNA significantly protected cardiomyocyte contractility from I/R-like injury. This was also associated with increased expression of myosin light chains 1 and 2 (MLC1/2) in comparison to scramble siRNA transfection. Moreover, the positive effect of MMP-2 siRNA transfection on cardiomyocyte contractility and MLC1/2 expression levels was also observed under control conditions, suggesting an important additional role for MMP-2 in physiological sarcomeric protein turnover. This study clearly demonstrates that intracellular expression of MMP-2 plays a significant role in sarcomeric protein turnover, such as MLC1 and MLC2, under aerobic (physiological) conditions. In addition, this study identifies intracellular/autocrine, cardiomyocyte-produced MMP-2, rather than paracrine/extracellular, as responsible for the degradation of MLC1/2 and consequent contractile dysfunction in cardiomyocytes subjected to I/R injury.

1. Introduction

The pathological role of matrix metalloproteinases (MMPs), including MMP-2, during the development of oxidative stress-mediated cardiac injury and contractile dysfunction has been well described [1–3]. We and others have shown increased activity of MMP-2 in ischemic reperfusion (I/R) injury [4–6], hypoxia-reoxygenation injury [7], and infusion of reactive oxygen species, namely, peroxynitrite ($ONOO^-$) [8, 9]. Furthermore, increased intracellular MMP-2 activity [10–13] is associated with degradation of contractile proteins such as troponin I [10], titin [11], myosin light chain 1 (MLC1) [12, 14, 15], and myosin light chain 2 (MLC2) [13]. All of these observations have been made in intact, isolated hearts during a relatively short time-course (minutes) and appear to be independent of changes in collagen content [16, 17], supporting an acute intracellular action of MMP-2.

MMP-2 can be found in most cardiac cell types, including vascular endothelial cells [18], smooth muscle cells [19], fibroblasts [20], and cardiomyocytes [10, 21]. The majority of MMP-2 synthesized is secreted (~60%) acting in a paracrine manner, with the remaining 40% being targeted to the cytosol [22] or mitochondrial associated membranes [23]. Therefore, it is possible that MMP-2 originating in endothelium, smooth muscle cells, or fibroblasts is upregulated in response to oxidative stress and can act in a paracrine manner

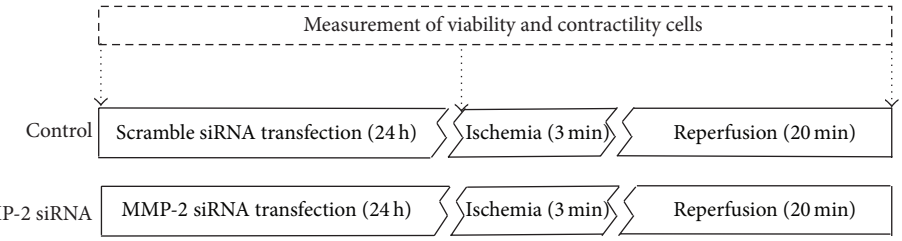

Figure 1: Schematic representation of the perfusion protocol for isolated cardiomyocytes. Scrambled siRNA was used as a control of MMP-2 siRNA. Arrows indicate when cell contractility was measured: (1) before siRNA transfection, (2) before ischemia, and (3) at the end of reperfusion.

on cardiomyocytes, contributing to the development of I/R injury and cardiac contractile dysfunction. Hence, the understanding of MMP-2's mechanism of action (paracrine versus autocrine) and determination of the cellular source/targets of MMP-2 are crucial in the development of novel and more selective drug design.

Greater than 20 MMPs have been described to date with all of them showing similarities in substrate specificities and response to known MMP inhibitors [24], limiting the clinical application of these broad spectra drugs. The vast majority of studies, looking at the roles of MMPs in the development of I/R injury, have been performed in whole heart or whole cardiac tissue homogenates, without the ability to discriminate the source between cell types. Moreover, the pharmacological approaches used to modulate MMP activity rely on the use of broad spectra MMP inhibitors (e.g., doxycycline, orthophenathroline) making it difficult to identify isoform specific effects. Inhibition of MMP-2 has been shown to protect isolated cardiomyocyte contractility in response to oxidative stress [21, 25]. Nonetheless, clinical usage of subantimicrobial doses of doxycycline in patients undergoing cardiopulmonary bypass surgery failed to show a protective effect on cardiac function despite the inhibition of MMP-2 [26]. Consequently, despite the wide body of preclinical evidence supporting inhibition of MMP-2 in cardiac pathologies, the failure of clinical translation makes it crucial to determine the physiological and pathological roles of MMP-2 in order to improve therapeutic strategies that target MMPs.

Here we show that specific, autocrine, intracellular action of MMP-2 on cardiomyocytes regulates not only contractile protein turnover under physiological conditions but also the development of I/R-induced cardiac contractile dysfunction, *via* increased degradation of contractile proteins. These observations, made with use of specific siRNA inhibition of MMP-2, provide novel and important knowledge of the role of MMP-2 in I/R injury and indicate potential therapeutic alternatives to the prevention and treatment of I/R injury.

2. Materials and Methods

This investigation conforms with the Guide to the Care and Use of Experimental Animals published by the Canadian Council on Animal Care.

2.1. Cardiomyocyte Isolation. Male Sprague-Dawley rats (weighing 100–150 g) were anaesthetized with sodium pentobarbital (60 mg/kg i.p.) and hearts were removed. Right ventricular myocytes were used as they provide a consistently higher ratio of live cardiomyocytes to contaminating fibroblasts and endothelial cells in comparison to preparations from the left ventricle [3]. Right ventricular myocytes were obtained by enzymatic dissociation as previously described [27].

2.2. Primary Culture of Cardiomyocytes. Isolated cardiomyocytes were seeded in 35 × 10 mm cell culture plates (Nunc, Roskilde, Denmark) at 2×10^5 cells per plate in DMEM medium (Lonza Walkersville, MD, USA) supplemented with 10% FBS and incubated in a 95% air, 5% CO_2 incubator at 37°C for 7 hours to stabilize cells. Viability and contractility of isolated cardiomyocytes were assessed after isolation, transfection with siRNA, and at the end of reperfusion (Figure 1).

2.3. siRNA Transfection. A mixture containing a pool of 3 target-specific 19–25 nucleotide small interfering RNAs (MMP-2 siRNA) designed to knock down rat MMP-2 gene expression (Santa Cruz Biotechnology, Santa Cruz, CA, USA) was resuspended in RNAse-free water to a final 10 μM concentration in a buffer containing 10 μM Tris-HCl, 20 mM NaCl, and 1 mM EDTA at pH 8.0. This solution was stored at −20°C. As a control, scrambled siRNA (Santa Cruz Biotechnology, Santa Cruz, CA, USA) was used under the same conditions.

Following the initial 7-hour stabilization period in DMEM and 10% FBS, cardiomyocytes were washed with siRNA transfection medium (Santa Cruz Biotechnology, Santa Cruz, CA, USA) and incubated for 24 hours at 37°C in 200 μL of transfection medium containing 0.8 μM of MMP-2 siRNA or scrambled siRNA (Figure 1) according to the manufacturer's protocol. For assessment of transfection efficiency, green fluorescent protein (GFP) was cotransfected with siRNA.

2.4. Simulated Ischemia/Reperfusion Protocol. After 24 hours of transfection with siRNA cardiomyocytes were subjected to chemical ischemia, as previously described [28]. Briefly, the transfection medium was removed and replaced with a solution containing 5 mM 2-deoxyglucose to inhibit glycolysis and 4 mM NaCN to inhibit mitochondrial respiration

(ischemia). After 1, 3, 5, and 7 minutes of incubation the solution was removed and replaced with culture medium without FBS (reperfusion).

2.5. Measurement of Viability and Contractility of Cardiomyocytes. Cardiomyocyte viability and contractility were evaluated at three time points throughout the experimental protocol: 7 hours after cell isolation, after transfection with siRNA (before ischemia), and at the end of reperfusion (Figure 1). The viability of cardiomyocytes was assessed by the trypan blue exclusion test [29–31]. Cardiomyocyte contractility was measured using the IonOptix system and IonWizard 6.0 software (IonOptix, Milton, MA USA). After a stabilization period the chamber containing the cells was perfused with an oxygenated buffer at a constant temperature of 37°C. Cells were continuously paced (stimulated) at 1 Hz and 5 V (IonOptix MyoPacer, Milton, MA, USA). The assessment of cardiomyocyte contractility was made by the measurement of peak shortening, maximal velocity of cell shortening, and maximal velocity of cell relengthening [21] on 8–10 cardiomyocytes per independent experiment, over a 10 min period to give an average measure per sample.

2.6. Preparation of Cell Extracts. Cardiomyocytes were collected and stored at −80°C. For biochemical studies, frozen cardiomyocytes were thawed and sonicated on ice twice for 5 seconds in 50 mM Tris-HCl buffer (pH 7.4) containing 3.1 mM sucrose, 1 mM DTT, 10 μg/mL leupeptin, 10 μg/mL soybean trypsin inhibitor, 2 μg/mL aprotinin, and 0.1% Triton X-100. Homogenates were then centrifuged at 10000 g at 4°C for 10 minutes and the supernatant was collected and stored at −80°C until further use. Protein content of the cardiomyocyte extract was measured using the Bradford protein assay (Bio-Rad, Hercules, CA, USA).

2.7. Measurement of MMP-2 Activity. Gelatin zymography was performed as previously described [4, 32, 33]. Briefly, homogenates from cardiomyocyte preparations containing 30 μg of protein were applied to 8% polyacrylamide gel copolymerized with 2 mg/mL gelatin. After electrophoresis, gels were rinsed three times for 20 minutes in 2.5% Triton X-100 to remove SDS. The gels were then washed twice in incubation buffer (50 mM Tris-HCl, 5 mM $CaCl_2$, 150 mM NaCl, and 0.05% NaN_3) for 20 minutes at room temperature and incubated in incubation buffer at 37°C for 24 hours. The gels were stained using 0.05% Coomassie Brilliant Blue G-250 in a mixture of methanol : acetic acid : water (2.5 : 1 : 6.5, v : v : v) and destained in aqueous solution of 4% methanol : 8% acetic acid (v : v). Developed gels were scanned with a GS-800 calibrated densitometer and MMP-2 activity was measured using Quantity One 4.6 software (Bio-Rad, Hercules, CA, USA).

2.8. Western Blot Analysis. Protein (30 μg) from cardiomyocyte homogenates was separated using 12% SDS-PAGE and transferred to a PVDF membrane (Bio-Rad, Hercules, CA, USA). Myosin light chains 1 and 2 (MLC 1 and MLC2) were identified using mouse monoclonal anti-MLC1 antibody and rabbit polyclonal anti-MLC2 antibody, respectively (Abcam, Cambridge, MA, USA), and MMP-2 was identified using rabbit monoclonal anti-MMP-2 antibody (Abcam, Cambridge, MA, USA). Membranes were developed using Versa Doc 5000 and band densities were measured with Quantity One 4.6 software (Bio-Rad, Hercules, CA, USA). Equal protein loading was additionally verified by measurement of tubulin level with mouse monoclonal antibody (Abcam, Cambridge, MA, USA).

2.9. Immunocytochemistry. For immunocytochemistry, cardiomyocytes were seeded on polylysine-coated coverslips and follow the same siRNA transfection protocol. After permeabilization with 0.25% Triton X-100 and fixation, cells were blocked for 1 h with PBS containing 5% bovine serum albumin (BSA, Sigma, St Louis, MO, USA). Proteins of cardiomyocytes were labeled by overnight incubation (at 4°C) with rabbit anti-MMP-2 (Abcam, Cambridge, MA, USA) antibody diluted at 1 : 200 in blocking buffer followed by brief wash (three times; 10 min each) and incubation with Alexa Fluor 555-conjugated goat anti-rabbit secondary antibodies (Invitrogen, Carlsbad, CA, USA) at 1 : 1000 for 1 h. After Hoechst (Sigma, St Louis, MO, USA) staining, the coverslips were mounted on newly cleaned slides using Prolong Gold Antifade Reagent (Invitrogen, Carlsbad, CA, USA) and observed with an LSM700 laser scanning confocal microscope (Carl Zeiss, Oberkochen, Germany). Images were acquired using a Zeiss Plan-Apochromat 63X/1.6 oil objective lens and analyzed with the Zeiss Zen 2009 software (version 5.5 SPI).

2.10. Immunoprecipitation. The immunoprecipitation of MMP-2 with MLC1 or MLC2 was initiated by incubating 200 μg of total protein extract with 10 μg mouse anti-MLC1 IgG or 10 μg rabbit anti-MLC2 IgG in a total volume of 500 μL RIPA buffer (150 mM NaCl, 1% IGEPAL CA-630, 0.5% sodium deoxycholate (DOC), 0.1% SDS, 50 mM Tris, pH 8.0, 1 mM PMSF) overnight at 4°C. This buffer was chosen because of its known high stringency to avoid unspecific binding. As a negative control, unrelated IgG was used instead of anti-MLC IgG. Following the initial incubation, 100 μL of slurry of protein A-Sepharose beads was added and the resulting mixture was incubated overnight at 4°C. After overnight incubation the mixture was washed three times with 0.5 mL of RIPA buffer at 4°C and 20 μL of sample buffer was added. Determination of colocalization of MLC1 or MLC2 with MMP-2 was determined by gelatin zymography of the immunoprecipitates.

2.11. Statistical Analysis. For contractility measurements, at least three independent experiments (myocyte preparations from different hearts) were run. Each experiment was performed in triplicate (myocytes from the same heart). ANOVA with Kruskal-Wallis post hoc analysis or Student's t-tests were used in this study. A $P < 0.05$ indicated statistical significance. Data are presented as the mean ± SEM.

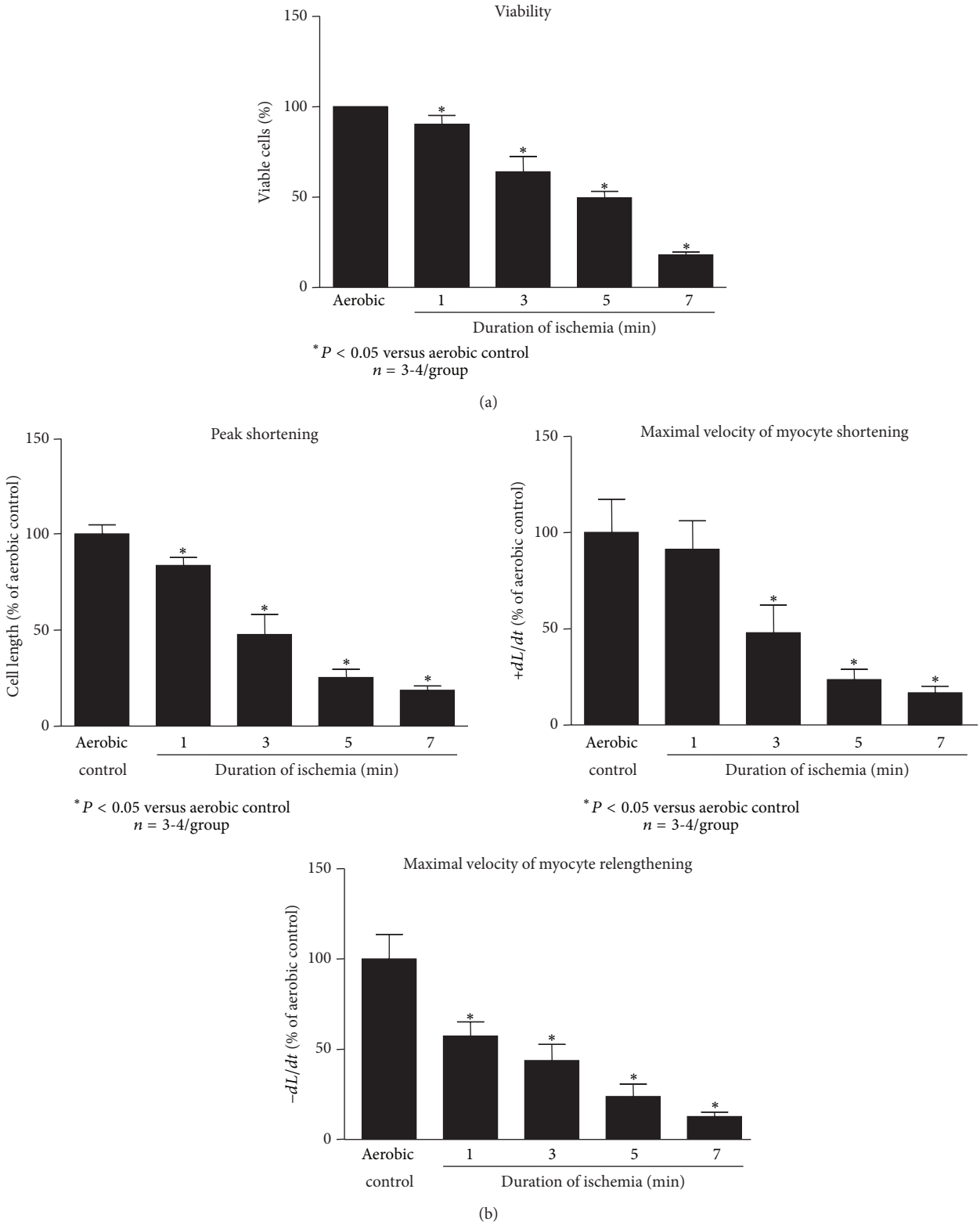

Figure 2: Effect of the duration of ischemia on cardiomyocyte viability (a) and contractility (b). Total number of live cells in aerobic condition is considered as a 100%. n = 3-4 heart preparations per group, $^{*}P < 0.05$ versus aerobic control.

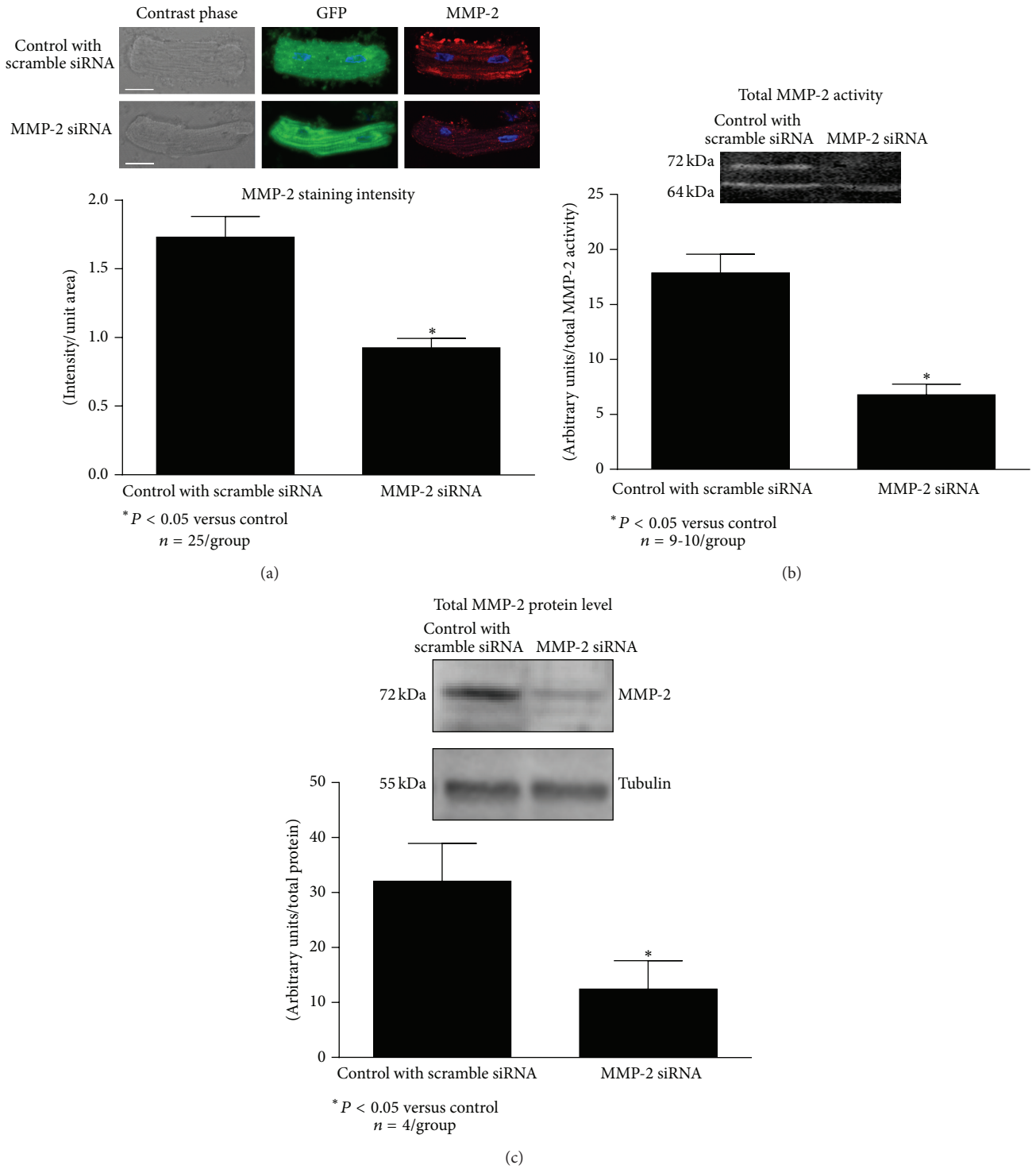

Figure 3: Effect of MMP-2 siRNA transfection on MMP-2 expression in isolated cardiomyocytes. (a) Efficiency of siRNA transfection and MMP-2 protein levels measured by immunocytochemistry. Scale bar, 50 μm. (b) Measurement of MMP-2 gelatinolytic activity by zymography. (c) MMP-2 protein level. (a) $n = 25$ cells from 3 different hearts per group; $n = 9$-10 heart isolates per group for MMP-2 activity (b), in (c) $n = 4$ heart isolates per group, $^{*}P < 0.05$ versus aerobic control.

3. Results

3.1. Cell Contractility and Duration of Ischemia. The effect of the duration of ischemia on cardiomyocyte viability and contractility was determined. One minute of ischemia decreased cardiomyocyte viability by approximately 10%, in comparison to aerobic control cells, with longer durations reducing viability further (Figure 2(a)). Cardiomyocyte contractility, namely, peak shortening and maximal velocity of myocyte relengthening, was decreased after 1 minute of ischemia; however maximal velocity of myocyte shortening was unaffected (Figure 2(b)). Three minutes of ischemia reduced contractility by 50% in all three measured parameters. Longer periods of ischemia (5 and 7 min) further reduced contractility to approximately 70–80% of aerobic values (Figure 2(b)). Based on cellular viability and contractility, 3 minutes of ischemia was chosen for further experimentation.

3.2. MMP-2 Expression and Activity in Cardiomyocytes Transfected with MMP-2 siRNA. MMP-2 siRNA transfection silencing of expression was evaluated by gelatin zymography, immunoblot analysis, and immunocytochemistry using confocal microscopy (Figure 3).

Transfection efficiency, determined by the measurement of GFP-tagged siRNA fluorescence that was cotransfected with either scrambled or MMP-2 siRNA (Figure 3(a), top panel), was approximately 95%. This efficiency of overall transfection was associated with a 50% decrease in the levels of MMP-2, evaluated by immunocytochemistry, in cardiomyocytes transfected with MMP-2 siRNA, in comparison to control cells transfected with scramble siRNA (Figure 3(a)).

Total MMP-2 activity, as determined by gelatin zymography, was reduced by approximately 70% in comparison to control cells transfected with scrambled siRNA (Figure 3(b)). Although the cleaved 64 kDa form of MMP-2 was detected after knocking down MMP-2 mRNA, the pro MMP-2 form (72 kDa) was undetectable (Figure 3(b)). A similar decrease was observed for MMP-2 protein level determined by immunoblotting (Figure 3(c)).

3.3. MMP-2 Knockdown Effects on Cardiomyocyte Contractility before and after I/R Injury. The effect of siRNA transfection on cell viability and contractility was evaluated using scrambled siRNA to control for possible effects independent of inhibition of MMP-2. Transfection of scrambled siRNA (control) did not impact either cardiomyocyte viability (Figure 4(a)) or contractility (Figure 4(b)).

Transfection of cardiomyocytes with MMP-2 siRNA resulted in an increase in the levels of the sarcomeric proteins myosin light chain 1 and myosin light chain 2 (MLC1 and MLC2, resp.) in comparison to control (Figure 5(a)). This increase in MLC1 and MLC2 was accompanied by a decrease in the formation of the protein complexes MMP-2-MLC1 and MMP-2-MLC2 (Figure 5(b)). A negative control (unrelated IgG to MLC1 or MLC2) did not show formation of complex with MMP-2. These observations at the protein level were associated with an increase in contractile function of aerobically perfused, MMP-2 siRNA transfected cardiomyocytes

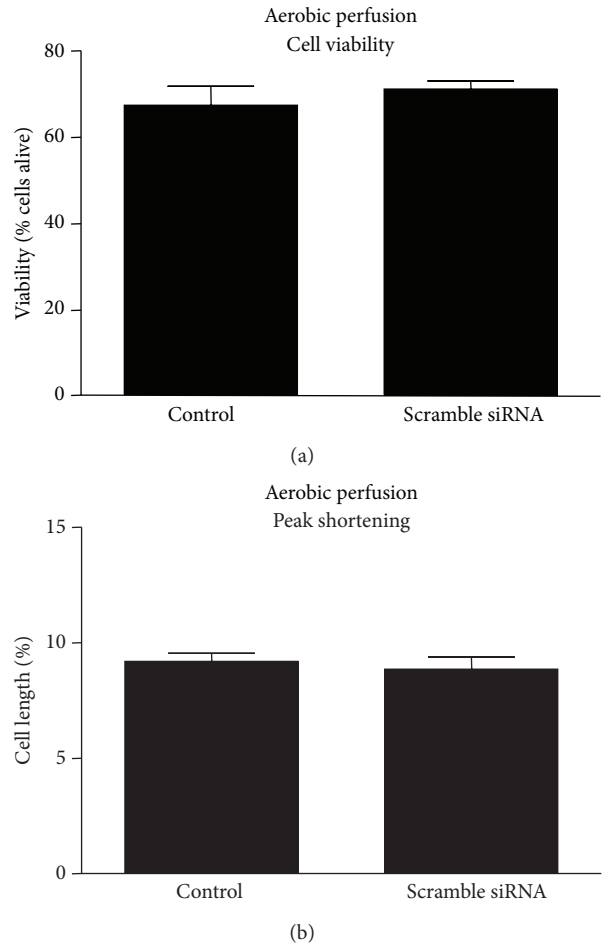

Figure 4: Effect of scrambled siRNA transfection on cardiomyocyte viability (a) and contractility (b). Control cells were transfected with scrambled siRNA. $n = 4$ heart isolations per group.

(before ischemia) in comparison to cells transfected with scrambled siRNA (Figure 5(c)).

The contractile function of cardiomyocytes, transfected with scrambled siRNA (control), in response to I/R was significantly decreased, whereas transfection with MMP-2 siRNA fully protected contractile function against I/R (Figure 6(a)). However, it should be noted that the contractility was higher in the MMP-2 knockdown cells than those with scrambled transfection (Figure 6(a)). The protective effects of MMP-2 inhibition by siRNA transfection were associated with increased levels of MLC1 and MLC2 that were 3- and 2-fold higher, respectively, in comparison to control scramble siRNA transfected cells under aerobic conditions (Figure 6(b)).

4. Discussion

While the cellular mechanisms of I/R injury are complex and not entirely understood, the degradation of contractile proteins is considered to be a major cause of heart injury [12, 34], with matrix metalloproteinase-2 (MMP-2) playing a significant role in contractile protein degradation [4, 10, 12, 13].

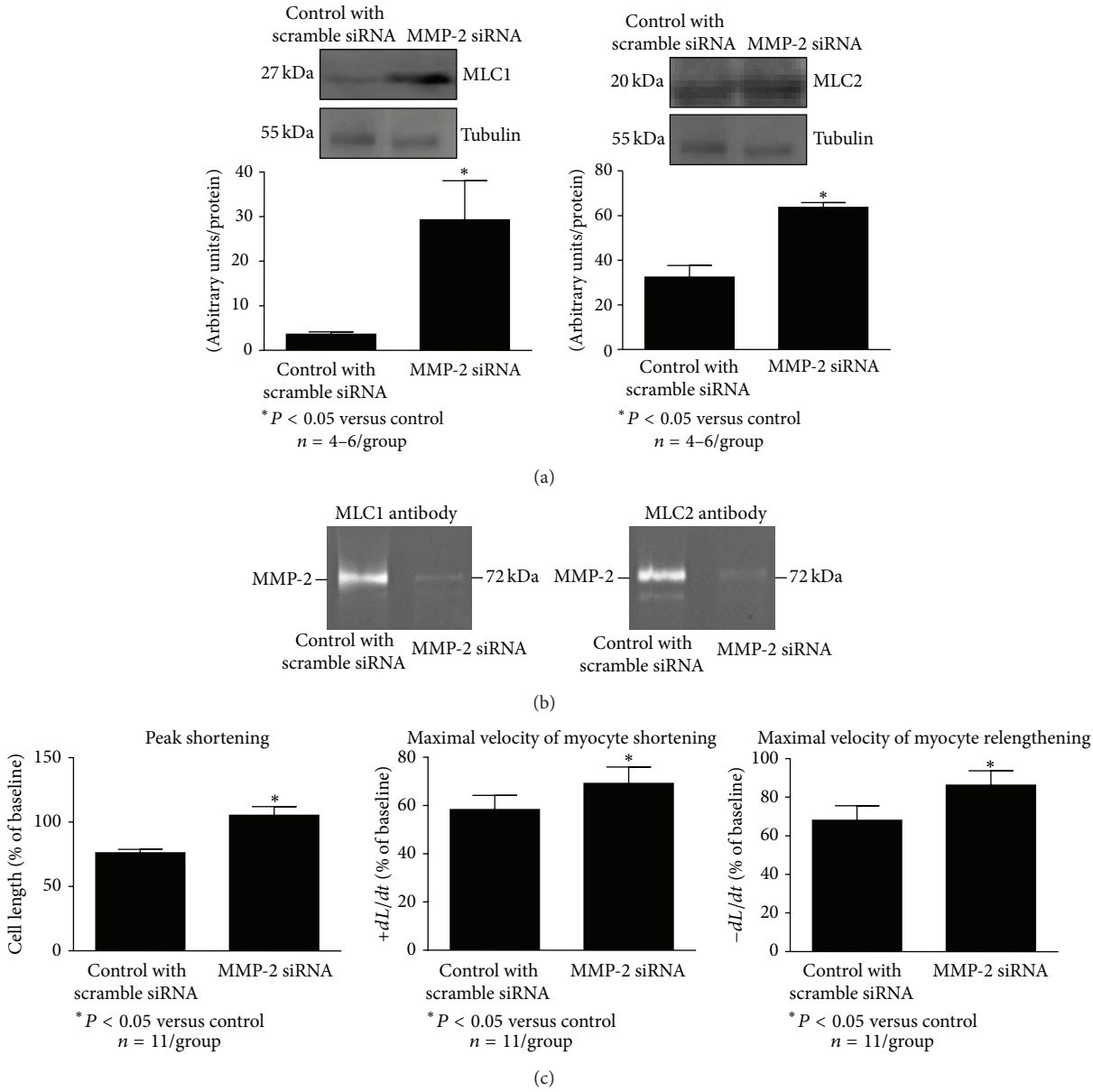

Figure 5: Effect of MMP-2 siRNA transfection on the level of the contractile proteins MLC1 and MLC2 (a), the formation of the complex between MMP-2 and MLC1 or MLC2 (b), and cardiomyocyte contractility (c). As a protein loading control the tubulin level was measured. Control cells were transfected with scrambled siRNA. $n = 4$–6 heart preparation isolations per group. $n = 11$ per group for contractility measurement and $n = 4$–6 for measurement of protein levels. $^{*}P < 0.05$ versus control.

However, degradation of contractile proteins is one from few mechanisms so far described. Metabolic remodeling expressed by ATP depletion, changes in signal transduction, structural remodeling, and oxidative stress are important players in heart failure [35–37].

To the best of our knowledge, this study is the first to demonstrate that, under physiological conditions, MMP-2 regulates MLC1 and MLC2 protein turnover. In response to I/R, intracellular MMP-2 activity increases leading to degradation of these contractile proteins and decreased cardiomyocyte contractility. Inhibition of MMP-2 by siRNA transfection (by reduction in MMP-2 protein levels) protects MLC1, MLC2, and cardiomyocyte contractility from I/R. Moreover, our study demonstrates that MMP-2 acts in an autocrine and intracellular fashion to regulate contractile protein turnover under physiological conditions. Furthermore, our study suggests that, in contrast to broad spectra MMP inhibitors, the use of MMP-2 siRNA to specifically modulate MMP-2 activity can become of clinical relevance in the prevention and treatment of I/R injury and contractile dysfunction associated with loss of contractile proteins.

MMPs are proteolytic enzymes known for their role in maintaining the structural integrity of the extracellular matrix [38]. However, studies over the last decade strongly

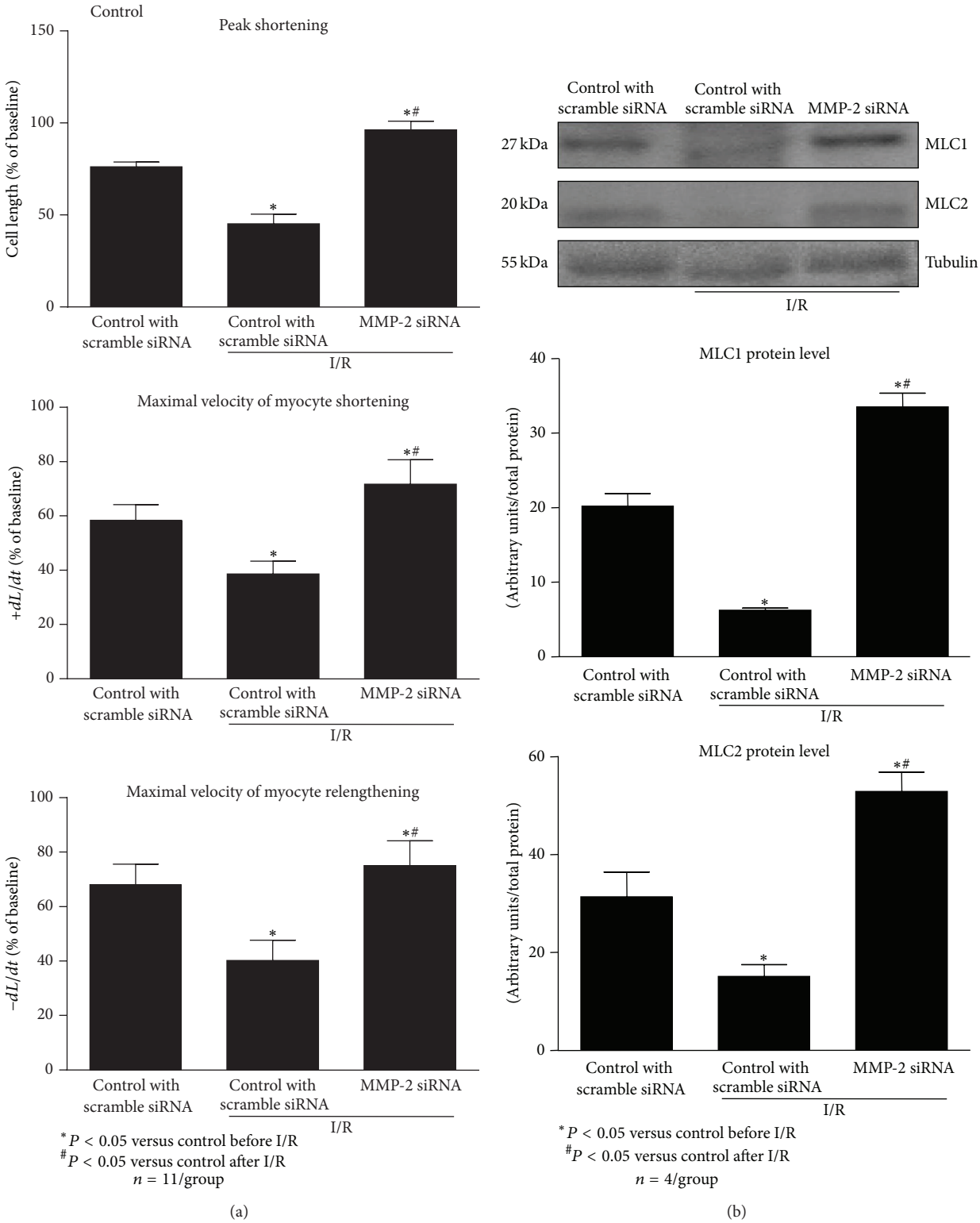

Figure 6: Effect of MMP-2 siRNA transfection on cardiomyocyte contractility (a) and MLC1 and MLC2 in cardiomyocytes subjected to I/R. As a protein loading control the tubulin level was measured. Control cells were transfected with scrambled siRNA. $n = 11$ per group for contractility measurement and $n = 4$ for measurement of protein levels. $^{*}P < 0.05$ versus control, $^{\#}P < 0.05$ versus I/R.

suggest that MMP-2, in addition to the role in remodeling and degradation of extracellular matrix, is also involved in intracellular degradation of contractile proteins in heart subjected to oxidative stress [3, 39, 40]. This increased degradation reduces sarcomeric integrity resulting in contractile dysfunction of the injured heart [15]. The study of the roles of MMP-2 in the heart has, almost exclusively, focused on pathological conditions. We have previously reported that MMP-2 may be involved in the physiological regulation of contractile proteins, namely, MLC1 and MLC2 [13, 14]. Here we show that the specific inhibition of MMP-2 protein levels and activity, in cardiomyocytes, with siRNA reduces the formation of the protein complex between MMP-2 and MLC1/2, resulting in an increase in MLC1/2 protein levels, in cells cultured under aerobic conditions. Importantly, the increase in MLC1/2 protein levels is associated with increased cardiomyocyte contractility. This observation suggests that inhibition of MMP-2 could be of potential usefulness in the therapeutic management of cardiac pathologies characterized by depressed cardiac function, such as heart failure [41].

Biological studies of specific MMP actions, including MMP-2, have been limited by the lack of selectivity and specificity of commercially available synthetic inhibitors [42] in addition to cytotoxicity [4, 43]. Moreover, genetic knockdown of MMP-2 has failed to provide a ubiquitously adequate model for the study of both the physiological and the pathological roles of MMP-2, since compensatory mechanisms have been observed to occur. For example, in MMP-2 knockout mice with autoimmune encephalomyelitis an increase of MMP-9 expression and activity is observed [44]. To bypass these limitations in modulating MMP-2 activity, use of small interfering RNA (siRNA) appears to be an apt approach. This genetic manipulation causes a transient and significant reduction in MMP-2 protein expression and consequently a reduction in overall enzymatic activity (Figure 3), and likely avoiding induction of potential compensatory mechanisms [45, 46].

Small interfering RNA has proven to be an effective method for reducing gene expression through the use of a small piece of antisense RNA complementary to a gene of interest [47]. In addition, siRNA has been successfully used in preclinical studies focused on cardiac tissue protection [48, 49]. By using MMP-2 siRNA we show that selective inhibition of intracellular MMP-2 protects the levels of myosin light chains 1 and 2 (MLC1/2) and contractility of cardiomyocytes subjected to I/R. Also, we show that the autocrine and intracellular actions of MMP-2 are responsible for contractile dysfunction and MLC1 degradation in I/R injured cardiomyocytes, independent from paracrine and extracellular MMP-2 actions since no other cell types are present. Although we cannot exclude the involvement of other proteolytic enzymes or nonproteolytic pathways in regulating sarcomeric contractility and protein turnover, we believe that the observed effects result mainly from MMP-2 selective silencing, without the enabling of adaptive mechanisms.

In summary, this study provides clear evidence that intracellular MMP-2 plays a crucial role in the heart under both physiological and pathological conditions, namely, at the level of regulation of contraction. The separation of intracellular from extracellular roles of MMP-2 has the potential to provide new directions for studying mechanisms underlying several cardiac pathologies, including heart failure. Furthermore, due to the potential for the use of siRNA therapies in clinical practice, these results can have a significant impact on the development of new approaches for the protection of hearts from reperfusion injury due to myocardial infarction or coronary revascularization.

Conflict of Interests

The authors declare that there is no conflict of interests regarding the publication of this paper.

Authors' Contribution

H.-B. Lin, V. J. J. Cadete, and F. Cayabyab were responsible for experimental work, experimental design, and paper writing; B. Sra, J. Sawicka, and Z. Chen were responsible for experimental work; L. K. Bekar was responsible for experimental design and paper writing; G. Sawicki was responsible for hypothesis generation, experimental design, and manuscript writing.

Acknowledgments

This project was funded by grants from Canadian Institutes of Health Research (CIHR), the Saskatchewan Health Research Foundation (SHRF), and Heart and Stroke Foundation of Canada (HSFC). Grzegorz Sawicki is a scholar supported by CIHR and SHRF.

References

[1] F. G. Spinale, J. S. Janicki, and M. R. Zile, "Membrane-associated matrix proteolysis and heart failure," *Circulation Research*, vol. 112, no. 1, pp. 195–208, 2013.

[2] F. G. Spinale, "Myocardial matrix remodeling and the matrix metalloproteinases: influence on cardiac form and function," *Physiological Reviews*, vol. 87, no. 4, pp. 1285–1342, 2007.

[3] M. A. M. Ali, X. Fan, and R. Schulz, "Cardiac sarcomeric proteins: novel intracellular targets of matrix metalloproteinase-2 in heart disease," *Trends in Cardiovascular Medicine*, vol. 21, no. 4, pp. 112–118, 2011.

[4] P. Y. Cheung, G. Sawicki, M. W. Wozniak, W. Wang, M. W. Radomski, and R. Schulz, "Matrix metalloproteinase-2 contributes to ischemia-reperfusion injury in the heart," *Circulation*, vol. 101, no. 15, pp. 1833–1839, 2000.

[5] L. Gao, L. Chen, Z. Z. Lu et al., "Activation of alpha1B-adrenoceptors contributes to intermittent hypobaric hypoxia-improved post-ischemic myocardial performance via inhibiting MMP-2 activation," *American Journal of Physiology*, 2014.

[6] P. Bencsik, J. Paloczi, G. F. Kocsis et al., "Moderate inhibition of myocardial matrix metalloproteinase-2 by ilomastat is cardioprotective," *Pharmacological Research*, vol. 80, pp. 36–42, 2014.

[7] E. Haase, D. L. Bigam, Q. B. Nakonechny, D. Rayner, G. Korbutt, and P. Cheung, "Cardiac function, myocardial glutathione, and matrix metalloproteinase-2 levels in hypoxic newborn pigs

reoxygenated by 21%, 50%, or 100% oxygen," *Shock*, vol. 23, no. 4, pp. 383–389, 2005.

[8] W. Wang, G. Sawicki, and R. Schulz, "Peroxynitrite-induced myocardial injury is mediated through matrix metalloproteinase-2," *Cardiovascular Research*, vol. 53, no. 1, pp. 165–174, 2002.

[9] H. León, I. Baczkó, G. Sawicki, P. E. Light, and R. Schulz, "Inhibition of matrix metalloproteinases prevents peroxynitrite-induced contractile dysfunction in the isolated cardiac myocyte," *British Journal of Pharmacology*, vol. 153, no. 4, pp. 676–683, 2008.

[10] W. Wang, C. J. Schulze, W. L. Suarez-Pinzon, J. R. B. Dyck, G. Sawicki, and R. Schulz, "Intracellular action of matrix metalloproteinase-2 accounts for acute myocardial ischemia and reperfusion injury," *Circulation*, vol. 106, no. 12, pp. 1543–1549, 2002.

[11] M. A. M. Ali, W. J. Cho, B. Hudson, Z. Kassiri, H. Granzier, and R. Schulz, "Titin is a target of matrix metalloproteinase-2: implications in myocardial ischemia/reperfusion injury," *Circulation*, vol. 122, no. 20, pp. 2039–2047, 2010.

[12] G. Sawicki, H. Leon, J. Sawicka et al., "Degradation of myosin light chain in isolated rat hearts subjected to ischemia-reperfusion injury: a new intracellular target for matrix metalloproteinase-2," *Circulation*, vol. 112, no. 4, pp. 544–552, 2005.

[13] A. Doroszko, D. Polewicz, V. J. J. Cadete et al., "Neonatal asphyxia induces the nitration of cardiac myosin light chain 2 that is associated with cardiac systolic dysfunction," *Shock*, vol. 34, no. 6, pp. 592–600, 2010.

[14] A. Doroszko, D. Polewicz, J. Sawicka, J. S. Richardson, P. Y. Cheung, and G. Sawicki, "Cardiac dysfunction in an animal model of neonatal asphyxia is associated with increased degradation of MLC1 by MMP-2," *Basic Research in Cardiology*, vol. 104, no. 6, pp. 669–679, 2009.

[15] V. J. J. Cadete, J. Sawicka, J. S. Jaswal et al., "Ischemia/reperfusion-induced myosin light chain 1 phosphorylation increases its degradation by matrix metalloproteinase 2," *The FEBS Journal*, vol. 279, no. 13, pp. 2444–2454, 2012.

[16] C. Q. Gao, G. Sawicki, W. L. Suarez-Pinzon et al., "Matrix metalloproteinase-2 mediates cytokine-induced myocardial contractile dysfunction," *Cardiovascular Research*, vol. 57, no. 2, pp. 426–433, 2003.

[17] C. J. Schulze, W. Wang, W. L. Suarez-Pinzon, J. Sawicka, G. Sawicki, and R. Schulz, "Imbalance between tissue inhibitor of metalloproteinase-4 and matrix metalloproteinases during acute myocardial ischemia-reperfusion injury," *Circulation*, vol. 107, no. 19, pp. 2487–2492, 2003.

[18] I. A. Arenas, Y. Xu, P. Lopez-Jaramillo, and S. T. Davidge, "Angiotensin II-induced MMP-2 release from endothelial cells is mediated by TNF-α," *American Journal of Physiology: Cell Physiology*, vol. 286, no. 4, pp. C779–C784, 2004.

[19] G. M. Risinger Jr., T. S. Hunt, D. L. Updike, E. C. Bullen, and E. W. Howard, "Matrix metalloproteinase-2 expression by vascular smooth muscle cells is mediated by both stimulatory and inhibitory signals in response to growth factors," *The Journal of Biological Chemistry*, vol. 281, no. 36, pp. 25915–25925, 2006.

[20] P. Stawowy, C. Margeta, H. Kallisch et al., "Regulation of matrix metalloproteinase MT1-MMP/MMP-2 in cardiac fibroblasts by TGF-β1 involves furin-convertase," *Cardiovascular Research*, vol. 63, no. 1, pp. 87–97, 2004.

[21] D. Polewicz, V. J. J. Cadete, A. Doroszko et al., "Ischemia induced peroxynitrite dependent modifications of cardiomyocyte MLC1 increases its degradation by MMP-2 leading to contractile dysfunction," *Journal of Cellular and Molecular Medicine*, vol. 15, no. 5, pp. 1136–1147, 2011.

[22] M. A. M. Ali, A. K. Chow, A. D. Kandasamy et al., "Mechanisms of cytosolic targeting of matrix metalloproteinase-2," *Journal of Cellular Physiology*, vol. 227, no. 10, pp. 3397–3404, 2012.

[23] B. G. Hughes, X. Fan, W. J. Cho, and R. Schulz, "MMP-2 is localized to the mitochondria-associated membrane of the heart," *The American Journal of Physiology—Heart and Circulatory Physiology*, vol. 306, pp. H764–H770, 2014.

[24] N. Oshiro and E. Miyagi, *Matrix Metalloproteinases: Biology, Functions, and Clinical Implications*, Nova Science Publishers, Hauppauge, NY, USA, 2011.

[25] H. León, N. Bautista-López, J. Sawicka, and R. Schulz, "Hydrogen peroxide causes cardiac dysfunction independent from its effects on matrix metalloproteinase-2 activation," *Canadian Journal of Physiology and Pharmacology*, vol. 85, no. 3-4, pp. 341–348, 2007.

[26] C. J. Schulze, M. M. Castro, A. D. Kandasamy et al., "Doxycycline reduces cardiac matrix metalloproteinase-2 activity but does not ameliorate myocardial dysfunction during reperfusion in coronary artery bypass patients undergoing cardiopulmonary bypass," *Critical Care Medicine*, vol. 41, pp. 2512–2520, 2013.

[27] P. Light, Y. Shimoni, S. Harbison, W. Giles, and R. J. French, "Hypothyroidism decreases the ATP sensitivity of K_{ATP} channels from rat heart," *The Journal of Membrane Biology*, vol. 162, no. 3, pp. 217–223, 1998.

[28] G. H. Borchert, M. Hlaváčková, and F. Kolář, "Pharmacological activation of mitochondrial BK_{Ca} channels protects isolated cardiomyocytes against simulated reperfusion-induced injury," *Experimental Biology and Medicine*, vol. 238, no. 2, pp. 233–241, 2013.

[29] R. J. Diaz and G. J. Wilson, "Studying ischemic preconditioning in isolated cardiomyocyte models," *Cardiovascular Research*, vol. 70, no. 2, pp. 286–296, 2006.

[30] R. J. Diaz, C. Zobel, H. C. Cho et al., "Selective inhibition of inward rectifier K+ channels (Kir2.1 or Kir2.2) abolishes protection by ischemic preconditioning in rabbit ventricular cardiomyocytes," *Circulation Research*, vol. 95, no. 3, pp. 325–332, 2004.

[31] R. J. Diaz, V. A. Losito, G. D. Mao, M. K. Ford, P. H. Backx, and G. J. Wilson, "Chloride channel inhibition blocks the protection of ischemic preconditioning and hypo-osmotic stress in rabbit ventricular myocardium," *Circulation Research*, vol. 84, no. 7, pp. 763–775, 1999.

[32] J. Fert-Bober, R. S. Basran, J. Sawicka, and G. Sawicki, "Effect of duration of ischemia on myocardial proteome in ischemia/reperfusion injury," *Proteomics*, vol. 8, no. 12, pp. 2543–2555, 2008.

[33] J. Fert-Bober, H. Leon, J. Sawicka et al., "Inhibiting matrix metalloproteinase-2 reduces protein release into coronary effluent from isolated rat hearts during ischemia-reperfusion," *Basic Research in Cardiology*, vol. 103, no. 5, pp. 431–443, 2008.

[34] S. F. Steinberg, "Oxidative stress and sarcomeric proteins," *Circulation Research*, vol. 112, no. 2, pp. 393–405, 2013.

[35] T. Doenst, T. D. Nguyen, and E. D. Abel, "Cardiac metabolism in heart failure: implications beyond ATP production," *Circulation Research*, vol. 113, no. 6, pp. 709–724, 2013.

[36] A. Nickel, J. Löffler, and C. Maack, "Myocardial energetics in heart failure," *Basic Research in Cardiology*, vol. 108, no. 4, article 358, 2013.

[37] W. Ge and J. Ren, "MTOR-STAT3-notch signalling contributes to ALDH2-induced protection against cardiac contractile dysfunction and autophagy under alcoholism," *Journal of Cellular and Molecular Medicine*, vol. 16, no. 3, pp. 616–626, 2012.

[38] W. C. Parks and R. P. Mecham, *Matrix Metalloproteinases*, Academic Press, San Diego, Calif, USA, 1998.

[39] G. Sawicki, "Synergistic effect of inhibitors of MMPs and ROS-dependent modifications of contractile proteins on protection hearts subjected to oxidative stress," *Current Pharmaceutical Design*, vol. 20, no. 9, pp. 1345–1348, 2014.

[40] A. D. Kandasamy, A. K. Chow, M. A. M. Ali, and R. Schulz, "Matrix metalloproteinase-2 and myocardial oxidative stress injury: beyond the matrix," *Cardiovascular Research*, vol. 85, no. 3, pp. 413–423, 2010.

[41] M. L. Coker, C. V. Thomas, M. J. Clair et al., "Myocardial matrix metalloproteinase activity and abundance with congestive heart failure," *The American Journal of Physiology*, vol. 274, no. 5, pp. H1516–H1523, 1998.

[42] J. F. Fisher and S. Mobashery, "Recent advances in MMP inhibitor design," *Cancer and Metastasis Reviews*, vol. 25, no. 1, pp. 115–136, 2006.

[43] A. H. Drummond, P. Beckett, P. D. Brown et al., "Preclinical and clinical studies of MMP inhibitors in cancer," *Annals of the New York Academy of Sciences*, vol. 878, pp. 228–235, 1999.

[44] J. Esparza, M. Kruse, J. Lee, M. Michaud, and J. A. Madri, "MMP-2 null mice exhibit an early onset and severe experimental autoimmune encephalomyelitis due to an increase in MMP-9 expression and activity," *The FASEB Journal*, vol. 18, no. 14, pp. 1682–1691, 2004.

[45] J. Zhang, S. Bai, X. Zhang, H. Nagase, and M. P. Sarras Jr., "The expression of gelatinase A (MMP-2) is required for normal development of zebrafish embryos," *Development Genes and Evolution*, vol. 213, no. 9, pp. 456–463, 2003.

[46] A. Ratajska and J. P. Cleutjens, "Embryogenesis of the rat heart: the expression of collagenases," *Basic Research in Cardiology*, vol. 97, no. 3, pp. 189–197, 2002.

[47] N. J. Caplen, "Gene therapy progress and prospects. Downregulating gene expression: the impact of RNA interference," *Gene Therapy*, vol. 11, no. 16, pp. 1241–1248, 2004.

[48] X. Zheng, D. Lian, A. Wong et al., "Novel small interfering RNA-containing solution protecting donor organs in heart transplantation," *Circulation*, vol. 120, no. 12, pp. 1099–1107, 2009.

[49] X. Zhang, M. Beduhn, X. Zheng et al., "Induction of alloimmune tolerance in heart transplantation through gene silencing of TLR adaptors," *American Journal of Transplantation*, vol. 12, no. 10, pp. 2675–2688, 2012.